



HAL
open science

Neuronal populations underlying locomotion in zebrafish

Jenna Sternberg

► **To cite this version:**

Jenna Sternberg. Neuronal populations underlying locomotion in zebrafish. *Neurons and Cognition* [q-bio.NC]. Université Pierre et Marie Curie - Paris VI, 2016. English. NNT : 2016PA066603 . tel-01591773

HAL Id: tel-01591773

<https://theses.hal.science/tel-01591773>

Submitted on 22 Sep 2017

HAL is a multi-disciplinary open access archive for the deposit and dissemination of scientific research documents, whether they are published or not. The documents may come from teaching and research institutions in France or abroad, or from public or private research centers.

L'archive ouverte pluridisciplinaire **HAL**, est destinée au dépôt et à la diffusion de documents scientifiques de niveau recherche, publiés ou non, émanant des établissements d'enseignement et de recherche français ou étrangers, des laboratoires publics ou privés.



THESE DE DOCTORAT DE
L'UNIVERSITE PIERRE ET MARIE CURIE

Ecole Doctorale Cerveau Cognition Comportement (ED3C)

Probing dynamic sensory-motor integration in spinal circuits team

Institut du cerveau et de la moelle épinière (ICM)

Neuronal populations underlying locomotion in zebrafish

Présentée par

Jenna STERNBERG

Pour obtenir le grade de

DOCTEUR de l'UNIVERSITÉ PIERRE ET MARIE CURIE

soutenue le 20 septembre 2016

devant le jury composé de :

Prof. Melina Hale	University of Chicago	<i>Rapporteur</i>
Prof. William SCHAFER	University of Cambridge	<i>Rapporteur</i>
Dr. Sabine LEVI	Institut du Fer à Moulin	<i>Examineur</i>
Dr. Jonathan MCDEARMID	University of Leicester	<i>Examineur</i>
Dr. Hugues PASCAL-MOUSSELLARD	Institut du cerveau et de la moelle épinière	<i>Directeur de thèse</i>
Dr. Claire WYART	Institut du cerveau et de la moelle épinière	<i>Chef d'équipe</i>

Acknowledgements

This thesis represents quite a road, and I wish to thank many people who made it possible.

The idea of doing a PhD in France starting simmering in the summer of 2010 while working with Drs. Natasha Zamudio and Déborah Bourc'his at the Curie Institute in Paris. I'd like to thank Natasha in particular for teaching me how to use pipettes and making me feel that I could pursue a career in science at a time when being a researcher didn't even seem like a remote possibility.

Erim Baumgartner at MIT-France, who made it possible for me to come to France in the first place and put me in touch with Claire, who happened to be looking for MIT interns, both of whom enthusiastically supported my coming to Paris to begin a masters and ultimately a PhD. Thanks to the Ecole des Neurosciences de Paris for recruiting me into the graduate program and supporting my move to France and studies, both administratively and financially.

Of course none of this would have been possible at all without Claire. Thank you for your constant support, boundless enthusiasm and creativity, crazy ideas, and desire for all of us to succeed. Being part of a new lab and watching it grow, change, and develop these last few years has been exciting, and I am proud to have worked here with you. Also thank you for putting together this amazing team. Thanks to all of the members of the Wyart lab past and present for your ideas, discussions, assistance, and making the lab a great place to be. In particular, thank you to Kris (for all of the black pixels), Kevin, Lydia, Urs, Andy, Laura, Johanna, Sophie, and Olivier who contributed in big ways to making the work here possible and for being great friends in good (and occasionally not-so-good) times.

I'd like to thank Dr. Hugues Pascal-Mousselard for agreeing to supervise me, making it possible for me to continue my time in the lab.

I would like to thank Dr. Joe McDearmid for teaching me how to patch at a time when the project was really stuck in a rut. Learning electrophysiology inspired me when my project was going nowhere, and never have I enjoyed failing as much as I did during the six months or so it took to get my first (and all subsequent) KAs patched. I am certain that I would not have gotten as far without your help nor realized how much I enjoyed tooling at the ephys rig.

Thank you to my jury members for accepting and taking the time to evaluate my thesis: Drs. Melina Hale, Bill Schafer, Joe McDearmid, and Sabine Lévi.

Thank you to my friends outside of the lab for being there and listening when times were rough, and most of all, thank you to my family: Mom, Dad, Marisa, Elma, and Larry for constantly encouraging me along the way and supporting me from afar, even though it maybe wasn't your first choice.

Table of Contents

	Page
Summary.....	1
Abbreviations.....	2
Introduction	3
I. The neural basis of behavior.....	3
II. Vertebrate spinal circuits.....	3
III. Zebrafish as a model organism for systems and sensory neuroscience.....	6
IV. Development of locomotion in the zebrafish.....	7
V. Thesis outline.....	9
Chapter 1. Automated tracking and characterization of behavior	
1. Introduction.....	11
I. Locomotion in larval zebrafish.....	11
II. Automated tracking and characterization of behavior.....	12
2. Article: “ZebraZoom: an automated program for high-throughput behavioral analysis and categorization”.....	13
3. Discussion.....	26
I. Defining behavioral motifs.....	26
II. Behavior and time.....	28
III. Manipulation of neural circuits.....	28
IV. Experimental Design.....	30
Chapter 2. Characterization of an optimized neurotoxin to probe the role of <i>chx10</i>⁺ excitatory interneurons in slow and fast swimming	
1. Introduction.....	32
I. Motivation.....	32
II. Genetic targeting in zebrafish.....	33
III. Tools to control neural activity: activation.....	34
IV. Tools to control neural activity: silencing.....	36
V. Neurotoxins to ablate or silence neurons.....	38
VI. Excitatory drive for locomotion.....	41
VII. V2a interneurons in the zebrafish.....	41
VIII. Aims.....	42
2. Article: “Optimization of a neurotoxin to investigate the contribution of excitatory interneurons to speed modulation <i>in vivo</i> ”.....	43
3. Discussion.....	64
I. Ongoing challenges to silencing <i>in vivo</i>	64

II.	Challenges for genetic targeting.....	66
III.	V2a interneurons in locomotion.....	67
IV.	Developmental effects of silencing GABAergic activity.....	69
V.	Conclusions.....	70
Chapter 3. Spontaneous activity in Cerebrospinal fluid-contacting neurons		
1.	Introduction.....	72
I.	Motivation.....	72
II.	Spontaneous activity during development.....	74
III.	Signal control and amplification in sensory systems.....	77
IV.	Spontaneous activity in the developing zebrafish embryo.....	78
V.	CSF-cNs in the spinal cord.....	80
VI.	CSF-cNs express TRP channel PKD2L1.....	83
VII.	Sensory function of PKD2L1.....	85
VIII.	CSF-cN function.....	87
IX.	Aims.....	90
2.	Materials and Methods.....	91
3.	Results.....	100
I.	Characteristics of spontaneous activity during early development.....	100
II.	Evaluation of developmental effects due to loss of activity.....	106
III.	Spontaneous activity of CSF-cNs relies on Pkd2l1 channel activity.....	110
IV.	Origins of activity in CSF-cNs.....	113
4.	Discussion.....	123
Overview.....		123
I.	Embryonic activity in CSF-cNs and development.....	124
II.	Challenges and limitations of interpreting calcium imaging data.....	129
III.	Properties of CSF-cNs.....	131
IV.	Conclusions.....	136
References		149
Annexes		
1.	Contribution statement.....	155
2.	Article: “Spinal cerebrospinal fluid-contacting neurons segregate by morphology and molecular markers”.....	156
3.	Article: “Hierarchy of neural organization in the embryonic spinal cord: Granger-causality graph analysis of <i>in vivo</i> calcium imaging data”.....	176
4.	Article: “Fast calcium imaging with optical sectioning via HiLo microscopy”.....	186

Summary

How do neurons dynamically control behavior? The neural networks that underlie actions are complex and involve integration of sensory input and physiological state of the animal. Locomotion is a key component of animal behavior, and the spinal circuits underlying locomotion provide a system to study how complex organization produces a behavioral output. Thanks to molecular and genetic techniques, basic understanding of how hindbrain and spinal circuits produce rhythmic locomotor patterns, known as central pattern generators (CPGs), has been achieved. However, understanding how these circuits function during locomotion, incorporating sensory input from the environment and the internal state of the animal, remains challenging to study because of the difficulty of manipulating and monitoring activity of neuronal populations *in vivo*. The zebrafish is an ideal vertebrate model organism to tackle these problems because of its simple locomotor repertoire at larval stages, transparency, and amenability to genetic manipulation.

Previous studies on larval zebrafish locomotion relied heavily on manual classification of single movements, and thanks to this work researchers defined a larval locomotor repertoire. Extensive morphological and single cell recordings established principles of population function in the spinal cord by morphologically-, physiologically-, or genetically-defined neuronal populations. In order to bridge neuronal properties and the behaviors they drive, we built a setup and developed a program named ZebraZoom to track larval behavior rapidly and automatically characterize locomotor patterns using previously defined behaviors (**Chapter 1**). ZebraZoom reached 90% accuracy, accomplishing tracking and analysis in a high-throughput manner. This work has allowed investigation of sensory-motor loops during active locomotion and analysis of behavioral deficits in genetic mutants.

V2a interneurons are excitatory interneurons in the spinal cord and hindbrain identified by the *chx10* transcription factor. These neurons are critical for proper locomotor patterns in many species. In the zebrafish, V2as drive high frequency rhythmic activity and are sufficient to generate locomotion when hindbrain V2as are stimulated. However, whether they contribute to ongoing slow locomotion and active fast locomotion is unknown. In order to probe their role during two different states of locomotion – slow or fast – we developed a genetically-encoded neurotoxin (*Tg(UAS:BoTxBLC-GFP)*) to silence the *chx10* population of V2as in zebrafish (**Chapter 2**). Using calcium imaging, behavior, and whole cell patch clamp electrophysiology, we validated the efficiency and lack of side effects of *Tg(UAS:BoTxBLC-GFP)*. Using behavior, fictive locomotor recordings, and calcium imaging, we showed that V2a interneurons contribute to slow and fast locomotion in distinct ways. Development of this tool has also allowed investigation of the contribution of other classes of neurons to behavior, used in conjunction with ZebraZoom, described in Chapter 1.

Cerebrospinal fluid-contacting neurons (CSF-cNs) are sensory neurons responsible for relaying mechanical and chemical sensory information locally to motor circuits. CSF-cNs in diverse species express GABA and the transient receptor potential (TRP) channel PKD2L1. Finally, I use genetic targeting, calcium imaging, pharmacology, and electrophysiology to investigate the role of Pkd channels in spontaneous activity in these neurons (**Chapter 3**). These results demonstrate that a single channel opening can generate an intrinsic source of spontaneous activity in sensory CSF-cNs that reflects sensory properties of CSF-cNs.

This work together shows how excitatory interneurons driving locomotion contribute to distinct motor patterns, and establishes the origin of activity of intraspinal sensory neurons that may contribute to their function as part of a sensory-motor loop. Together with establishing new tools to probe the dynamic roles of sensory input and neuronal populations during active locomotion, a more complete picture of how dynamic interactions shape locomotor output may be achieved.

Abbreviations

Arch	archaeorhodopsin-3
ASIC	acid sensing ion channel
BoNT	botulinum neurotoxin
CaP	caudal primary motor neuron
ChR2	channelrhodopsin-2
CSF-cN	cerebrospinal fluid contacting neuron (see also KA)
CICR	calcium-induced calcium release
CiA	circumferential ascending interneuron
CiD	circumferential descending interneuron
CoPA	commissural primary ascending interneuron
CoSA	commissural secondary ascending interneuron
CPG	central pattern generator
DoLA	dorsal longitudinal neuron
DRG	dorsal root ganglion
dpf	days post fertilization
GCaMP	genetically-encoded calcium indicator
hpf	hours post fertilization
IC	ipsilateral caudal neuron
KA	Kolmer-Agduhr neuron (see also CSF-cN)
KCC2	potassium chloride co-transporter
MCoD	multipolar commissural descending interneuron
MN	motor neuron
OKR	optokinetic response
OMR	optomotor response
PCA	principal component analysis
PKD2L1	Polycystic kidney disease 2-like-1
PMN	primary motor neuron
RB	Rohon-Beard neuron
ROS	reactive oxygen species
SERT	serotonin transporter
SHH	Sonic hedgehog
SNARE	soluble N-ethyl maleimide-sensitive factor attachment protein receptor
SMN	secondary motor neuron
TeNT	tetanus toxin
TRC	taste receptor cell
TRP	transient receptor potential
TTX	tetrodotoxin
VeLD	ventral lateral descending interneuron
VMAT	vesicular monoamine transporter
Wnt	Wingless signaling pathway

Introduction

I. The neural basis of behavior

Understanding how neural networks generate and modulate behavior is not a new question but remains elusive to study. Over 100 years ago, Sherrington first proposed that neurons may form networks that are controlled dynamically (Sherrington, 1906). The complexity of actions that a neuron can perform function along the difference scales of anatomical and neuronal organization from cellular and firing properties, synaptic properties, connectivity, and system constraints (Getting, 1983; Wilson, 2014). Beyond the level of the individual neuron and its connectivity, neuromodulation can affect the activity of a circuit (Harris-Warrick and Marder, 1991; Katz et al., 1994; Marder and Thirumalai, 2002; Sakurai and Katz, 2003), resulting in state-dependent circuit operation that can involve single neurons or circuits capable of generating excitation or inhibition (Getting, 1983; Fields, 2004; Buonomano and Maass, 2009; Marder et al., 2014).

II. Vertebrate spinal circuits

Motor tasks are vital elements of behavior for all animals and understanding motor behavior will lead to better understanding of how the nervous system is organized and functions to generate coordinated output. Work in a variety of vertebrate species revealed that intrinsic networks in the spinal cord can generate rhythmic oscillations without sensory input (Marder and Calabrese, 1996). These networks that can act without external input to generate organized patterns of activity are known as central pattern generators (CPG) (Grillner and Wallen 1985). In vertebrates, the CPG consists of local interneurons and motor neurons that can produce oscillatory activity resembling the activity occurring during repetitive locomotion (**Figure 1**; Marder and Calabrese, 1996; Grillner, 2003; Grillner et al., 2007; Goulding, 2009). The brain determines a motor output, and descending projections excite spinal circuits to achieve the action (Grillner and Shik, 1973; Steeves and Jordan, 1980; Armstrong 1988). The spinal cord itself effects movement, integrating sensory information from the periphery and descending commands while sending feedback to the brain via ascending connections (Rossignol et al., 2006).

Introduction

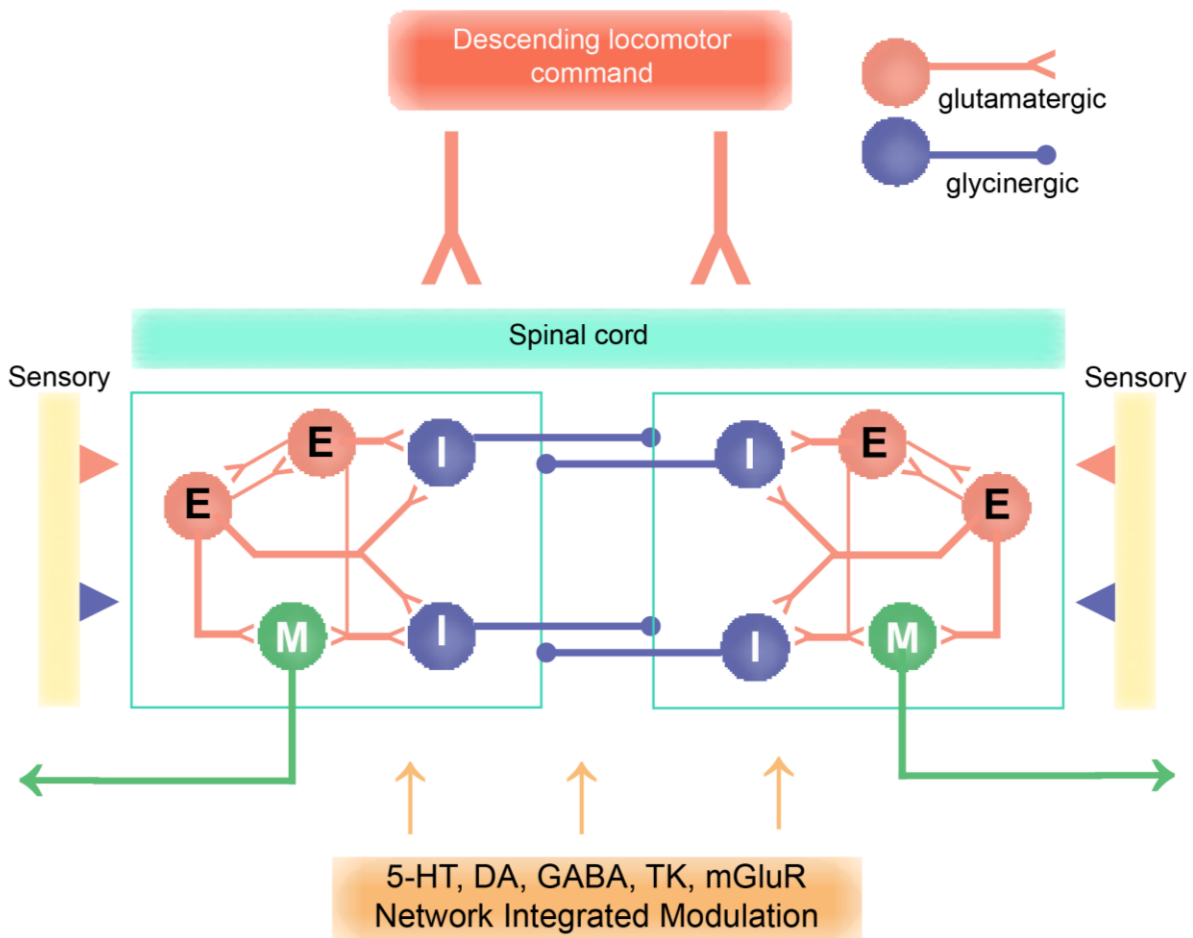


Figure 1. The central pattern generator network.

Diagrams show a schematic representation of the spinal cord components of the networks that generate rhythmic locomotor activity. All neuron symbols denote populations, not single cells. Excitatory glutamatergic inputs excite spinal interneurons and motor neurons, including inhibitory glycinergic interneurons that project axons across the midline to inhibit interneurons and motor neurons on the contralateral side. Sensory input from the periphery provides feedback during ongoing locomotion. Metabotropic receptors, monoamines, dopamine, and GABA, among other factors, exert modulatory control over locomotion. Adapted from Grillner and Jessell, 2009.

Interneurons in the spinal cord comprise CPG elements to activate motor neurons in a coordinated manner and integrate sensory inputs. Genetic programs control how these interneurons are patterned in the embryonic spinal cord. Neuronal identity is determined by morphogen gradients acting on neuronal progenitors in the ventricular zone to establish dorsoventral position (Goulding, 2009). The notochord and floor plate produce sonic hedgehog (SHH), while the dorsal epidermis secretes bone morphogenetic protein (BMP; **Figure 2**; Jessell, 2000; Shirasaki and Pfaff, 2002; Lee and Jessell, 1999). Distinct concentrations of morphogens allow subdivisions between progenitor domains to generate unique classes of neurons in the embryonic spinal cord (Shirasaki and Pfaff,

Introduction

2002). The transcription factor domains as well as morphology and in some cases function are conserved between vertebrate species, including mouse and zebrafish (**Figure 3**; Goulding 2009).

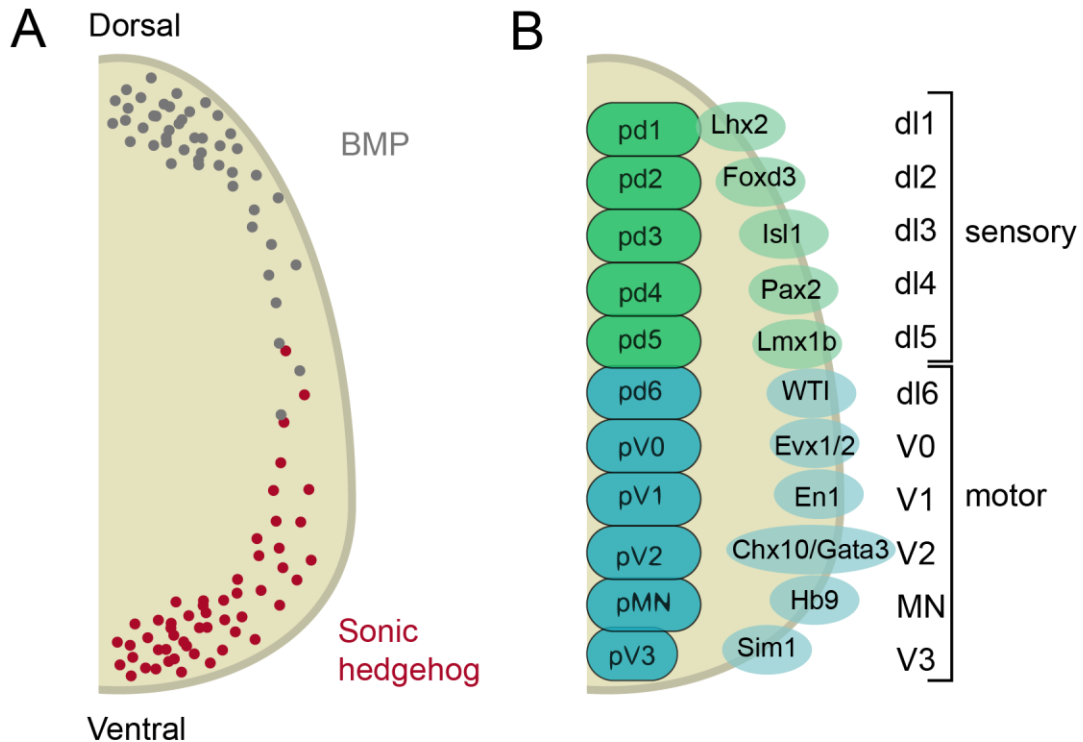


Figure 2. Early development of the spinal cord.

Schematic cross sections through the developing spinal cord. (A) A gradient of sonic hedgehog (red, ventral) and bone morphogenetic proteins (BMP) provide instructive positional signals to dividing progenitors in the ventricular zone. This leads to restricted activation of patterning factors in discrete dorsoventral domains. (B). Restricted activation of patterning factors leads to dorsoventral spatial segregation of different classes of neurons in the spinal cord. dI1-dI5 neurons derived from dorsal progenitors (green) primarily contribute to spinal sensory pathways, whereas dI6, MN and V0-V3 neurons that develop from intermediate and ventral progenitors (blue) are involved in locomotor circuitry. Adapted from Goulding, 2009.

Functions of these diverse interneuron classes and heterogeneity within classes is an active field of research (Jessell, 2000; Goulding, 2009; Grillner and El Manira, 2015; Kiehn 2016).

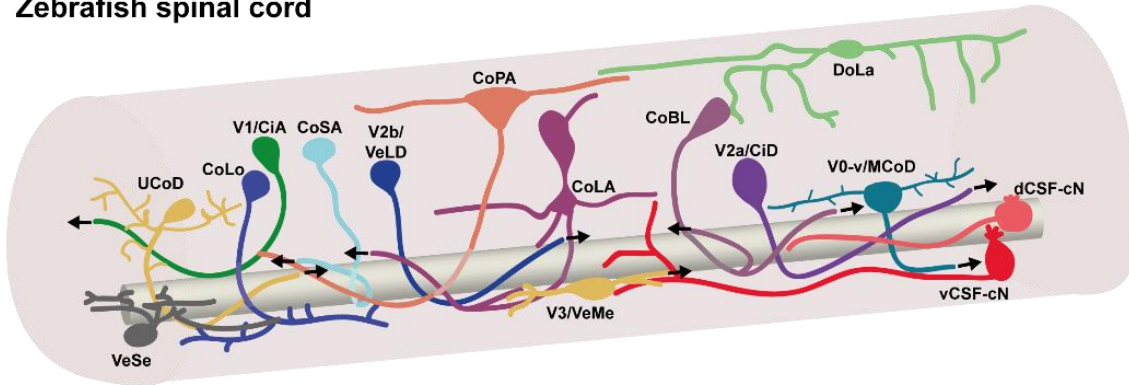
However, understanding the contribution of sensory input and modulation of these circuits by both external sensory input and physiological state of the animal remains difficult to tackle.

Most knowledge relies on *in vitro* preparations due to embryonic lethality of knockouts or difficulty of accessing the neurons (Crone et al., 2008; Zhang et al., 2008). Although combinatorial genetic strategies are being developed to target subclasses of neurons that will not lead to embryonic death

Introduction

by restricting manipulation, often neurotoxin-mediated silencing, to the spinal cord (Talpalar et al., 2013), *in vivo* analysis of spinal circuits and sensory input remains a challenge.

Zebrafish spinal cord



Embryonic mouse spinal cord

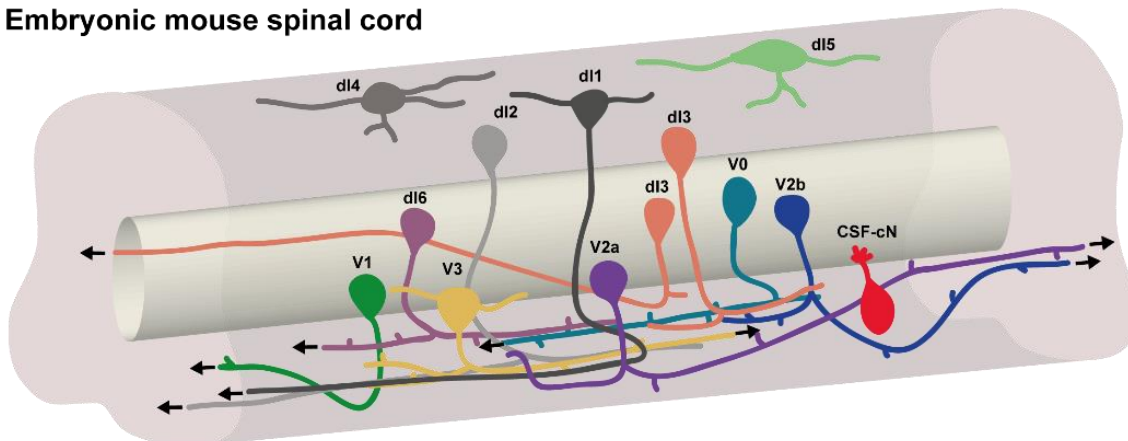


Figure 3. Similar neuronal cell types are present in the embryonic spinal cords of aquatic and terrestrial vertebrates. The putative zebrafish homologues of V0, V1, V2, and V3 locomotor interneurons are indicated by the same color. These include V0 and MCoD neurons (teal), V1 and CiA neurons (dark green), V2a and CiD neurons (purple), V2b and VeLD neurons (dark blue), V3, UCoD, and VeME neurons (yellow), and CSF-cNs (red). Adapted from Goulding, 2009.

III. Zebrafish as a model organism for systems and sensory neuroscience

Obtaining an understanding at the mechanistic level of nervous system functioning requires detailed analysis of neural circuits. Advances in optogenetics, high resolution functional imaging, molecular and genetic tools, *in vivo* electrophysiology, and synaptic tracing are making this understanding more feasible *in vivo*. Thanks to its transparency at embryonic and larval stages and genetic tractability, the zebrafish is an ideal model organism for understanding the principles underlying network function and behavior in vertebrates (Grunwald and Eisen, 2002).

Introduction

The zebrafish has been used as a genetic model organism now for over thirty years (Streisinger et al., 1981) and has primarily been exploited in development biology thanks to its external fertilization and rapid development. Larval zebrafish are approximately 4 mm long, and their brain is less than 500 um thick, making the entire brain accessible for functional imaging (Grunwald and Eisen, 2002). The locomotor network of embryonic and larval zebrafish evolves rapidly between fertilization and mature swimming over the course of a few days (**Figure 4**; Drapeau et al., 2002; Lewis and Eisen, 2003). In the spinal cord, classes of interneurons are highly conserved between zebrafish and mammalian species, including neurotransmitter phenotype and morphology in some cases (**Figure 3**; Goulding 2009; Djenoune et al., 2014).

IV. Development of locomotion in the zebrafish

Locomotor activity begins prior to sensory input (Hamburger and Balaban, 1963), thus basic circuits develop independent of activation or of sensory input (Haverkamp, 1986). Spontaneous electrical activity in the zebrafish spinal cord begins around 17 hpf and develops into a mature locomotor network by 4 dpf (**Figure 4**; Drapeau et al., 2002). Vertebrates at embryonic stages display spontaneous motor behavior that consists of alternating bending of the trunk (Hooker 1952; Hamburger and Balaban, 1963). In the zebrafish this behavior begins at 17 hpf, as the earliest born motor neurons start extending growth cones into muscle, pioneering the ventral root (Kimmel et al., 1995; Saint-Amant and Drapeau, 1998; Lewis and Eisen, 2003) and is independent of descending commands from the brain (Saint-Amant and Drapeau, 1998; Downes and Granato 2006). The underlying neuronal activity consists of periodic depolarizations that trigger action potentials, and thus coiling, as well as synaptic bursts of glycinergic inputs that originate from the contralateral side of the spinal cord (Saint-Amant and Drapeau, 2000). This behavior relies on electrical coupling, occurring independently of glycinergic and glutamatergic transmission but blocked by heptanol, a gap junction blocker (Saint-Amant and Drapeau 2000; Saint-Amant and Drapeau, 2001).

Introduction

Chemical transmission in the zebrafish begins to appear around 21 hpf as embryos develop an immature touch response. Swimming begins at 3 dpf, consisting of occasional swimming episodes that last several seconds. By 4 dpf, larvae exhibit beat-and-glide locomotion that occurs frequently, and by 5 dpf, larvae swim more frequently (approximately 1 Hz) and feeding starts. Additionally, by 5 dpf larvae respond to visual, vestibular, mechanical, nociceptive, and acoustic stimuli (Metcalf et al., 1985; Knaut et al., 2005; Fleisch and Neuhauss, 2006; Burgess and Granato, 2007a; Kohashi and Oda, 2008). Thus, the zebrafish larvae serves as a useful model for studying the extensive pathways for sensing and responding to the external environment and their contribution to motor behavior.

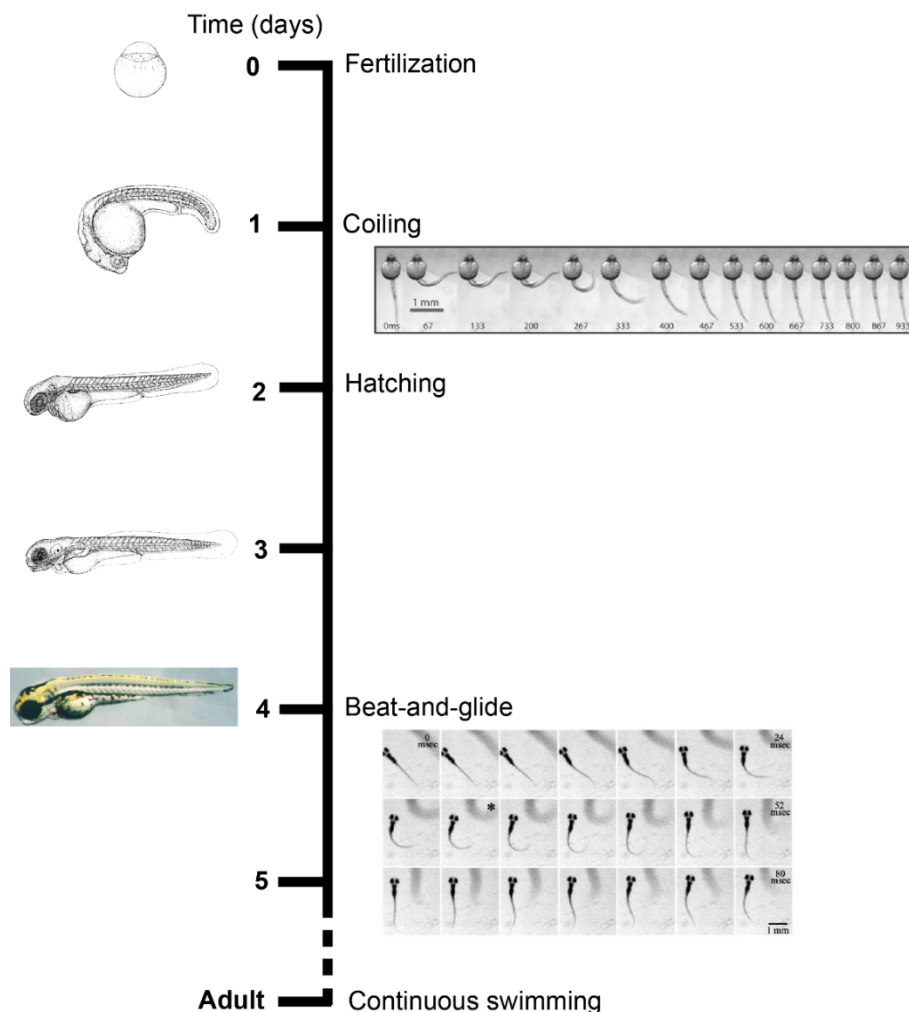


Figure 4. Developmental timing for appearance of motor behaviors in the zebrafish embryo prior to hatching and larva. Schematic adapted from Drapeau et al., 2002. Images on the left are from Kimmel et al., 1995. The coiling sequence is from Knogler et al., 2014. The example of beat-and-glide locomotion is from Budick and O'Malley, 2000.

Introduction

V. Thesis outline

This thesis will address three aims. I first establish methods to investigate behavior and its neural underpinnings in intact animals. Next, I will address how interneurons within the hindbrain and spinal cord contribute to either locomotion or the development of the motor networks within the spinal cord.

First, I **establish and validate an automated and high-throughput method to analyze larval zebrafish behavior**. Using kinematic characterization of swimming bouts, we isolated distinct types of swim bouts in 5-7 dpf zebrafish larvae, analyzed effects of bath application of pharmacological agents, and characterized sequences of movements. Together this work establishes a framework in which sensory integration and active behavior can be studied in a quantitative and high-throughput manner (Chapter 1) in combination with techniques to manipulate neuronal activity.

Second, I will present **validation of a genetically-encoded neurotoxin**, a tool to study behavior in actively swimming animals by potently silencing neurons. This tool serves as an alternative to other techniques for silencing and manipulating neural populations during active behavior. I will then demonstrate use of this tool to **reveal novel roles of excitatory *chx10*⁺ premotor interneurons during different modes of active locomotion** (Chapter 2).

Finally, I will address the role of spontaneous activity of a unique population of intraspinal sensory neurons during development of the spinal cord with the goal of **understanding how spontaneous activity of these GABAergic sensory neurons contributes to development and function of the spinal cord**. (Chapter 3).

Automated tracking and characterization of behavior

I. Locomotion in larval zebrafish

As the zebrafish has emerged as a model organism to study how neural circuits drive behavior, efforts in the last couple of decades have aimed to quantify and characterize the repertoire of zebrafish locomotion. Early work by Budick and O'Malley established a subjective framework by which researchers could isolate defined locomotor patterns (2000). Unlike the continuous swimming of adult zebrafish, larvae swim in a "beat-and-glide" fashion, periods of rhythmic tail movements called swim bouts alternate with periods of rest.

Spontaneous motor patterns for zebrafish larvae are discretized into a few simple patterns that operate in distinct gaits (Thorsen et al., 2004). Basic spontaneous swims can be characterized as spontaneous slow swims or routine turns. Routine turns have a shallow initial bend angle of 14 to 27° as part of a low-speed swim, whereas spontaneous slow swims are low-speed swims with mean yaw angles of less than 3° (Budick and O'Malley, 2000). Escape responses are high-velocity turns initiated by a fast C-shaped bend of the tail (Foreman and Eaton, 1993; Liu and Fetcho, 1999) and followed by a burst swim (Hale, 1996; Budick and O'Malley, 2000) that involves larger bend angles and faster speeds than spontaneous slow swimming.

In addition to this basic repertoire, larvae are able to perform diverse types of goal or reflex-directed behavior, including O-bends in response to a dark flash (Burgess and Granato, 2007a), J-turns for tracking prey (McElligott and O'Malley, 2005), burst swims for prey capture (Borla et al., 2002), long-latency C-starts (Burgess and Granato, 2007b), and struggles in response to aversive stimuli (O'Malley et al., 2004). Larvae also perform highly stereotyped visually-mediated reflexive behavior, including the optomotor response (OMR) (Neuhauss et al., 1999), which has been extensively used to elicit slow swimming for probing the role of individual neurons in controlling distinct parameters of locomotion (Orger et al., 2008, Severi et al., 2014). These different types of locomotion were identified by manual

classification (Borla et al., 2002; McElligott and O'Malley, 2005), or short (400 ms – 1000 ms) video acquisitions of stimulus-driven behavior coupled with kinematic analysis (Burgess and Granato, 2007a; Burgess and Granato, 2007b)

II. Automated tracking and characterization of behavior

Automated analysis continues to generate more complete pictures of the behavioral repertoires of model organisms such as *C. elegans* (Zheng et al., 2011; Brown et al., 2013), *Drosophila* (Branson et al. 2009; Dankert et al., 2009), and mouse (Jhuang et al. 2010; de Chaumont F, et al., 2012). For the purposes of mapping neural circuits, the ultimate goal would be to obtain high speed tracking of behavior in real-time combined with a wide array of stimuli, including activating or silencing tools that act on a millisecond scale. This has been achieved in *C. elegans*, for which acquisition speed demands are not as high as zebrafish (Leifer et al., 2011; Stirman et al., 2011) and to some extent in *Drosophila* (Wu et al., 2014) and rodents (Armstrong et al., 2013).

Refined analysis to understand how circuits are integrating information at the level of the spinal cord or how sensory feedback is incorporated to generate this wide diversity of behavior in zebrafish requires high-throughput analysis of kinematics in freely behaving larvae. By developing new tracking and categorization software, we sought to develop a program that would address two challenges of quantifying locomotor behavior: automating tracking of larvae over long time scales (minutes) and categorizing this behavior into previously-defined and subjective motifs in order to be able to investigate the neural underpinnings of distinct locomotor patterns during active locomotion.

Article

ZebraZoom: an automated program for high-throughput behavioral analysis and categorization

Olivier Mirat, Jenna R. Sternberg,
Kristen E. Severi, Claire Wyart

Published in:
Frontiers in Neural Circuits
Volume 7, 2013



ZebraZoom: an automated program for high-throughput behavioral analysis and categorization

Olivier Mirat^{1,2}, Jenna R. Stenberg^{1,3}, Kristen E. Severi¹ and Claire Wyart^{1*}

¹ Centre de Recherche de l'Institut du Cerveau et de la Moelle Épineière, UPMC, Inserm UMR S975, CNRS UMR 7225, Fondation ICM, Campus Hospitalier Pitié Salpêtrière, Paris, France

² Université Paris Descartes, Paris, France

³ Université Pierre et Marie Curie, Paris, France

Edited by:

Gonzalo G. De Polavieja, Instituto Cajal. CSIC, Spain

Reviewed by:

Kristin Branson, HHMI Janelia Farm Research Campus, USA

Alfonso Perez-Escudero, Consejo Superior de Investigaciones Científicas, Spain

*Correspondence:

Claire Wyart, Centre de Recherche de l'Institut du Cerveau et de la Moelle Épineière, Inserm U975, CNRS UPMC UMR 975, Fondation ICM, Campus Hospitalier Universitaire, Pitié-Salpêtrière, 83, Bld de l'hôpital, 75013 Paris, France
e-mail: claire.wyart@icm-institute.org

The zebrafish larva stands out as an emergent model organism for translational studies involving gene or drug screening thanks to its size, genetics, and permeability. At the larval stage, locomotion occurs in short episodes punctuated by periods of rest. Although phenotyping behavior is a key component of large-scale screens, it has not yet been automated in this model system. We developed ZebraZoom, a program to automatically track larvae and identify maneuvers for many animals performing discrete movements. Our program detects each episodic movement and extracts large-scale statistics on motor patterns to produce a quantification of the locomotor repertoire. We used ZebraZoom to identify motor defects induced by a glycinergic receptor antagonist. The analysis of the blind mutant *atoh7* revealed small locomotor defects associated with the mutation. Using multiclass supervised machine learning, ZebraZoom categorized all episodes of movement for each larva into one of three possible maneuvers: slow forward swim, routine turn, and escape. ZebraZoom reached 91% accuracy for categorization of stereotypical maneuvers that four independent experimenters unanimously identified. For all maneuvers in the data set, ZebraZoom agreed with four experimenters in 73.2–82.5% of cases. We modeled the series of maneuvers performed by larvae as Markov chains and observed that larvae often repeated the same maneuvers within a group. When analyzing subsequent maneuvers performed by different larvae, we found that larva–larva interactions occurred as series of escapes. Overall, ZebraZoom reached the level of precision found in manual analysis but accomplished tasks in a high-throughput format necessary for large screens.

Keywords: machine learning, tracking, analysis of kinematics, collective behavior, support vector machine classifier, multiclass categorization, locomotion in intact behaving animals

A central question in systems neuroscience is how neural circuit assembly and function relate to animal behavior. Genetic screens in invertebrate models, such as *Drosophila melanogaster* and *Caenorhabditis elegans* have begun to unravel the genetic basis of circuit function and behavior (Chalfie et al., 1985; Moore et al., 1998; Scholz et al., 2000). Automated methods have recently been developed in these species to track the position of individuals alone or in a group (Branson et al., 2009; Swierczek et al., 2011) and to categorize behavior (Dankert et al., 2009; Kabra et al., 2013). The zebrafish has emerged as an important vertebrate model organism for developmental biology, neurobiology, and human disease models, and is now used as a genetic model organism for the study of the mechanisms modulating complex behaviors in vertebrates such as depression and anxiety (Blaser et al., 2010; Lee et al., 2010; Cachat et al., 2011; Vermoesen et al., 2011; Zakhary et al., 2011; Ziv et al., 2013), sleep (Zhdanova et al., 2001; Appelbaum et al., 2009), or addiction (Petzold et al., 2009; Khor et al., 2011). The permeability, small size, genetic tractability, transparency, and low cost of zebrafish make them highly suitable for large-scale genetic and chemical screens (Driever

et al., 1996; Granato et al., 1996; Haffter and Nusslein-Volhard, 1996).

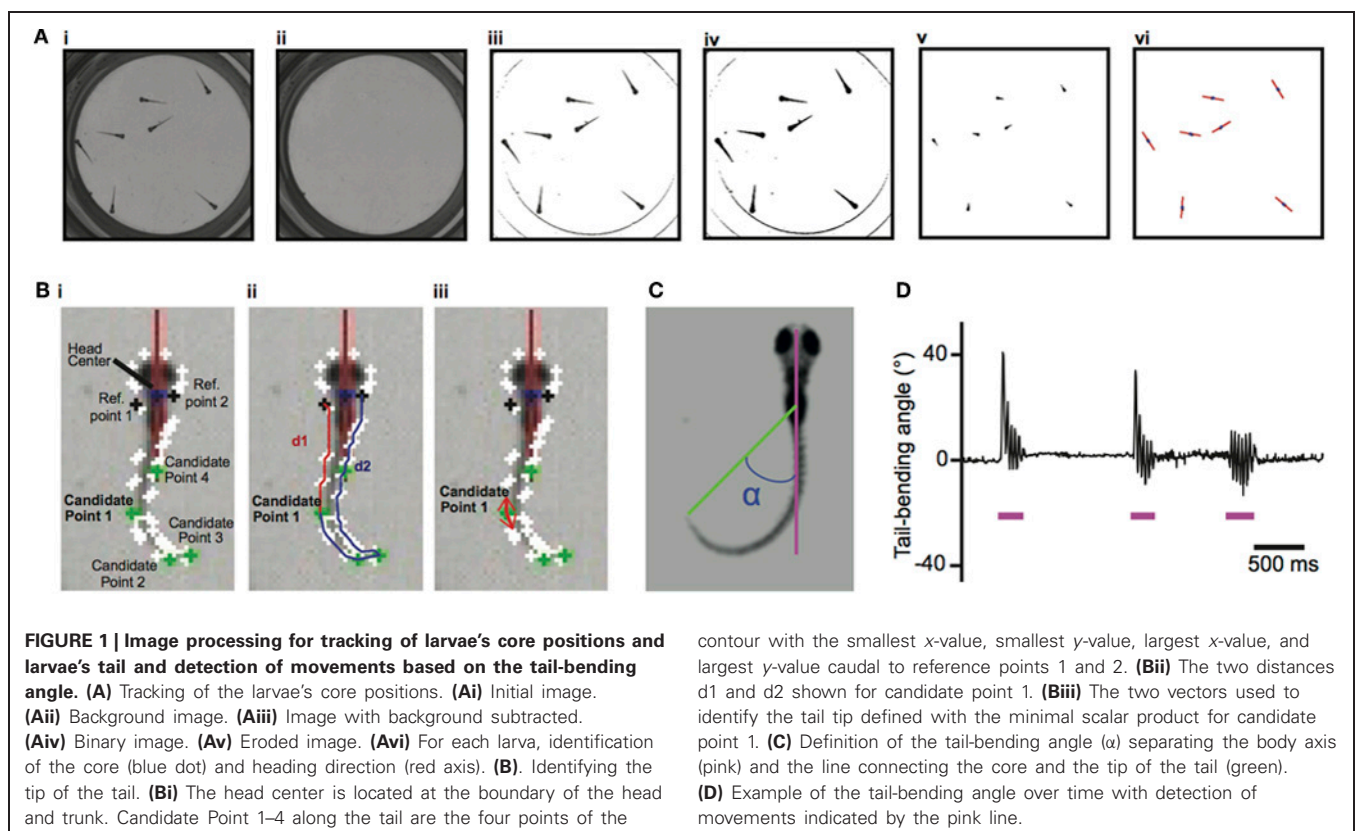
Although simple for a vertebrate, the locomotor patterns of the zebrafish larva bring technical challenges to automated analysis. Larvae spontaneously swim in discrete bouts in a manner often described as “beat and glide,” which can be classified as individual maneuvers, including slow forward swim, routine turn, or escape. These short movements are characterized by a large range of tail-beat frequencies (15–100 Hz), which require high-speed imaging to capture accurately and can be separated by long resting periods of up to a few seconds. Manual tracking via frame-by-frame analysis has formed the basis of contemporary knowledge and has enabled initial characterization of the larval zebrafish locomotor repertoire (Budick and O'Malley, 2000; Borla et al., 2002; McElligott and O'Malley, 2005). However, manual techniques are both laborious and limited in scope for high-throughput screens (Driever et al., 1996; Granato et al., 1996; Haffter and Nusslein-Volhard, 1996). The currently available automated tools have limitations in either refinement or time-scale. Recent chemical or genetic screens have relied on commercial software that estimates

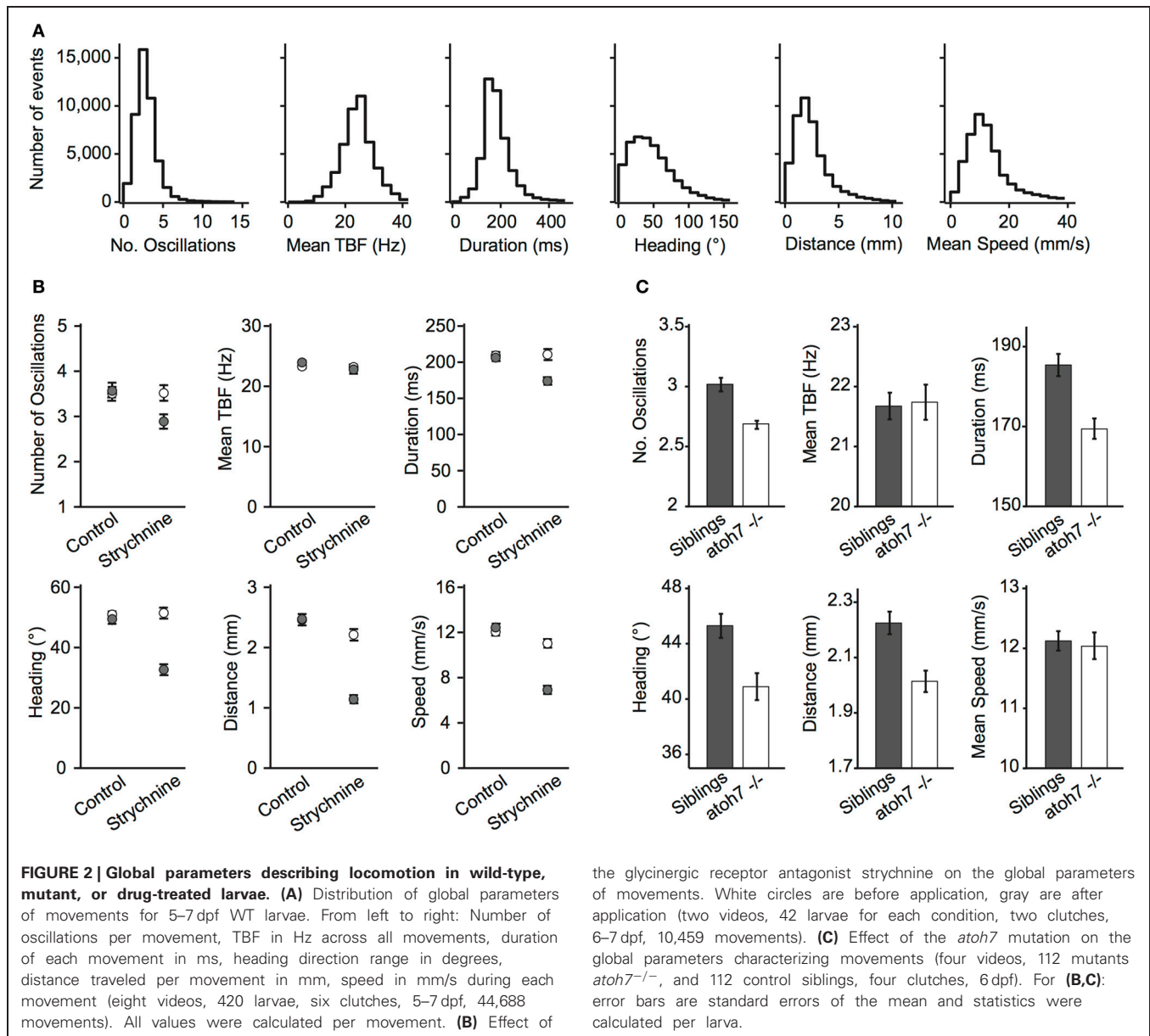
an index of mobility of the larvae, usually measured as the distance traveled during a recording session or the amount of time spent moving (Rihel et al., 2010; Elbaz et al., 2012; Rihel and Schier, 2012). These approaches for high-throughput screens provide information about average velocity and distance traveled by tracking the animals' center-of-mass over minutes to hours. Previous studies have either focused on analyzing movement duration and speed at low frequency over long periods of time or on fine analysis of kinematics at high frequency but for very short acquisition (typically 1000 ms, Burgess and Granato, 2007; Liu et al., 2012). Accurate categorization of maneuvers for each individual in a group requires novel methods to record behavior with high temporal resolution and over long durations, automatically tracking and categorizing thousands of maneuvers.

Here we developed a new program, ZebraZoom, to track the full body position over a multiple-minute timescale of 56 larvae simultaneously recorded at high frequency and to finely characterize each maneuver. To identify core and tail positions for large datasets, videos were obtained on multiple larvae simultaneously over long periods of time and at high resolution using a high-speed camera run in a streaming-to-disk interface (Methods). Typically 500–1000 movements from seven larvae were recorded per dish in four minutes and eight dishes were monitored in parallel. To simplify tracking, we placed larvae in conditions that reduced overlapping in the z-plane during swimming (Methods; overlaps occurred on average once every 145 s per larva). We developed an offline 2D tracking method for identifying and separating each animal even when in close contact (Methods,

Figure 1). For each larva several features were identified, a core position that included the head and swim bladder (**Figure 1A**) and ten points along the tail (Methods and **Figure 1B**; **Video S1**). As movements occurred as discrete episodes, ZebraZoom detected movements based on the tail-bending angle over time (Methods and **Figures 1C–D**). To validate the accuracy of movement detection, one trained experimenter manually identified all movements occurring in a subset of videos. In three videos representing a total of 189 events, movements occurred with a false negative rate of 2.7% and a false positive rate of 3.7%.

To quantify movements in a consistent manner, we used the location of the head, the position of the tail, the heading direction and the tail-bending angle to estimate global parameters of locomotion (**Figure 2A**, Methods). We observed that movements for 5–7 dpf wild-type (WT) larvae occurred every 2.22 s on average per larva (at 0.4495 ± 0.0117 Hz). For all movements identified, larvae performed on average 3.19 ± 0.01 oscillations per movement, had a 24.29 ± 0.03 Hz tail-beat frequency (TBF), lasting 189.5 ± 0.0004 ms with a $51.14 \pm 0.18^\circ$ heading direction range, 2.49 ± 0.008 mm traveled distance and 13.35 ± 0.04 mm/s speed per maneuver. We illustrated the use of ZebraZoom for quantifying the effects of a known glycinergic receptor antagonist, and for analyzing a blind genetic mutant. Glycine is responsible for reciprocal inhibition in the spinal cord that permits left-right alternation to sustain oscillations (Dale, 1985; Grillner et al., 1995; Granato et al., 1996; Drapeau et al., 2002; Li et al., 2004). In zebrafish, mutants for glycinergic receptors or transporters have been associated with defects in motor pattern generation





(Granato et al., 1996; Odenthal et al., 1996; Hirata et al., 2005; Masino and Fetcho, 2005). We measured the effect of bath application of 75 μ M strychnine on spontaneous locomotor activity in larvae and compared to control siblings that were not exposed to the drug (Figure 2B, Methods). For control larvae, we did not observe a significant change in the occurrence of movements over time (0.35 ± 0.05 movements per larva/s before and 0.27 ± 0.03 movements per larva/s after), or on any of the global parameters (Figure 2B; all $p > 0.15$). However the locomotor behavior of larvae treated with strychnine was significantly impacted (Figure 2B). Overall, movements occurred less frequently (0.30 ± 0.04 Hz before and 0.12 ± 0.02 Hz after, $p < 0.0002$). Although the average TBF during a movement did not change ($p > 0.81$), the number of oscillations decreased (3.52 ± 0.17 before and 2.89 ± 0.16 after; $p < 0.0078$), an effect that was associated with a

decrease in movement duration ($p < 0.0001$), distance traveled ($p < 10^{-5}$), and average speed ($p < 10^{-5}$). Strychnine application also resulted in a decrease in the range of heading direction ($p < 10^{-5}$). *atoh7* mutant larvae lack retinal ganglion cells, rendering them blind (*atoh7*^{-/-}, Kay et al., 2001). Considering the importance of vision for zebrafish larvae, analyzing their locomotor output could reveal corresponding behavioral differences. Overall *atoh7*^{-/-} mutants generated episodic movements less frequently than control siblings (0.33 ± 0.02 Hz vs. 0.51 ± 0.02 Hz, 112 larvae for each condition). Quantitative analysis of global parameters of the blind mutants showed no difference in the average TBF or the average speed per larva (Figure 2C; $p > 0.85$ and $p > 0.83$, respectively) but there were small but significant decreases in the number of oscillations, duration, heading direction range, and distance traveled (Figure 2C; all $p < 10^{-3}$).

These defects were observed systematically in four clutches. *atoh7^{-/-}* mutants thus display small but substantial differences in basic motor behavior when compared to control siblings.

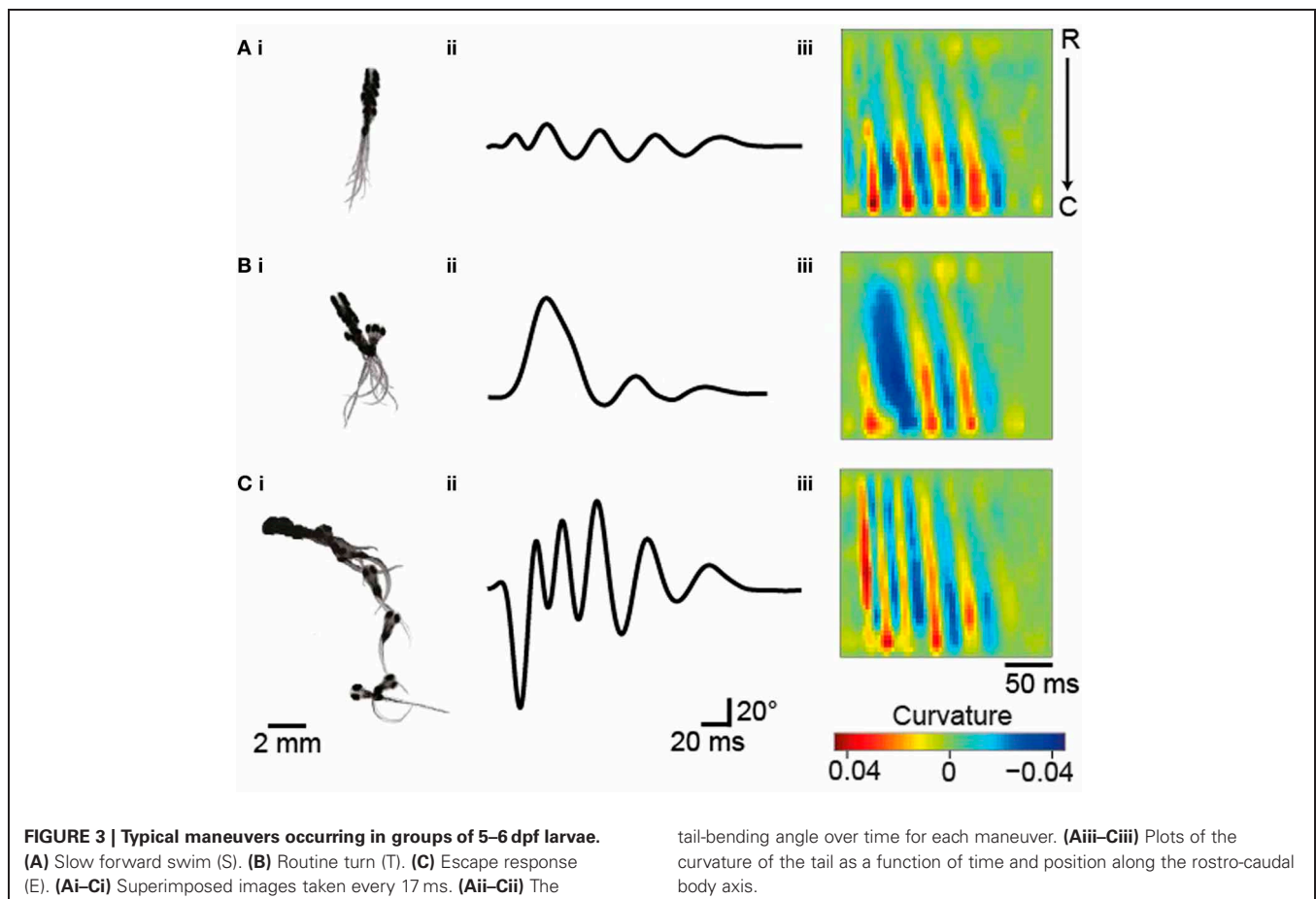
Zebrafish larvae display a variety of locomotor maneuvers that are often grouped into discrete categories. In these experimental conditions, three types of movement occur in groups of larvae at early stages: slow forward swims (S), routine turns (T, also referred to as slow turns), and escapes (E, including C-turns or burst swims). **Figure 3** shows examples of these movements reported by ZebraZoom. For each maneuver, we superimposed a succession of images (**Figures 3Ai–Ci**), the tail-bending angle over time (**Figures 3Aii–Cii**) and the curvature along the rostro-caudal axis and as a function of time (**Figures 3Aiii–Ciii**). The three types of maneuvers included a series of slow left-right alternation; high values of curvature were confined to the caudal tail (**Figures 3Aiii–Ciii**). While high values of curvature of the tail were confined to the caudal end for slow forward swims (**Figure 3Aiii**), high values of curvature were distributed from head to tail for routine turns and escapes (**Figures 3Biii,Ciii**). Stereotypical routine turns and escapes differed by the frequency of left-right alternation in the tail bend (**Figures 3Biii,Ciii**). As larvae did not always exhibit a canonical slow forward swim, routine turn or escape, some movements were ambiguous. To estimate the percentage of these movements, four experimenters subjectively classified 390 movements distributed over eight

videos. Overall about 82% of all movements were classified uniformly by at least three out of four experimenters (Methods) indicating that 18% of movements were difficult to categorize.

Using knowledge of stereotypical locomotor events, we designed a multiclass categorization approach with supervised machine learning to automatically sort each movement into one of the three categories. To implement the multiclass categorization, we used two successive support vector machine (SVM) classifiers: the first classifier sorted S vs. all other maneuvers, and when necessary the second classifier sorted T vs. E. Locomotor events were segregated subjectively in the training set ($n = 201$). This machine learning approach relied on associating dynamic parameters extracted from the tail-bending angle over time with each maneuver type identified in the training set (**Figure 4A** and Methods). To reduce the dimensionality of the data, we

Table 1 | Estimation of ZebraZoom categorizing accuracy based on the different reference experimenters.

	All movements (%)	S (%)	T (%)	E (%)
Experimenter #1	82.5	85	82	79
Experimenter #2	73.2	85	60	53
Experimenter #3	74.3	73	80	58
Experimenter #4	75.4	79	77	47



performed Principal Component Analysis (PCA). Based on the selection of a trained experimenter on the learning set, we validated the multiclass categorization to sort maneuvers by comparison with the subjective classification performed by a trained experimenter for a recognition set ($n = 189$; **Figures 4B,C**). We observed that ZebraZoom agreed with the trained experimenter 82.5% of the time for the recognition dataset (85% for S, 82% for T, and 79% for E; **Figures 4B,C; Table 1** and Methods). When compared to four independent experimenters, ZebraZoom reached 91% accuracy for categorization of stereotypical maneuvers that all experimenters had unanimously identified and 76.4% on average for all maneuvers (73.2–82.5%, **Table 1**). Once validated, we applied the ZebraZoom categorization algorithm on a large dataset of 44,688 movements of WT larvae (**Figure 4D**). We identified 14,911 S (33.36%), 21,432 T (49.96%), and 8,345 E (18.67%). The distribution of global parameters for the three classes of maneuvers were similar in terms of number of oscillations and duration, but they differed in terms of mean TBF, heading direction range, distance traveled and speed (**Figure 4D**).

The investigation of interactions between individuals leading to coordinated motion in animal groups has been a long-standing challenge that is central to elucidating the mechanisms and evolution of collective behavior. Most studies have focused on the analysis of speed or directionality to reflect the interaction between animals (Katz et al., 2011; Gautrais et al., 2012). We availed ourselves of ZebraZoom's features to accurately identify each larva and categorize their maneuvers to study how larvae interacted. In comparison to juvenile and adult zebrafish that swim continuously, larval zebrafish swim episodically with maneuvers that occur in a beat-and-glide manner. Each movement can be regarded as a discrete event, therefore we were motivated to explore how local perturbations of a single individual could impact the group. The program switched identity of larvae once every 109 s (once every 49 movements on average), allowing us to track single larvae. We modeled sequences of maneuvers performed by larvae within a group as Markov chains. Utilizing the classifier, we described larva–larva interactions in a group and intrinsic properties of individuals. We calculated a transition index (I) for each sequence of two maneuvers as the transition probability between first and second maneuvers divided by the probability of random occurrence of the second maneuver (**Figure 5; Table 2** and Methods). When the two successive maneuvers were the same, a higher transition index indicated the probability of repetition of this maneuver was greater than chance. The transition index was equal to one when the order of sequential maneuvers was random. Overall I was greater than one for repetition of the same maneuvers (**Table 2**). We sorted the data into interactions between different animals and the repetition within the same animal. We analyzed how the transition index for a given succession of maneuvers depended on the distance between the two larvae's core positions at the onset of the movement and the time between the onset of each movement (**Figure 5** and Methods). Individual larvae often performed the same type of maneuver sequentially (maximal values $I_{S \text{ max (same)}} = 1.43$, $I_{T \text{ max (same)}} = 1.37$, $I_{E \text{ (same)}} = 2.38$, all $p < 0.002$; **Figure 5A**,

Table 2, and Methods). Although slow forward swims or routine turns were not frequently repeated between larvae (I close to 1: maximal values $I_{S \text{ (diff)}} = 1.09$ and $I_{T \text{ (diff)}} = 1.01$, $p > 0.05$; **Figures 5Bi,ii, Table 2**, and Methods), we found that recurrent escapes were very frequent between different larvae (maximal value $I_{E \text{ (diff)}} = 3.6$, $p < 0.002$; **Figure 5Biii, Table 2**, and Methods). Five to seven dpf larvae do not show evidence for social interactions (Buske and Gerlai, 2011). By taking advantage of the algorithm for identifying single larva and categorizing simple maneuvers, we reveal that larva–larva interactions primarily occurred for escape responses. These series of escapes occurred after direct collisions (in one third of the cases) or via long distance interaction (two third of cases). Blind *atoh7^{-/-}* larvae showed a similar profile of interactions for escapes (data not shown); these interactions were most likely mechanically triggered.

Large-scale chemical and genetic screens would benefit from a quantitative approach to analyze fine locomotor patterns over long periods of time. Compared to other genetic models, zebrafish locomotion is difficult to analyze because larvae initiate maneuvers intermittently and during these short events, the larvae swim at a high speed with TBFs ranging from 15–100 Hz. The quantitative analysis of motor behavior for large-scale screens requires solving the problem of recording multiple animals simultaneously at high frequency (above 200 Hz) and for long periods of time (minutes). Here we implemented a reliable method for quantifying global parameters of movements based on stream-to-disk recordings acquired at high frequency and over long periods of time, limited only by data storage. Next we developed a robust method for tracking the full body position of zebrafish larvae swimming in groups. We first manually validated that the tracking accurately detected discrete movements, and then used the global parameters obtained to characterize the locomotion of WT larvae. Quantification of the global parameters describing larval movements corroborates previous observations based on fewer samples (Budick and O'Malley, 2000; Danos and Lauder, 2007; Liu et al., 2012). Similar estimates of the duration of movements, distance traveled and speed were obtained from the recent application of C-trax (designed originally for *Drosophila*) to zebrafish larvae [Lambert et al. (2012) based on Branson et al. (2009)]. In these conditions, recordings at low frequency over long periods of time, typically 60 Hz for minutes or hours, revealed the global level of activity over time but no information on fine kinematics during individual maneuvers (Elbaz et al., 2012). When recordings were performed at high frequency to capture the dynamics of motion, they usually lasted 1000 ms (Burgess and Granato, 2007).

We illustrated the benefit of ZebraZoom to quantify global parameters of movements by analyzing the effect of a drug to block glycinergic neurotransmission, which has been known to be involved in motor pattern generation and alternation between the left and right side of the spinal cord across vertebrate species (Grillner, 2003; Korn and Faber, 2005; Nishimaru and Kakizaki, 2009). Most studies relied on ventral nerve root recordings where muscles were dissected out or paralyzed in order to record the activity of motor neurons at the level of a few segments at most. Our automated quantification of locomotor events enabled

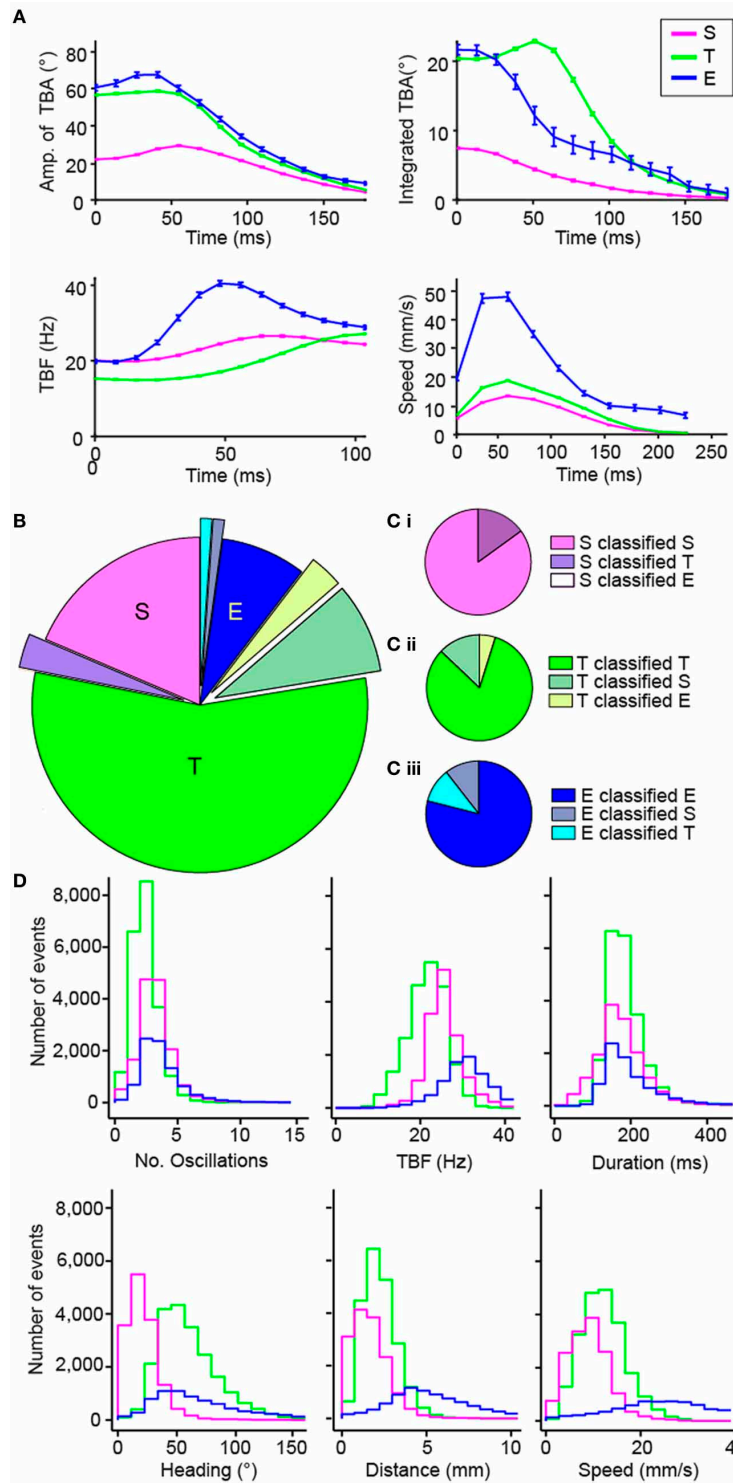


FIGURE 4 | Validation of the automated categorization of maneuvers: slow forward swim (S), routine turn (T) and escape (E). (A) Dynamic parameters used for categorizing the different maneuvers: amplitude of tail-bending angle (TBA) in degrees, integrated TBA in degrees, TBF in Hz, and speed in mm/s. The mean of each parameter for each time bin is shown and error bars are standard error of the mean: S in pink, T in green and E in blue. Time 0 is taken at the peak of the first bend of the movement. (B,C) Comparison of the results of the automatic categorization from

ZebraZoom with the subjective categorization by a trained experimenter on 189 movements from one video. The comparison of the categorization is shown overall (B) and for each maneuver (C: Ci for S, Cii for T, Ciii for E). The proportion of movements categorized the same way by both methods is shown in addition to the proportion of movements miscategorized and how they were categorized. (D) Distribution of global parameters for each maneuver S, T, and E of WT larvae (same color code as in A; 44,688 movements total from eight videos, six clutches).

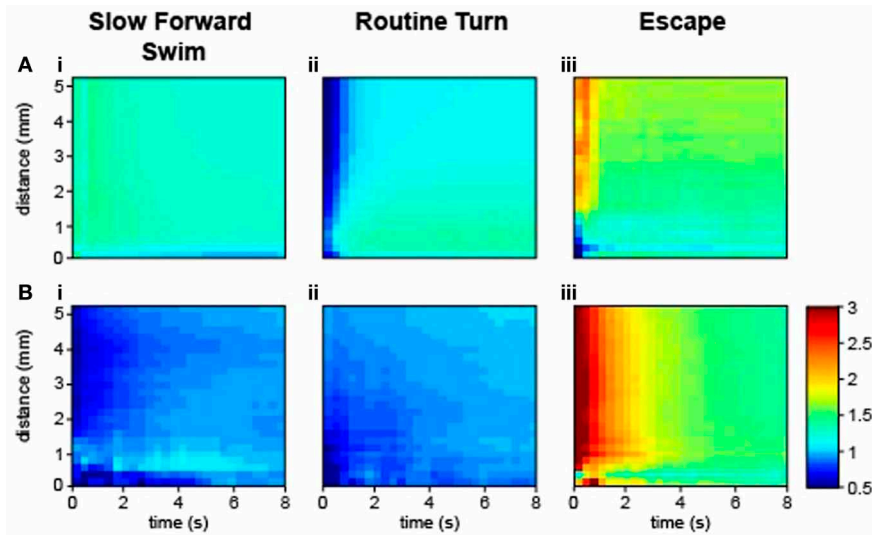


FIGURE 5 | Larva-larva interactions occurred most frequently as sequences of escapes. Transition index for the same larvae **(A)** and for different larvae **(B)**. Time is plotted in seconds from the time of initiation of the first movement. Distance is plotted from the core

position of the larva at the beginning of a movement. **(Ai,Bi)** The sequence S-S. **(Aii,Bii)** The sequence T-T. **(Aiii,Biii)** The sequence E-E (36,068 total movements from five videos, 280 WT larvae, four clutches, 5–6 dpf).

Table 2 | Transition index for sequence of two maneuvers estimated as the probability of transition from maneuver 1 to maneuver 2 divided by the occurrence of the maneuver 2.

	S	T	E
INTERACTIONS BETWEEN DIFFERENT ANIMALS			
S	1.0498	1.0152	0.8481
T	1.0087	1.0413	0.8606
E	0.8549	0.8493	1.7528
REPETITIONS WITHIN THE SAME ANIMAL			
S	1.2162	0.8947	0.8413
T	0.9091	1.1185	0.8499
E	0.8263	0.8887	1.6995

identification of effects induced by bath application of the glycinergic antagonist strychnine on locomotion in intact animals. As predicted, bath application of strychnine dramatically reduced the occurrence of movements and the number of oscillations per movement, that was correlated with a reduction of the duration of movement and of the distance traveled. While mean TBF was not affected, we observed a reduction in the heading direction range and in speed. Our approach pinpointed effects of glycinergic blockade, including a reduction in the number of oscillations per movement, a kinematic feature not estimated in commercially available software. The analysis of the mutant *atoh7* revealed that although TBF and speed were not affected in the blind mutant, there was a small but significant decrease in the number of oscillations, heading direction range, distance, and duration of each bout compared to their control siblings. These effects were systematically observed on four clutches suggesting that visual feedback may impact some global parameters of locomotion. However since the pattern of expression of *atoh7* has not

yet been fully characterized, it cannot be excluded that the gene may be expressed in cells other than retinal ganglion cells.

The originality of ZebraZoom lies in categorizing all maneuvers performed by individual larvae in a group. The subjective analysis of maneuvers based on four independent experimenters revealed that locomotor maneuvers were not obvious to categorize. Based on subjective estimates, 18% of all movements corresponded to ambiguous maneuvers. By using a machine-learning paradigm, we trained ZebraZoom to categorize all maneuvers over tens of thousands of movements with 82.5% accuracy, a similar value to the 72% agreement rate of all four experimenters measured over a few hundreds of movements. The approach we developed here could be expanded to include directionality of the turns, sequences of maneuvers such as those occurring during prey tracking, and subcategories of escapes.

This study constitutes an important first step for accurate tracking of multiple larvae in groups over long periods of time and for categorizing maneuvers. Some improvements could be implemented in the future. While our tracking method currently relies on a simple “blob” approach solely based on raw image analysis, a model-based approach may be more reliable in particular when animals are in close contact (Fontaine et al., 2008). We show here that ZebraZoom can achieve an accurate categorization of maneuvers, comparable to experimenters’ estimates, based solely on the dynamics of movement of head and tail. An interesting avenue of exploration to address this could be investigation of novel dynamic parameters for the learning and recognition process of the classifier to yield subtler methods for detection of defects. Quantification of motor patterns in *C. elegans* is based on a description of all possible positions of the animal over time (Stephens et al., 2008). In order to fully understand larval zebrafish behavior we need to identify a minimal set of parameters sufficient to describe all motor patterns. All together this

work brings new insight to the complexity of behavior determination in zebrafish larvae and could be applied to investigation of the mechanisms of addiction, arousal, feeding, social interaction and aggression in larvae and juveniles (Gahtan et al., 2005; Bianco et al., 2011; Buske and Gerlai, 2011; Miller and Gerlai, 2012; Ziv et al., 2013). The observation of complex interactions in juveniles raises the hope that it will soon be possible to investigate the neuronal circuits and molecular pathways underlying social interactions. The fact that we can track individual larva and analyze their interactions is a major advance over existing methods. Our approach that systematically quantifies and categorizes thousands of motor patterns was designed to bring efficiency and reliability to drug screening and forward genetic screens. ZebraZoom can detect, quantify, and categorize movements to provide a quantitative description of global parameters as well as a qualitative description of all maneuvers performed by individual larvae.

METHODS

ZEBRAFISH HUSBANDRY

All experiments were performed on *Danio rerio* larvae between 5 and 7 dpf. AB and TL strains of WT larvae were obtained from our laboratory stock of adults. Embryos and larvae were raised in an incubator at 28.5°C under a 14/10 light/dark cycle (lights on, 8:00 A.M.; lights off, 10:00 P.M.) until the start of behavioral recordings. The mutant line for *atoh7* (Kay et al., 2001) was given by Dr. Herwig Baier, MPI Munich. Double recessive *atoh7*^{-/-} mutants were identified at 5 dpf by their dark pigmentation. All procedures were approved by the Institutional Ethics Committee at the Research Center of the Institut du Cerveau et de la Moelle épinière (CRICM).

BEHAVIORAL RECORDINGS

Motor behavior of 56 larvae split into eight dishes (seven larvae per dish, **Figure 1Ai**) on a homogeneous illumination plate (light intensity 0.78 mW/cm², Phlox, ref. LEDW-BL-200/200-LLUB-Q-1R24) in egg water (http://zfin.org/zf_info/zfbook/chapt1/1.3.html, methylene blue added at 0.5 ppm). Following acclimation, larvae were recorded for 4 min at 337 Hz with a high-speed camera (VC-2MC-M340E0-C, CMOS chip 2048 × 1088 pixels, Vieworks, South Korea) placed above the setup and coupled to a camera objective (AF Nikkor 50 mm f/1.8D, Nikon, Japan). Pixel size was 66 μm. We developed a direct-to-disk high-speed imaging system designed for long acquisitions of raw images in collaboration with R&D Vision, France. Behavioral recordings were performed between 2:00 and 5:00 P.M. Larvae were acclimated for 60 minutes on the light source at room temperature (21–22°C) and kept at room temperature during all recordings. Larvae were kept in dishes with an inner diameter of 2.2 cm and an outer diameter of 3.5 cm (**Figure 1A**). Water was kept at a low level (2 mm) in order to reduce the occurrence of crossings between larvae. Typically 500–1000 movements were recorded in each 4-min session for each well.

ZEBRAZOOM TRACKING ALGORITHM

The first step is to track the core and then the tail for all larvae over time. Written in C++ using the *openCV* library, the

program identified the center position and heading direction of each larva (**Figures 1Ai–vi**). The algorithm used a Hough transform to identify the eight wells. For each well the background was estimated as the maximum pixel value over all frames of the video recording (**Figure 1Aii**) and then subtracted for all frames for that well (**Figure 1Aiii**). The resulting image was converted to binary (**Figure 1Aiv**). An erosion filter was applied twice in a row with a 3 by 3 structuring element (**Figure 1Av**). The “core” of the larva referred to the resulting connected components that had an appropriate area (between 0.0871 and 0.8712 mm²). The core of the larva included the head and the trunk with swim bladder (**Figure 1Avi**). The algorithm identified the head center position as the center of mass of the putative cores for each larva in a frame. To follow each larva across subsequent frames, ZebraZoom used the information from the previous two frames (core position and speed) to predict the position of the larva and located the closest core out of all the possible cores. The heading direction for each larva was calculated simultaneously using the moments of the eroded body (up to the second order, see red lines in **Figure 1Avi**).

For each larva with an identified core, we determined the “full body” referring to the connected component of the binary image in **Figure 1Aiv**. In order to track the tail, the full body was rotated so that the head axis was parallel to the y-axis, always in the same orientation. To identify the contour of the tail in the coordinate system defined by the head axis, a series of points was extracted from the full body by using the algorithm of Suzuki and Abe (1985), (white dots in **Figures 1Bi–iii**). Reference point A1 was the closest point on the contour line from the head center and reference point A2 was the point symmetrical along the head axis to reference point A1 on the contour. In order to identify the tip of the tail, four candidate points on the contour were selected with minimal and maximal x- and y-values (**Figures 1Bi–iii**). For the maximal y-value the point also had to be above a given distance away from the two reference points [below a 20% threshold for the ratio $|(d_1 - d_2)/(d_1 + d_2)|$, **Figure 1Bii**]. Distances d1 and d2 were calculated from each candidate point to the reference points A1 and A2 along the contour (**Figure 1Bii**). Candidate points with a ratio $|(d_1 - d_2)/(d_1 + d_2)|$ over 0.25 were excluded. The tip of the tail was then identified as the point associated with the smallest scalar product of the tangential vectors pointing in opposite directions (**Figure 1Biii**). The midline of the larva was defined as the line equidistant to the contour line on the left and right side.

ERRORS IN CORE AND TAIL TRACKING

If an error occurred in the core tracking, the larva was missing for that frame and there was no tracking of its tail. If the core of a larva was identified, the algorithm proceeded to the tail tracking. To confirm that the tail tracking was correct, the algorithm checked that the tail length was greater than 1.32 and less than 3.96 mm. If this criterion was invalid, the tail position was set to the previous frame. This happened in 13.46% of frames on average but was compensated by a smoothing spline on the center positions between the left and right contour points of the tail and a median filter applied on the tail-bending angle over time. The tail-bending angle was defined as the angle between the axis formed by the tip of the tail and the center of the head with respect to the larva heading direction (**Figures 1C,D**).

SEPARATING LARVAE DURING CONTACTS

Tracking was optimized to separate larvae in close vicinity to one another or in direct contact. For core tracking, if the trajectories of the two cores merged at a given time point, then the algorithm considered that a collision occurred between the two larvae. When the predicted positions of two larvae based on core position and speed in the two previous frames were closest to the same core, the algorithm considered that a collision between the two larvae occurred at that frame. When a collision was detected, the algorithm applied erosion filters in the region of interest defined by the core until more than one isolated core emerged. In rare cases, the multiple cores were not resolved and the larva could not be tracked for that frame. For the tail tracking, if the area of the larva's full body was greater than 1.9 mm^2 , the algorithm considered that two larvae were in direct contact. The distance separating the larvae's cores determined which of two algorithms was used to isolate the tails: if the distance was less than 1.32 mm , a line separation algorithm was applied. A line was created to separate the two larvae by optimizing the area of the resulting tails, calculated by maximizing the sum of the two largest areas containing a head center position. If the distance was greater than 1.32 mm , a pixel intensity separation algorithm was applied instead. The threshold used to convert the image into binary was adjusted until two separate full bodies, each a connected component, emerged and contained the head center position. Larvae crossings occurred once every 145 s on average per larva (0.0069 ± 0.0019 events per second) and the switching of identification between two larvae after a collision was estimated manually to occur every 109 s on average (0.0092 ± 0.0036 events per second per larva based on 720 s of recordings from four videos, and 28 larvae).

DETECTION OF MOVEMENTS

Algorithms for the detection of movements and the behavior analysis were written in MATLAB (The Mathworks, Inc., USA). The detection of movement was based solely on thresholding the tail-bending angle measured over time (Figures 1C,D). ZebraZoom detected the start of a movement when the value for the tail-bending angle at a given frame varied over 1.15° from the mean value of the tail-bending angle for the ten surrounding frames, or 29.7 ms . To avoid separating single maneuvers into multiple events, movements that occur within 14.8 ms of each other were merged. To avoid false positives we considered only movements in which the larva core had moved more than 0.099 mm and where the range of tail-bending angle values was above 2.86 degrees. Additionally, only events during which the eroded binary image of the larva had moved more than a set number of pixels between subsequent images were considered based on the parameters used for the erosion. Rarely we have observed two distinct movements occurring without a pause, such as a slow forward swim followed by an escape due to a collision. In these few cases when two movements occurred without a noticeable stabilization in the tail-bending angle over time, the movements were merged into one movement in our analysis.

Our tracking method was robust in these experimental conditions. We cannot probe the impact of a reduction of contrast or spatial resolution. All numerical thresholds used above for

tracking were fixed empirically, but they could easily be modified for other users to adapt to other recording conditions.

CALCULATION OF THE CURVATURE

After alignment of the body axis with the y -axis in a consistent orientation, the tail was represented parametrically in Cartesian coordinates as $[x(t), y(t)]$. The midline of the tail was fitted to the $x(t), y(t)$ function with a spline. Curvature was calculated in Cartesian coordinates:

$$c = \frac{|x'y'' - y'x''|}{(x'^2 + y'^2)^{\frac{3}{2}}}$$

where the derivatives were all calculated with respect to t , the distance along the tail.

EXTRACTION OF GLOBAL PARAMETERS

For all frames of a video, ZebraZoom outputs variables for each larva in each dish including: the position of its core, head axis, midline position of its tail and tail-bending angle. For each detected movement, a reference number for the larvae was extracted along with the corresponding well number, start and end time of the movement, and global parameters such as the number of oscillations, TBF, movement duration, heading direction range referring to the range of values of the heading axis for one movement with the heading angle reset to zero at the onset of movement, distance traveled, average speed (distance traveled divided by movement duration).

AUTOMATIC MULTICLASS CATEGORIZATION

We automatically attributed each movement detected in the video to either one of the three maneuvers: slow forward swim, routine turn or escape response. Our method relied on a dynamic set of parameters extracted from the bending angle of the tail estimated from the first tail bend over a limited time window (Figures 1C, 4A). We based our categorization on the four following parameters: (1) the amplitude of the tail-bending angle (0 – 178 ms , bins of 12 ms), (2) the instantaneous frequency (0 – 104 ms , bins of 7 ms), (3) the cumulative tail-bending angle calculated as the average angle value over time (0 – 178 ms , bins of 12 ms), and (4) the speed (0 – 240 ms , bins of 24 ms) (Figure 4A). The values of these four dynamic parameters were interpolated with a spline for a given time window during the movement and then used for categorization of every movement. PCA was first performed to reduce noise and dimensionality. Each movement was subsequently represented by the fourteen first principal components of the PCA out of 53 components (representing all together about 93% of the variance), to which the total duration of the movement was added. Multiclass categorization was implemented in two steps: a series of two subsequent SVM classifiers with linear kernel was applied for automatic categorization of movements: the first SVM classifier discriminated slow forward swims vs. turns and escapes, and if necessary a second SVM discriminated between a routine turn and an escape. We used two distinct datasets from WT 5–7 dpf larvae, one for learning the three maneuver types (five videos, $n = 201$ movements) and one for testing their recognition (three videos, $n = 189$ movements).

ESTIMATING THE RECURRENCE OF MANEUVERS

Successions of maneuvers performed by larvae in a given dish were modeled as Markov chains. Out of the nine possible sequences of two maneuvers (S–S, S–T, S–E, T–S, T–T, T–E, E–S, E–T, E–E), we estimated the frequency of occurrence of each sequence. For a given movement classified as S, T, or E occurring at a given time in one dish, we calculated the transition probability for the subsequent movement to be classified as S, T, or E. We calculated a weighted transition index (I) for each sequence of two sequential maneuvers as the ratio of the transition probability from the first maneuver to the second, divided by the probability of occurrence of the second maneuver (Table 2 for values of all transition indexes). When I is equal to 1, the probability of repeating a maneuver is equal to the probability of random occurrence of the maneuver (probability of random occurrence was 0.35 for S; 0.48 for T and 0.16 for E; Table 2). Thus the index of recurrence I was defined as:

$$I(B1, B2) = \frac{p(x_i = B1 | x_{i-1} = B2)}{p(x_i = B1)}$$

with $B1$ and $B2$ as two possible maneuvers (S, T, or E) and x_{i-1} and x_i as two successive movements. WT larvae were used to estimate the transition index (36,068 movements from 280 larvae originating from four clutches and obtained from 40 wells). To investigate the recurrence of maneuvers as a function of time and distance, we calculated I as a function of the distance separating the two head centers of the larvae at the onset of their respective movement and the time as the time interval between the onsets of the first and second movement. I was calculated for many different time and distance windows. In Figure 5, we plotted these indexes for the sequences S–S, T–T, and E–E. We first calculated the index for the same larva (Figures 5Ai–iii) and across different larvae (Figures 5Bi–iii).

STATISTICAL ANALYSIS

The data used for Figure 2A were based on eight videos, 420 WT AB larvae from six different clutches between 5 and 7 dpf. All values were given as mean \pm standard error of the mean (s.e.m.) calculated per movement. For the pharmacology experiments (Figure 2B), strychnine was bath applied at 75 μ M and the data were based on two videos of 84 WT larvae coming from two clutches (42 for controls and 42 for strychnine) between 6 and 7 dpf. The data on *atoh7*^{-/-} mutants in Figure 2C were generated using four videos, 224 larvae total originating from four clutches (112 *atoh7*^{-/-} and 112 control siblings). All global parameters plotted in Figures 2B,C were calculated per larva then averaged across all larvae and means were given \pm s.e.m. across all larvae. Since the distributions of global parameters were not normal, a standard non-parametric Wilcoxon rank sum test was used in MATLAB for calculating differences between conditions with vs. without drugs for Figure 2B and *atoh7*^{-/-} vs. siblings for Figure 2C. The data used for Figure 4D were based on 44,688 movements from eight videos, 448 larvae, six clutches and for Figure 5 from 36,068 movements from five videos, 280 WT AB larvae from four clutches. To test how the maximal values of the transition index were different from random, we calculated

I_{\max} after randomly permuting maneuvers while keeping track of the larva identity, time, and location the same for 50 iterations. For each comparison, S–S, T–T, E–E across different larvae or within the same larva, we compared the values of I_{\max} after randomization to the measured value I_{\max} using a two-sample T -test.

DATA AND ALGORITHM SHARING

The software ZebraZoom is documented and available online from Source Forge in the code tab (<http://sourceforge.net/p/zebrazoom/wiki/Home/>). ZebraZoom requires MATLAB and works reliably on an Ubuntu 11.04 computer with OpenCV installed and MATLAB 7.10.

CONTRIBUTIONS

Claire Wyart and Olivier Mirat designed the project with help from Jenna R. Sternberg. Olivier Mirat wrote all algorithms of the ZebraZoom program. Jenna R. Sternberg and Claire Wyart assembled the experimental setup. Jenna R. Sternberg performed all experiments. Olivier Mirat and Claire Wyart analyzed the data. Kristen E. Severi, Olivier Mirat, and Claire Wyart prepared the figures. All authors tested and validated the program and wrote the paper.

ACKNOWLEDGMENTS

We thank Dr. Stanley Durlleman, Dr. Lionel Moisan, Dr. Carlos Pantoja, and Claire Oldfield for critical reading of the manuscript. We thank Dr. Olivier Colliot, and Drs. Stanley Durlleman and Lionel Moisan again for advice on machine learning, tracking, and Markov chain analysis. We thank Caroline Vidal, Philippe Domineaux, and Antoine Mongay for data server access. We thank Laura Garnerio, Audrey Baradel, Lydia Djenoune, Victor Adenis, Devika Nair, and Maxime Gaudin for technical assistance and fish care. We thank Dr. Herwig Baier for kindly sharing the *atoh7* mutant line. This work received critical support from the Institut du Cerveau et de la Moelle Epinière (ICM/CR), the Ecole des Neurosciences de Paris (ENP), the Fondation Bettencourt Schueller, Mr. Pierre Belle, the City of Paris Emergence program, the ATIP-AVENIR program from INSERM and CNRS, the Fyssen Foundation, the International Reintegration Grant from Marie Curie Actions Framework Program 6, and the European Research Council (ERC) starter grant “OptoLoco.” Jenna R. Sternberg is affiliated with the graduate program of the Ecole des Neurosciences de Paris (ENP) associated with the ED3C. Olivier Mirat is funded by a DIGITEO PhD fellowship associated with the Ecole Doctorale Interdisciplinaire Européenne Frontières du vivant ED474 program doctoral Bettencourt.

SUPPLEMENTARY MATERIAL

The Supplementary Material for this article can be found online at: http://www.frontiersin.org/Neural_Circuits/10.3389/fncir.2013.00107/abstract

Video S1 | ZebraZoom tracking of seven larvae in a dish. Acquisition was performed at 300 Hz, and one out of every ten images is displayed (every 33.3 ms).

REFERENCES

- Appelbaum, L., Wang, G. X., Maro, G. S., Mori, R., Tovin, A., Marin, W., et al. (2009). Sleep-wake regulation and hypocretin-melatonin interaction in zebrafish. *Proc. Natl. Acad. Sci. U.S.A.* 106, 21942–21947. doi: 10.1073/pnas.906637106
- Bianco, I. H., Kampf, A. R., and Engert, F. (2011). Prey capture behavior evoked by simple visual stimuli in larval zebrafish. *Front. Syst. Neurosci.* 5:101. doi: 10.3389/fnsys.2011.00101
- Blaser, R. E., Chadwick, L., and McGinnis, G. C. (2010). Behavioral measures of anxiety in zebrafish (*Danio rerio*). *Behav. Brain Res.* 208, 56–62. doi: 10.1016/j.bbr.2009.11.009
- Borla, M. A., Palecek, B., Budick, S., and O'Malley, D. M. (2002). Prey capture by larval zebrafish: evidence for fine axial motor control. *Brain Behav. Evol.* 60, 207–229. doi: 10.1159/000066699
- Branson, K., Robie, A. A., Bender, J., Perona, P., and Dickinson, M. H. (2009). High-throughput ethomics in large groups of *Drosophila*. *Nat. Methods* 6, 451–457. doi: 10.1038/nmeth.1328
- Budick, S. A., and O'Malley, D. M. (2000). Locomotor repertoire of the larval zebrafish: swimming, turning and prey capture. *J. Exp. Biol.* 203(Pt 17), 2565–2579.
- Burgess, H. A., and Granato, M. (2007). Modulation of locomotor activity in larval zebrafish during light adaptation. *J. Exp. Biol.* 210(Pt 14), 2526–2539. doi: 10.1242/jeb.003939
- Buske, C., and Gerlai, R. (2011). Shoaling develops with age in Zebrafish (*Danio rerio*). *Prog. Neuropsychopharmacol. Biol. Psychiatry* 35, 409–415. doi: 10.1016/j.pnpb.2010.09.003
- Cachat, J., Stewart, A., Utterback, E., Hart, P., Gaikwad, S., Wong, K., et al. (2011). Three-dimensional neurophenotyping of adult zebrafish behavior. *PLoS ONE* 6:e17597. doi: 10.1371/journal.pone.0017597
- Chalfie, M., Sulston, J. E., White, J. G., Southgate, E., Thomson, J. N., and Brenner, S. (1985). The neural circuit for touch sensitivity in *Caenorhabditis elegans*. *J. Neurosci.* 5, 956–964.
- Dale, N. (1985). Reciprocal inhibitory interneurons in the *Xenopus* embryo spinal cord. *J. Physiol.* 363, 61–70.
- Dankert, H., Wang, L., Hoopfer, E. D., Anderson, D. J., and Perona, P. (2009). Automated monitoring and analysis of social behavior in *Drosophila*. *Nat. Methods* 6, 297–303. doi: 10.1038/nmeth.1310
- Danos, N., and Lauder, G. V. (2007). The ontogeny of fin function during routine turns in zebrafish *Danio rerio*. *J. Exp. Biol.* 210(Pt 19), 3374–3386. doi: 10.1242/jeb.007484
- Drapeau, P., Saint-Amant, L., Buss, R. R., Chong, M., McDearmid, J. R., and Brustein, E. (2002). Development of the locomotor network in zebrafish. *Prog. Neurobiol.* 68, 85–111. doi: 10.1016/S0301-0082(02)00075-8
- Driever, W., Solnica-Krezel, L., Schier, A. F., Neuhauss, S. C., Mallicki, J., Stemple, D. L., et al. (1996). A genetic screen for mutations affecting embryogenesis in zebrafish. *Development* 123, 37–46.
- Elbaz, I., Yelin-Bekerman, L., Nicenboim, J., Vatine, G., and Appelbaum, L. (2012). Genetic ablation of hypocretin neurons alters behavioral state transitions in zebrafish. *J. Neurosci.* 32, 12961–12972. doi: 10.1523/JNEUROSCI.1284-12.2012
- Fontaine, E., Lentink, D., Kranenbarg, S., Müller, U. K., van Leeuwen, J. L., Barr, A. H., et al. (2008). Automated visual tracking for studying the ontogeny of zebrafish swimming. *J. Exp. Biol.* 211(Pt 8), 1305–1316. doi: 10.1242/jeb.010272
- Gahtan, E., Tanger, P., and Baier, H. (2005). Visual prey capture in larval zebrafish is controlled by identified reticulospinal neurons downstream of the tectum. *J. Neurosci.* 25, 9294–9303. doi: 10.1523/JNEUROSCI.2678-05.2005
- Gautrais, J., Ginelli, F., Fournier, R., Blanco, S., Soria, M., Chaté H., et al. (2012). Deciphering interactions in moving animal groups. *PLoS Comput. Biol.* 8:e1002678. doi: 10.1371/journal.pcbi.1002678
- Granato, M., van Eeden, F. J., Schach, U., Trowe, T., Brand, M., Furutani-Seiki, M., et al. (1996). Genes controlling and mediating locomotion behavior of the zebrafish embryo and larva. *Development* 123, 399–413.
- Grillner, S. (2003). The motor infrastructure: from ion channels to neuronal networks. *Nat. Rev. Neurosci.* 4, 573–586. doi: 10.1038/nrn1137
- Grillner, S., Deliagina, T., Ekeberg, O., el Manira, A., Hill, R. H., Lansner, A., et al. (1995). Neural networks that co-ordinate locomotion and body orientation in lamprey. *Trends Neurosci.* 18, 270–279. doi: 10.1016/0166-2236(95)80008-P
- Haffter, P., and Nusslein-Volhard, C. (1996). Large scale genetics in a small vertebrate, the zebrafish. *Int. J. Dev. Biol.* 40, 221–227.
- Hirata, H., Saint-Amant, L., Downes, G. B., Cui, W. W., Zhou, W., Granato, M., et al. (2005). Zebrafish bandoneon mutants display behavioral defects due to a mutation in the glycine receptor beta-subunit. *Proc. Natl. Acad. Sci. U.S.A.* 102, 8345–8350. doi: 10.1073/pnas.0500862102
- Kabra, M., Robie, A. A., Rivera-Alba, M., Branson, S., and Branson, K. (2013). JAABA: interactive machine learning for automatic annotation of animal behavior. *Nat. Methods* 10, 64–67. doi: 10.1038/nmeth.2281
- Katz, Y., Tunström, K., Ioannou, C. C., Huepe, C., and Couzin, I. D. (2011). Inferring the structure and dynamics of interactions in schooling fish. *Proc. Natl. Acad. Sci. U.S.A.* 108, 18720–18725. doi: 10.1073/pnas.1107583108
- Kay, J. N., Finger-Baier, K. C., Roeser, T., Staub, W., and Baier, H. (2001). Retinal ganglion cell genesis requires lakritz, a Zebrafish atonal Homolog. *Neuron* 30, 725–736.
- Khor, B. S., Jamil, M. F., Adenan, M. I., and Shu-Chien, A. C. (2011). Mitragnine attenuates withdrawal syndrome in morphine-withdrawn zebrafish. *PLoS ONE* 6:e28340. doi: 10.1371/journal.pone.0028340
- Korn, H., and Faber, D. S. (2005). The Mauthner cell half a century later: a neurobiological model for decision-making? *Neuron* 47, 13–28. doi: 10.1016/j.neuron.2005.05.019
- Lambert, A. M., Bonkowsky, J. L., and Masino, M. A. (2012). The conserved dopaminergic diencephalospinal tract mediates vertebrate locomotor development in zebrafish larvae. *J. Neurosci.* 32, 13488–13500. doi: 10.1523/JNEUROSCI.1638-12.2012
- Lee, A., Mathuru, A. S., Teh, C., Kibat, C., Korzh, V., Penney, T. B., et al. (2010). The habenula prevents helpless behavior in larval zebrafish. *Curr. Biol.* 20, 2211–2216. doi: 10.1016/j.cub.2010.11.025
- Li, W. C., Higashijima, S., Parry, D. M., Roberts, A., and Soffe, S. R. (2004). Primitive roles for inhibitory interneurons in developing frog spinal cord. *J. Neurosci.* 24, 5840–5848. doi: 10.1523/JNEUROSCI.1633-04.2004
- Liu, Y. C., Bailey, I., and Hale, M. E. (2012). Alternative startle motor patterns and behaviors in the larval zebrafish (*Danio rerio*). *J. Comp. Physiol. A Neuroethol. Sens. Neural Behav. Physiol.* 198, 11–24. doi: 10.1007/s00359-011-0682-1
- Masino, M. A., and Fetcho, J. R. (2005). Fictive swimming motor patterns in wild type and mutant larval zebrafish. *J. Neurophysiol.* 93, 3177–3188. doi: 10.1152/jn.01248.2004
- McElligott, M. B., and O'Malley, D. M. (2005). Prey tracking by larval zebrafish: axial kinematics and visual control. *Brain Behav. Evol.* 66, 177–196. doi: 10.1159/000087158
- Miller, N., and Gerlai, R. (2012). From schooling to shoaling: patterns of collective motion in zebrafish (*Danio rerio*). *PLoS ONE* 7:e48865. doi: 10.1371/journal.pone.0048865
- Moore, M. S., DeZazzo, J., Luk, A. Y., Tully, T., Singh, C. M., and Heberlein, U. (1998). Ethanol intoxication in *Drosophila*: genetic and pharmacological evidence for regulation by the cAMP signaling pathway. *Cell* 93, 997–1007. doi: 10.1016/S0092-8674(00)81205-2
- Nishimaru, H., and Kakizaki, M. (2009). The role of inhibitory neurotransmission in locomotor circuits of the developing mammalian spinal cord. *Acta Physiol. (Oxf.)* 197, 83–97. doi: 10.1111/j.1748-1716.2009.02020.x
- Odenthal, J., Rossnagel, K., Haffter, P., Kelsh, R. N., Vogelsang, E., Brand, M., et al. (1996). Mutations affecting xanthophore pigmentation in the zebrafish, *Danio rerio*. *Development* 123, 391–398.
- Petzold, A. M., Balciunas, D., Sivasubbu, S., Clark, K. J., Bedell, V. M., Westcot, S. E., et al. (2009). Nicotine response genetics in the zebrafish. *Proc. Natl. Acad. Sci. U.S.A.* 106, 18662–18667. doi: 10.1073/pnas.0908247106
- Rihel, J., Prober, D. A., Arvanites, A., Lam, K., Zimmerman, S., Jang, S., et al. (2010). Zebrafish behavioral profiling links drugs to biological targets and rest/wake regulation. *Science* 327, 348–351. doi: 10.1126/science.1183090
- Rihel, J., and Schier, A. F. (2012). Behavioral screening for neuroactive drugs in zebrafish. *Dev. Neurobiol.* 72, 373–385. doi: 10.1002/dneu.20910
- Scholz, H., Ramond, J., Singh, C. M., and Heberlein, U. (2000). Functional ethanol tolerance in *Drosophila*. *Neuron* 28, 261–271.
- Stephens, G. J., Johnson-Kerner, B., Bialek, W., and Ryu, W. S. (2008). Dimensionality and dynamics in the behavior of *C. elegans*. *PLoS Comput. Biol.* 4:e1000028. doi: 10.1371/journal.pcbi.1000028
- Suzuki, S., and Abe, K. (1985). Topological structural analysis of

- digital binary image by border following. *Comput. Vis. Graph. Image Process.* 30, 32–46.
- Swierczek, N. A., Giles, A. C., Rankin, C. H., and Kerr, R. A. (2011). High-throughput behavioral analysis in *C. elegans*. *Nat. Methods* 8, 592–598. doi: 10.1038/nmeth.1625
- Vermoesen, K., Serruys, A. S., Loyens, E., Afrikanova, T., Massie, A., Schallier, A., et al. (2011). Assessment of the convulsant liability of antidepressants using zebrafish and mouse seizure models. *Epilepsy Behav.* 22, 450–460. doi: 10.1016/j.yebeh.2011.08.016
- Zakhary, S. M., Ayubcha, D., Ansari, F., Kamran, K., Karim, M., Leheste, J. R., et al. (2011). A behavioral and molecular analysis of ketamine in zebrafish. *Synapse* 65, 160–167. doi: 10.1002/syn.20830
- Zhdanova, I. V., Wang, S. Y., Leclair, O. U., and Danilova, N. P. (2001). Melatonin promotes sleep-like state in zebrafish. *Brain Res.* 903, 263–268. doi: 10.1016/S0006-8993(01)02444-1
- Ziv, L., Muto, A., Schoonheim, P. J., Meijsing, S. H., Strasser, D., Ingraham, H. A., et al. (2013). An affective disorder in zebrafish with mutation of the glucocorticoid receptor. *Mol. Psychiatry* 18, 681–691. doi: 10.1038/mp.2012.64
- Conflict of Interest Statement:** The authors declare that the research was conducted in the absence of any commercial or financial relationships that could be construed as a potential conflict of interest.
- Received: 28 February 2013; accepted: 21 May 2013; published online: 12 June 2013.
- Citation: Mirat O, Sternberg JR, Severi KE and Wyart C (2013) *ZebraZoom: an automated program for high-throughput behavioral analysis and categorization.* *Front. Neural Circuits* 7:107. doi: 10.3389/fncir.2013.00107
- Copyright © 2013 Mirat, Sternberg, Severi and Wyart. This is an open-access article distributed under the terms of the Creative Commons Attribution License, which permits use, distribution and reproduction in other forums, provided the original authors and source are credited and subject to any copyright notices concerning any third-party graphics etc.

Motion is the final output of the neural networks underlying behavior. Historically, manual observations generated key observations about how animals interact with their environments. However, changes in behavior often take place on short (millisecond) or long (minutes to hours) time scales, which are difficult to detect with subjective analysis. Thanks to genetic model systems and the development of tools for controlling neuronal activity, probing the role of circuits in natural locomotion is primarily challenged by the lack of automated analysis. We developed software that can address this problem in zebrafish larvae by performing fine kinematic analysis and quantification of behavior on a millisecond to minute time scale.

I. Defining behavioral motifs

Classic ethology defined behavioral motifs using subjective measures of an experimenter. A major question for linking neural activity and behavioral output is whether these experimenter-defined behavior motifs are sufficient to understand behavior and relevant in classifying distinct locomotor sequences or whether new motifs revealed by unsupervised methods are more pertinent for investigating behavior.

In developing ZebraZoom, we relied heavily on locomotor sequences extensively characterized with classic ethology techniques (Foreman and Eaton, 1993; Liu and Fetcho, 1999; Budick and O'Malley, 2000). This approach proved advantageous because we could use these defined patterns to validate our approach and quantify the occurrence of these behaviors over time. Although this approach provided a useful starting point, our work has several limitations. We limited the algorithm to three classic behaviors, ignoring the diversity of movement types that zebrafish larvae perform. However, our classification system forced all movements into one of the three categories. In segregating behavior in this manner, certainly movements that did not fall within classical definitions were determined by

ZebraZoom to fall into one category, even if the movement may have reflected a different type of behavior. Therefore, knowledge about diversity or possible subtypes of behavioral motifs was not considered. For future studies looking at spontaneous locomotion over time, integrating these movements or performing unsupervised learning may provide new insight without the limitations of subjectively-defined motifs.

The problem of classification was further exacerbated by the difficulty in finding suitable parameters to define a behavioral sequence. When looking at raw data, the tail curvature allowed for distinguishing between slow swims and turns in particular, which are similar in kinematics but differ in yaw at the beginning of the movement (Budick and O'Malley, 2000). However, curvature proved difficult to quantify and integrate into the algorithm to classify behaviors (**Figure 3**). Ultimately, the tail bend angle, measured from a point between the two eyes to the tip of the tail, served as a readout of tail movement over time (**Figure 1**).

However, tail bend angle does not fully consider, for example, the point along the tail with the maximum angle, which is different for different types of movement (Budick and O'Malley, 2000). Recent work has emphasized the importance of quantifying tail angle at many points along the tail or curvature to identify and characterize movements (Huang et al., 2013; Jouary and Sumbre, 2016). In the future, expanding the list of distinct behavioral motifs that might otherwise overlap will depend on having a quantitative method to include the vector position of the tail over time.

Although larval zebrafish move along a continuum of speeds, these tend to cluster into distinct gaits or modules (Thorsen et al., 2004; Severi et al., 2014). A question to be resolved is how the circuits that underpin this continuum and the distinct gaits are integrated in the nervous system and at what level this integration occurs. Advances in tracking, kinematic analysis, and classification will help to provide the answers to these questions in the most physiological conditions possible.

II. Behavior and time

Behavior can encompass an animal or person's activity across time scales. For example, a blink can take place in a hundred milliseconds, whereas sleep-wake cycles can operate on a scale of hours or days. At the level of the nervous system, by studying one or the other, we can be privy to rapid circuitry or long-term neuroendocrine influence that shape patterns of activity over time. Because of computational demands to resolve complex movements, events that occur on millisecond timescales are often studied in isolation, whereas patterns that occur over long time are studied in low resolution, i.e. "Did the animal move or not?" Ultimately the interplay of actions across temporal scales will need to be considered. Establishing a balance that allows capturing of fine kinematics over long periods of time is a tradeoff to be considered in terms of data acquisition, analysis, and the demands of a biological question.

Other tools to analyze zebrafish locomotion focused on fine kinematic analysis for the duration of a bout or cruder analytics over hours. Our goal was to develop a tool that could address questions that demand fine kinematic analysis of individual movements for multiple larvae over time. Thanks to elimination of buffering by using a direct-to-disk acquisition system, the software is capable of collecting data for up to a few minutes. As a larval zebrafish of five to seven days post fertilization (dpf) perform on average one bout every one to three seconds, a few minutes of recording is sufficient to permit a larger picture of the behavior of larvae over time. This software served as a step to consider movement over time without yet being able to analyze very long time frames that encompass circadian rhythms and other long-term effects on behavior.

III. Manipulation of neural circuits

In this study, we relied on pharmacological manipulations of behavior to validate the utility of our approach. One problem with combining pharmacology and behavior is the lack

of readout to measure the extent to which a drug penetrates the nervous system. Unlike mutants, in which the defect is known, or in single cell electrophysiology, in which changes can be measured at the level of the cell, motor output represents the final measure of what many neurons organized into circuits accomplish together. In large-scale screens to identify potential therapeutics or drug mechanisms, frequently a single concentration of each compound is applied and behavioral changes are observed (Rihel et al., 2010).

For validation of ZebraZoom, we tested the effects of applying a glycine receptor antagonist, strychnine. Glycine is the primary inhibitory neurotransmitter in the spinal cord (Legendre, 2001) and underlies reciprocal inhibition required for sustained left-right alternations (Dale, 1985; Grillner et al., 1995; Granato et al., 1996; Drapeau et al., 2002; Li et al., 2004) In zebrafish diverse classes of commissural glycinergic interneurons are active during swimming, escape responses, and struggles (Liao and Fetcho, 2008). We hypothesized that a systemic block of glycine receptors would dramatically affect the ability of larval zebrafish to perform rhythmic locomotion.

Bath application of 75 μ M of strychnine generated a consistent and clear behavioral phenotype; larvae swam shorter distances for shorter durations with a corresponding decrease in swimming speed and fewer oscillations of the tail. Surprisingly, tail beat frequency was unaffected. However, the resulting observation that the number of oscillations, duration, heading degree, distance, and speed traveled for each bout were affected without a change in tail beat frequency could be related to dose-dependent effects of blocking glycinergic transmission. As with all behavioral studies, interpretation of these results should be taken with caution. Ideally, manipulating neural circuits with pharmacology should involve comparisons at different doses or in conjunction with other methods.

One motivation for creating ZebraZoom was to analyze kinematic parameters of movements in mutants for which specific ion channels or receptors are eliminated. The *atoh*^{-/-}

mutant is blind because of a loss of retinal ganglion cells (Kay et al., 2001). These mutants had significant differences from sibling controls in number of oscillations, duration, heading degree, and distance, but not in tail beat frequency or speed. Whether these effects are directly related to blindness or loss of *atoh7* expression in other cells is unknown. This again highlights the need to have highly specific manipulations to be able to resolve effects from the cellular to behavioral level.

IV. Experimental design

The ZebraZoom setup operates with a fixed frame rate camera mounted to a stand that images larvae placed in wells on top of an evenly illuminated plate, allowing for simultaneous imaging of 50-100 larvae, ideal for high-throughput screens or analysis. Despite its utility for these purposes, some drawbacks limit the breadth of uses for the setup. First, only a limited number of stimuli can be applied. In this work, pharmacological agents applied between imaging sessions prevented tracking of behavior immediately following application of the drug. With a maximum acquisition time of four minutes, monitoring behavior over time proved difficult. Moreover, currently all analysis is performed offline. For integrating on-line tracking, critical for implementing behavior triggered stimulus application, the software would need to operate in real time.

This work in zebrafish represents a step in integrating various demands, including the need for tracking multiple larvae simultaneously for high-throughput acquisition and analysis of both spontaneous and evoked locomotor patterns, fine kinematics, and extending the temporal scale beyond milliseconds to understand spontaneous and evoked behavior over time.

**Characterization of an optimized neurotoxin to probe the
role of *chx10*⁺ excitatory interneurons
during slow and fast swimming**

Efficient tools to control neuronal activity with spatial and temporal specificity are critical to understanding how populations of neurons contribute to behavior. Previous efforts relied on classical approaches that primarily included electrophysiological recording combined with pharmacology (Saint-Amant and Drapeau, 2001; Roeser and Baier, 2003). Although in many cases these methods could be used to establish general principles of neural network function, they are limited by the challenge of identifying the same type of neuron and restrict manipulation to one or few neurons. Over the last few decades, molecular genetics advances have allowed specific targeting of populations that share common molecular markers. In genetic model organisms such as fruit flies, zebrafish, and mice, dissecting the neural basis for behavior has been greatly helped by techniques that allow identification of populations of neurons and expressing reporters or sensors in these neurons to manipulate or monitor their activity.

I. Motivation

Although various chemical, optical, and toxin-mediated approaches to silencing or ablation in conjunction are available for use in zebrafish, many of these tools are not currently feasible for use in freely swimming assays to investigate the role of interneurons and neural populations during active locomotion (Arrenberg et al., 2009; Lee et al., 2010). The first aim will be to validate a new genetically-encoded botulinum neurotoxin *Tg(UAS:BoTxBLC-GFP)* by testing its efficacy for chronic silencing *in vivo*. Because of the importance of synaptic activity during development, this characterization included evaluation of neurotransmitter phenotype and spinal cord excitability when GABAergic cerebrospinal fluid-contacting neurons (CSF-cNs) were silenced.

The second aim will be to investigate the effect of silencing *chx10*⁺ V2a interneurons during active locomotion. These neurons are well characterized in zebrafish, but their role in

active locomotion or spontaneous swimming was unknown. By choosing this population, it becomes possible to compare the results of silencing with *Tg(UAS:BoTxBLC-GFP)* to previously established literature, determine their role in innate behavior and whether they play a similar role during distinct gaits, either slow or fast swimming.

II. Genetic targeting in zebrafish

The zebrafish benefits from the Gal4/UAS system, a combinatorial method developed first in *Drosophila* to express genes in identified neurons of interest (Fischer et al., 1988), then extended to zebrafish (**Figure 1**; Scheer and Campos-Ortega, 1999). The Gal4/UAS system is a combinatorial expression system. Gal4, a yeast transcriptional activator, is controlled under a specific promoter. In a separate effector line, the gene of interest is fused to the DNA-binding motif of Gal4, the upstream activating sequence, or UAS. The effector gene can only be activated when a cell is also expressing a Gal4, and whether the cell contains the Gal4 is dependent on the promoter of interest used to express it (Ornitz et al., 1991; Scheer and Campos-Ortega 1999). This system allows for specific tools to monitor and control neuronal activity to be expressed in specific tissues or cell populations of interest.

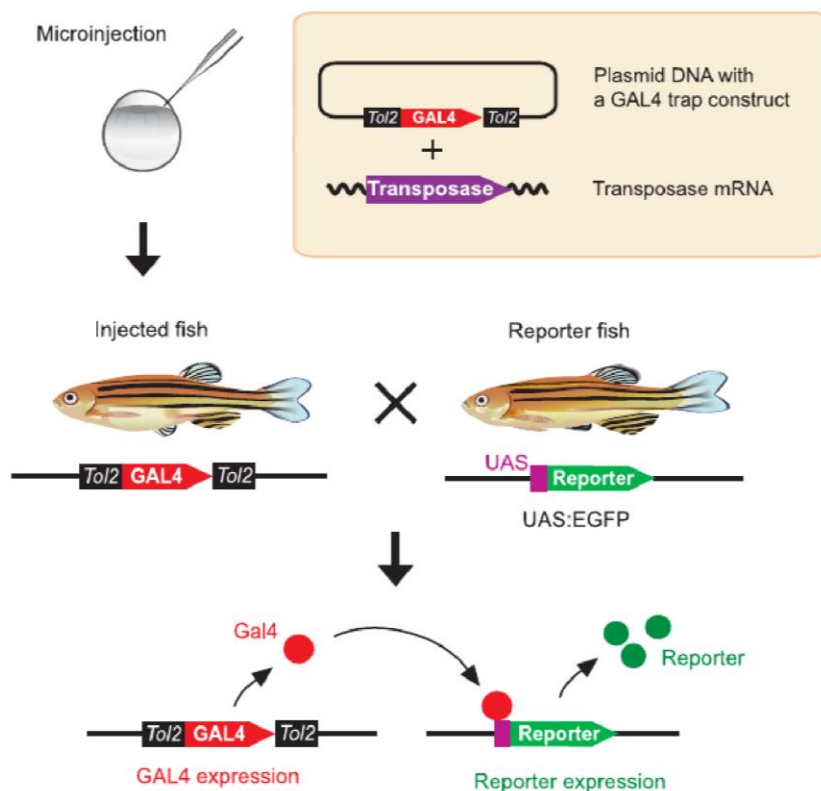


Figure 1. The Tol2-mediated Gal4 enhancer trap and gene trap screen. The scheme for Gal4 enhancer and gene trap screen by using the upstream activating sequence (UAS:eGFP) reporter. The synthetic transposase mRNA and a transposon donor plasmid containing a Gal4 trap construct are co-injected into zebrafish fertilized eggs. The trap construct is excised from the donor plasmid and integrated in the genome. Tol2 insertions created in the germ cells are transmitted to the next generation. In double transgenic embryos obtained from a cross of the injected fish and the UAS-reporter fish, Gal4 expressing cells are visualized by the fluorescent reporter. Adapted from Asakawa and Kawakami, 2008.

III. Tools to control neural activity: activation

Development of tools to activate specific populations of neurons have provided immense knowledge about neural pathways underlying behavior (Kramer et al., 2009; Bernstein and Boyden, 2011). Classically, neuroscientists relied on single cell recordings that allowed control of that cell's firing, but newer tools provide the ability to control single cells or populations using non-invasive techniques. In the 2000s, several groups established the use of light-gated channels and pumps (Nagel et al., 2002; Lima and Miesenböck, 2005; Gorostiza and Isacoff, 2008). In particular, Channelrhodopsin-2 (ChR2), a light-activated cation channel found naturally in *Chlamydomonas reinhardtii* that is activated by blue light, could be expressed in hippocampal neurons *in vitro* (Nagel et al., 2003; Boyden et al., 2005). These findings launched the field of optogenetics dedicated to using isolated microbial opsins to control neurons *in vivo*, extending use of these tools for studying behavior in species from *C.*

elegans to primates. The major advantage of opsins is remote manipulation, possible as long as light can be delivered with sufficient power density. This obviates the need to dissect tissue in order to access neurons and also allows study of actively behaving animals. Thousands of studies published have showed the extent to which these methods can be applied to study neural circuits (reviewed in Bernstein and Boyden, 2011; Yizhar et al., 2011; Deisseroth, 2015).

Some limitations and reservations must be made about the use of optical techniques to activate populations of neurons. First, simultaneous activation of many cells confounds the physiological role these neurons play and demonstrates sufficiency to perform a certain action. However, gross manipulation may lead to invalid conclusions about the role of neurons activated optogenetically. Recent work has emphasized the need to take results of ChR2 studies in context (Otchy et al., 2015), as activating with ChR2 and silencing or ablating can result in vastly different conclusions about the role of the neurons studied. Techniques are being developed to provide activation to three-dimensionally restricted spots (Vaziri and Emiliani, 2011; Hernandez et al., 2016), however, these methods are challenging to implement and require samples to be immobilized, often limiting the number of questions related to behavior that can be addressed. Additionally, opsins require a relatively high power density *in vivo* to be activated (Yizhar et al., 2011). In the case of classic ChR2, this may be as low as one to five milliwatts per millimeter, which is reasonable to achieve through an objective but challenging to provide for freely moving animals that are not tethered to the light source.

Thanks to the transparency of zebrafish larvae, optogenetic techniques have been implemented with success for studying behavior in restrained or enucleated zebrafish larvae (Douglass et al., 2008; Wyart et al., 2009; Fidelin et al., 2015). However, light power requirements (Arrenberg et al., 2008) and photosensitive behaviors (Friedmann et al., 2015;

Rihel and Schier, 2012; Kokel et al., 2010) limit use of these tools in freely swimming larvae. New chemogenetic tools utilize small molecules or temperatures to induce activation (Armbruster et al., 2007; Arenkiel et al., 2008; Sternson and Roth, 2014). Although these tools avoid light-induced behavioral confounds or the need to deliver light, many have not been developed for use in zebrafish. A recently developed tool used genetic targeting of TRP channels in conjunction with thermal or chemical agonists to activate or ablate neurons (Chen et al., 2016). More research in this field should result in better tools for specifically activating neurons during active locomotion without unwanted behavioral side effects.

Thanks for extensive genetic identification of neuronal populations, all of these techniques are afforded some form of spatial control when used under the control of a specific promoter. The diversity of techniques also allows for control at a diversity of temporal scales; opsins acts in milliseconds, whereas TRPV activation occurs over minutes, and Designer Receptor Exclusively Activated by Designer Drugs (DREADDs) act over hours (Boyden et al., 2005; Rogan and Roth, 2011; Chen et al., 2016). All of these tools require expression of an exogenous protein or receptor, either for light or for small molecules (Rogan and Roth, 2011), which can create experimental confounds. Overall, activation has been easier to implement than silencing. Although studies must be taken in context, as it is assumed that activation does not generally mimic physiological activation, they have provided critical insight to understanding the activity and pathways of neural circuits.

IV. Tools to control neural activity: silencing

Although activation demonstrates sufficiency, only silencing can demonstrate necessity. Compared to activation, silencing neurons has posed a greater challenge in neuroscience. Targeted laser ablation (Liu and Fetcho, 1999; Roeser and Baier, 2003) and pharmacology (Saint-Amant and Drapeau, 2001) are classical methods to silence output or remove specific

circuit elements *in vivo*. Modern techniques include methods to genetically silence output or to ablate neurons entirely, eliminating them from their circuits. Some of the major techniques currently used in zebrafish include Nitroreductase- or KillerRed-mediated ablation (Bulina et al., 2006; Curado et al., 2008), TRP channel mediated silencing (Chen et al., 2016), and ablation or silencing with neurotoxins (Kurita et al., 2003; Asakawa et al., 2008; Chou et al., 2016).

Although optical tools are widely used and effective for *in vivo* activation, similar tools for silencing have been more difficult to implement. Halorhodopsin (NpHR), an inward chloride pump, operates on the assumption that forcing chloride into the neuron will hyperpolarize the neuron, when in fact changing the chloride gradient can lead to a depolarizing shift of the reversal potential of chloride, which can be sufficient to turn hyperpolarizing GABA to depolarizing signaling. Use of NpHR *in vivo* often causes post-inhibitory rebound as well and requires much higher light power density than ChR2, on the order of 20-50 milliwatts per millimeter squared (Arrenberg et al., 2009). Archaeorhodopsins are proton pumps that are slightly more efficient than NpHR but are also associated with increased spontaneous release (Mahn et al., 2016). Although these tools have been used with some success to probe neural circuits on a millisecond timescale, questions remain on whether effects are due to silencing or the side effect of increased neurotransmitter release. This and high light power requirements render opsins currently incapable of silencing neuronal activity in freely behaving zebrafish.

Targeted ablation can be used for killing neurons can are superficial and individually identifiable, but frequently neurons or tissues of interest do not fulfill these criteria. In these cases, approaches relying on genetic targeting can be used. Nitroreductase ablation allows targeting of genetically identified populations of any cell type using a hybrid chemical-genetic approach (Curado et al., 2008; Mathias et al., 2014). Nitroreductase catalyzes the reduction of

prodrug metronidazole (Mtz), and the cytotoxic product produced induces cell death (Curado et al., 2008). This method provides a method to ablate any genetically-identified tissue, and can be highly effective. However, some drawbacks include tissues are not fully ablated or induction of cell death requires bathing in Mtz for up to 72 hours, limiting the developmental timepoints that can be evaluated. Furthermore unwanted ablation can occur when used in conjunction with the Gal4/UAS system (Curado et al., 2008). Many transgenic lines that are specific, for example, to one cell population in the spinal cord, also have “leaky” expression in non-neuronal tissues such as the heart or muscle. If nitroreductase was used, these tissues would also be ablated, rendering conditions impossible to distinguish effects from the different types of tissues affected.

KillerRed is another form of targeted ablation that has been implemented for use in zebrafish. KillerRed is a photosensitizer that generates reactive oxygen species (ROS) when KillerRed-expressing cells are activated with green or white light, triggering plasma membrane damage and cell death and works well in zebrafish (Bulina et al., 2006, Teh et al., 2010; Lee et al., 2010). However, this technique is associated with photodamage, requires tissue transparency, and needs high expression level, and illumination power must be optimized for each transgenic line or tissue to elicit desired level of photodamage (Teh et al., 2010).

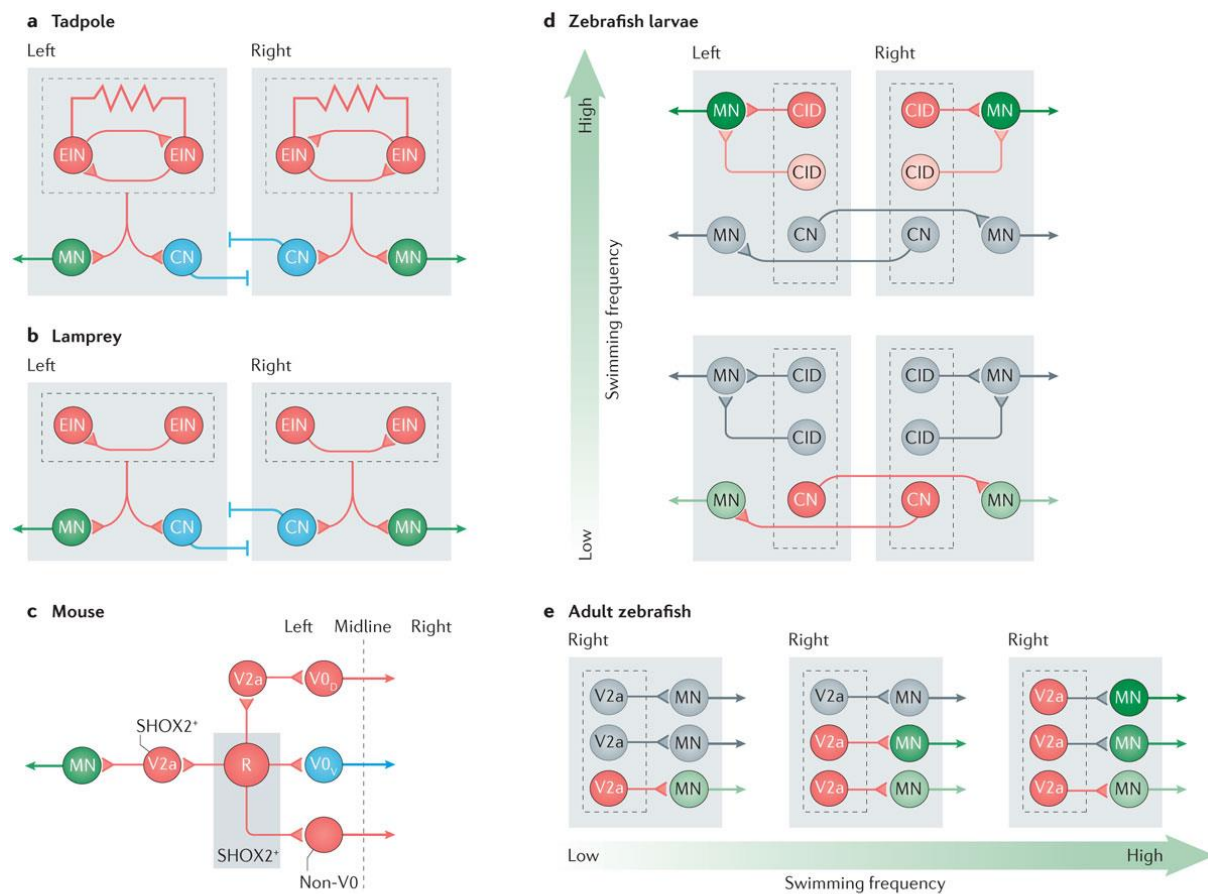
V. Neurotoxins to ablate or silence neurons

Neurotoxins are widely used in neuroscience for channel pharmacology, specific ablation, or silencing of neuronal populations. For ablation purposes, genetically-encoded diphtheria toxin can effectively ablate a target cell population, however undesired ablation of other cells or animal death due to its potency has prevented establishment of a stable zebrafish transgenic line (Kurita et al., 2003; Wan et al., 2006).

Tetanus and botulinum toxins (BoNTs) are extremely toxic poisons that block vesicular release at the synaptic cleft and thus block synaptic transmission (Schiavo et al., 1992). BoNTs are proteins synthesized as single inactive polypeptide chains which become active by proteolysis. The active form of the toxin is a dimer composed a heavy chain (HC) coupled to a light chain metalloprotease (LC). The HC binds to receptors on neurons to allow endocytosis of the toxin. Once endocytosed, the acidic environment leads to a conformational change that results in a translocation of the LC into the cytosol (Simpson, 2004). The light chain is a zinc-dependent endopeptidase that cleaves one on the SNARE (Soluble NSF Attachment Protein Receptor) proteins, which are critical for vesicle fusion and neurotransmitter release (Stecher et al., 1989; Pellizzari et al., 1999; Aoki and Guyer, 2001). The fatal effects of the toxins are not due to cell death, but rather to toxin-induced inhibition of acetylcholine release within the motor neuron synaptic cleft.

Use of neurotoxins is ideal for neuroscientists because the possibility of blocking output while leaving the neurons intact, in addition to not affecting heart, muscle, or other non-neuronal tissues. For neural specific silencing, several labs have generated transgenic lines carrying the tetanus toxin light chain (Asakawa et al., 2008; Chou et al., 2016). Tetanus toxin operates by cleaving vesicle membrane protein, synaptobrevin-2, blocking neurotransmitter release from synaptic vesicles. Unfortunately, technical problems with using transgenics for targeted tetanus toxin prevented widespread use, including the need to perform immunohistochemistry to detect expression *in vivo* (Lee et al., 2010), low levels of expression with the transgenic line forcing the need to inject RNA at the single cell stage (David Lyons, *personal communication*), and methylation of the UAS transgene across generations, leading to silencing of the transgenic over time. Efficacy has also been difficult to evaluate for this and other techniques because of the lack of published information *in vivo*. Although purified BoTxLC proteins have been extensively used in basic research, genetically encoded forms of

BoTxLC, which can be easily modified, expressed in zebrafish, and used for active behavioral assays have not been actively developed.



Nature Reviews | Neuroscience

Figure 2. Rhythm-generating circuits are excitatory in all the vertebrates that have been investigated. (A)-(B) |In tadpoles, the circuit is composed of reciprocally and electrically connected glutamatergic and cholinergic neurons (excitatory interneurons (EINs)) that are located in the hindbrain and the spinal cord. In lampreys, EINs are glutamatergic, with synaptic connections to other EINs and are located in each segment along the spinal cord. EINs drive motor neurons (MNs), which project to the muscles) and inhibitory commissural neurons (CNs), with axons projecting to the other half of the cord) on the same side of the cord. (C) Proposed circuits for the rhythm-generating circuit in the mouse spinal cord. The rhythm-generating circuit (R) is composed of neurons that express the transcription factor short stature homeobox protein 2 (SHOX2). Rhythm-generating circuits drive left–right alternating circuits ($V0_D$ – $V0_V$), including V2a neurons that express the transcription factor *chx10* homeodomain containing homologue (CHX10), and neurons that are both CHX10- and SHOX2-positive ($V2a$ SHOX2⁺) that presumably connect to motor neurons. Rhythm-generation circuits also drive left–right synchronizing circuits (non- $V0$, possibly of the V3 class). Only the left side of the circuit is shown. Blocking the synaptic output of SHOX2⁺ neurons or optogenetically silencing these neurons disrupts the rhythm without completely abolishing it, suggesting that as yet unidentified EINs contribute to the rhythm. (D) The rhythm-generating circuits in zebrafish larvae are composed of CNs that belong to the excitatory multipolar commissural descending type (MCoD) neurons and circumferential ipsilateral descending (CID) neurons, which are analogues of $V0_V$ and V2a mouse neurons, respectively. The MCoDs (CNs) are active at low swimming frequencies but are silenced as the swimming frequencies increase (>40 Hz). The probability of CID ($V2a$) neuron firing increases with frequency, with the most dorsal neuron active at the highest frequencies (60–90 Hz). Laser ablation of MCoD neurons abrogates slow swimming, whereas ablation of dorsal CID ($V2a$) neurons abolishes high frequency swimming frequency. (E) In the adult zebrafish, three groups of rhythm-generating V2a neurons innervate slow, intermediate and fast MNs. The three groups of V2a neurons are recruited incrementally (as indicated by the color change) in a modular manner that reflects an ordered recruitment of slow, intermediate and fast MNs as the speed of swimming increases. Adapted from Kiehn, 2016.

VI. Excitatory drive for locomotion

In vertebrates, excitatory signals from the brainstem interneurons send processes into the spinal cord to activate spinal circuits necessary to execute the target motor output (Drew et al., 2004; Gahtan et al., 2005; Jordan et al., 2008). In the lamprey, amphibian tadpoles, zebrafish, and mouse, networks that coordinate locomotor movements depend primarily on ipsilateral projecting excitatory neurons (Jordan et al., 2008; Goulding, 2009; Roberts et al., 2010). In tadpoles and lamprey, electrophysiological methods identified these neurons based on their connections in the spinal cord, though without genetic markers, the causal role of these neurons remains unknown (Grillner et al., 1991; Roberts et al., 2010; Kiehn 2016). In mammals, excitatory and ipsilaterally-projecting interneurons consist of CHX10⁺ V2a interneurons to a large extent (**Figure 2**; Al-Mosawie et al., 2007; Lundfald et al., 2007).

VII. V2a interneurons in the zebrafish

V2 neurons comprise a mixed population of glutamatergic *chx10*⁺ V2a and *gata2/3*⁺ GABAergic V2b neurons that project ipsilaterally and span many spinal cord segments (Karunaratne et al., 2002; Kimura et al., 2006; Peng et al., 2007; Al-Mosawie et al., 2007; Lundfald et al., 2007). In the zebrafish, V2as, also referred to as circumferential descending interneurons (CiDs), provide a primary source of excitatory drive to spinal circuits. Paired recordings from *chx10*⁺ V2as form monosynaptic connections with motor neurons, in particular those involved in fast swimming (**Figure 2**, Kimura et al., 2006). Targeted ablation of these neurons also resulted in a loss of fast frequencies during electrically-induced swimming (Eklöf-Ljunggren et al., 2012). Activation with ChR2 in a behaving head-embedded animal demonstrated that V2a neurons in the hindbrain but not spinal cord are sufficient to elicit slow frequency swimming, and silencing with NpHR halts ongoing slow swimming bouts in 3 dpf larvae (Kimura et al., 2013). Together, these data suggest that V2as

are necessary for high frequency fictive swimming elicited by electrical stimulation and that a subset are necessary for initiation of slow frequency locomotion at early larval stages.

As with mammals, in which movement occurs along a continuum of speeds but clusters into specified gaits (Hoyt and Taylor 1981; Bramble and Carrier, 1983), larval zebrafish similarly display gaits for slow and fast locomotion (Thorsen et al., 2004). In addition to the V2a population, multipolar commissural descending interneurons (MCoDs), also known as V0-v interneurons, are active during slow swimming frequencies and are silenced at higher swimming frequencies (Mclean et al., 2008). V2as are active at the highest swimming frequencies. *In vivo* electrophysiology demonstrated that the spinal interneuron classes active at slow speeds are inhibited at fast speeds, during which other classes of neurons become active (Masino et al., 2005; Mclean et al., 2008). Based on these results, it appears that the circuits driving slow and fast locomotion are distinct and that excitatory drive for these separate gaits may originate from unique sources.

VIII. Aims

The first aim is to validate a new genetically-encoded botulinum neurotoxin *Tg(UAS:BoTxBLC-GFP)* for use *in vivo*. Because of the chronic nature of silencing and importance of activity-dependent development, this characterization included evaluation of neurotransmitter phenotype and spinal cord excitability when GABAergic CSF-cNS were silenced. The second aim was to investigate the effect of silencing *chx10*⁺ V2a interneurons during active locomotion. These neurons are well characterized in zebrafish, but their role in active locomotion or spontaneous swimming is unknown. By choosing this population, it was possible to compare the results of silencing with BoTxBLC-GFP to previously establish literature that showed that V2as are required for fastest swimming speeds and probe whether the V2a population played roles during spontaneous slow swimming and active locomotion.

Article

Optimization of a neurotoxin to investigate the contribution of excitatory interneurons to speed modulation *in vivo*

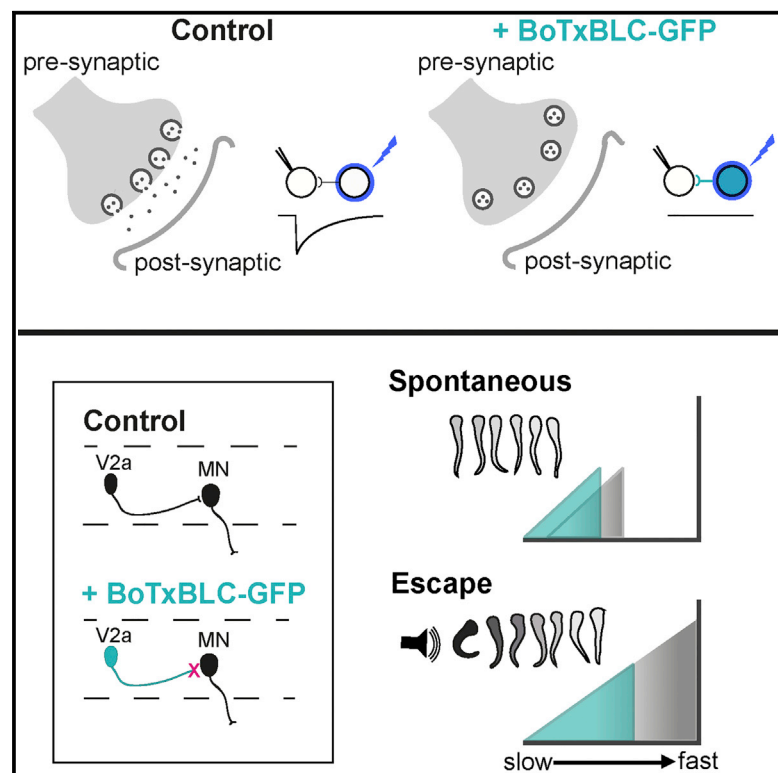
Jenna R. Sternberg*, Kristen E. Severi*,
Kevin Fidelin, Johanna Gomez, Hideshi Ihara, Yara Alcheikh, Jeffrey
M. Hubbard, Koichi Kawakami, Maximiliano Suster, Claire Wyart

Published in:
Current Biology
VOL. 26, SEPTEMBER 2016

Current Biology

Optimization of a Neurotoxin to Investigate the Contribution of Excitatory Interneurons to Speed Modulation In Vivo

Graphical Abstract



Authors

Jenna R. Sternberg, Kristen E. Severi, Kevin Fidelin, ..., Koichi Kawakami, Maximiliano Suster, Claire Wyart

Correspondence

kokawaka@nig.ac.jp (K.K.),
claire.wyart@icm-institute.org (C.W.)

In Brief

Silencing of neuronal populations in moving animals remains a challenge to investigating neural control of behavior. By developing an optimized botulinum toxin to block synaptic release in vivo, Sternberg, Severi et al. show that excitatory V2a interneurons contribute to locomotor frequency in distinct ways during slow or fast locomotion.

Highlights

- Optimized, genetically encoded botulinum neurotoxin silences synaptic output in vivo
- Excitatory V2a interneurons drive high-frequency components of fast locomotion
- Silencing of V2as shifts locomotor frequency downward during the slow regime



Optimization of a Neurotoxin to Investigate the Contribution of Excitatory Interneurons to Speed Modulation In Vivo

Jenna R. Sternberg,^{1,2,3,4,8} Kristen E. Severi,^{1,2,3,4,8} Kevin Fidelin,^{1,2,3,4} Johanna Gomez,^{1,2,3,4} Hideshi Ihara,⁵ Yara Alcheikh,^{1,2,3,4} Jeffrey M. Hubbard,^{1,2,3,4} Koichi Kawakami,^{6,*} Maximiliano Suster,^{6,7} and Claire Wyart^{1,2,3,4,*}

¹Institut du Cerveau et de la Moelle Épineuse (ICM), 47 Boulevard de l'Hôpital, 75013 Paris, France

²INSERM UMRS 1127, 75013 Paris, France

³CNRS UMR 7225, 75013 Paris, France

⁴UPMC Université Paris 06, 75005 Paris, France

⁵Department of Biological Science, Graduate School of Science, Osaka Prefecture University, Sakai, Osaka 599-8531, Japan

⁶Division of Molecular and Developmental Biology, National Institute of Genetics, and Department of Genetics, SOKENDAI (The Graduate University for Advanced Studies), Mishima, Shizuoka 411-8540, Japan

⁷Neural Circuits and Behaviour Group, Uni Research AS, Thormøhlensgate 55, Bergen 5008, Norway

⁸Co-first author

*Correspondence: kokawaka@nig.ac.jp (K.K.), claire.wyart@icm-institute.org (C.W.)

<http://dx.doi.org/10.1016/j.cub.2016.06.037>

SUMMARY

Precise control of speed during locomotion is essential for adaptation of behavior in different environmental contexts [1–4]. A central question in locomotion lies in understanding which neural populations set locomotor frequency during slow and fast regimes. Tackling this question in vivo requires additional non-invasive tools to silence large populations of neurons during active locomotion. Here we generated a stable transgenic line encoding a zebrafish-optimized botulinum neurotoxin light chain fused to GFP (BoTxBLC-GFP) to silence synaptic output over large populations of motor neurons or interneurons while monitoring active locomotion. By combining calcium imaging, electrophysiology, optogenetics, and behavior, we show that expression of BoTxBLC-GFP abolished synaptic release while maintaining characterized activity patterns and without triggering off-target effects. As *chx10*⁺ V2a interneurons (V2as) are well characterized as the main population driving the frequency-dependent recruitment of motor neurons during fictive locomotion [5–14], we validated our silencing method by testing the effect of silencing *chx10*⁺ V2as during active and fictive locomotion. Silencing of V2as selectively abolished fast locomotor frequencies during escape responses. In addition, spontaneous slow locomotion occurred less often and at frequencies lower than in controls. Overall, this silencing approach confirms that V2a excitation is critical for the production of fast stimulus-evoked swimming and also reveals a role for V2a excitation in the production of slower spontaneous locomotor behavior. Altogether, these results establish BoTxBLC-GFP

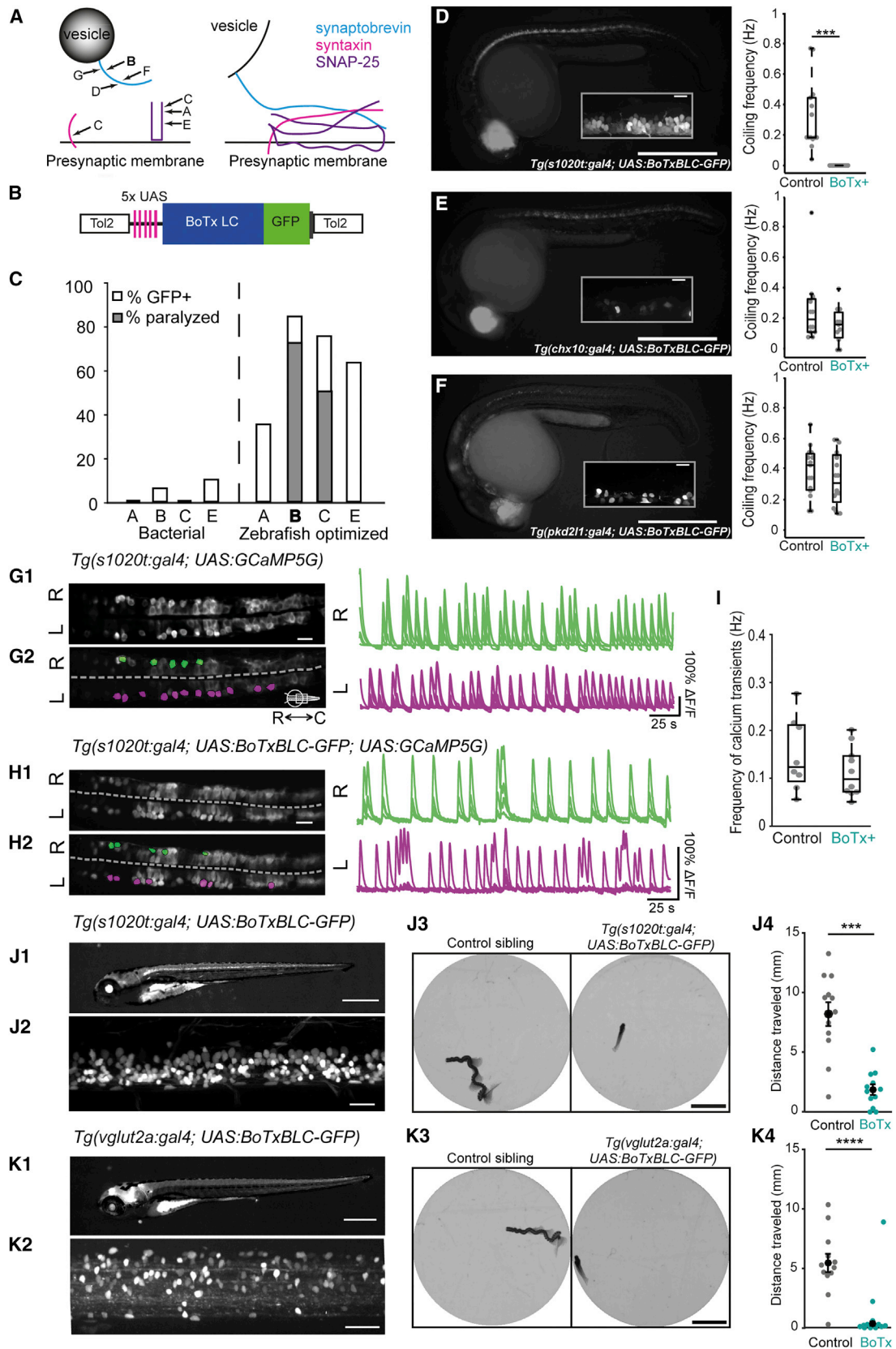
as an ideal tool for in vivo silencing for probing the development and function of neural circuits from the synaptic to the behavioral level.

RESULTS

Generation of a Zebrafish-Optimized Transgenic Line for Botulinum Neurotoxin Light Chain

In order to understand the neural circuits underlying behavior, efficient tools to silence distinct classes of neurons in behaving animals are necessary. Botulinum toxins are potent poisons that block vesicular release at the synaptic cleft by cleaving SNARE (soluble NSF attachment protein [SNAP] receptor) proteins and thus eliminate synaptic transmission [15–18]. The efficacy and specificity of action of botulinum toxin light chains (BoTxLCs) make them ideal tools for silencing neurons. However, stable transgenic lines optimized for expression have not yet been generated and characterized in zebrafish.

We utilized the two-part Gal4/UAS combinatorial gene expression system [19, 20] to generate a stable and efficient zebrafish-optimized transgenic line encoding BoTxLC fused to GFP to abolish synaptic release in vivo. To test the efficiency of neuronal silencing of different botulinum neurotoxin serotypes (Figure 1A), we expressed distinct serotypes fused to GFP under the control of a 5× repeat of UAS (Figure 1B). We quantified the touch escape response of embryos transiently expressing either the bacterial or zebrafish codon-optimized variants of each serotype under a ubiquitous driver (Figure 1C) [19]. The bacterial forms were unable to induce paralysis, whereas the zebrafish codon-optimized form of the B serotype paralyzed 72% of embryos (Figure 1C). We established a stable transgenic line for the B serotype, *Tg(UAS:BoTxBLC-GFP)*. Offspring of *Tg(UAS:BoTxBLC-GFP)* fish mated to *Tg(SAGFF73A:gal4)* fish [19] (Table S1), which expresses ubiquitously, were unable to generate spontaneous and touch-evoked movement (>99%; data not shown). *Tg(UAS:BoTxBLC-GFP)* fish of at least the tenth generation were used for the remainder of this article.



(legend on next page)

Expression of BoTxBLC-GFP in Spinal Motor Neurons Selectively Abolishes Coiling at the Embryonic Stage

To test the efficiency and evaluate off-target effects of BoTxBLC-GFP, we performed a behavioral assay using Gal4 lines driving expression in either motor neurons or spinal interneurons [5, 20, 21]. Embryos 17–25 hr post-fertilization (hpf) perform a gap junction driven stereotyped coiling behavior [22, 23]. To determine whether BoTxBLC-GFP expressed in motor neurons could block muscle contraction, we used *Tg(s1020t:gal4)*, which drives expression in a large subset of motor neurons [24, 25] (Figure S1). Embryos lost the ability to coil when BoTxBLC-GFP was expressed in this line (Figure 1D; Movie S1). We then went on to test Gal4 lines expressing in interneurons that do not drive embryonic coiling [23]. Coiling persisted when embryos expressed BoTxBLC-GFP in *chx10*⁺ interneurons (V2as) or in GABAergic *pkd2l1*⁺ cerebrospinal-fluid-contacting neurons (CSF-cNs) (Figures 1E and 1F) [14, 26]. Together, these results indicate that BoTxBLC-GFP efficiently blocks synaptic output without off-target effects in zebrafish embryos.

BoTxBLC-GFP-Expressing Motor Neurons Maintain Their Characteristic Activity

To test whether the loss of coiling in *Tg(s1020t:gal4; UAS:BoTxBLC-GFP)* embryos (Figure 1D) was due to off-target effects of BoTxBLC-GFP expression, we performed calcium imaging in motor neurons expressing both BoTxBLC-GFP and GCaMP5G [21, 27, 28] (Figures 1G and 1H). Motor neurons in *Tg(s1020t:gal4; UAS:BoTxBLC-GFP; UAS:GCaMP5G)* embryos showed calcium transients occurring at comparable frequencies to non-BoTxBLC-GFP-expressing *Tg(s1020t:gal4; UAS:GCaMP5G)* embryos at 24 hpf (Figures 1G–1I; Movie S2).

This result indicates that expression of BoTxBLC-GFP silenced motor output without noticeably affecting motor neuron properties, suggesting that paralysis resulted from a loss of presynaptic release rather than cell death.

BoTxBLC-GFP Expression in Essential Neuronal Populations Effectively Disrupts the Escape Response in Freely Swimming Larvae

To test the utility of BoTxBLC-GFP in an active behavioral assay, we measured the escape response to an acoustic stimulus, which at 5 days post-fertilization (dpf) consists of a high amplitude turn followed by fast swimming [29, 30]. The expression of BoTxBLC-GFP in *Tg(s1020t:gal4)* (Figures 1J and S1), targeting a large subset of motor neurons, or in *Tg(vglut2a:gal4)*, targeting glutamatergic neurons (Figure 1K) [31], severely disrupted the escape response (Movie S3). When the larva responded, the distance traveled was significantly reduced (Figures 1J4 and 1K4), confirming that expression of BoTxBLC-GFP in essential motor circuit populations leads to a predictable massive deficit in locomotion at larval stages.

BoTxBLC-GFP Completely Blocks Synaptic Release In Vivo

To directly test the capacity of BoTxBLC-GFP to abolish vesicular release, we took advantage of a reliable monosynaptic connection between GABAergic CSF-cNs and caudal primary motor neurons (CaPs) (J.M.H., unpublished data). Using transgenic *Tg(pkd2l1:gal4; UAS:ChR2-mCherry)* larvae, we elicited single spikes with a 5 ms light pulse in CSF-cNs while performing whole-cell recordings in CaPs [21, 26] (Figures 2A and 2B). Light-mediated spiking of CSF-cNs induced large short-latency inhibitory postsynaptic currents (IPSCs) in CaPs (J.M.H., unpublished

Figure 1. Generation and Validation of the Transgenic Line *Tg(UAS:BoTxBLC-GFP)*

(A) Botulinum serotype B targets synaptobrevin, a SNARE complex protein essential for neurotransmitter release (after [17, 18]; A–G denote cleavage sites of distinct Botulinum serotypes).

(B) Design of the zebrafish codon-optimized *UAS:BoTxLC-GFP* constructs for the A, B, C, and E serotypes tested in transient.

(C) Percentage of *Tg(SAGFF73:gal4)* embryos paralyzed upon transient expression of BoTx serotypes, with and without codon optimization for zebrafish (embryos tested, from left to right: n = 11, 16, 18, 20, 20, 25, 16, and 30).

(D) Expression pattern of *Tg(s1020t:gal4; UAS:BoTxBLC-GFP)* double transgenic embryos (left) and reduction in coiling frequency (right). n = 14 BoTxBLC-GFP⁺ embryos and n = 14 control siblings.

(E) Same as (D) but for *Tg(chx10:gal4; UAS:BoTxBLC-GFP)*. n = 11 BoTxBLC-GFP⁺ embryos and n = 12 control siblings.

(F) Same as (D) but for *Tg(pkd2l1:gal4; UAS:BoTxBLC-GFP)*. n = 16 BoTxBLC-GFP⁺ embryos and n = 15 control siblings.

(G and H) Representative examples of calcium imaging in *Tg(s1020t:gal4; UAS:GCaMP5G)* control (G) and *Tg(s1020t:gal4; UAS:GCaMP5G; UAS:BoTxBLC-GFP)*

(H) embryos. Imaging plane (G1 and H1) and selected regions of interest (ROIs) (G2 and H2) (left and right hemicords are indicated in magenta and green, respectively) are shown, with the corresponding $\Delta F/F$ traces on the right. Differences in $\Delta F/F$ amplitude result from higher levels of baseline GFP expression in BoTxBLC-GFP⁺ embryos.

(I) Frequency of calcium transients in control and BoTxBLC-GFP⁺ embryos. Each point represents the average frequency of all ROIs within an embryo (n = 8 BoTxBLC-GFP⁺ and n = 8 non-sibling control embryos).

(J) Comparison of control siblings and *Tg(s1020t:gal4; UAS:BoTxBLC-GFP)* 5 dpf larvae in a freely swimming acoustic escape assay. Whole-larva lateral view (J1), lateral view of the spinal cord (J2), and trajectories of swimming larvae in the assay (J3) are shown. Control siblings are *Tg(UAS:BoTxBLC-GFP)* only. (J4) shows the average distance traveled during a responsive trial (in millimeters) (n = 12 control larvae, 109 responses out of 118 trials; n = 11 BoTxBLC-GFP⁺ larvae, 72 responses out of 118 trials).

(K) Same as (J) but for *Tg(vglut2a:gal4; UAS:BoTxBLC-GFP)*. n = 12 control larvae, 98 responses out of 128 trials; n = 10 BoTxBLC-GFP⁺ larvae, 67 responses out of 128 trials.

Control sibling embryos for (D)–(F) had the Gal4, the UAS, or neither transgene. Insets for (D)–(F) are z projection stacks of a few optical sections imaged on the lateral side between segments 7 and 10. Scale bars represent 500 μ m in (D)–(F), 20 μ m for the insets in (D)–(F), 20 μ m in (G) and (H), 100 μ m in (J1) and (K1), 25 μ m in (J2) and (K2), and 5 mm in (J3) and (K3). (D)–(F), (J1), (J2), (K1), and (K2) are lateral views with dorsal up. (G) and (H) are dorsal views. Rostral is to the left in all panels. In (D)–(F), individual points correspond to coiling frequency for one embryo. For (J4) and (K4), the average responses of each larva are represented by a single gray point for control or teal point for BoTxBLC-GFP⁺ larvae, respectively. Means are shown \pm SEM in black. The central line on each boxplot is the median value, and the box limits are the 25th and 75th percentiles. The whiskers include all data points not considered outliers. ***p < 0.001, ****p < 0.0001, Student's t test (D–F and I). L, left; R, right. See also Figure S1, Table S1, and Movies S1, S2, and S3.

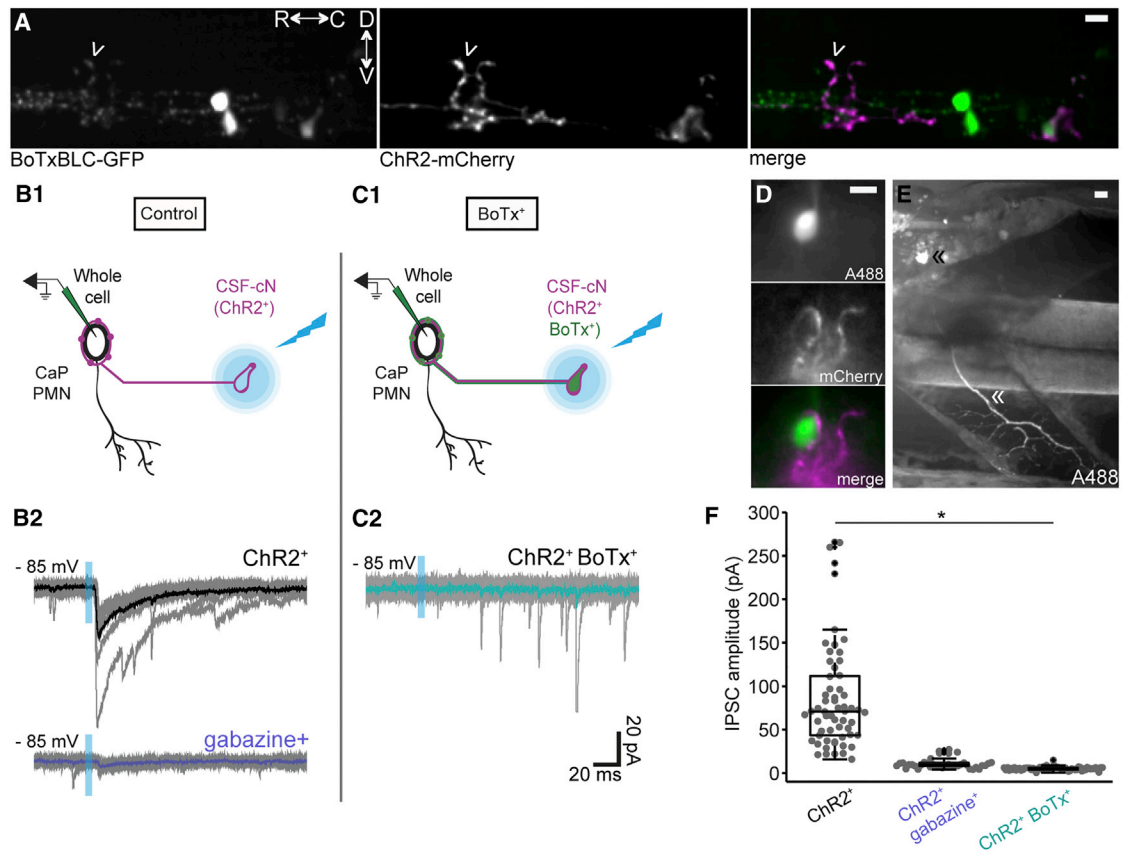


Figure 2. ChR2-Mediated Activation of Presynaptic Neurons Expressing BoTxBLC-GFP Demonstrates a Complete Block of Synaptic Release In Vivo

(A) Expression of BoTxBLC-GFP and ChR2-mCherry in *Tg(pkcd211:gal4; UAS:BoTxBLC-GFP; UAS:ChR2-mCherry)*. GFP and mCherry co-labeling in a CSF-cN innervating a CaP primary motor neuron is shown (innervation of a CaP by a CSF-cN is indicated by an arrowhead).

(B) Full field light-mediated activation of CSF-cNs in *Tg(pkcd211:gal4; UAS:ChR2-mCherry)* induces a monosynaptic IPSC in a CaP that is reduced by gabazine. (B1) is a schematic representation of light-mediated activation of ChR2⁺ CSF-cNs coupled with a whole-cell recording of a CaP. Individual traces from one CaP (gray) and the average of ten trials (black) are shown in the top panel of (B2); the bottom panel shows that gabazine strongly reduces the induced IPSC (individual traces from one CaP [gray] and the average of ten trials [purple]).

(C) No IPSC was observed after light-mediated activation of CSF-cNs in *Tg(pkcd211:gal4; UAS:ChR2-mCherry; UAS:BoTxBLC-GFP)* larvae. (C1) shows the schematic representation of experimental setup. (C2) shows individual traces from one CaP (gray) and the average of ten trials (teal).

(D and E) Confirmation of CaP identity after filling with Alexa 488 dye. (D) shows a cell body with Alexa 488 (top), ChR2-mCherry (middle), merge (bottom), and axonal projections onto ventral musculature in (E) (black double arrowhead, CaP soma; double white arrowhead, axon exiting the spinal cord).

(F) Quantification of peak IPSC amplitude in control and BoTxBLC-GFP⁺ larvae (control, *n* = 3 cells from three larvae, 60 trials; gabazine, *n* = 2 cells from two larvae, 40 trials; BoTxBLC-GFP⁺, *n* = 3 cells from three larvae, 60 trials).

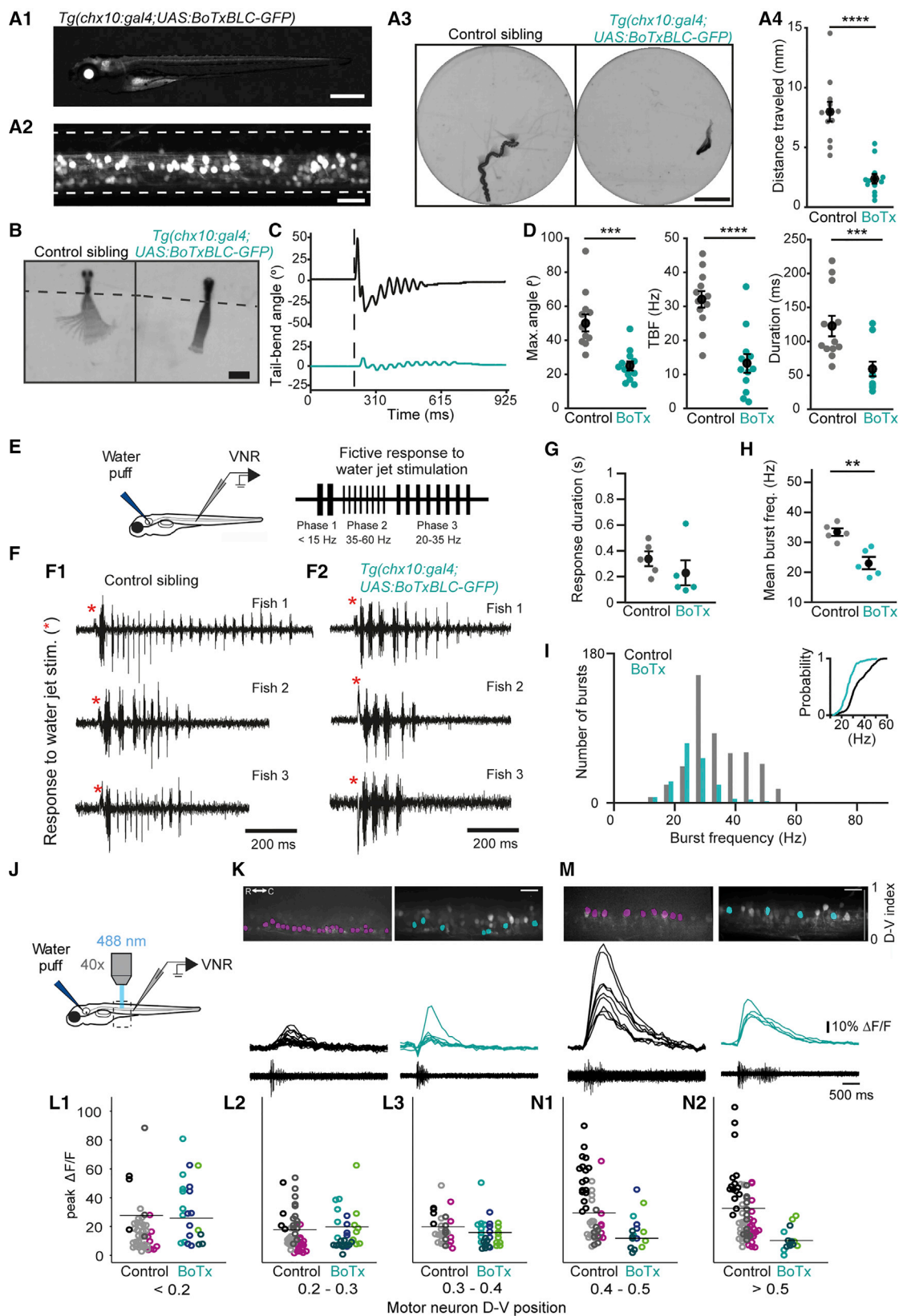
(A) and (E) are z projection stacks from a few optical sections imaged on the lateral side. (D) is a single plane image. All images are oriented with rostral to the left and dorsal up. Scale bars represent 10 μ m (approximated in D). The central line on each boxplot is the median value, and the box limits are the 25th and 75th percentiles. The whiskers include all data points not considered outliers. **p* < 0.05, one-way ANOVA with repeated measures. R, rostral; C, caudal; D dorsal; V, ventral. See also [Figure S2](#) and [Table S1](#).

data) that were strongly reduced by bath application of GABA_AR antagonist gabazine ([Figure 2B2](#)). In *Tg(pkcd211:gal4; UAS:BoTxBLC-GFP; UAS:ChR2-mCherry)* larvae, light-mediated spiking in CSF-cNs did not generate IPSCs in CaPs ([Figure 2C](#)). The identity of the CaP was confirmed by filling the cells with Alexa 488 dye ([Figures 2D](#) and [2E](#)). In 59 out of 60 trials, expression of BoTxBLC-GFP abolished the evoked current in CaPs ([Figure 2F](#)). Despite the block of synaptic release, *Tg(pkcd211:gal4; UAS:BoTxBLC-GFP)* transgenic larvae did not exhibit any defects in spinal cord formation ([Figure S2](#)). Furthermore, CSF-cNs retained their standard morphology, and the animals lived to adulthood (data not shown). These results demonstrate the

complete loss of vesicular release from BoTxBLC-GFP-expressing neurons in vivo.

BoTxBLC-Mediated Silencing of V2a Interneurons Confirms Their Critical Role in Fast Locomotion

V2a interneurons are known to drive motor neuron activation, and their recruitment is frequency dependent during fictive locomotion [8, 9, 14]. Therefore, we tested how V2a silencing impacts fast and slow locomotor regimes during active locomotion. Expression of BoTxBLC-GFP under the control of the *chx10* promoter [5] targeted most V2a interneurons ([Figures 3A1](#) and [3A2](#)). Consequently, acoustic escape responses in these larvae



(legend on next page)

showed a large reduction in the distance traveled in responsive trials compared to control siblings (Figures 3A3 and 3A4; Movie S3). In *Tg(chx10:gal4; UAS:BoTxBLC-GFP)* larvae assayed in a head-embedded and tail-free configuration (Figures 3B–3C; Movie S4), the maximum bend angle, average tail-beat frequency, and response duration were all significantly reduced compared to control siblings during the acoustic escape response (Figure 3D).

Although the *Tg(chx10:gal4)* transgenic line recapitulated *chx10* expression in the hindbrain and rostral spinal cord [5], a few neurons with axons exiting the spinal cord were labeled caudally (Figure 3A2), which could contribute to the response by affecting muscle contraction. To circumvent this confound, we performed fictive ventral nerve root (VNR) recordings in 4 dpf paralyzed larvae, which allowed monitoring of the motor neuron output upstream of the neuromuscular junction. In control siblings, fast escape responses induced by otic vesicle stimulation [32] consisted of a few large amplitude bursts (phase 1), followed by fast-frequency swimming (~35–60 Hz; phase 2), which transitioned to slow-frequency swimming (<35 Hz; phase 3) (Figure 3E). Silencing of V2a output selectively disrupted fast swimming (Figure 3F); the response duration was not significantly reduced (Figure 3G). Fast locomotor frequencies above 40 Hz were abolished, whereas lower frequencies were unaffected (Figures 3H and 3I).

Motor neurons are incrementally recruited along the dorsoventral axis with swimming frequency [7]. To investigate how motor neuron recruitment was affected when V2as were silenced, we generated a novel transgenic line, *Tg(mnx1:GCaMP5G)*, in which

motor neurons express the genetically encoded calcium sensor GCaMP5G, and coupled calcium imaging of motor neurons with otic-vesicle stimulation and VNR recordings [28, 33] (Table S1; Experimental Procedures; Figures 3J–3N). The amplitude of calcium transients varied as a function of the dorsoventral position within the motor pool in a different manner for control *Tg(mnx1:GCaMP5G)* larvae and V2a-silenced *Tg(mnx1:GCaMP5G; chx10:gal4; UAS:BoTxBLC-GFP)* larvae (Figures 3K and 3M; $p = 0.000005$). Overall, the average peak $\Delta F/F$ amplitude was highest in the most dorsal motor neurons in control larvae. Ventral motor neurons exhibited similar $\Delta F/F$ amplitude whether V2as were silenced or not (Figure 3L). In contrast, the activity of dorsal motor neurons was largely reduced in V2a-silenced larvae compared to controls (Figure 3N). A reduction in the recruitment of dorsal motor neuron is consistent with our observations that fast locomotor frequencies (>40 Hz) in both active and fictive locomotion are abolished when V2as are silenced.

Silencing of V2a Interneurons Decreases the Locomotor Frequency during Spontaneous Slow Swimming

Despite the role of hindbrain V2a neurons in initiating locomotion in zebrafish larva [5], the V2a contribution to spontaneous slow swimming has not been directly addressed. In freely swimming larvae, we noted that the occurrence of spontaneous slow swimming was largely reduced in *Tg(chx10:gal4; UAS:BoTxBLC-GFP)* (Figures 4A–4D; Movie S5), indicating that these neurons normally drive spontaneous locomotion. We observed that the rarely occurring swim bouts were on average longer in duration (Figure 4E). In V2a-silenced larvae, fictive

Figure 3. V2a Interneurons Are Critical for Induced Fast-Frequency Swimming

- (A) Comparison of control siblings and *Tg(chx10:gal4; UAS:BoTxBLC-GFP)* 5 dpf larvae in a freely swimming acoustic escape assay. Whole-larva lateral view (A1), lateral view of the spinal cord with borders denoted by dotted line (A2), and trajectories of swimming larvae in the assay (A3) are shown. Control siblings are *Tg(UAS:BoTxBLC-GFP)* larvae. (A4) shows the average distance traveled during a responsive trial (in millimeters) ($n = 11$ control larvae, 81 responses out of 120 trials; $n = 12$ BoTxBLC-GFP⁺ larvae, 107 responses out of 120 trials).
- (B–D) Comparison of control siblings and *Tg(chx10:gal4; UAS:BoTxBLC-GFP)* 5 dpf larvae in a head-embedded, tail-free acoustic escape assay. (B) Left: control larva (*Tg(UAS:BoTxBLC-GFP)*). Right: *Tg(chx10:gal4; UAS:BoTxBLC-GFP)* larva with its head embedded in agarose and the tail free to move. The dotted line indicates the agar border. (C) Example tail-bend angle (degrees) extracted for head-restrained control larvae (*Tg(UAS:BoTxBLC-GFP)* alone, black, top) and BoTxBLC-GFP (*Tg(chx10:gal4; UAS:BoTxBLC-GFP)*), teal, bottom). The dotted line indicates the time of stimulus delivery. (D) Kinematic analysis of head-embedded acoustic-induced escape responses. Maximum bend angle in the trial (left, degrees), average tail-beat frequency within a bout (center, Hz), and average bout duration (right, ms). $n = 12$ control larvae, 104 trials; $n = 12$ *Tg(chx10:gal4; UAS:BoTxBLC-GFP)* larvae, 118 trials.
- (E–I) Analysis of fictive VNR recordings during escape responses in 4 dpf larvae. (E) Left: schematic of the otic vesicle stimulation used to evoke fast escape responses in combination with fictive VNR recordings. Right: three phases of the response can be distinguished in the escape response. (F) Representative traces of fictive escape responses from three larvae for control (F1) and *Tg(chx10:gal4; UAS:BoTxBLC-GFP)* (F2) larvae. Red asterisks indicate the stimulus onset. (G and H) Response duration (G, s) and mean burst frequency (H, Hz) for $n = 57$ stimulations for five control larvae and $n = 54$ stimulations for five BoTxBLC-GFP⁺ larvae. (I) Distribution of burst frequencies (Hz) in control larvae (gray) and BoTxBLC-GFP⁺ larvae (teal). Inset: cumulative distribution function.
- (J–N) Calcium transients, imaged in motor neurons as a function of dorsoventral position, when V2as are silenced (BoTxBLC-GFP⁺) or not (control) with simultaneous fictive VNR recording. (J) Schematic of the calcium imaging configuration performed in combination with otic vesicle stimulation and VNR recordings as described in (E). (K) GCaMP5G expression in *Tg(mnx1:GCaMP5G)* with ROIs overlaid (top), calcium transients (center), and fictive VNR recording during a fictive escape in ventral motor neurons (bottom). Control larva: purple ROIs, black $\Delta F/F$ trace (left). BoTxBLC-GFP⁺ larva: teal ROIs, teal $\Delta F/F$ trace (right). (L) Peak $\Delta F/F$ response for an individual ROI, color-coded by larva, with the average across larvae indicated by a black line. Comparison of control versus BoTxBLC-GFP⁺ larvae for ventral motor neurons at dorsoventral positions: 0–0.2 (L1), 0.2–0.3 (L2), or 0.3–0.4 (L3). (M) Same as (K) but for dorsal motor neurons. (N) Same as (L) but for dorsoventral positions: 0.4–0.5 (N1) or 0.5–1 (N2).

For (L) and (N), $n = 199$ ROIs from 55 stimulations with swimming episodes for five control larvae and $n = 102$ ROIs from $n = 30$ stimulations with swimming episodes for four BoTxBLC-GFP⁺ larvae. Scale bars represent 100 μm in (A1), 25 μm in (A2), 5 mm in (A3), 1 mm in (B), and 20 μm in (K) and (M). For (A4), (D), (G), and (H), each data point is the average across all trials for a single larva. Control sibling *Tg(UAS:BoTxBLC-GFP)* larvae are in gray and *Tg(chx10:gal4; UAS:BoTxBLC-GFP)* are in teal. Means are shown \pm SEM in black. ** $p < 0.01$, *** $p < 0.001$, **** $p < 0.0001$. See also Table S1 and Movies S3 and S4.

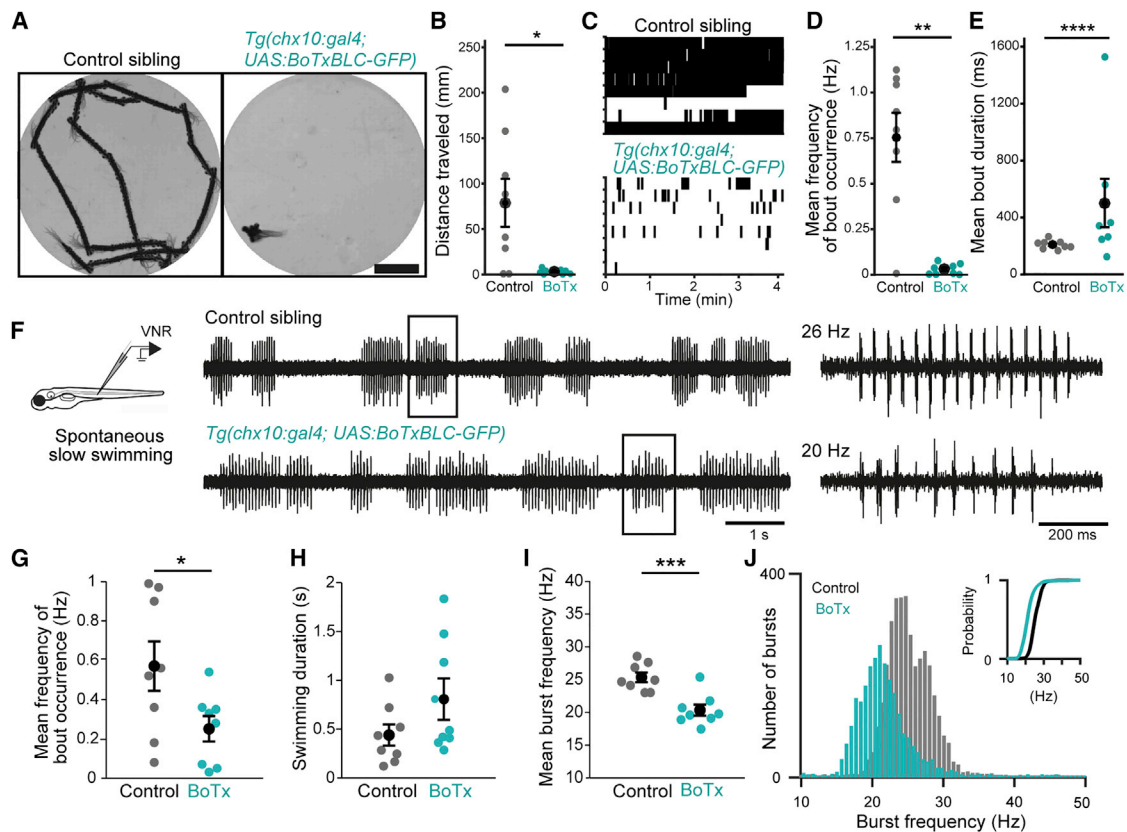


Figure 4. V2a Interneurons Drive Most of Spontaneous Slow Swimming and Adjust the Locomotor Frequency in the Slow Regime

(A–E) Spontaneous slow swimming assay comparing control and *Tg(chx10:gal4; UAS:BoTxBLC-GFP)* larvae at 5 dpf.

(A) The trajectory of a 5 dpf larvae spontaneously swimming for the first minute of a 4 min recording. Left: control sibling (*Tg(UAS:BoTxBLC-GFP)*) alone. Right: *Tg(chx10:gal4; UAS:BoTxBLC-GFP)* larva recorded simultaneously.

(B) Average distance traveled (mm; measured during the first minute of the trial).

(C) Rastergram of the timing of swim bout initiation over the 4 min spontaneous swimming trial recorded. The y axis represents a different individual larva. Top: control siblings. Bottom: *Tg(chx10:gal4; UAS:BoTxBLC-GFP)*.

(D) Mean frequency of bout occurrence (bouts per second, Hz) measured over a 4 min trial.

(E) Average bout duration (ms) across all bouts recorded spontaneously in a 4 min trial.

(B–E) $n = 8$ control larvae and $n = 8$ BoTxBLC-GFP⁺ larvae.

(F) Schematic and example trace of fictive slow swimming in a control (top) and a BoTxBLC-GFP⁺ (bottom) larva. Boxes indicate expanded regions at right. Note the reduced burst frequency in BoTxBLC-GFP⁺ larvae when V2as are silenced.

(G) Reduction in frequency of bout occurrence (bouts per second) in BoTxBLC-GFP⁺ larvae compared to control siblings ($n = 1265$ bouts for eight control larvae; $n = 938$ bouts for eight BoTxBLC-GFP⁺ larvae).

(H) Fictive bout duration (s).

(I) Mean burst frequency during fictive slow swim bouts (Hz).

(H and I) $n = 741$ bouts from eight control larvae; $n = 497$ bouts from eight BoTxBLC-GFP⁺ larvae.

(J) Distribution of burst frequencies (Hz) in control larvae (gray) and BoTxBLC-GFP⁺ larvae (teal). Inset: cumulative distribution function.

For (B), (D), (E), (G), (H), and (I), control siblings (gray, *Tg(UAS:BoTxBLC-GFP)*) were compared to *Tg(chx10:gal4; UAS:BoTxBLC-GFP)* larvae (teal), and each point represents a single larva. Means are shown \pm SEM in black. * $p < 0.05$, ** $p < 0.01$, *** $p < 0.001$, **** $p < 0.0001$, Student's *t* test (D and G). See also [Table S1](#) and [Movie S5](#).

slow swim bouts occurred less frequently and tended to last longer than in control siblings (Figures 4F–4H). In contrast to fast escapes, in which a reduction of frequency occurred via a suppression of the highest frequencies (Figure 3I), in the slow regime swim frequency was reduced by a downward shift of locomotor frequencies (Figures 4I and 4J). Taken together, the active and fictive data demonstrate that V2a interneurons contribute to generation of spontaneous swim events and setting the range of locomotor frequencies during slow locomotion.

DISCUSSION

Silencing with the Optimized Botulinum Toxin Light Chain

Silencing large populations of neurons in vivo is critical to understanding their role in circuits that control behavior. To be readily implemented, silencing tools should be genetically encoded, efficient, and non-toxic. BoTxBLC-GFP is efficient at blocking presynaptic vesicular release, as demonstrated here by probing monosynaptically connected pairs of neurons in vivo.

Neurotoxins have been used extensively for eliminating neuronal activity. Persistent problems for diphtheria use include off-target damage and establishing stable transgenic lines, while in the case of tetanus, detection of fluorescence is difficult *in vivo* [19, 34–36]. The stable transgenic BoTxBLC-GFP has been effective for many generations, and fluorescence could be detected *in vivo*. Codon optimization of BoTxBLC-GFP was critical for expression and silencing in zebrafish, demonstrating the need to design model-specific tools.

Other strategies such as Nitroreductase, KillerRed, or transient receptor potential channels developed for targeted cell ablation or silencing in zebrafish work *in vivo* but require a chemical cofactor or light delivery [34–37]. With chemically mediated methods, ablations can require long incubation times, depending on the expression level, and if driver lines express in non-neuronal tissues [36], these tissues will be ablated. Although opsins can silence with precise spatial and temporal resolution, light delivery can interfere with light-sensitive behaviors, and opsins are currently unfeasible for silencing across large spatial regions during active behavior because they require high power density [38–40]. BoTxBLC-GFP offers a straightforward alternative to these existing methods, potently and chronically silencing in neuronal tissue without additional cofactors or off-target effects. Implementing inducible expression in the future would allow dissection of the relative contributions of acute versus chronic silencing.

The Contribution of V2a Interneurons to Locomotion

chx10⁺ V2a glutamatergic neurons are involved in initiation [5], termination [6], left-right alternation [41], and setting of locomotor frequency [7, 11, 42] in vertebrate species. V2a interneurons recorded during fictive locomotion in zebrafish are recruited in a frequency-dependent manner along the dorsoventral axis and are necessary for generation of high-frequency swimming [8, 12]. Here we investigated the effects of silencing a majority of V2as during two motor behaviors: slow spontaneous swimming and fast escape responses. The escape response in zebrafish larva includes a wide range of locomotor frequencies from 15–100 Hz [2, 43]. Fast components of the escape were suppressed when V2a interneurons were silenced, confirming the critical role of V2as in fast locomotion [8, 44]. By performing calcium imaging on the motor pool, we showed that this suppression effect corresponds to the diminished recruitment of dorsal motor neurons essential for fast swimming. This suggests that the excitation of motor neurons by V2as is necessary to generate fast locomotor frequencies.

Spontaneous slow locomotion occurs in a narrow range of locomotor frequencies (20–30 Hz) [2, 43], during which a subset of ventral V2as is active [8]. Spontaneous active slow swimming rarely occurred when V2as were silenced, and those swim bouts lasted longer. These effects could be related to hindbrain V2a populations involved in initiating locomotion [5] or controlling the duration of locomotor events [6]. In addition, we observed that V2as adjust the locomotor frequency in the slow regime. Further investigation should clarify how excitation by V2as from the hindbrain and spinal cord contribute to this effect. The remaining source of excitation driving slow swimming when V2as are silenced could be glutamatergic V0-v neurons, referred to as MCoDs in zebrafish, which are selectively recruited

at these frequencies [8], suggesting that MCoDs and V2as may work in concert during slow locomotion.

Our results confirm important contributions for V2as in fast and slow regimes of locomotion. Previous work showed that spinal V2as are a heterogeneous population of neurons based on their dorsoventral positioning, morphology, intrinsic properties, and connectivity [8, 9, 12]. Our results, obtained by silencing of the V2a population in the hindbrain and spinal cord, indicate speed-dependent roles for V2as. Although V2as are critical for sustaining fast locomotion, they appear to adjust locomotor frequency and modulate bout duration in the slow regime. New genetic tools will be required to distinguish how hindbrain and spinal cord V2as accomplish these unique functions.

EXPERIMENTAL PROCEDURES

Generation of Stable Transgenic Zebrafish Lines

25 ng μl^{-1} of *Tol2* transposase mRNA and either *pT2S-UAS:zBoTxBLC-GFP* or *pT2S-UAS:zBoTxBLC* were co-injected into one-cell-stage embryos of the TAB (AB/TUB) strain. 188 injected embryos from seven unique clutches were raised. 47 embryos injected with *pT2S-UAS:zBoTxBLC-GFP* were screened after mating with selected Gal4FF lines for behavioral phenotypes and GFP fluorescence. 13 embryos injected with *pT2S-UAS:zBoTxBLC* were screened by PCR. We used Gal4FF drivers (*Tg(SAGFF73A)* and others) for screening the UAS founder fish. We selected six founders, identified single integrations by Southern blot, and mapped the integration sites from F1 progeny (834 F1 fish examined). A single homozygous F2 line, *Tg(UAS:zBoTxBLC-GFP)34b*, has been stably maintained for over ten generations and used for the experiments shown for all figures except Figure 1C. The sequences are available on the zTrap database (<http://kawakami.lab.nig.ac.jp/ztrap/>). The *Tg(mnx1:GCaMP5G)icm25* stable transgenic line was generated based on the *mnx1* promoter [33] integrated in a 5' entry gateway clone [45] and combined to the pME-GCaMP5G and the 3' polyA entry clone into the destination vector carrying *tol2* sites and *cryaa:venus* [46]. Table S1 lists all transgenic lines used in this study, long-form names, and expression patterns if applicable.

All procedures were approved by the Institut du Cerveau et de la Moelle Épinrière (ICM) and the National Ethics Committee (Comité National de Réflexion Ethique sur l'Expérimentation Animale Ce5/2011/056) based on EU legislation or were in accordance with institutional and national guidelines and regulations at the National Institute of Genetics in accordance with the Guide for the Care and Use of Laboratory Animals of the Institutional Animal Care and Use Committee (IACUC, approval identification number 27-2) in Japan.

ACCESSION NUMBERS

The accession number for the transgenic UAS:BoTxBLC-GFP reported in this paper is ZFIN: ZDB-ALT-160119-9. The accession number for the transgenic *mnx1:GCaMP5G* reported in this paper is ZFIN: ZDB-ALT-160427-5.

SUPPLEMENTAL INFORMATION

Supplemental Information includes Supplemental Experimental Procedures, two figures, one table, and five movies and can be found with this article online at <http://dx.doi.org/10.1016/j.cub.2016.06.037>.

AUTHOR CONTRIBUTIONS

M.S. generated the BoTx constructs and lines in K.K.'s lab, which provided the fish facility and technical assistance to map the integration. M.S. conceived and initiated the BoTx project and generated the plasmid constructs and the stable transgenic line *Tg(UAS:BoTxBLC-GFP)*. M.S. actively worked to validate and maintain active carriers over generations from the line used in this manuscript. J.R.S., K.E.S., and C.W. conceived this study with input from

K.F. J.R.S. performed and analyzed coiling experiments, *in vivo* patch recordings, calcium imaging, VNR recordings, and cell counting. K.E.S. performed and analyzed larval behavioral experiments with help from Y.A. K.F. performed and analyzed VNR recordings. J.G. generated the *Tg(mnx1:GCaMP5G)* transgenic line. H.I. provided the original clones for BoTxLC serotypes. J.H. provided unpublished essential electrophysiological data. C.W. and K.K. supervised the research. J.R.S., K.E.S., and C.W. wrote and revised the manuscript with feedback from K.F., K.K., and M.S.

ACKNOWLEDGMENTS

We thank Professor Shin-Ichi Higashijima for the *Tg(chx10:gal4)* line; Professor Shunji Kozaki for bacterial BoTx plasmids; Dr. Tom Auer and Dr. Filippo Del Bene for the *mnx1* promoter; Professor David McLean for useful feedback; Urs Böhm, Dr. Andrew Prendergast, and Dr. Steven Knafo for support with behavior and tracking; Vincent Guillemot for assistance with statistics; Sophie Nunes Figueiredo, Natalia Maties, and Bogdan Buzurin for fish care; Drs. Ruben Portugues, Ana Faustino, and David Lyons for helpful comments on the manuscript; and the Plateforme d'Imagerie Cellulaire Pitié-Salpêtrière, cloning facility, and biostatistics facility at ICM. This work received support from the JSPS postdoc fellowship (M.S.), National BioResource Project and 15H02370 from MEXT of Japan (K.K.), The Philippe Foundation (C.W., K.E.S., and J.M.H.), and the Chaire d'Excellence of the Ecole des Neurosciences de Paris (E.N.P.), European Research Council starting grant Optoloco no. 311673, and NIH Brain Initiative grant no. 5U01NS090501 (C.W.).

Received: February 19, 2016

Revised: May 24, 2016

Accepted: June 17, 2016

Published: August 11, 2016

REFERENCES

- Severi, K.E., Portugues, R., Marques, J.C., O'Malley, D.M., Orger, M.B., and Engert, F. (2014). Neural control and modulation of swimming speed in the larval zebrafish. *Neuron* 83, 692–707.
- Budick, S.A., and O'Malley, D.M. (2000). Locomotor repertoire of the larval zebrafish: swimming, turning and prey capture. *J. Exp. Biol.* 203, 2565–2579.
- Talpalar, A.E., Bouvier, J., Borgius, L., Fortin, G., Pierani, A., and Kiehn, O. (2013). Dual-mode operation of neuronal networks involved in left-right alternation. *Nature* 500, 85–88.
- Gosgnach, S., Lanuza, G.M., Butt, S.J., Saueressig, H., Zhang, Y., Velasquez, T., Riethmacher, D., Callaway, E.M., Kiehn, O., and Goulding, M. (2006). V1 spinal neurons regulate the speed of vertebrate locomotor outputs. *Nature* 440, 215–219.
- Kimura, Y., Satou, C., Fujioka, S., Shoji, W., Umeda, K., Ishizuka, T., Yawo, H., and Higashijima, S. (2013). Hindbrain V2a neurons in the excitation of spinal locomotor circuits during zebrafish swimming. *Curr. Biol.* 23, 843–849.
- Bouvier, J., Caggiano, V., Leiras, R., Caldeira, V., Bellardita, C., Balueva, K., Fuchs, A., and Kiehn, O. (2015). Descending command neurons in the brainstem that halt locomotion. *Cell* 163, 1191–1203.
- McLean, D.L., Fan, J., Higashijima, S., Hale, M.E., and Fetcho, J.R. (2007). A topographic map of recruitment in spinal cord. *Nature* 446, 71–75.
- McLean, D.L., Masino, M.A., Koh, I.Y., Lindquist, W.B., and Fetcho, J.R. (2008). Continuous shifts in the active set of spinal interneurons during changes in locomotor speed. *Nat. Neurosci.* 11, 1419–1429.
- Menelaou, E., VanDunk, C., and McLean, D.L. (2014). Differences in the morphology of spinal V2a neurons reflect their recruitment order during swimming in larval zebrafish. *J. Comp. Neurol.* 522, 1232–1248.
- Dougherty, K.J., and Kiehn, O. (2010). Functional organization of V2a-related locomotor circuits in the rodent spinal cord. *Ann. N Y Acad. Sci.* 1198, 85–93.
- Ljunggren, E.E., Haupt, S., Ausborn, J., Ampatzis, K., and El Manira, A. (2014). Optogenetic activation of excitatory premotor interneurons is sufficient to generate coordinated locomotor activity in larval zebrafish. *J. Neurosci.* 34, 134–139.
- Ampatzis, K., Song, J., Ausborn, J., and El Manira, A. (2014). Separate microcircuit modules of distinct v2a interneurons and motoneurons control the speed of locomotion. *Neuron* 83, 934–943.
- Ritter, D.A., Bhatt, D.H., and Fetcho, J.R. (2001). *In vivo* imaging of zebrafish reveals differences in the spinal networks for escape and swimming movements. *J. Neurosci.* 21, 8956–8965.
- Kimura, Y., Okamura, Y., and Higashijima, S. (2006). *alx*, a zebrafish homolog of *Chx10*, marks ipsilateral descending excitatory interneurons that participate in the regulation of spinal locomotor circuits. *J. Neurosci.* 26, 5684–5697.
- Kao, I., Drachman, D.B., and Price, D.L. (1976). Botulinum toxin: mechanism of presynaptic blockade. *Science* 193, 1256–1258.
- Schiavo, G., Benfenati, F., Poulain, B., Rossetto, O., Poverino de Laureto, P., DasGupta, B.R., and Montecucco, C. (1992). Tetanus and botulinum-B neurotoxins block neurotransmitter release by proteolytic cleavage of synaptobrevin. *Nature* 359, 832–835.
- Sutton, R.B., Fasshauer, D., Jahn, R., and Brunger, A.T. (1998). Crystal structure of a SNARE complex involved in synaptic exocytosis at 2.4 Å resolution. *Nature* 395, 347–353.
- Brunger, A.T., Jin, R., and Breidenbach, M.A. (2008). Highly specific interactions between botulinum neurotoxins and synaptic vesicle proteins. *Cell. Mol. Life Sci.* 65, 2296–2306.
- Asakawa, K., Suster, M.L., Mizusawa, K., Nagayoshi, S., Kotani, T., Urasaki, A., Kishimoto, Y., Hibi, M., and Kawakami, K. (2008). Genetic dissection of neural circuits by Tol2 transposon-mediated Gal4 gene and enhancer trapping in zebrafish. *Proc. Natl. Acad. Sci. USA* 105, 1255–1260.
- Scott, E.K., Mason, L., Arrenberg, A.B., Ziv, L., Gosse, N.J., Xiao, T., Chi, N.C., Asakawa, K., Kawakami, K., and Baier, H. (2007). Targeting neural circuitry in zebrafish using GAL4 enhancer trapping. *Nat. Methods* 4, 323–326.
- Fidelin, K., Djenoune, L., Stokes, C., Prendergast, A., Gomez, J., Baradel, A., Del Bene, F., and Wyart, C. (2015). State-dependent modulation of locomotion by GABAergic spinal sensory neurons. *Curr. Biol.* 25, 3035–3047.
- Saint-Amant, L., and Drapeau, P. (1998). Time course of the development of motor behaviors in the zebrafish embryo. *J. Neurobiol.* 37, 622–632.
- Saint-Amant, L., and Drapeau, P. (2000). Motoneuron activity patterns related to the earliest behavior of the zebrafish embryo. *J. Neurosci.* 20, 3964–3972.
- Warp, E., Agarwal, G., Wyart, C., Friedmann, D., Oldfield, C.S., Conner, A., Del Bene, F., Arrenberg, A.B., Baier, H., and Isacoff, E.Y. (2012). Emergence of patterned activity in the developing zebrafish spinal cord. *Curr. Biol.* 22, 93–102.
- Wyart, C., Del Bene, F., Warp, E., Scott, E.K., Trauner, D., Baier, H., and Isacoff, E.Y. (2009). Optogenetic dissection of a behavioural module in the vertebrate spinal cord. *Nature* 461, 407–410.
- Djenoune, L., Khabou, H., Joubert, F., Quan, F.B., Nunes Figueiredo, S., Bodineau, L., Del Bene, F., Burcklé, C., Tostivint, H., and Wyart, C. (2014). Investigation of spinal cerebrospinal fluid-contacting neurons expressing PKD2L1: evidence for a conserved system from fish to primates. *Front. Neuroanat.* 8, 26.
- Lauterbach, M.A., Ronzitti, E., Sternberg, J.R., Wyart, C., and Emiliani, V. (2015). Fast calcium imaging with optical sectioning via HiLo microscopy. *PLoS ONE* 10, e0143681.
- Akerboom, J., Chen, T.W., Wardill, T.J., Tian, L., Marvin, J.S., Mutlu, S., Calderón, N.C., Esposti, F., Borghuis, B.G., Sun, X.R., et al. (2012). Optimization of a GCaMP calcium indicator for neural activity imaging. *J. Neurosci.* 32, 13819–13840.
- Kohashi, T., Nakata, N., and Oda, Y. (2012). Effective sensory modality activating an escape triggering neuron switches during early development in zebrafish. *J. Neurosci.* 32, 5810–5820.

30. Böhm, U.L., Prendergast, A., Djenoune, L., Nunes Figueiredo, S., Gomez, J., Stokes, C., Kaiser, S., Suster, M., Kawakami, K., Charpentier, M., et al. (2016). CSF-contacting neurons regulate locomotion by relaying mechanical stimuli to spinal circuits. *Nat. Commun.* 7, 10866.
31. Satou, C., Kimura, Y., Hirata, H., Suster, M.L., Kawakami, K., and Higashijima, S. (2013). Transgenic tools to characterize neuronal properties of discrete populations of zebrafish neurons. *Development* 140, 3927–3931.
32. Kohashi, T., and Oda, Y. (2008). Initiation of Mauthner- or non-Mauthner-mediated fast escape evoked by different modes of sensory input. *J. Neurosci.* 28, 10641–10653.
33. Zelenchuk, T.A., and Brusés, J.L. (2011). In vivo labeling of zebrafish motor neurons using an *mxn1* enhancer and Gal4/UAS. *Genesis* 49, 546–554.
34. Lee, A., Mathuru, A.S., Teh, C., Kibat, C., Korzh, V., Penney, T.B., and Jesuthasan, S. (2010). The habenula prevents helpless behavior in larval zebrafish. *Curr. Biol.* 20, 2211–2216.
35. Curado, S., Anderson, R.M., Jungblut, B., Mumm, J., Schroeter, E., and Stainier, D.Y. (2007). Conditional targeted cell ablation in zebrafish: a new tool for regeneration studies. *Dev. Dyn.* 236, 1025–1035.
36. Curado, S., Stainier, D.Y., and Anderson, R.M. (2008). Nitroreductase-mediated cell/tissue ablation in zebrafish: a spatially and temporally controlled ablation method with applications in developmental and regeneration studies. *Nat. Protoc.* 3, 948–954.
37. Chen, S., Chiu, C.N., McArthur, K.L., Fetcho, J.R., and Prober, D.A. (2016). TRP channel mediated neuronal activation and ablation in freely behaving zebrafish. *Nat. Methods* 13, 147–150.
38. Mattis, J., Tye, K.M., Ferenczi, E.A., Ramakrishnan, C., O’Shea, D.J., Prakash, R., Gunaydin, L.A., Hyun, M., Fenno, L.E., Gradinaru, V., et al. (2011). Principles for applying optogenetic tools derived from direct comparative analysis of microbial opsins. *Nat. Methods* 9, 159–172.
39. Friedmann, D., Hoagland, A., Berlin, S., and Isacoff, E.Y. (2015). A spinal opsin controls early neural activity and drives a behavioral light response. *Curr. Biol.* 25, 69–74.
40. Rihel, J., and Schier, A.F. (2012). Behavioral screening for neuroactive drugs in zebrafish. *Dev. Neurobiol.* 72, 373–385.
41. Crone, S.A., Quinlan, K.A., Zagoraïou, L., Droho, S., Restrepo, C.E., Lundfald, L., Endo, T., Setlak, J., Jessell, T.M., Kiehn, O., and Sharma, K. (2008). Genetic ablation of V2a ipsilateral interneurons disrupts left-right locomotor coordination in mammalian spinal cord. *Neuron* 60, 70–83.
42. Dougherty, K.J., Zagoraïou, L., Satoh, D., Rozani, I., Doobar, S., Arber, S., Jessell, T.M., and Kiehn, O. (2013). Locomotor rhythm generation linked to the output of spinal *shox2* excitatory interneurons. *Neuron* 80, 920–933.
43. Mirat, O., Sternberg, J.R., Severi, K.E., and Wyart, C. (2013). ZebraZoom: an automated program for high-throughput behavioral analysis and categorization. *Front. Neural Circuits* 7, 107.
44. Eklöf-Ljunggren, E., Haupt, S., Ausborn, J., Dehnisch, I., Uhlén, P., Higashijima, S., and El Manira, A. (2012). Origin of excitation underlying locomotion in the spinal circuit of zebrafish. *Proc. Natl. Acad. Sci. USA* 109, 5511–5516.
45. Kwan, K.M., Fujimoto, E., Grabher, C., Mangum, B.D., Hardy, M.E., Campbell, D.S., Parant, J.M., Yost, H.J., Kanki, J.P., and Chien, C.B. (2007). The Tol2kit: a multisite gateway-based construction kit for Tol2 transposon transgenesis constructs. *Dev. Dyn.* 236, 3088–3099.
46. Ni, T.T., Lu, J., Zhu, M., Maddison, L.A., Boyd, K.L., Huskey, L., Ju, B., Hesselson, D., Zhong, T.P., Page-McCaw, P.S., et al. (2012). Conditional control of gene function by an invertible gene trap in zebrafish. *Proc. Natl. Acad. Sci. USA* 109, 15389–15394.

Current Biology, Volume 26

Supplemental Information

**Optimization of a Neurotoxin to Investigate
the Contribution of Excitatory Interneurons
to Speed Modulation In Vivo**

Jenna R. Sternberg, Kristen E. Severi, Kevin Fidelin, Johanna Gomez, Hideshi Ihara, Yara Alcheikh, Jeffrey M. Hubbard, Koichi Kawakami, Maximiliano Suster, and Claire Wyart

Table S1. List of stable transgenic lines used and generated in this study.

Name used in text	Long form or alternate name	Labeling	Reference
<i>Tg(pkd2l1:gal4)</i>	<i>Tg(pkd2l1:gal4)icm10</i>	CSF-cNs	Fidelin et al., 2015 [S1]
<i>Tg(s1020t:gal4)</i>	<i>Et(-0.6hsp70l:Gal4-VPI6)s1020t</i>	Motor neurons, CSF-cNs, VeLDs	Scott et al., 2007 [S2]
<i>Tg(SAGFF73:gal4)</i>	<i>SAGFF(nedd4b1);gal4FF</i>	Ubiquitous	Asakawa et al., 2008 [S3]
<i>Tg(chx10: R -GFP)</i>	<i>Tg(chx10:lox:DsRed:lox:GFP)</i>	V2a interneurons	Kimura et al., 2006 [S4]
<i>Tg(chx10:gal4)</i>	<i>Tg(chx10:gal4)</i>	V2a interneurons	Kimura et al., 2013 [S5]
<i>Tg(UAS:BoTxBLC-GFP)</i>	<i>Tg(Nk(UAS:zBoTxBLC-GFP)34b)</i> <i>Tg(UAS:BoTxBLC-GFP)icm21</i>	N/A	This study (see Auer et al., 2015; Böhm et al., 2016) [S6,S7]
<i>Tg(UAS:ChR2-mCherry)</i>	<i>Tg(UAS:Cr.ChR2_H134R-mCherry)</i>	N/A	Schoonheim et al., 2010 [S8]
<i>Tg(UAS:GCaMP5G)</i>	<i>Tg(UAS:GCaMP5G)icm08</i>	N/A	Fidelin et al., 2015 [S1]
<i>Tg(vglut2a:gal4)</i>	<i>Tg(vglut2a:gal4)</i>	Glutamatergic cells expressing vGluT2	Satou et al., 2013 [S9]
<i>Tg(vglut2a: R -GFP)</i>	<i>Tg(vglut2:lox:DsRed:lox:GFP)</i>	Glutamatergic cells expressing vGluT2	Satou et al., 2013 [S9]
<i>Tg(gad1b: R -GFP)</i>	<i>Tg(gad1b:lox:DsRed:lox:GFP)</i>	GABAergic cells	Satou et al., 2013 [S9]
<i>Tg(mnx1:GCaMP5G)</i>	<i>Tg(mnx1:GCaMP5G)icm25</i>	Motor neurons	This study
<i>Tg(HuC:GCaMP5G)</i>	<i>Tg(elavl3:GCaMP5G)</i>	Most neurons	Ahrens et al., 2013 [S10]

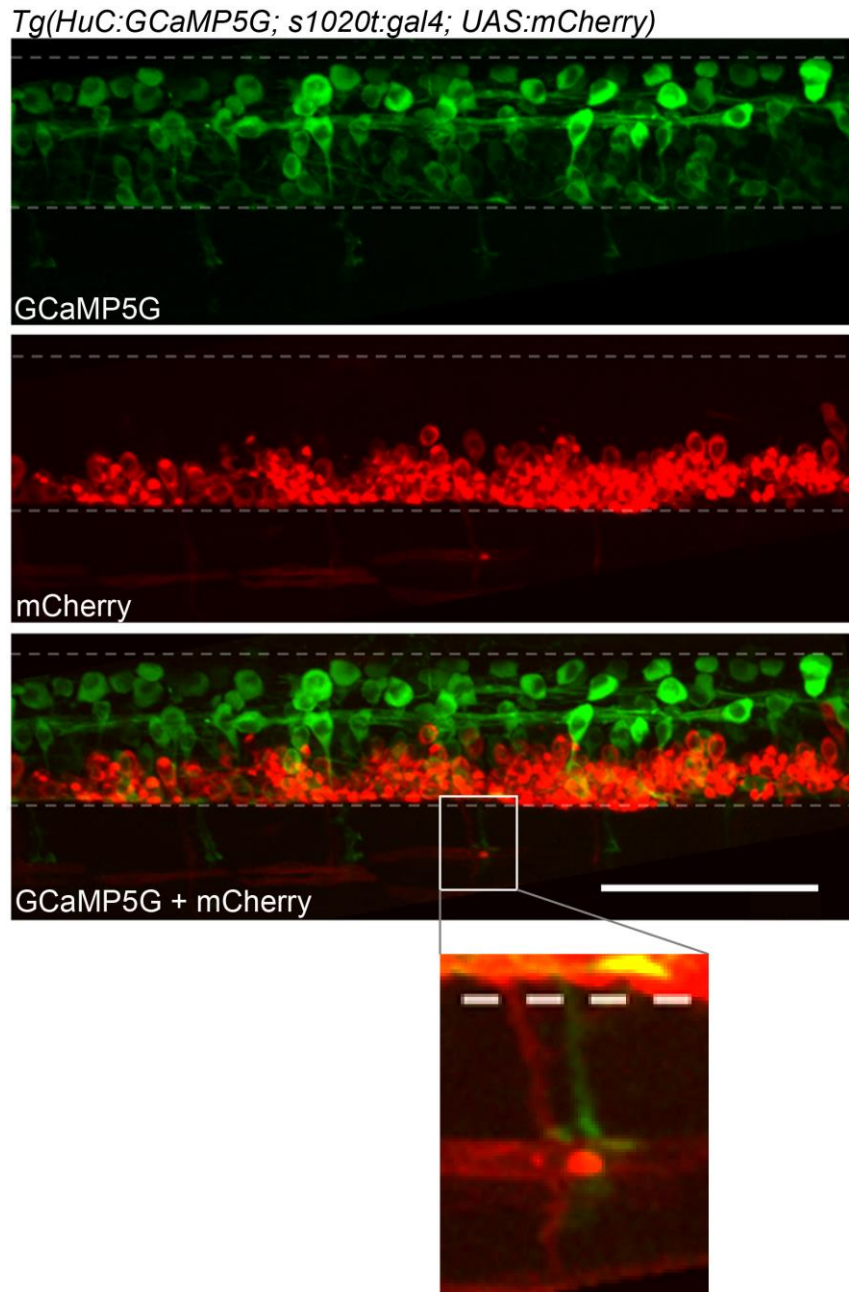


Figure S1. Related to Figure 1. *Tg(s1020t:gal4)* enhancer trap line labels most but not all motor neurons.

Image of 1 dpf *Tg(HuC:GCaMP5G; s1020t:gal4; UAS:mCherry)* embryo. Top: The *HuC* promoter labels a diverse population of interneurons and motor neurons in the spinal cord. Middle: In the *Tg(s1020t:gal4)* enhancer trap line, most primary motor neurons are labeled in the spinal cord. Merge: GCaMP5G and mCherry expression.

Magnification: axons from motor neurons exiting the spinal cord are visible in non-overlapping populations of motor neurons from both transgenic lines. Rostral is left, dorsal is up. Scale bar is 50 μ m.

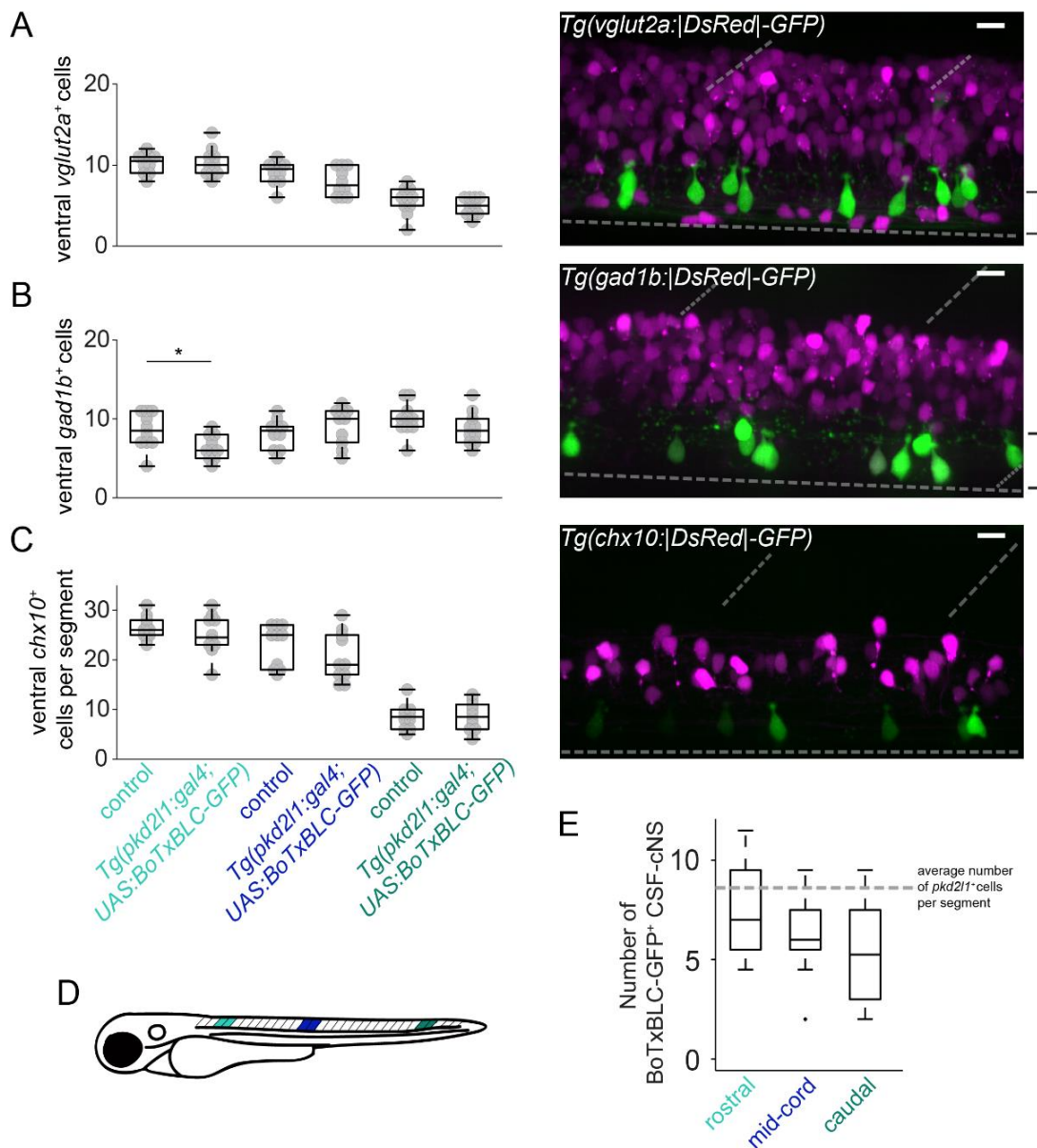


Figure S2. Related to Figure 2. Neurotransmitter specification in the spinal cord is unaffected when GABAergic CSF-cNs are silenced in *Tg(pkd211:gal4; UAS:BoTxBLC-GFP)*.

(A-C) Quantification of ventral glutamatergic, GABAergic, and *chx10*⁺ interneurons per segment in rostral (segments 3-4), mid-cord (segments 10-11), and caudal (segments 25-26) regions in 3 dpf larvae. (A) Left: quantification of ventral glutamatergic cells in control and *Tg(pkd211:gal4; UAS:BoTxBLC-GFP)*. Right: image of *Tg(vglut2a:|R|)-GFP; pkd211:gal4; UAS:BoTxBLC-GFP* at segment 10. n = 14 control siblings, n = 13 BoTxBLC-GFP⁺. (B) Left: quantification of ventral GABAergic cells in control and *Tg(pkd211:gal4; UAS:BoTxBLC-GFP)*. Right: image of *Tg(gad1b:|R|)-GFP; pkd211:gal4; UAS:BoTxBLC-GFP* at segment 10. n = 12 control siblings, n = 12 BoTxBLC-GFP⁺. (C) Left: quantification of *chx10*⁺ V2as in control and *Tg(pkd211:gal4; UAS:BoTxBLC-GFP)*. Right: image of *Tg(chx10:|R|)-GFP; pkd211:gal4; UAS:BoTxBLC-GFP* at segment 10. n = 10 control siblings, n = 10 BoTxBLC-GFP⁺. (D) Schema of regions for quantification. (E) Number of BoTxBLC-GFP⁺ CSF-cNs per segment. Dotted line indicates average number of *pkd211*⁺ CSF-cNs in the spinal cord per segment.

* p < 0.05. Student's t-test. All comparisons were performed per region between control and BoTxBLC-GFP⁺ conditions.

Supplemental Experimental Procedures

Zebrafish husbandry

All procedures were approved by the Institut du cerveau et de la moelle épinière (ICM) and the National Ethics Committee (Comité National de Réflexion Ethique sur l'Expérimentation Animale Ce5/2011/056) based on E.U legislation or were in accordance with institutional and national guidelines and regulations at the National Institute of Genetics in accordance with the Guide for the Care and Use of Laboratory Animals of the Institutional Animal Care and Use Committee (IACUC, approval identification number 27-2) in Japan. All experiments were performed on *Danio rerio* embryos and larvae of AB, TL, TU, or mixed background. For some experiments, *mitfa*^{-/-} animals were used. Embryos and larvae were raised in an incubator at 28.5°C under a 14/10 light/dark cycle until the start of experimentation. Experiments were performed at room temperature (22-26°C) on 1 to 5 dpf larvae.

Generation of plasmids for conditional expression of Botulinum Toxin Light Chain (BoTxLC) in zebrafish embryos

Plasmids encoding published bacterial BoTxLC proteins A, B, C, D, E, F and G were obtained in vector pQE3 (3416 bp) (a gift to KK). In parallel, cDNA sequences encoding full BoTxLC serotypes A (1398bp), B (1350 bp), C (1401 bp), and E (1320 bp) were constructed *in silico* based on entries from NCBI, then modified in-house for optimal translation in zebrafish, and finally purchased from GenScript (New Jersey, USA). Synthetic cDNAs were blunt-end cloned at the *EcoRV* site of pUC57, and in most cases subsequently amplified by PCR using high-fidelity PfuUltra II Fusion HS DNA polymerase, TOPO cloned in pCR8GW (Invitrogen, Carlsbad, California) and fully sequenced thereafter to confirm that no mutations had been introduced by PCR. To generate GFP reporter plasmids that express BoTxLC under Gal4/UAS control, we first generated a custom *Tol2* transgenesis and expression vector containing the Gal4-target sequence, 5x UAS, followed by an atg-less GFP. A Gateway-compatible vector pT2UASMSGW-R1R2 (5419 bp) was digested with *SaII/XhoI* to introduce an *XhoI/SaII* GFP fragment (740 bp). The resulting plasmid was digested with *EcoRI/XhoI* to ligate either a bacterial or zebrafish-codon optimized BoTxLC cDNA fragment containing 5' *EcoRI* and 3' *XhoI* compatible ends. The resulting plasmids *pT2UAS:BoTxLC-GFP* or *pT2UAS:zBoTxLC-GFP* encode an in-frame fusion of GFP at the C-terminus of BoTxLC (see supplemental material in [S6, S7]).

Transient expression of botulinum toxin serotypes and behavioral scoring

Groups of $n > 30$ were raised for each injected group and examined at 36 or 48 hours post fertilization (hpf). Embryos were placed in 5 cm plastic petri dishes filled with E3 media and allowed to settle for 5 minutes before recording touch-evoked motor behaviors. Embryos were firmly touched at the tail, head, and yolk region at least 3 times with a fine syringe needle, and those that displayed no motion at all (escape response or swimming) were considered paralyzed. Paralysis was confirmed in 500 fps high-speed video recordings (Photron, United Kingdom).

Coiling Assay in transgenic lines expressing the optimized BoTxBLC-GFP

Embryos expressing BoTxBLC-GFP under the control of either *Tg(pkd211:gal4)*, *Tg(s1020t:gal4)*, or *Tg(chx10:gal4)* were screened for fluorescence and dechorionated. Coiling was evaluated between 24 and 25 hpf for 1 minute. All experiments were performed simultaneously with sibling embryos not expressing BoTxBLC-GFP as controls. All images were obtained using a uEye camera (IDS Imaging Development Systems GmbH, Obersulm, Germany).

Fluorescent imaging of transgenic lines

A Nikon AZ100 Multizoom microscope system was used for all images of whole embryos or larvae. Stacks of spinal neurons in diverse transgenics lines were obtained using a 20x or 40x water immersion objective on a spinning disk confocal microscope or 2-photon laser scanning microscope using a 20x water immersion objective (3i Intelligent Imaging Innovations, Inc., Denver, CO, USA).

Calcium imaging in zebrafish embryos

Adults of homozygous *Tg(UAS:BoTxBLC-GFP)* were crossed to double transgenic *Tg(s1020t:gal4; UAS:GCaMP5G)* and *Tg(s1020t:gal4; UAS:GCaMP5G)* were crossed to wild type AB adults for age-matched

controls. Embryos were maintained at 28.5°C and staged according to [S11], dechorionated manually, then embedded in 1.5% low melting point agarose. All imaging was performed following injection in caudal axial muscle with approximately 2 nL of 500 μ M α -bungarotoxin (Tocris Bioscience, Bristol, United Kingdom). Calcium imaging was performed at 4 or 5 Hz with a spinning disk confocal (3i Intelligent Imaging Innovations, Inc., Denver, CO, USA) for 4 or 8 minutes. Images were acquired using Slidebook software (3i Intelligent Imaging Innovations, Inc., Denver, CO, USA) and reconstructed online using Fiji (fiji.sc/). ROIs were manually selected based on a standard deviation Z-projection stack and dorsolateral position in the spinal cord. Peak detection was performed using an open-source signal processing toolbox [S12]. Individual ROI peak frequencies were averaged within embryos to determine coiling frequency from $\Delta F/F$ calculated using custom scripts written in MATLAB (The Mathworks, Natick, MA, USA).

Electrophysiology

Whole cell recording were performed in 3 dpf larvae in artificial CSF (concentrations in mM: 134 NaCl, 2.9 KCl, 1.2 MgCl₂, 10 HEPES, 10 glucose, 2 CaCl₂; 290 mOsm \pm 3 mOsm, pH adjusted to 7.8 with NaOH). Larvae were pinned through the notochord with 0.025 mm tungsten pins. Larvae were decapitated to prevent visual light response, and skin and muscle from two segments between segments 8 and 18 were dissected using a glass suction pipette. A MultiClamp 700B amplifier, a Digidata series 1440A Digitizer, and pClamp 10.3 software (Axon Instruments, Molecular Devices 446 Sunnyvale, CA, USA) were used for acquisitions. Patch pipettes (1B150F-4, WPI, Sarasota, FL, USA) with a tip resistance of 8-11 M Ω were filled with internal solution (concentrations in mM: K-gluconate 115, KCl 15, MgCl₂ 2, Mg-ATP 4, HEPES free acid 10, EGTA 0.5, 290 mOsm, adjusted to pH 7.2 with KOH with Alexa 488 at 10 μ M final concentration). Holding potential was -85 mV, away from the calculated chloride reversal potential (-51 mV). Liquid junction potential in our experiments was -19 mV, stated values for holding potential are not corrected as it did not affect the outcome of the experiments. Gabazine (Tocris Bioscience, Bristol, United Kingdom) was applied in the bath for a final concentration of 10 μ M. Recordings with gabazine in the bath were initiated at least 2 minutes after bath application. Analysis of electrophysiological data was performed offline using Clampex 10 software (Molecular Devices, California, USA).

Cell selection for electrophysiology

For experiments in *Tg(pkd211:gal4; UAS:ChR2-mCherry)*, larvae were pre-screened for fluorescence to identify motor neuron somas encircled by CSF-cN axons expressing ChR2-mCherry. For experiments in *Tg(pkd211:gal4; UAS:ChR2-mCherry; UAS:BoTxBLC-GFP)*, larvae were pre-screened for fluorescence to identify motor neurons encircled by presynaptic CSF-cNs expressing both ChR2 and BoTxBLC-GFP. After recordings, motor neuron identity was confirmed by visualization of Alexa 488 dye and post hoc imaging of ChR2-mCherry. One cell per larva was used for data analysis.

Optogenetic stimulation

Activation of CSF-cNs was achieved by whole field stimulation through a 40x objective for 5 ms with a blue LED (UHP-Mic-LED-460, Prismatic Ltd., Israel, power = 3.88 mW / mm²) through a Digital Micromirror Device with all mirrors in the “on” position. All experiments were run as sets of 10 trials. Two sets of experiments were performed for each cell.

Behavioral recordings and analysis of acoustic escape responses from freely swimming larvae

Depending on the severity of the defects, embryos that could not hatch on their own were dechorionated manually at 2 dpf, as well as their control siblings. 5 dpf larvae were placed individually in dishes with 2.2 cm inner diameter and 3.5 cm outer diameter in 400 μ L of fish facility water on a homogeneous illumination plate (light intensity 0.78 mW / cm² Phlox, ref. LEDW-BL-200/200-LLUB-Q-1R24). Only undamaged, healthy-looking larvae were selected for testing. Larvae were habituated for 10 minutes on the light source at room temperature not lower than 22°C and kept at room temperature during all recordings. For the acoustic startle assay, following acclimation, larvae were given a 500 Hz acoustic stimulus for 10 ms at frame 130 and recorded for a total of 1 second at 650 frames per second with a high-speed camera (Basler AG, ac12040-180km) placed above the setup. Synchronization of the camera and the stimulus was achieved by a custom built Arduino setup. For each group of four dishes, 10 trials were recorded with an inter-trial interval of 2-5 minutes. The acquired images had pixel dimensions of 2000 x 544 and an exposure time of 500 μ s. Behavioral recordings were acquired between 1:00 and 6:00 P.M. The behavior setup used here was described in [S7]. To determine the distance traveled in each trial, using custom-written MATLAB, videos

were analyzed to detect the center of mass of the larva at each frame and to determine the distance traveled between successive frames, which was summed over the trial.

Behavioral recordings and analysis of acoustic escape responses from head-embedded larvae

Due to failure to inflate the swim bladder in *Tg(chx10:gal4; UAS:BoTxBLC-GFP)* larvae, a common problem in larvae with locomotor defects, we utilized the head-embedded configuration to record high-speed kinematics in upright larvae. Recordings were performed in an identical way to freely swimming acoustic-induced escape assay (above) with the exception that larvae were embedded in 2% low-melting temperature agarose and the agarose surrounding the tail was manually removed. Tracking was performed with custom written MATLAB software. A skeleton of the tail was extracted using 10 segments. Depending on the quality of the tracking, traces were individually manually excluded from the dataset in cases of tracking failure, and parameters were manually adjusted to achieve excellent tracking. Kinematic parameters were extracted for each trial including: escape duration, escape latency, the number of tail oscillations, the average tail-beat frequency over the escape bout, and the maximum tail bend angle.

Behavioral recordings and analysis of spontaneously freely swimming larvae

5 dpf larvae in the same wells and on the same setup as in freely swimming acoustic escape experiments above were recorded following a minimum 10 minute acclimation period with no stimulation provided by the experimenter. Videos were recorded at 60 Hz for four minutes at 2000 x 1088 pixel resolution. Videos were scored manually and frames where swim bouts started or ended were recorded. To determine the distance traveled, the same custom MATLAB code as above was employed on the first minute of the four minute acquisition sequence.

Fictive ventral nerve root (VNR) recordings

The fictive locomotion protocol was based on published procedures ([S1,S13]). Thin-walled, borosilicate glass capillaries (Sutter Instruments, Novato, CA, USA) were pulled and fire-polished from a Flaming/Brown pipette puller (Sutter Instruments, Novato, CA, USA) to obtain peripheral nerve recording micropipettes. Pipettes were filled with artificial CSF and positioned next to the preparation using motorized micromanipulators under the microscope. Light suction was applied when the pipette reached the muscle region located at the vicinity of intermyotomal junctions, ventral to the axial musculature midline. The larva was laterally mounted and the otic vesicle was stimulated by a jet of water delivered by a glass pipette and powered by a picospritzer (WPI, Sarasota, FL, USA) on the same side of the body as the VNR pipette. VNR signals were acquired at 10 kHz in current clamp IC=0 mode using a MultiClamp 700A amplifier, a Digidata series 1322A digitizer, and pClamp 8.2 software (Molecular Devices–Axon Instruments, Sunnyvale, CA, USA). Recordings were considered for analysis when the background noise did not exceed 0.05 mV amplitude and signal to noise ratio for fictive locomotor events detection was above three. VNR recordings were analyzed offline using custom MATLAB scripts. For analysis of fast evoked locomotion, the phase 1 portion of elicited fast responses consisted of low frequency bursts between 10 and 20 Hz, lower frequencies than the typical slow swimming frequency range (between 20 to 30 Hz). Because our assay was designed to induce fast locomotor frequencies, we did not perform double VNR recordings to determine if the initial and variable phase 1 slow component corresponds to fictive struggles characterized by locomotor activity back propagating caudal to rostral ([S14]). Since these bursts were always followed by fast frequencies (above 40 Hz) and were part of induced responses, we included them in frequency analysis because it did not affect interpretation of results with respect to the generation of fast locomotion.

Fictive VNR recordings combined with calcium imaging of motor neurons

Calcium imaging was performed at 10 Hz with a spinning disk confocal microscope (3i Intelligent Imaging Innovations, Inc., Denver, CO, USA) in either *Tg(mnx1:GCaMP5G)* or *Tg(mnx1:GCaMP5G; chx10:gal4; UAS:BoTxBLC-GFP)* larvae at 4 dpf. Fictive recordings were performed as described above with otic vesicle stimulation. Up to 12 trials total were performed per larva. Trials in which the fictive recording had at least four bursts in response to otic vesicle stimulation were included for analysis. ROIs were manually selected based on a standard deviation of a Z projection stack computed over few optical sections. For experimental larvae expressing BoTxBLC-GFP in V2a interneurons and GCaMP5G in motor neurons, only neurons with obvious nuclear-excluded GCaMP5G were included in analysis to ensure that background BoTxBLC-GFP expression did not impact $\Delta F/F$ amplitude analysis.

Cell counts in *Tg(pkd2II:gal4; UAS:BoTxBLC-GFP)*

Tg(pkd2II:gal4; UAS:BoTxBLC-GFP) adults were crossed to *Tg(vglut2:IRI-GFP)*, *Tg(gad1b:IRI-GFP)*, or *Tg(chx10:IRI-GFP)* to obtain triple transgenic larvae. Siblings expressing only *Tg(vglut2:IRI-GFP)*, *Tg(gad1b:IRI-GFP)*, or *Tg(chx10:IRI-GFP)* were used as controls. Larvae were embedded in agar and anesthetized in 0.02% tricaine for imaging. From each larva, separate stacks from three regions were obtained: segments 3-4, 10-11, and 25-26. Segment boundaries were identified with a transmitted image, and cells were counted in Fiji (fiji.sc/).

Statistics

For larval behavioral and fictive data, statistical results were generated from a linear mixed effect models (LME) estimated with R version 3.2.3, where the individual fish was considered as random in order to take into account repeated measurements. When non-LME tests were appropriate, statistical tests were used as specified in figure legends.

Supplemental References

- S1. Fidelin, K., Djenoune, L., Stokes, C., Prendergast, A., Gomez, J., Baradel, A., Del Bene, F., and Wyart, C. (2015). State-dependent modulation of locomotion by GABAergic spinal sensory neurons. *Curr. Biol.* *26*, 103-109.
- S2. Scott, E.K., Mason, L., Arrenberg, A.B., Ziv, L., Gosse, N.J., Xiao, T., Chi, N.C., Asakawa, K., Kawakami, K., and Baier, H. (2007). Targeting neural circuitry in zebrafish using GAL4 enhancer trapping. *Nat. Methods* *4*, 323-326.
- S3. Asakawa, K., Suster, M.L., Mizusawa, K., Nagayoshi, S., Kotani, T., Urasaki, A., Kishimoto, Y., Hibi, M., and Kawakami, K. (2008). Genetic dissection of neural circuits by Tol2 transposon-mediated Gal4 gene and enhancer trapping in zebrafish. *Proc. Natl. Acad. Sci. USA.* *105*, 1255-1260.
- S4. Kimura, Y., Okamura, Y., and Higashijima, S. (2006). *alx*, a zebrafish homolog of *Chx10*, marks ipsilateral descending excitatory interneurons that participate in the regulation of spinal locomotor circuits. *J. Neurosci.* *26*, 5684-5697.
- S5. Kimura, Y., Satou, C., Fujioka, S., Shoji, W., Umeda, K., Ishizuka, T., Yawo, H., and Higashijima, S. (2013). Hindbrain V2a neurons in the excitation of spinal locomotor circuits during zebrafish swimming. *Curr. Biol.* *23*, 843-849.
- S6. Auer, T.O., Xiao, T., Bercier, V., Gebhardt, C., Durore, K., Condoret, J-P., Wyart, C., Suster, M., Kawakami, K., Wittbrodt, J., Baier, H., and Del Bene, F. (2015). Deletion of a kinesin 1 motor unmasks a mechanism of homeostatic branching control by neurotrophin-3. *eLife* *4*, e05061.
- S7. Böhm, U.L., Prendergast, A., Djenoune, L., Nunes Figueiredo, S., Gomez, J., Stokes, C., Kaiser, S., Suster, M., Kawakami, K., Charpentier, M., Concordet, J-P., Rio, J-P., Del Bene, F., and Wyart, C. (2016). CSF-contacting neurons regulate locomotion by relaying mechanical stimuli to spinal circuits. *Nat. Commun.* *7*, 10866.
- S8. Schoonheim, P. J., Arrenberg, A. B., Del Bene, F., and Baier, H. (2010). Optogenetic localization and genetic perturbation of saccade-generating neurons in zebrafish. *J. Neurosci.* *30*, 7111-7120.
- S9. Satou, C., Kimura, Y., Hirata, H., Suster, M.L., Kawakami, K., and Higashijima, S. (2013). Transgenic tools to characterize neuronal properties of discrete populations of zebrafish neurons. *Development* *140*, 3927-3931.
- S10. Ahrens, M.B., Orger, M.B., Robson, D.N., Li, J.M., and Keller, P.J. (2013). Whole-brain functional imaging at cellular resolution using light-sheet microscopy. *Nat. Methods* *10*, 413-20.
- S11. Kimmel, C.B., Ballard W.W., Kimmel S.R., Ullmann, B., and Schilling, T.F. (1995). Stages of embryonic development of the zebrafish. *Dev. Dyn.* *203*, 253-310.

- S12. O'Haver, T.C. (1995). A pragmatic introduction to signal processing with applications in scientific measurement. <https://terpconnect.umd.edu/~toh/spectrum/PeakFindingandMeasurement.htm>.
- S13. Masino, M.A., and Fetcho J.R. (2005). Fictive swimming motor patterns in wild type and mutant larval zebrafish. *J. Neurophysiol.* 93, 3177-3188.
- S14. Liao, J.C., and Fetcho J.R. (2008) Shared versus specialized glycinergic spinal interneurons in axial motor circuits of larval zebrafish. *J. Neurosci.* 28, 12982-12992.

I. Ongoing challenges to silencing *in vivo*

A major problem to understanding the role of neurons in the brain and spinal cord involved in locomotion is the difficulty of monitoring and manipulating their activity during active behavior. In the mouse, studies on specified classes of spinal cord interneurons are restricted to pre- or post-natal animals because genetic ablation of neurons involved in rhythm generation, causes defects in the respiratory rhythm generating centers or neurons are difficult to access with light for optogenetic manipulations at later stages (Lanuza et al., 2004; Crone et al., 2008; Zhang et al., 2014; Bouvier et al., 2016). Combinatorial genetic tools now allow study of neural populations *in vivo* at adult stages in mammals (Sato et al., 2016), but use of optogenetic techniques *in vivo* require implantation of optical fibers, feasible in the brain but not spinal cord (Bouvier et al., 2016; Tovote et al., 2016).

Even in the zebrafish, in which the larvae is transparent, analysis of causal roles of neural populations in the spinal cord has been restricted to using fictive locomotion as a readout of motor activity, often in combination with single cell recordings (McLean et al., 2007; McLean et al., 2008; Eklöf-Ljunggren et al., 2012) or in head-fixed preparations (Wyart et al., 2009). Active locomotion has proved harder to investigate. Both genetic silencing has been difficult to achieve and manipulation of neural circuits during active locomotion requires application of pharmacological agents that act systemically or requires spatial targeting with high temporal resolution for optogenetic manipulation.

Often a fine balance between the advantages and drawbacks of different techniques are used to tackle unique questions about neural populations underlying behavior. For example, optogenetic activation will indicate what a system is capable of doing when widely activated. Often these manipulations involve synchronous activation of many neurons not found in physiological activation resulting in behavioral output that would not occur in physiological conditions (Otchy et al., 2015). Opsins intended for silencing such as light-gated chloride

pump NpHR (Zhang et al., 2007) or proton pump Arch (Chow et al., 2010), can lead to undesired activation. NpHR must be carefully used to account for changes in chloride reversal potential (Raimondo et al., 2012) or rebound following a light pulse (Arrenberg et al., 2009). Sustained proton pump activity induces pH-dependent calcium influx that leads to increased spontaneous release (Mathias et al., 2016). Optogenetic techniques therefore afford the ability to control activity remotely, leaving the animal alive and intact, but should be supported by other methods for interpreting the roles of neural populations in behavior.

Chemogenetic tools use genetically engineered receptors that interact with small molecules and can be used *in vivo* to activate, ablate, or silence neurons (Sternson and Roth, 2014). In zebrafish, nitroreductase ablation is most widely used to ablate tissues (Curado et al., 2008; Mathias et al., 2014). The efficacy of nitroreductase ablation depends on the tissue being ablated and requires 12-72 hours to ablate tissues (Curado et al., 2008). However, in tissues that can be ablated, these techniques provide a way to eliminate entirely a population from its networks. Targeted ablation can precisely kill single neurons and researchers have temporal control, choosing the stage at which the neurons are ablated, but neurons must be identifiable, easily accessible, and limited in number.

A critical question in determining which silencing or ablation tool to use to link activity to behavior is whether the method used should be acute or chronic. For behavior, ideally neurons could be silenced on a millisecond timescale, however, optogenetic tools cannot be used in freely swimming larvae due to technical constraints of light power, the confound of light-induced behaviors (Arrenberg et al. 2009; Rihel and Schier, 2012; Friedmann et al., 2015), and can provide activation instead of silencing (Arrenberg et al., 2009; Warp et al., 2012; Mahn et al., 2016). However, some of these techniques can be implemented in head-restrained configurations (Ritter et al., 2001), in which the tail can still be monitored. Chronic silencing or ablation methods using laser, chemical, neurotoxin-induced ablation, or

neurotoxin-mediated silencing provide varying levels of temporal specificity. Bathing in chemical cofactors for up to three days required for Nitroreductase-mediated ablation (Curado et al., 2008; Mathias et al., 2014) limits the timeframe during which experiments can be performed but avoids some of the rewiring that probably occurs when neurons are genetically silenced from their birth as with genetically-encoded neurotoxins. In the case of silencing *chx10*⁺ V2a neurons with BoTxBLC-GFP, understanding whether the effects on locomotion resulted from developmental changes or reflected the role of V2as during active locomotion remains to be determined.

II. Challenges for genetic targeting

The Gal4/UAS system is practical for use *in vivo* but has limitations of silencing over time and in all cases, the Gal4 is not expressed in every cell within a given class. The *Tg(chx10:gal4)* provides highly specific expression in V2as compared to other transgenic lines isolated for targeting a single cell class, but even in this line only 60-70% of neurons are affected, rendering results difficult to interpret. The remaining 30% could, via redundancy or developmental rewiring, carry the primary functions of V2as. Also, some *chx10*-negative neurons are frequently labeled in the transgenic line *Tg(chx10:gal4)*, a common drawback of the Gal4/UAS system. Although most of the neurons in the Gal4 are glutamatergic (Kimura et al., 2013 and *data not shown*), a small number of motor neurons are present and could confound behavioral results if they were silenced in addition to V2as. Thankfully, the effect of ectopic motor neuron expression could be eliminated by performing fictive recordings, in which motor output is recorded upstream of the neuromuscular junction. If a significant proportion of *chx10*-negative interneurons were also labeled, the results would be uninterpretable, highlighting again the need for adequate genetic tools to target neural populations.

III. V2a interneurons in locomotion

In our study, silencing V2as selectively abolished fast locomotor frequencies during escape responses. Additionally, spontaneous, slow locomotion occurred less often and at frequencies lower than controls. Overall, this silencing approach confirmed that V2a excitation is critical for the production of fast, stimulus-evoked swimming. Moreover, V2as are critical for generation of spontaneous slow locomotion and set the range of frequencies at which slow swimming occurs. When optogenetically activated, hindbrain V2as can elicit a slow swim bout in head-fixed larvae, and when optogenetically silenced with Arch, larvae stop ongoing swimming (Kimura et al., 2013). Most likely, abolishment of initiation of slow locomotion is a function carried by hindbrain V2a interneurons.

In a morphological characterization of the spinal V2a population, axon projection patterns and synapse distribution varied with respect to dorsoventral position and recruitment order (Menelaou et al., 2014). In lampreys, tadpoles, and mice, V2a-like neurons form connections with motor neurons, other V2a-like neurons, and commissural inhibitory interneurons (Grillner, 2003; Roberts et al., 2010; Crone et al., 2008; Dougherty and Kiehn, 2010; Menelaou et al., 2014). Whether spinal or hindbrain V2as contribute to setting slow swim frequency is unclear, however, spinal V2as are recruited differentially at different swimming frequencies (Menelaou et al., 2014), and ablation of spinal V2as is sufficient to eliminate the fastest swimming frequencies (Eklöf-Ljunggren et al., 2012) suggesting this function is at least partially carried by spinal V2as. With the morphological and paired recording approach in zebrafish and complementary genetic approaches in mammals, a better picture of the diversity of V2a interneurons can be established.

In our experiments, BoTxBLC-GFP expression was not restricted to the hindbrain or spinal cord, and our results reflect widespread silencing of subtypes of V2a interneurons.

Brainstem V2a neurons can initiate or stop rhythmic motor networks in the spinal cord (Kimura et al., 2013; Bouvier et al., 2016), which could result from dual functionality or a heterogeneous population of V2a neurons. Recent work in mammals demonstrated V2a contribution to frequency control, left-right alternation, burst variability, stabilizing burst amplitude and duration (Crone et al., 2008; Zhong et al., 2011; Dougherty et al., 2013). Together, this work has established that V2as are critical for locomotion and contribute to diverse functions across species, with differences possibly relating to different motor demands. Subtypes of neurons providing excitatory drive in the mouse, including subtypes of V2as or Chx10⁺ neurons are beginning to be identified (Dougherty et al., 2013).

In the zebrafish, MCoDs/V0-s are rhythmically active at slow swimming frequencies (McLean et al., 2008) MCoDs/V0-vs, identified as a unique class by their morphology and neurotransmitter phenotype (Hale et al., 2001; Higashijima et al., 2004a, 2004b), are active at slow swimming frequencies, but their role beyond causation cannot be established without genetic targeting. In mice, excitatory V0 interneurons express Dbx1 during early development. Using diphtheria toxin to genetically ablate the Dbx1 population, V0 neurons were determined to control left-right alternation at high speeds, whereas inhibitory V0 interneurons appear to ensure alternation at low frequencies (Lanuza et al., 2004; Talpalar et al., 2013). Whether subtypes of these neurons exist in zebrafish and how they contribute to locomotion in concert with V2a interneurons during slow and fast swimming remains to be studied.

Another question to be addressed in the future is how circuits are wired and modulated pre-synaptically to the V2as. What are the sources of excitation to V2as? Some of the functional diversity of the *chx10*⁺ interneurons may be due to differences in which populations are activating or silencing these neurons. Evidence in both mouse and zebrafish suggests that these neurons receive input related to sensory feedback (Pfaff, 2016;

unpublished results) and the effect of silencing the *chx10*⁺ V2as, decreased swimming frequency, is consistent with the results of silencing sensory afferents during ongoing locomotion (Knafo et al., *in preparation*). V2as may play a critical role in integrating both descending and peripheral inputs to generate smooth, coordinated movements at a diversity of locomotor speeds.

In order to further decipher the roles of V2a and other populations during active locomotion, tools need to be developed. First, more specific genetic markers to identify coherent subpopulations of neurons are needed, for examples *Shox2*, expressed in a subpopulation of V2as (Dougherty et al., 2013) or *Satb2* (Pfaff, 2016), already identified in mice. Second, intersectional genetic approaches will need to be developed in order to restrict expression of the reporter, activator, or silencer of interest. Additionally, generating a genetically-encoded, quickly inducible form of *Tg(UAS:BoTxBLC-GFP)* would eliminate the confound of developmental rewiring. This would also provide insight in the role of developmental activity in producing functional neural circuits by comparing chronically silenced and acutely silenced populations.

IV. Developmental effects of silencing GABAergic activity

In addition to probing activity during ongoing locomotion, one use of genetically-encoded botulinum toxin is for chronic silencing to investigate activity-dependent development. *Tg(UAS:BoTxBLC-GFP)* allows for silencing throughout development. Indeed, one original goal of my work was to chronically silence CSF-cNs, which are GABAergic and highly active at early stages of development, in order to investigate the role of their GABAergic signaling during embryonic motor behaviors and during development. Silencing the CSF-cNs, validated by whole cell patch clamp, did not lead to a defect of coiling, alter the number of neurons expressing either GABA or glutamate, or lead to premature cell death. These results

indicated that synaptic release from CSF-cNs during early development does not play a significant role in excitability of motor circuits, when early rhythmic activity of spinal CPGs is taking place. Although, other developmental processes might be affected. Relying on the Gal4/UAS system, it is possible that the remaining GABAergic signaling was sufficient to contribute to proper development as mediated by CSF-cNs, however the lack of any developmental changes suggests that this early activity has other functions not examined here.

V. Conclusions

Determining the role of a neuron or neural population during active behavior ideally entails silencing these neurons on a millisecond timescale during ongoing locomotion. However, due to constraints with optical methods, the only currently available tools with such high temporal precision, these experiments are not currently possible. As both genetic and silencing or ablation tools continued to be developed with the goal of use in actively behaving animals, it will be possible to achieve this goal. These results emphasize the complementarity of *in vivo* and *in vitro* approaches and silencing methods, and the diversity of functions a population such as the V2as can perform. Future studies should investigate whether BoTx-mediated silencing effects result from acute or chronic block of synaptic release and how different populations of V2as contribute to their unique roles. Thanks to parallel development of tools to probe behavior in freely moving animals and genetic tools to isolate neuronal populations, a more complete picture of how the brain and spinal cord generate locomotor output will continue to emerge.

**Spontaneous activity in
cerebrospinal fluid-contacting neurons**

I. Motivation

The challenge of investigating behavior *in vivo* often necessitates researchers attempting to understand the spinal cord to perform experiments *in vitro* (Grillner and Zangger, 1979; Wallen and Williams, 1984; Kjaerulff and Kiehn, 1996). By removing the spinal cord and adding excitatory neuromodulators, the isolated spinal cord can perform rhythmic oscillations without sensory input (Delcomyn 1980; Buchanan and Grillner, 1987; Smith and Feldman, 1987). With these tools, understanding of the mechanisms by which locomotion is generated and elements of the central pattern generator (CPG) were established. However, locomotion is a product of dynamic interactions between descending command from the brain, rhythmic motor elements in the spinal cord, and sensory feedback (**Figure 1**; Rossignol et al., 2006).

Sensory feedback can allow, prevent, or select motor patterns, modulate excitation levels, and demands flexibility from motor networks (Rossignol et al., 2006). Thanks to extensive work, primarily in decerebrate cats, we know that muscle and skin afferents as can adapt a locomotor pattern to environmental demands (Loeb et al., 1977; Duysens and Pearson, 1980; Aoyagi et al., 2003; Rossignol et al., 2006) in addition to input from visual, auditory, and vestibular systems.

A major challenge to understanding the neural basis of behavior is quantifying kinematics of locomotion in awake behaving animals, described in **Chapter 1**. In **Chapter 2**, I addressed the challenge of manipulating circuits to enable study of their function, characterizing an optimized neurotoxin and using it to investigate the role of a population of interneurons that provide excitatory drive during locomotion. Having tools to probe neural function *in vivo*, we can address how sensory input contributes to activity in the spinal cord during development and in conjunction with the motor system. In this chapter, I will focus on single cell and population activity with electrophysiological recordings and calcium imaging to investigate how sensory neurons contribute to activity in the spinal cord.

Cerebrospinal fluid-contacting neurons (CSF-cNs) are a unique class of neurons originally described over a hundred years ago and thought to contribute to sensory function thanks to their morphology and location around the CSF-filled central canal of the spinal cord (Kolmer 1921; Agduhr 1922; Kolmer 1931; Vigh and Vigh-Teichmann, 1971). However, their location within the spinal cord has hampered efforts to study their function.

Here I will address the question of whether CSF-cNs are active during development of the motor network, and whether this activity contributes to development of the motor network or CSF-cN function as intraspinal sensory cells *in vivo*.

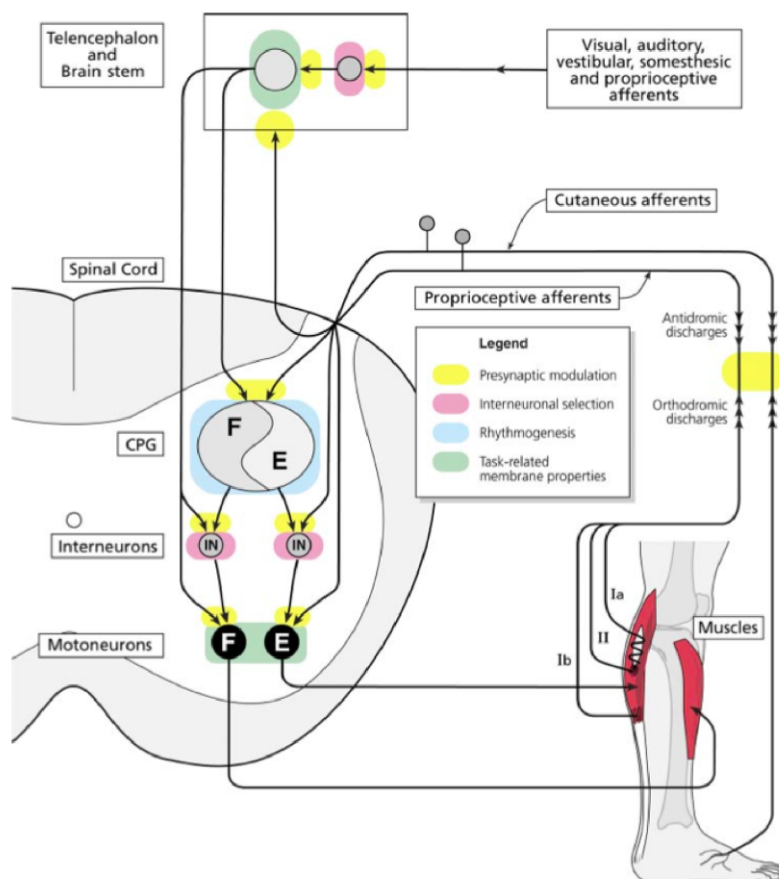
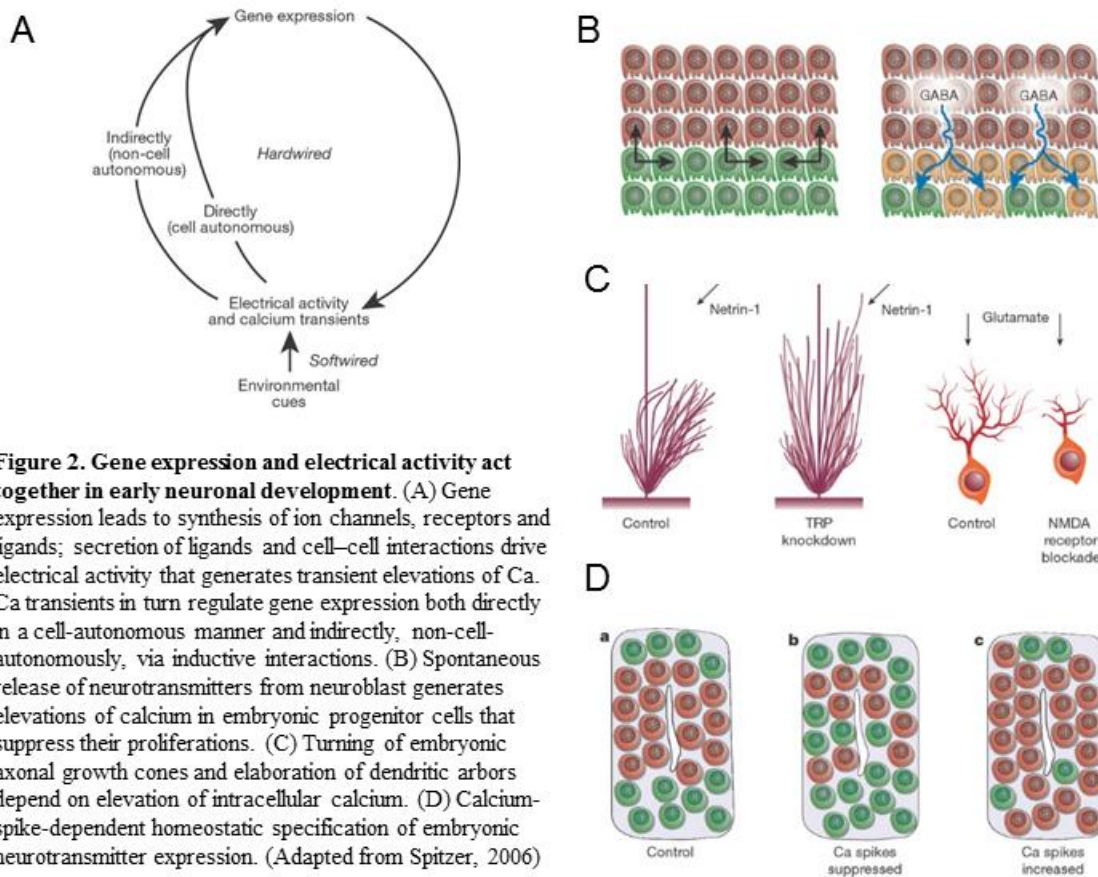


Figure 1. Some sites for dynamic sensorimotor interactions during locomotion. Sensory inputs of various modalities reach the spinal cord or the brain stem and are generally subjected to a phasic presynaptic inhibitory control (yellow) at their entry. Afferent inputs make contact with second-order neurons that are themselves modulated by the rhythmic process such that some pathways may be opened or closed in different phases of the cycle or else the same input may give rise to excitatory or inhibitory responses in the various phases of the cycle (interneuronal selection in pink). This is achieved either by inputs processed by those interneurons implicated directly in the pattern generation or through interneurons whose excitability is modulated cyclically by the central pattern generator (CPG). Interneurons enclosed within the dashed area are considered to be cyclically influenced by the CPG but are not part of the rhythm generation process itself of the CPG. Membrane properties of motoneurons and interneurons apparent only during locomotion can also change the gain of the responses to sensory stimuli. (From Rossignol et al., 2006)

II. Spontaneous activity during development

During early development of the nervous system, spontaneous activity occurs in many neural circuits in the nervous system including the retina, cochlea, cerebellum, hippocampus, neocortex, and the spinal cord (Moody and Bosma, 2005; Blankenship and Feller, 2010). This activity plays important roles in development, including synapse formation, excitatory-inhibitory balance, organization of brain regions, developmental timing, activity-dependent wiring, axonal guidance, differentiations, neurotransmitter phenotype (Katz and Shatz, 1996; Kirkby et al., 2003). In sensory systems, spontaneous and synchronized events allow projection neurons to form sensory maps. Mammalian retinal ganglion cells are active during the period when the ganglion cell axons reach the superior colliculus and the lateral geniculate nucleus as many projections are refined (Galli and Maffei, 1988; Meister et al., 1991). Depolarization of hair cells before the onset of hearing is essential for cochlear neurons to reach their targets (Tritsch et al., 2007).

Even before synapses form, neurons and their precursors display chemical and electrical activity that regulates differentiation, neurotransmitter phenotype, and neuronal migration (**Figure 2**; Desarmenien et al., 1991; Gu and Spitzer 1995; LoTurco et al., 1995; Demarque et al., 2002; Manent et al., 2005; Spitzer, 2006). Much of this early uncoordinated activity is generated by neurotransmitters depolarizing neurons and activating voltage-gated calcium channels, leading to changes in calcium concentrations that regulate intracellular cascades (Vanhoutte and Bading, 2003). Additionally, calcium entry can regulate development via channels that do not rely on classical voltage- or neurotransmitter-gating. Metabotropic glutamate receptor activation and activation of GABA_A receptors can lead to depolarization of neural progenitors (Flint et al., 1999; Wang, et al., 2003). Transient receptor potential (TRP) channels can also generate calcium transients in growth cones of developing axons (Greka et al., 2003).



Later, when circuits are beginning to form, activity becomes correlated and patterned between neighboring cells. Spontaneous patterned activity often shares common mechanisms for their generation, including pacemaker neurons (Rockhill et al., 2009; Tong and McDearmid, 2012), gap junction coupling (Singer et al., 2001; Personius et al., 2007), transient synaptic connectivity (Tritsch et al., 2007), paracrine or extra synaptic transmission (Demarque et al., 2002), or depolarizing GABA (Leinekugel et al., 1997; Garaschuk et al., 1998).

In the spinal cord, coordinated spontaneous bursting in chick is driven by depolarizing acetylcholine, GABA acting on GABA_A receptors, and glycine (Milner and Landmesser 1999). Later in development in the mouse and rat, activation of spinal circuits by the brainstem drives correlated activity between the left and right sides of the spinal cord (Nishimaru and Kudo, 2000). Pharmacological and optogenetic activation to alter the

frequency of these bursts induced defects in motor neuron pool-specific pathfinding to target appropriate muscles (**Figure 3**; Hanson and Landmesser, 2006; Kastenenka and Landmesser, 2013), maturation of synapses (Gonzalez-Islas and Wenner, 2006), and development of CPG networks (Myers et al., 2005; Marder and Rehm, 2005). In *Drosophila*, spontaneous motor neuron activity drives muscle contraction from 17 hpf, leading to sequential activation of muscles segments. When ChR2 was used to alter the frequency of neural activity before appearance of coordinated muscle contractions, the contractions were delayed, indicating that maturation of motor function requires a specified frequency of coordinated neural activity (Crisp et al., 2011). Together, these results demonstrate a functional role for spontaneous activity in the development of motor networks.

Coordinated activity in the spinal cord thus plays a role in development and maturation of the networks underlying locomotion. Although the motor network can develop independent of sensory input (Suster and Bate; 2002; Goulding 2009), early born and active sensory neurons could contribute to refining of the spinal motor network.

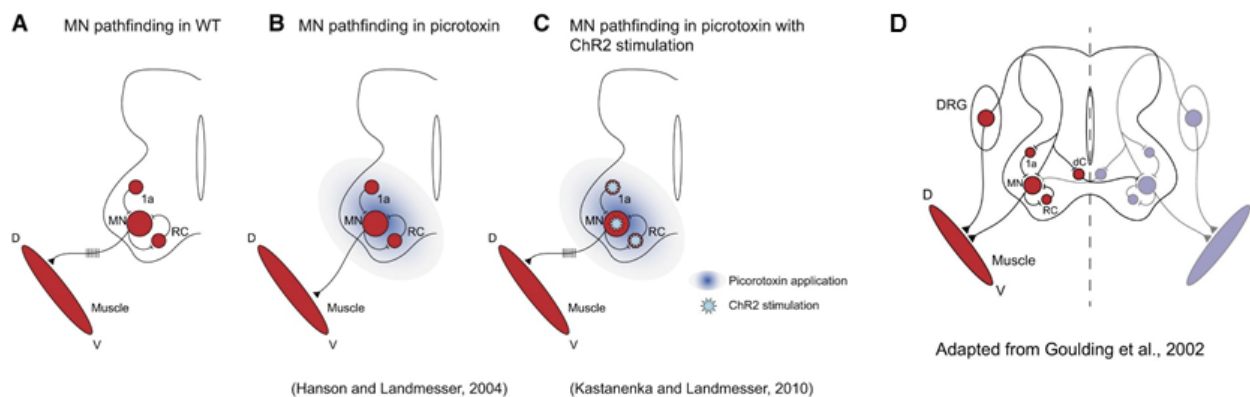


Figure 3. Motor neuron pathfinding in the developing spinal cord under normal and disrupted activity patterns.

Schematic representation of motoneuron pathfinding in the developing spinal cord during normal development (A), in the presence of the GABA_A antagonist picrotoxin (B), and in the combination of picrotoxin and ChR2 stimulation (C). (D) Schematic of a subset of spinal cord cell types and their connections. V, ventral; D, dorsal; MN, motoneuron; RC, Renshaw cell; 1a, 1a inhibitory interneuron; ChR2, channelrhodopsin-2; dC, commissural interneurons (Adapted from Kirkby et al., 2013)

III. Signal control and amplification in sensory systems

Spontaneous activity is a key developmental feature of neural circuits but also plays important roles in coding inputs in functional sensory systems. Animals encounter diverse stimuli in their environments that can rapidly change, and thus modulation of how neurons respond to these inputs enables correct readout by the central nervous system. However, firing and vesicular release rates cannot be negative, necessitating a need for a basal firing rate to enable sensitivity to a dynamic range of inputs (Wilson, 2014). Sensory systems also cope with the need to respond to a wide range of stimuli by having neurons respond to opposing stimuli, such as with ON-OFF neurons and color opponent neurons. This strategy is also employed by auditory, thermosensory, and mechanosensory systems (Jacobs et al., 2008; Yorozu et al., 2009; Ma, 2010; Wilson, 2014).

Metabolic constraints limit the extent to which a single neuron can code for extensive stimuli and incentivize systems to implement adaptation or gain control. By adapting basal firing, neurons can adjust their sensitivity and constantly change the relationship between input and output based on the state of the environment at any given time (Wark et al., 2007). TRP channels are mostly cation non-selective ion channels (Owsianik et al., 2006) and are involved in transduction of diverse stimuli, such as vision, olfaction, taste, chemosensation, thermosensation, and mechanosensation as well as amplifying these sensory responses (Clapham 2003; Voets et al., 2005; Christensen and Corey, 2007).

In sensory neurons, TRP channels can contribute to both sensory transduction and controlling sensitivity of a neuron to relevant stimuli. In the *Drosophila* auditory system, one TRPN channel, NompC amplifies sound evoked motion by the auditory organ but is not required for signal transduction, while Nanchung and Inactive are TRPV channels that are required for responses, forming components of the transduction complex (Gopfert et al., 2006; Lehnert et al., 2013). A great debate in the mechanosensation field is whether TRP

channels are the primary transducers that sense force or whether they play a secondary role in the signal transduction pathway, such as in amplification or modulation of the primary transduction signal (**Figure 4**; Christensen and Corey, 2007; Hu et al., 2015). This system of separating transduction and amplification could play critical roles in ensuring a dynamic system to finely decipher and integrate sensory inputs to ensure coordinated locomotion.

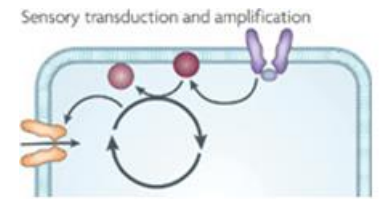


Figure 4. Distinct mechanisms can transduce and amplify sensory signals in receptor neurons. (Adapted from Faisal et al., 2008)

IV. Spontaneous activity in the developing zebrafish embryo

The zebrafish is an ideal organism to probe the role of sensory neurons *in vivo* thanks to their transparency and rapid development. The earliest motor activity in the zebrafish consists of spontaneous contractions ("coiling") that appears at 17 hpf (Saint Amant and Drapeau 1998) when few spinal motor neurons and interneurons have extended axons (Bernhardt et al., 1990; Kuwada et al., 1990; Saint-Amant and Drapeau, 1998). Coiling is early motor network activity that is independent of supraspinal input (Saint Amant and Drapeau, 1998; Downes et al., 2006). Glutamatergic neurons with pacemaker properties that are known as ipsilateral caudal (IC) cells (Tong and McDearmid, 2012) drive a gap junction coupled network of early born motor neurons and primary interneurons (Saint Amant and Drapeau, 2001). This activity is characterized by spontaneous coordinated activation of motor neurons and early born interneurons of one hemicord out of phase with the other hemicord, which manifests as alternated muscle contraction of the tail (Saint Amant and Drapeau, 2000; Muto et al., 2011; Warp et al., 2012). Motor neuron activity is uncorrelated at 18 hpf and becomes correlated by 20 hpf via progressive synchronization of subgroups of cells (Warp et al., 2012). Coiling behavior starts around 17 hpf and increases to approximately 1 Hz at 19-21 hpf before steadily decreasing until 25-26 dpf, after which very little spontaneous contraction occurs (Eaton and Farley, 1973; Kimmel et al., 1995; Saint-Amant and Drapeau, 1998).

While coiling occurs, embryos also become touch-sensitive around 21 hpf and can generate short swim bursts in response to touch by 27 hpf (Saint Amant and Drapeau, 1998). At 2 and 3 dpf, embryos and larvae generate infrequent immature swim bursts of long duration before displaying mature beat-and-glide swimming that includes a range of behaviors by 4 and 5 dpf, at which point they start to feed and exhibit complex predation behavior (Drapeau et al., 2002; Borla et al., 2002; McElligott and O'Malley, 2005). Thus, spontaneous coiling sets an early electrically-coupled network that contributes to early motor behaviors as chemical transmission begins developing, whereas by 4 dpf, mature beat-and-glide swimming mediated by chemical neurotransmission predominates (Drapeau et al., 2002). Sensory input could also contribute to development of the spinal cord at this stage, either via regulating frequency of motor neuron activation or through an alternative mechanism.

Recently population imaging with GCaMP at embryonic stages demonstrated rostral to caudal propagation of motor neuron activity underlying coiling (Muto et al., 2011). Altering activity frequency with NpHR led to fewer neurons integrated into the coordinated oscillating network (Warp et al., 2012). This evidence suggests that oscillations play a role in setting developmental timing and permitting newly born neurons beginning to extend axons into the CPG network.

In work by Warp et al., enhancer trap line *Tg(s1020t:gal4)*, used to monitor coordinated oscillations, also labeled ventral longitudinal descending neurons (VeLD) and a small fraction of dorsal cerebrospinal fluid-contacting neurons (CSF-Cns) (2012). VeLDs are 100% correlated with the motor network (Saint Amant and Drapeau, 2001). Both motor neurons (MNs) and VeLDs are located laterally. Some medially-located neurons displayed long uncorrelated calcium transients, suggesting that CSF-cNs might display spontaneous activity early in development (**Figure 5**).

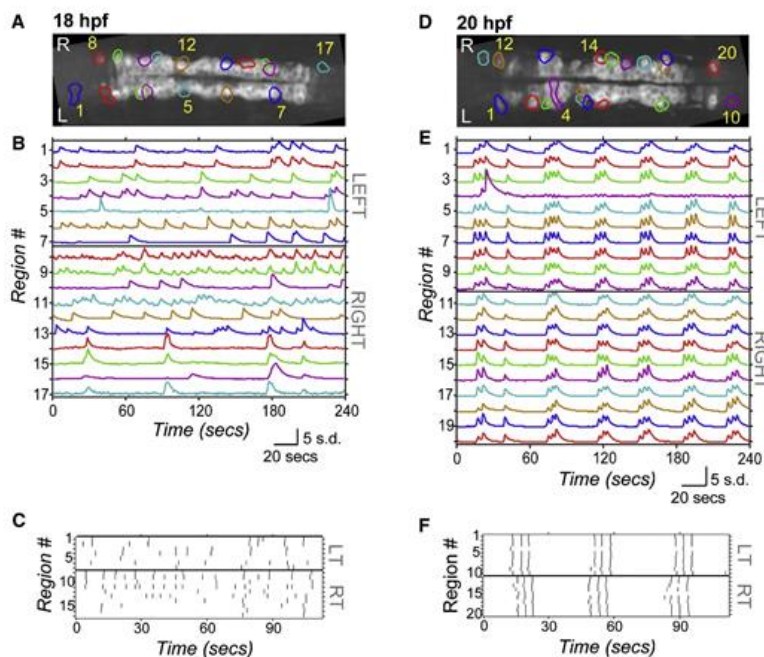


Figure 5. Spontaneous Calcium Activity in Spinal Neurons Progresses from Sporadic to Locomotor-Like During Embryonic Development

GfCaMP3 activity in single neurons in one embryo at 18 hpf (left) and 20 hpf (right). (A and D) Dorsal views of GfCaMP3 baseline fluorescence with active regions circled (rostral left). (B and E) Normalized intensity traces for active regions (identified on y axis) for the left and right sides of the cord, with amplitude corresponding to standard deviations (s.d.) of fluorescence away from baseline. At 18 hpf (B), ipsilateral neurons have little correlated firing, though some synchronization is observed. At 20 hpf (E), ipsilateral neurons are tightly synchronized, with few exceptions, **note the elongated cell extending to the midline** (C and F) Raster plots of detected events for subsection of data in (B) and (E). At 18 hpf (C), population activity is uncoordinated. By 20 hpf (F), ipsilateral cells are synchronized, contralateral cells alternate, and a higher order left/right bursting organization is observed. From Warp et al., 2012

V. CSF-cNs in the spinal cord

Cerebrospinal fluid (CSF) is a fluid that is secreted from the choroid plexus, an epithelial structure found in the ventricles of the brain. Its roles are not well understood but are thought to include homeostasis, mechanical protection, sleep, transportation of chemical signals, migration and guidance of neuroblasts (Bito et al., 1966; Sawamoto et al., 2006). In the spinal cord, CSF flows in the lumen of the central canal, which extends the length of the spinal cord (Bradbury and Lathem, 1965). A diverse populations of cells surround the vertebrate central canal, including ependymocytes, tanyctes (Seitz et al., 1981; Hugnot and Franzen, 2010), and neurons known as CSF-contacting neurons or CSF-cNs, which represent an interface between the CSF and the nervous system.

CSF-cNs were originally described in the early twentieth century by Kolmer and Agduhr (Kolmer 1921; Agduhr, 1922; Kolmer 1931). Kolmer and Agduhr described the cells as neurosensory and intraependymal, respectively. Based on the morphology of these "*Liquorkontakt-Neuronensystem*" or liquor-contacting neural system cells, consistent with the morphology of known receptor cells, they proposed that the cells might carry sensory

function. Kolmer proposed calling them a "parasagittal organ" and Agduhr a "sense organ" (Kolmer 1921; Agduhr 1922; Kolmer 1931).

Following Kolmer and Agduhr's observations, Vigh and Vigh-Teichmann used electron microscopy to investigate the morphology of these neurons in a variety of structures (Vigh and Vigh-Teichmann, 1971; Vigh and Vigh-Teichmann, 1973; Vigh and Vigh-Teichmann, 1998). They reported that CSF-cNs in the spinal cord protrude into the lumen of the central canal that contains microvilli and a motile kinocilium (**Figure 6**; Vigh and Vigh-Teichmann, 1971; Vigh and Vigh-Teichmann, 1973). These morphological details were expanded by backfilling with horseradish peroxidase to describe ipsilateral and rostral projecting axons in *Xenopus* (Dale et al., 1987a; Dale et al., 1987b), later confirmed in rat (Stoeckel et al., 2003) and zebrafish (Wyart et al., 2009). Since initial descriptions of the morphology and projections of CSF-cNs, immunohistochemistry demonstrated that across diverse species CSF-cNs are always GABAergic (**Figure 6**; Barber et al., 1982; Dale et al., 1987a; Dale et al., 1987b; Bernhardt et al., 1992).

Thanks to this extensive morphological characterization, CSF-cNs can be viewed as a conserved class of neurons across species. In the spinal cord, CSF-cNs are ovoid shaped and possess an apical extension that extends into the central canal (Vigh and Vigh-Teichmann, 1971; Vigh and Vigh-Teichmann, 1973). This extension has a tuft of microvilli and a kinocilium, a primary motile cilium, in the zebrafish (Bohm et al., 2016). In addition GABA expressio, in various species CSF-cNs can express, for example, neuropeptides such as somatostatin (Buchanan et al., 1987; Wyart et al., 2009), urotension-II related peptide (Quan et al., 2015), serotonin (Annex 2; Montgomery et al., 2015), and dopamine (Roberts and Meredith, 1987; Roberts et al., 1989).

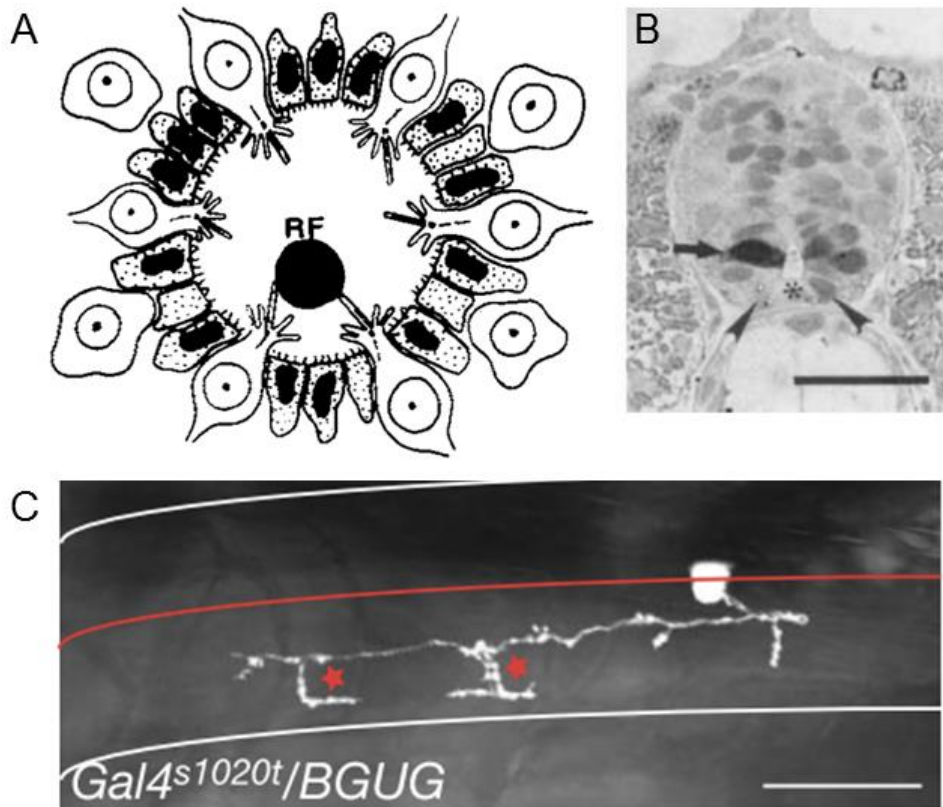


Figure 6. CSF-cNs surround the central canal and express GABA

(A) CSF-cNs (white) surround and contact the central canal. From Vigh and Vigh-Teichmann, 1970. (B) Coronal sections of GABA immunohistochemistry in a 27 hpf zebrafish embryo. The black arrow indicates a dorsal CSF-cN expressing GABA. Scale is 25 μ m. From Bernhardt et al., 1992. (C) Dorsal view of a CSF-cN in zebrafish projecting an axon rostrally and ipsilaterally in the spinal cord. From Wyart et al., 2009.

In the zebrafish, genetic characterization has demonstrated the CSF-cNs originate from two separate progenitor domains in the spinal cord. Dorsal CSF-cNs, also designated as KA', originate from pMN and *olig2*⁺ precursors, whereas ventral CSF-cNs, also known as KA'', originate from the lateral floor plate p3 *nkx2.2*⁺ precursors (Bernhardt et al., 1992; Park et al., 2004; Schäfer et al., 2007; Yang et al. 2010). Both populations are present by the beginning of electrical activity in the spinal cord and express GABA by 20 hpf (Djenoune et al., 2014). Additionally, dorsal CSF-cNs express somatostatin-1 from 24-55 hpf, a period during which extensive axonal outgrowth and birth of secondary motor neurons occurs. Ventral CSF-cNs express serotonin from 48-72 hpf, before the onset of mature locomotion (Annex 2).

Expanding on this knowledge, extensive characterization of CSF-cNs in the zebrafish demonstrated that although ventral and dorsal CSF-cNs both have ipsilateral and rostral projecting axons, dorsal CSF-cN axons remain ventral in the spinal cord, whereas ventral CSF-cN axons branch and project more dorsally in the spinal cord by larval stages (Annex 2). Connectivity of dorsal versus ventral CSF-cNs onto spinal circuits may also differ. Ventral CSF-cNs preferentially project onto interneurons involved in both slow (Fidelin et al., 2015) and fast (Hubbard et al., *in revision*) locomotion as well as primary motor neurons active during fast locomotion. Connectivity of dorsal CSF-cNs has not been established.

CSF-cNs are among the earliest born neurons in the spinal cord (Bernhardt et al., 1992). GABAergic from the earliest stages of electrical activity in the spinal cord, CSF-cNs could function to set the excitability of the motor network via GABA release or develop early in response to a requirement for communicating sensory responses from the CSF to the central nervous system.

VI. CSF-cNs express TRP channel PKD2L1

TRP channels belong to a large family of ion channels implicated in a diversity of neural signaling processes and found primarily in sensory receptor cells. These channels are identified by their homology instead of their function or selectivity because their functions are diverse and difficult to understand (Clapham, 2003). TRP channels are identified by their structure, six-transmembrane polypeptide subunits that form tetrameric assemblies that are permeable to cations. Many TRP channels are almost ubiquitously expressed, and most have splice variants (Clapham 2003). TRP channels function widely in sensory systems and can respond to touch, temperature (Peier et al., 2002; Voets et al., 2004), pain (Caterina et al., 1997; Jordt et al., 2004), osmolarity (Strotmann et al., 2000), pheromones (Liman et al., 1999), taste (Perez et al., 2002; Huang et al., 2006), and other sensory stimuli. Ongoing

debate remains concerning the primary function of TRP channels in sensory pathways; evidence suggests they transduce sensory signals but also activate indirectly and play roles in modulating gain for responses to sensory inputs (Lin and Corey, 2005; Christensen and Corey, 2007).

The TRPP (polycystin, also known as PKD channels because they are deleted in polycystin kidney disease) subfamily includes calcium permeant channels that require a partner of another PKD to form a cation channel at the cell membrane. PKD2L1 (PKD2L1 (Polycystic-kidney-disease-like ion channel 2 – Like 1), also known as TRPP3, is expressed in a subset of taste receptor cells (TRC) (Huang et al., 2006; Bushman and Liman, 2015). Additionally, PKD2L1 is also expressed in neurons surrounding the central canal of the spinal cord (**Figure 7**; Huang et al., 2006) Recent work demonstrated further that expression of PKD2L1 is specific to CSF-cNs in the spinal cord and brainstem of mouse, macaque, and zebrafish from early in development of the spinal cord (**Figure 8**; Djenoune et al., 2014; Orts-Del'Immagine et al., 2014).

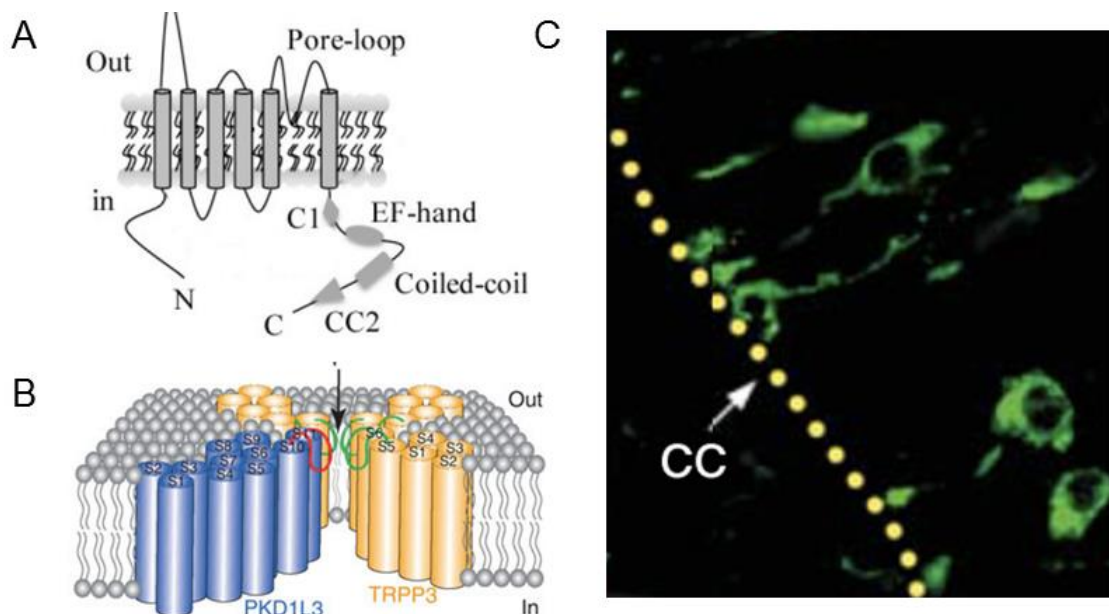


Figure 7. PKD2L1 structure and expression in the spinal cord

(A) Schematic illustration of PKD2L1 membrane topology. From Zheng et al., 2015 and Djenoune, 2015. (B) Schematic of a heteromeric PKD2L1-PKD1L3 viewed from the side. The channel is composed of three PKD2L1 (TRPP3) subunits and one PKD1L3, the arrow points to the channel pore. From Yu et al., 2012. (C) Immunohistochemistry for PKD2L1 on a coronal section of a mouse spinal cord. CSF-cNs (green) contact the central canal (CC). From Huang et al., 2006.

In both mouse and macaque, species in which immunohistochemistry for PKD2L1 was performed, PKD2L1 localizes to the soma and more densely to the apical bulbous extension protruding into the central canal. CSF-cNs have a motile cilium in zebrafish (Bohm et al., 2016). Heteromeric PKD2L1-PKD1L1 complexes in mice and humans acts as a ciliary calcium channel controlling ciliary calcium concentration leading to activation of hedgehog pathways directly in the cilium (Delling et al., 2013). PKD2L1 can also form a complex with PKD1L3 in order to localize to the cell surface, whereas PKD2L1 itself has ER retention sequences that relegate PKD2L1 homotetramers to the endoplasmic reticulum (Murakami et al., 2005). In spinal CSF-cNs in the mouse, PKD2L1 is co-expressed with PKD1L2, indicating that PKD2L1 is most likely trafficked to the cell surface (Petracca et al., 2016).

VII. Sensory function of PKD2L1

PKD2L1 was originally identified in a subset of taste receptor cells that lost sour taste response when PKD2L1 was genetically ablated from those cells (Huang et al., 2006). Therefore, PKD2L1 is thought to be involved in sour taste, however its role in pH detection is unclear. When overexpressed in *Xenopus* oocytes, channel opening decreased when pH was lowered (Chen et al., 1999). An "off" response following acidification activates the PKD2L1-PKD1L3 complex. Alkaline increases in pH increases PKD2L1 activity up to pH 8-9 and decreases its activity at higher pH (Inada et al., 2008).

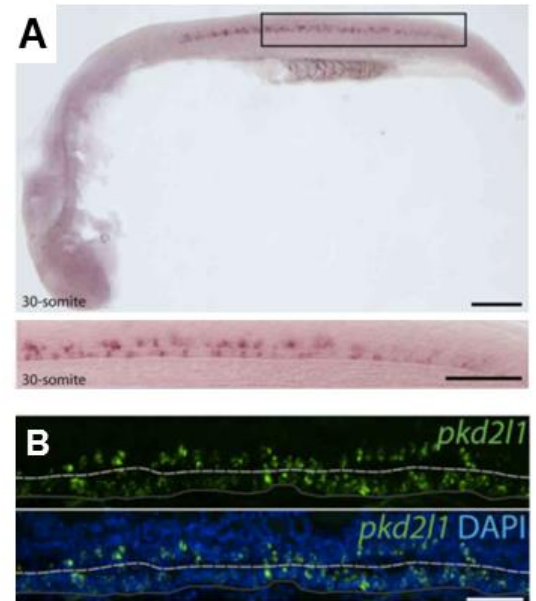


Figure 8. *pkd2l1* is expressed in the zebrafish spinal cord from embryonic to adult stages. (A) Whole mount *in situ* hybridization for *pkd2l1* in a 24 hpf zebrafish embryo. The bottom image is a magnified region of the boxed region (top). Scale is 100 μ m (top) and 50 μ m (bottom). (B) In sagittal sections from the adult spinal cord, *pkd2l1*⁺ CSF-contacting cells are located ventral and dorsal to the central canal. Scale is 40 μ m. Adapted from Djenoune et al., 2014.

PKD2L1 channels have an increased opening probability in hypo-osmotic solutions and a decreased opening probability in hyperosmotic solutions (Murakami et al., 2005; Shimizu et al., 2009). PKD2L1 channel opening probably also increases after heating followed by rapid cooling and is decreased at high temperatures (Higuchi et al., 2014).

Several reports PKD2L1 may open constitutively (Chen et al., 1999, Liu et al., 2002). However it is difficult to disentangle sensory-induced high frequency opening from constitutive opening. Expression of recombinant PKD2L1-PKD1L3 tetramers in HEK293 cells show that this complex may not serve as a sensory transduction element, but that Ca^{2+} spikes controlled by Ca^{2+} influx through the channel may serve to amplify sensory signals. A recent report demonstrated that Ca^{2+} -dependent activation amplifies a small Ca^{2+} influx via the PKD2L1-PKD1L3 complex triggered by rapid onset/offset of Ca^{2+} , voltage, or acidic stimuli (Hu et al., 2015).

PKD2L1 may also play a role in mechanosensation, though no direct evidence is available to support this claim (Lin and Corey, 2005), and calcium imaging showed that primary cilia, where PKDs are generally expressed, do not appear to be calcium-responsive mechanosensors (Delling et al., 2016). PKD2 senses fluid flow to establish left-right determination (Praetorius and Spring, 2005; Yoshida et al., 2012). However, PKD1L1-PKD2L1 expressed *in vitro* showed that although channel activity increased at high pressures of 11-13 kPa, the PKD1L1-PKD2L1 channel lacks sensitivity found in classical mechanosensitive channels such as Piezo (Coste et al., 2012) or MscL (Sukharev et al., 1994), and in TRPP knockout and double and triple knockout mice, mechanotransduction persists in hair cells (Wu et al., 2016). Indeed in other systems, such as *Drosophila* audition, nematode touch, and mechanical pain or hair cell transduction in mouse, TRP channels are critical for mechanosensation without playing a direct role in transduction of the mechanical stimulus (Christensen and Corey, 2007).

VIII. CSF-cN function

Despite their presence in every vertebrate species investigated (Kolmer, 1921; Agduhr 1922; Kolmer 1931; Vigh and Vigh-Teichmann, 1971; Vigh et al., 1973; Barber et al, 1982; Dale et al., 1987a; Stoeckel et al., 2003; Reali et al., 2011; Jalalvand et al., 2014; Djenoune et al., 2014), the physiological role of CSF-cNs is only beginning to be understood. Their location around the central canal, morphology, and conserved expression of PKD2L1 and GABA suggest that CSF-cNs probably carry mechanosensory or chemosensory functions, transmitting changes in flow or composition of the CSF to regulate activity in the spinal cord. Thanks to recent development of genetic and optical tools, the function of CSF-cNs has been probed directly in recent years.

Knowledge of expression of PKD2L1 in sour taste receptor cells strongly suggested a role in monitoring pH (Huang et al., 2006). Comparative work in taste receptor cells and CSF-cNs demonstrated although PKD2L1-positive taste receptor cells transduce acidic stimuli via a proton current, sour taste persists in knockouts of the PKD channels (Horio et al., 2011; Nelson et al., 2010). The responses of CSF-cNs to acidification in the spinal cord, rapid activation and decay kinetics, were reminiscent of ASIC channels (Bushman and Liman, 2015). In the mouse and lamprey, CSF-cNs respond to pH in a bell-shaped manner, possibly using ASIC channels to respond to acidic pH and PKD2L1 to respond to alkaline pH (**Figure 9**; Orts-Del'Immagine et al., 2016, Jalalvand et al., 2016b). Firing rates are lowest when the pH is closest to physiological conditions, suggesting CSF-cNs may be active during any departures from healthy conditions (Jalalvand et al., 2016b).

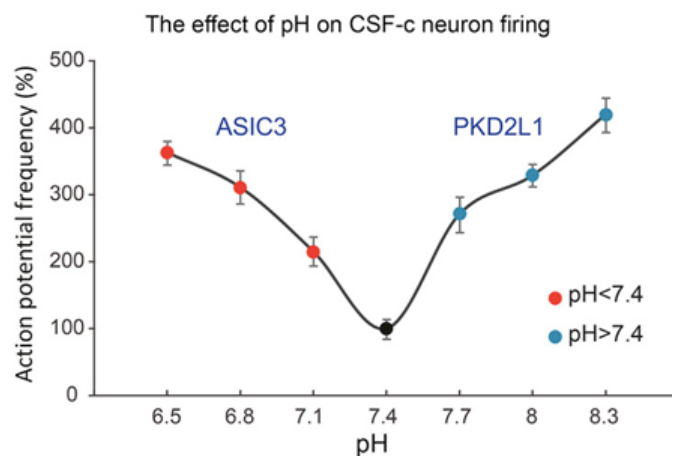


Figure 9. CSF-cNs respond to changes in pH through ASIC channels and PKD2L1 in the adult lamprey. Adapted from Jalalvand et al., 2016b

However, the impact of changing firing rates to cope with pH changes on behavior is unknown.

The Wyart lab has undertaken extensive characterization of the connectivity of CSF-cNs and their sensory responses in zebrafish, in which circuits can be manipulated and monitored in actively behaving animals. CSF-cNs form monosynaptic connections with excitatory interneurons involved in slow locomotion (Fidelin et al., 2015) as well as CaP primary motor neurons (Hubbard et al., *in revision*). During slow locomotion, simultaneous optogenetic activation of all CSF-cNs is sufficient to silence ongoing locomotor bouts, while activation of CSF-cNs during rest can trigger a slow swim bout, a phenomenon enhanced in a state of high excitability following bath application of NMDA (Wyart et al., 2009; Fidelin et al., 2015).

Spinal CSF-cNs in the zebrafish also respond to both passive and active bending of the tail that is abolished in a *pkd21l* null mutant (**Figure 10**; Bohm et al., 2016), which suggests that Pkd21l in zebrafish may play a critical role in transduction or facilitation of mechanical inputs. However, the role of Pkd21l in this pathway or other sensory modalities is not established. Expression of neuropeptides suggests that CSF-cNs may play a long lasting modulatory role on behavioral state or neuronal plasticity, but this is challenging to test on a long time scale. Location around the central canal and GABA expression have also lead to investigation on whether CSF-cNs could enabling the differentiation of progenitors in the ependymal neurogenic niche via GABA release (Reali et al., 2011). However the contexts in which CSF-cNs are physiologically activated and the extent to which they play diverse roles in the spinal cord are not known.

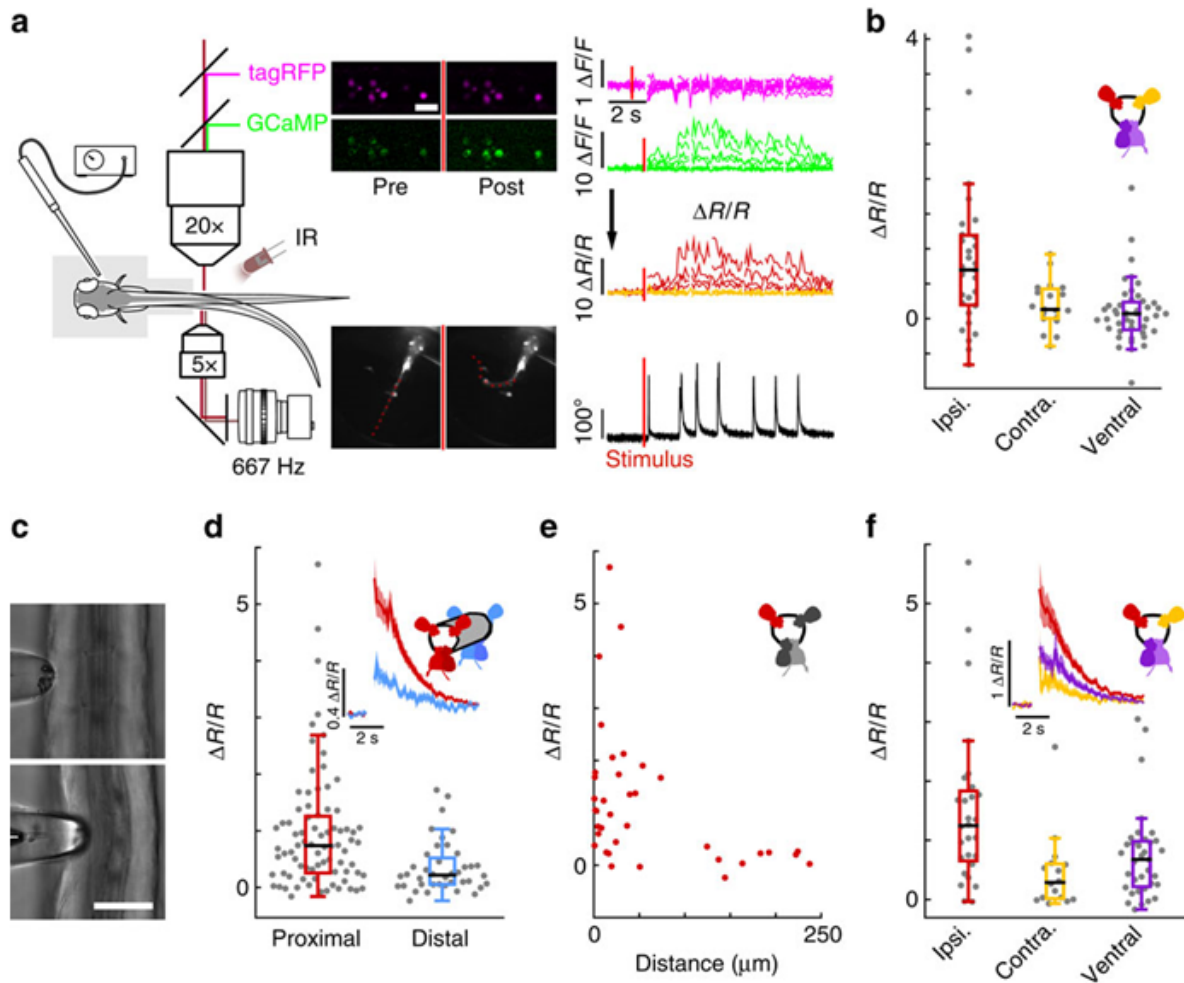


Figure 10. CSF-cNs respond to active muscle contraction as well as to passive mechanical bending of the spinal cord. (a) Schematic describing 2-photon imaging experiments used to record simultaneously from CSF-cNs expressing tagRFP (magenta) and GCaMP5 (green) in head-embedded Tg(pkcd211:GCaMP5, pkcd211:tagRFP) larvae. Infrared illumination combined with high-speed video recording shows unidirectional tail deflections induced by a water jet to the otic vesicle. Sample traces for $\Delta F/F$ of tagRFP and GCaMP shown with tail deflection during escape (note: vertical scale is 10 times larger for GCaMP compared to tagRFP signals). Subtracting the tagRFP signal from the GCaMP signal removed motion artifacts; breaks in the trace arise from frames when cells escaped from the focal plane. Scale bar: 10 μm . (b) Quantification of calcium transient amplitude in response to muscle contraction ($n=11$ larvae) in dorsal CSF-cNs either ipsilateral or contralateral (yellow) or ventral (purple). Only dorsal ipsilateral cells exhibited responses greater than baseline and all other cell types responded significantly less than dorsal ipsilateral cells. (c) Passive mechanical stimulation of CSF-cNs in paralyzed larvae was implemented with mechanical pressure exerted by pushing a glass probe laterally against the fish tail. Scale bar: 50 μm . (d) Response of proximal (<100 μm) and distal (>100 μm) CSF-cNs. Inset: average calcium response of proximal (red) versus distal (blue) CSF-cNs. (e) Response of dorsal ipsilateral (red) CSF-cNs as function of distance from the probe. (f) Response of dorsal ipsilateral (red), dorsal contralateral (yellow) and ventral (purple) CSF-cNs relative to the location of mechanical stimulation. Inset: Average calcium response of dorsal ipsilateral versus dorsal contralateral and ventral CSF-cNs. Adapted from Böhm et al., 2016.

IX. Aims

Spontaneous activity is critical for developmental processes and function of sensory cells. CSF-cNs in zebrafish express GABA and Pkd211 early in development as spontaneous activity transitions from uncorrelated electrical activity to correlated activation of CPG neurons within each spinal hemicord.

1. What are the spontaneous activity levels of CSF-cNs *in vivo* from embryonic development to stages in which mature motor networks are formed? I will address this question using genetic targeting, calcium imaging with genetically-encoded calcium indicator GCaMP5G.
2. Can spontaneous activity contribute to development of spinal cord networks? Using immunohistochemistry and quantification, optogenetics, and electrophysiology, I will evaluate the effects of reducing spontaneous activity in CSF-cNs.
3. What is the origin of spontaneous activity and does it reflect sensory properties of CSF-cNs? I address this question with pharmacology, calcium imaging, and electrophysiological recordings.

Zebrafish husbandry

All procedures were approved by the Institut du cerveau et de la moelle épinière (ICM) and the National Ethics Committee on E.U. legislation. All experiments were performed on *Danio rerio* embryos or larvae of AB, TL, or mixed background. For some experiments, *mifta*^{-/-} were used. Embryos or larvae were raised in an incubator at 28.5°C under a 14/10 light/dark cycle until the start of experimentation. In the case of some experiments at 24 hpf, embryos were raised at 28.5°C until at least 60% epiboly then moved to 26.5°C to delay development in order to perform experiments at the correct stage (Kimmel et al., 1995). Experiments were performed at room temperature (22-26°C) on 24 hpf embryos to 5 dpf larvae.

Table 1. Transgenic lines used

Short name	Alternate name	Labels	Reference
<i>Tg(pkd211:GCaMP5G)</i>	<i>Tg(pkd211:GCaMP5G)icm07</i>	CSF-cNs	Böhm et al., 2016
<i>Tg(olig2:dsred2)</i>	<i>Tg(olig2:dsred2)</i>	Diverse, includes motor neurons and dorsal CSF-cNs in the spinal cord	Kucenas et al., 2008
<i>Tg(HuC:GCaMP5G)</i>	<i>Tg(elavl3:GCaMP5G)</i>	Most neurons	Ahrens et al., 2013
<i>Tg(s1020t):gal4</i>	<i>Et(-0.6hsp70l:Gal4-VP16)s1020t</i>	Motor neurons, CSF-cNs, VeLDs	Scott et al., 2007
<i>Tg(pkd211:gal4)</i>	<i>Tg(pkd211:gal4)icm10</i>	CSF-cNs	Fidelin et al., 2015
<i>Tg(pvalb6):gal4</i>	<i>Tg(pvalb6):gal4</i>	ventral CSF-cNs	Isaac Bianco and Florian Engert, <i>unpublished</i>
<i>Tg(UAS:GCaMP5G)</i>	<i>Tg(UAS:GCaMP5G)icm08</i>	N/A	Fidelin et al., 2015
<i>Tg(UAS:ChR2-mCherry)</i>	<i>Tg(UAS:Cr.ChR2_H134R-mCherry)</i>	N/A	Schoonheim et al., 2010
<i>Tg(UAS:mCherry)</i>	<i>Tg(UAS:mCherry)</i>	N/A	Herwig Baier lab, <i>unpublished</i>

Generation of transgenic lines

The *pkd211*^{-/-} mutant was generated by Lydia Djenoune and Andrew Prendergast, methods are adapted from Böhm et al., 2016.

To generate the Tg(*pkd211*:GCaMP5G)*icm10* transgenic line expressing the GCaMP5G reporter gene in *pkd211* expressing cells, we amplified 3.8kbp of genomic sequence immediately upstream of the predicted ATG site for the zebrafish *pkd211* gene (ENSDARG00000022503)¹³ as well as 630 bp of highly conserved DNA in intron 2. Both DNA fragments were then subcloned into the pT2KhspGFF plasmid using restriction digestion and T4 ligation. The 3.8 kb promoter region was cloned in place of the hsp promoter, while the intronic sequence was placed after the Gal4 stop codon and before the SV40 poly-A site. For establishing the Tg(*pkd211*:GCaMP5G)*icm07*, the same strategy was used by regular cloning with the PT2 vector containing the GCaMP5G construct.

RNA coding for each TALEN monomer (left arm target: 50-TGAGAAAGGATACAAAAG-30; right arm target: 50-TTGAG ATTTGCTTTGACG-30) was synthesized by the mMessage mMachine in vitro transcription kit (Invitrogen) and injected into *Tg(pkd211:GCaMP5G)icm07* embryos at the one-cell stage. Injected embryos were pooled and a crude DNA extract was harvested. A DNA cassette containing the target site was amplified by PCR (primers: 50-AGGGCAAGAGAATGGCAAGACG-30 and 50-TGTGTGCTA GGACTGTGGGG-30), and the resulting band was digested by SacI (Roche) to confirm disruption of the TALEN site. The mutant alleles were cloned by TOPO cloning (Invitrogen) and sequenced to determine the exact nature of the mutations. The *pkd211*^{*icm02*} mutant allele is an 8 bp deletion in exon 2 causing a β 1 frameshift that terminates in a stop codon within 35 amino acids of the substitution, upstream of the first transmembrane domain of Pkd211. All analysis was performed blind to genotype, which was only assayed at the conclusion of each experiment.

Coiling Assay in *pkd211* ^{-/-}

Heterozygotes for *pkd211* were crossed together to obtain a mix of *pkd211*^{+/+} *pkd211*^{+/-}, and *pkd211*^{-/-} offspring. Coiling was evaluated blindly at 24 hpf for 2 minutes. Embryos were genotyped following experiments. All images were obtained using a uEye camera (IDS Imaging Development Systems GmbH, Obersulm, Germany).

Preparation of embryos or larvae for calcium imaging

Tg(pkd211:GCaMP5G); pkd211^{+/-} adults were crossed to obtain *pkd211*^{+/+} *pkd211*^{+/-}, and *pkd211*^{-/-} offspring from 24 hpf to 5 dpf. Embryos or larvae were anesthetized in 0.02% MS 22 and mounted laterally in 1.5% low melting point agarose in glass-bottomed dishes filled with fish facility water. Once embedded in agarose, approximately 2 nl of 0.5 mM α -Bungarotoxin (Tocris, Bristol, UK) was injected inn the caudal ventral axial musculature to induce paralysis.

Multiday calcium imaging

Embryos and larvae were imaged between segments 5-12 using an upright microscope (Examiner Z1, Zeiss, Germany) with a spinning disk head (CSU-X1, Yokogawa), and a modular laser light source (3i Intelligent Imaging Innovations, Inc., Denver, Colorado, USA, Examiner Z1, Zeiss, Germany) using a long distance water-immersion 20X objective (Zeiss, NA=1). Calcium transients were acquired from GCaMP5G expressing CSF-cNs at 4Hz using Slidebook software (3i Intelligent Imaging Innovations, Inc., Denver, CO, USA) and reconstructed online using Fiji (fiji.sc/). All experiments were performed blind; embryos and larvae were genotyped following experiments.

Quantification

For analysis, ROIs were selected manually based on maximum z-projections. Analysis of $\Delta F/F$ was calculated using custom scripts written in MATLAB (The Mathworks, Natick, MA, USA). Photobleaching was corrected for all calcium traces by fitting a polynomial decay function. The baseline F_0 was manually selected based on periods of time with low spontaneous activity. $\Delta F/F$ for each ROI was calculated as $\Delta F/F = (F(t) - F_0) / F_0$ from the adjusted trace. To estimate the contribution of background fluorescence to the calculated signal, ROIs from the dorsal spinal cord that did not have GCaMP labeled cells were selected from twenty traces and averaged. Cross-correlation between ROI was performed in MATLAB (The Mathworks, Natick, MA, USA) with the *xcorr* function, which measures the similarity between one time sequence and shifted (time-lagged) copies of a second time sequence as a function of the lag.

Integral analysis

Due to unstable baselines due to high levels of activity, calcium traces were additionally corrected by identifying minima along the calcium trace using an open-source signal processing toolbox (<https://terpconnect.umd.edu/~toh/spectrum/PeakFindingandMeasurement.htm>.) A second degree polynomial function was fitted to thresholded minima on the $\Delta F/F$ trace, and then integral $\int \Delta F/F$ was calculated based on this corrected $\Delta F/F$ trace using a trapezoidal integral approximation. $\Delta F/F$ for all ventral or dorsal ROIs were averaged per embryo or larvae for comparison (**Figure**).

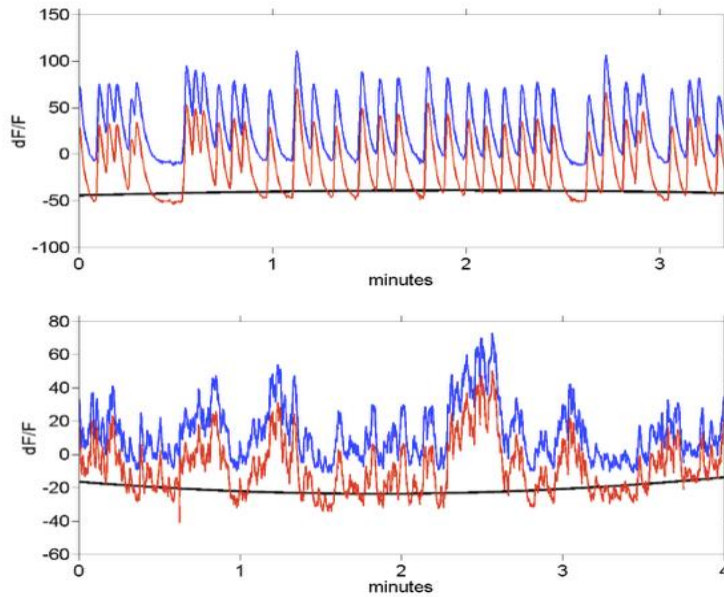


Figure. Baseline correction for calcium imaging integral quantification

Traces in red are $\Delta F/F$ based on raw fluorescence values. The black line indicates a second-degree polynomial fit to thresholded minima on the red trace. The blue trace represents correlated $\Delta F/F$ from which the integral was calculated.

Pharmacology

24 hpf *Tg(s1020t:gal4:UAS:GCaMP5G)* or *Tg(pkd211:GCaMP5G)* embryos were prepared as described above (preparation for calcium imaging) Following a four minute baseline recording, embryos were injected in the yolk sac with approximately 3 nl of 500 μ M TTX or artificial CSF artificial CSF (concentrations in mM: 134 NaCl, 2.9 KCl, 1.2 MgCl₂, 10 HEPES, 10 glucose, 2 CaCl₂; 290 mOsm \pm 3 mOsm, pH adjusted to 7.8 with NaOH). Post-injection recordings were recording after 15-30 minutes.

Immunohistochemistry

Immunohistochemistry was performed in *pkd211^{+/+} pkd211^{+/-}*, or *pkd211^{-/-}* embryos and larvae that were also *Tg(pkd211:GCaMP5G)*. Embryos and larvae were all stained for GFP plus either 5-HT or GABA. Imaging was performed on an upright laser scanning confocal Olympus FV-1000 microscope (PICPS, ICM).

5-HT: Embryos and larvae from 24 hpf to 3 dpf were fixed in 4% PFA, 1% DMSO prior to incubation in 50mM of glycine in 0.1% PBS-Triton X-100 (PBSTx). Following blocking for 2 hours in 1% DMSO, 1% NGS, 1% BSA, and 0.7% Triton X-100, the primary antibody was applied (rabbit anti-5-HT, 1:2000, provided by Dr. Steinbusch, Maastricht University, Netherlands; chicken anti-GFP, 1:500, Abcam, Cambridge, UK) in blocking buffer overnight at 4°C. Following washing, Alexa- conjugated secondary antibodies IgG (1:500, Invitrogen, Carlsbad, CA, USA) were applied in blocking buffer overnight at 4°C. 3 dpf larvae were treated prior to staining with For IHC at 3 dpf, 30% sucrose was added in fixation solutions, and prior to staining, larvae were treated with 0.2mg/ml collagenase in PBS for 5min and the skin was removed with forceps to increase permeabilization.

GABA: Larvae at 3 dpf were fixed in 4% PFA, 0.1% glutaraldehyde, and 30 % sucrose, then the skin was removed. Larvae were dehydrated stepwise in increasing concentrations of methanol, incubated at -20°C for at least 2 hours, then rehydrated step-wise. Larvae were digested with 0.5U/mL dispase (Invitrogen, Carlsbad, CA, USA) in PBS-Tween for 72 hours. Following blocking in 1% DMSO/2% BSA/5% NGS/PBS-Tween, larvae were incubated overnight in the primary rabbit anti-GABA antibody at 4°C (1:2000, Sigma-Aldrich A2052, St. Louis, MO, USA; chicken anti-GFP, 1:500, Abcam, Cambridge, UK) in blocking solution. Larvae were incubated with Alexa conjugated secondary antibodies overnight at 4°C (1:500, Invitrogen, Carlsbad, CA, USA).

Electrophysiology

Embryos or larvae were anesthetized in 0.02% MS-222 dissolved in aCSF (concentrations in mM: 134 NaCl, 2.9 KCl, 1.2 MgCl₂, 10 HEPES, 10 glucose, 2 CaCl₂; 290 mOsm +/- 3 mOsm, pH adjusted to 7.8 with NaOH), then pinned to a Sylgard-lined dish with 0.025 mm diameter tungsten wires inserted in the notochord and paralyzed by injection into

caudal axial muscle with 0.5 mM α -Bungarotoxin (Tocris, Bristol, UK). A region of 2-3 segments was dissected, skin and muscle were removed by gentle suction. Patch clamp electrodes (6-10 M Ω resistance) were pulled from borosilicate glass (World Precision Instruments, USA) using a P-1000 micropipette puller (Sutter Instruments, USA).

For loose patch recordings, electrodes were filled with aCSF and low resistance seals of 15-35 M Ω were obtained to extracellularly observe cell firing. When loose-patch recordings were coupled with calcium imaging. *Tg(pkd211:GCaMP5G)* embryos of 25-27 hpf were used, and experiments were acquired with using a MultiClamp 700A amplifier, a Digidata series 1322A Digitizer, and pClamp 8.2 software (Axon Instruments, Molecular Devices). Calcium imaging was performed as described above (Multiday calcium imaging).

For whole cell recordings of CSF-cNs, patch clamp electrodes (6-10 M Ω resistance) were pulled. Experiments were performed in *Tg(pkd211:gal4: UAS:mCherry)* or *Tg(pvalb6:gal4); UAS:mCherry* for ventral CSF-cNs, *Tg(pkd211:gal4: UAS:mCherry)* or *Tg(olig2:dsred)* for dorsal CSF-cNs. For motor neuron recordings at 3 dpf, higher resistance electrodes (8-13 M Ω resistance) were used. Patch electrodes were filled with intracellular solution (concentrations in mM: K-gluconate 115, KCl 15, MgCl₂ 2, Mg-ATP 4, HEPES free acid 10, EGTA 0.5, 290 mOsm, adjusted to pH 7.2 with KOH, Alexa 488 added to 5 mM final concentration). Liquid junction potential was calculated to be -19 mV and corrected for analysis.

Whole cell recordings were obtained with a MultiClamp 700B amplifier, a Digidata series 1440A Digitizer, and pClamp 10.3 software (Axon Instruments, Molecular Devices 446 Sunnyvale, CA, USA). Raw signals were acquired at 15 kHz and low-pass filtered at 10 kHz. Analysis of electrophysiological data was performed offline using Clampex 10 software (Molecular Devices, California, USA) or MATLAB (The Mathworks, Natick, MA, USA).

To identify single channel events in whole cell recordings, cells were held in gap-free voltage clamp configuration at -85 mV. Events were segregated into those lasting less than

1.5 ms or longer than 2 ms because events shorter than 2 ms had highly variable currents associated with partial channel opening. A manual threshold was used to determine the amplitude of a single channel opening based on visualization. Initial channel opening frequency was based on an arbitrary 20 s window of a gap-free voltage clamp recording at least 1 minute after breaking into the cell.

Evaluation of monosynaptic connection between CSF-cNs and CaP PMNs in *pkd211*^{-/-}

Homozygous *pkd211*^{-/-} adults were incrossed to obtain *pkd211*^{-/-} offspring. In order to sparsely label CSF-cNs with ChR2, fertilized embryos were injected with DNA constructs *pkd211:gal4* and *UAS:ChR2-mCherry* at the single-cell stage at 25 ng/ul. Larvae were screened at 3 dpf for ChR2-mCherry⁺ CSF-cNs with an axon that formed a basket-like structure midway along the dorsoventral axis, suggestive of the CSF-cN-CaP connection. Whole cell recordings of CaPs were performed as described above. Activation of CSF-cNs was achieved by whole field stimulation through a 40x objective for 5 ms with a blue LED (UHP-Mic-LED-460, Prizmatix Ltd., Israel, power = 3.88 mW/mm²) through a digital micro mirror device with all mirrors in the "on" position (described in Chapter 2). All experiments were run as a set of ten trials. Two sets of experiments were performed for each cell.

CSF-flow stimulus

For testing the response of CSF-cNs to flow in the central canal, 26-29 hpf *Tg(pkd211:GCaMP5G)* embryos were prepared as for electrophysiology: embryos were anesthetized in 0.02% MS-222 dissolved in aCSF (concentrations in mM: 134 NaCl, 2.9 KCl, 1.2 MgCl₂, 10 HEPES, 10 glucose, 2 CaCl₂; 290 mOsm +/- 3 mOsm, pH adjusted to 7.8 with NaOH), then pinned through the notochord to a Sylgard-lined dish with 0.025 mm diameter tungsten wires and paralyzed by injection into caudal axial muscle with 0.5 mM α -

Bungarotoxin (Tocris, UK). A region of 2-3 segments was dissected, skin and muscle were removed by gentle suction. A patch pipette (3-5 M Ω) connected to a pico-spritzer was filled with aCSF and inserted into the central canal. Visualization of a 300 ms stimulus at 5 psi confirmed that the flow was contained in the central canal. Each stimulus comprised a 300-500 ms long stimulus applied with a pressure of 5-10 psi. Experiments were performed as sets of three stimuli with twenty second intervals between stimuli. Calcium imaging was performed with an EM-CCD camera (Hamamatsu Photonics, Japan), and images were acquired at 10 Hz using a custom script (Urs Böhm) written in LabVIEW (National Instruments, USA). The stimulus and calcium imaging were triggered and synchronized via pClamp 10.3 software (Axon Instruments, Molecular Devices, USA). Analysis of calcium transients was performed offline as described above. Peak $\Delta F/F$ was the maximal value in the five frames following the end of the stimulus. For each acquisition, a background ROI was used to estimate contribute of out-of-focus signals to the change in fluorescence. On average, these signals represented approximately 5% $\Delta F/F$.

Dual color two-photon imaging

27-30 hpf embryos were embedded in agar as described above in either a dorsal or lateral orientation. Calcium imaging was performed on a two-photon microscope (2p-*vivo*, Intelligent Imaging Innovations, Inc., USA) using a 20x objective. Images were acquired at 6.5 Hz. Regions of interest around CSF-cN cell bodies expressing both GCaMP5G and tagRFP were manually defined in MATLAB (The Mathworks, UAS). To correct for motion artifacts due to muscle contraction-related motion, the ratio of the GCaMP and the tagRFP signal ($\Delta R/R$) was calculated. Maximum $\Delta R/R$ for each ROI was calculated following the return of the cell to its initial position prior to muscle contraction in the 10 frames following the end of the contraction.

I. Characteristics of spontaneous activity during early development

Previous studies in zebrafish described in detail rhythmic oscillations that underlie coiling behavior occurring from 17-25 hpf (Saint Amant and Drapeau, 1998; Saint Amant and Drapeau, 2000; Warp et al., 2012). Motor neurons and early born interneurons that will become part of the CPG network to generate locomotion in the spinal cord integrate into a gap junction coupled network driven by glutamatergic descending interneurons in the hindbrain and rostral spinal cord (Saint Amant and Drapeau 2001; Tong and McDearmid, 2012). At these stages, activity is restricted to ventrally-located cells that participate in the rhythmic coiling network (**Figure 1A**). The electrophysiological signature is periodic inward currents and synaptic bursts (**Figure 1B**). These oscillations require gap junction coupling (**Figure 1C**). GABAergic and *pkd211*⁺ CSF-cNs are present at this stage but were presumed to be silent, likely because access to these cells for electrophysiological recording is difficult as they are medially located in the spinal cord around the viscous central canal and the ventral longitudinal axonal fasciculus.

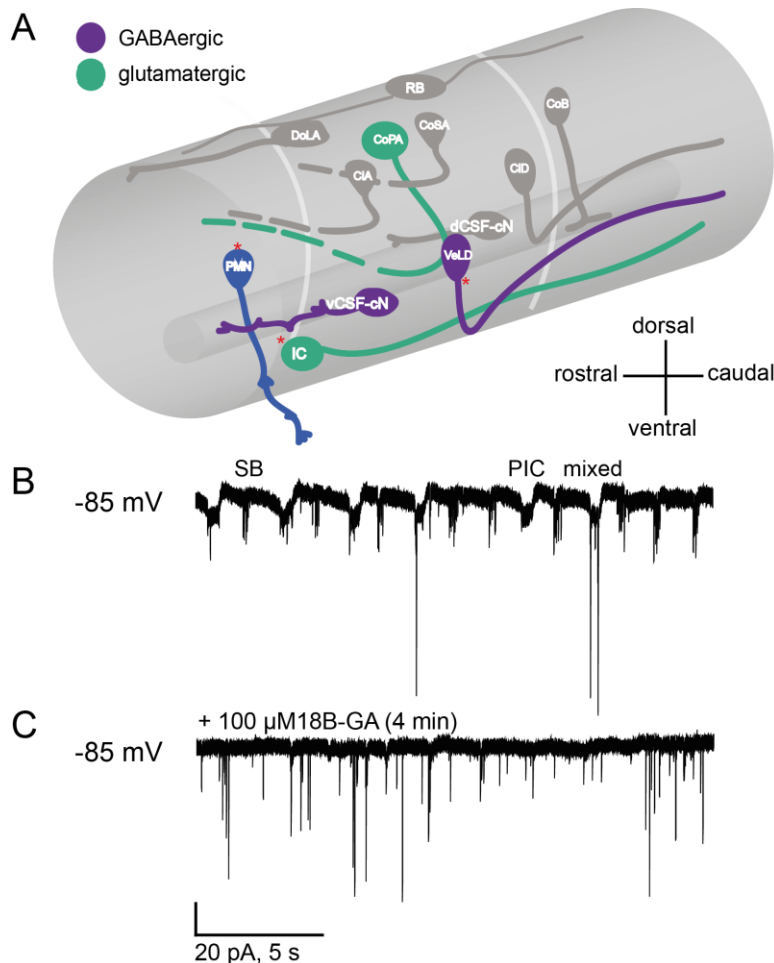


Figure 1. Rhythmic embryonic activity in the zebrafish spinal cord.

(A) Schematic of interneurons and motor neurons present in the spinal cord at 1 dpf. Red asterisks indicate neurons that are always rhythmically active: pacemaker IC cells, primary motor neurons, and GABAergic VeLDs. Neurons in gray are inactive at the earliest stages when coiling appears. All neurons in gray except for DoLAs and RBs incorporate into the rhythmic circuit after coiling has begun (Adapted from Lewis and Eisen, 2003 and Goulding 2009). (B) Electrophysiological signature of embryonic activity at 27 hpf. Periodic inward currents (PIC) are low amplitude, long duration inward current steps following by smaller short duration outward currents. Synaptic bursts (SB) are large and fast individual current events that do not generate action potentials, which are a correlate of contralateral depolarization. Mixed glutamatergic/glycinergic events begin to occur from 23-24 hpf and are present in all motor neurons from 26-30 hpf (Knogler et al., 2014) (C) Rhythmic activity is abolished by application of gap junction blocker, 18 β -glycyrrhetic acid.

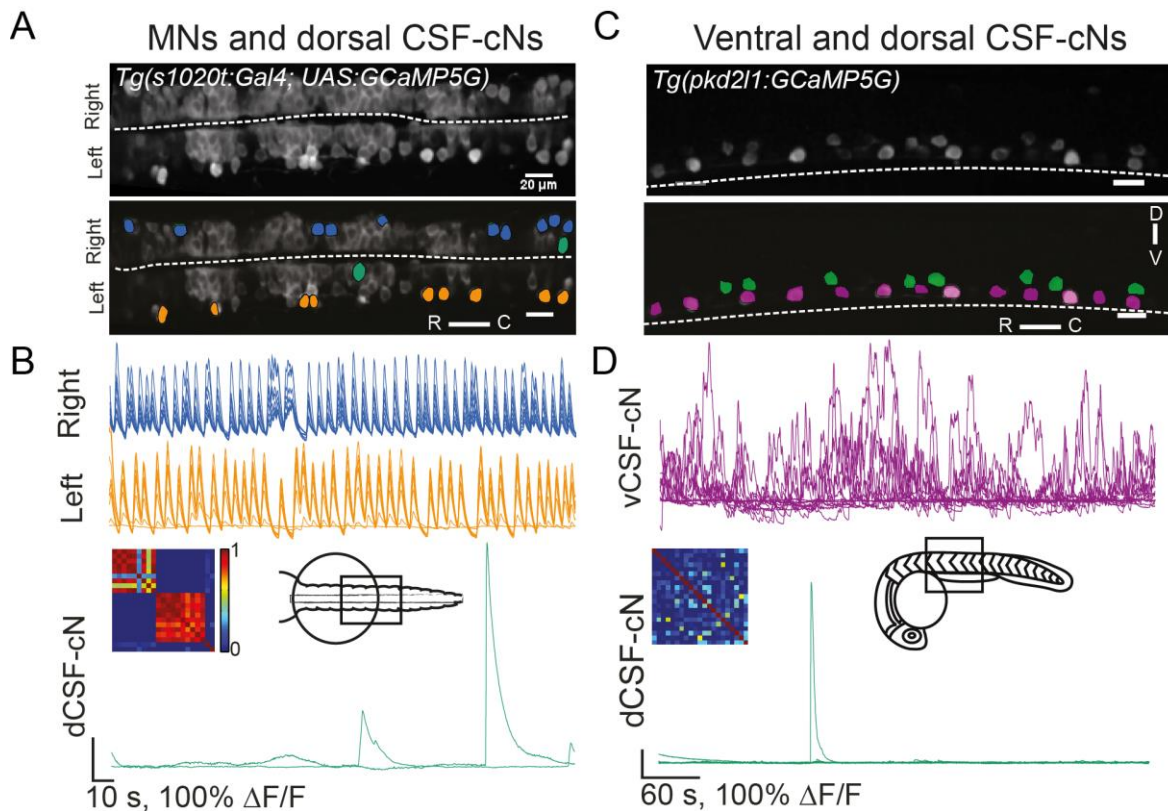


Figure 2. Spontaneous activity in spinal cord neurons of zebrafish embryos at 24 hpf.

(A) Dorsal view of motor neurons and dorsal CSF-cNs are labeled in *Tg(s1020t:gal4; UAS:GCaMP5G)* at 24 hpf. Top: Z-projection between spinal cord segments 7 and 11. Bottom, same image with ROIs selected for calcium imaging analysis superimposed. Blue ROIs are motor neurons on the right hemicord, orange ROIs are motor neurons on the left hemicord, and green ROIs are putative dorsal CSF-cNs, identified by their medial location. (B) $\Delta F/F$ and cross-correlation for ROIs shown in A. Motor neurons oscillate and mostly alternate between the left and right sides (top). A subset of dorsal CSF-cNs is active but do not generate rhythmic oscillations. Motor neuron activity is highly correlated along one hemicord, CSF-cNs are not correlated. The schematic shows a dorsal view of an embryo and the imaging region. (C) Lateral view of CSF-cNs, all labeled in *Tg(pkd211:GCaMP5G)* (top). Ventral CSF-cNs are magenta ROIs, dorsal CSF-cNs are green (bottom). (D) $\Delta F/F$ and cross-correlation for ROIs in C. Ventral cells are highly active and uncorrelated. Schematic shows the lateral region of interest in a 24 hpf embryo. Scale in A and C is 20 μ M.

Dorsal CSF-cNs, VeLDs and motor neurons are labeled at the embryonic stage in the transgenic enhancer trap line *Tg(s1020t:gal4)* (Warp et al., 2012). A previous study reported that a small subpopulation of medially-located putative CSF-cNs appeared to be active when this population was imaged with the genetically-encoded calcium indicator GCaMP3 (Warp et al., 2012). Calcium imaging in *Tg(s1020t:Gal4; UAS:GCaMP5G)* at 24 hpf confirmed that these few CSF-cNs did not participate in the rhythmic network, and their activity did not correlate with motor neurons or each other (**Figure 2A-2B**). In order to characterize better this sparse activity, I performed calcium imaging at 24-25 hpf in a transgenic line labeling all CSF-cNs *Tg(pkd211:GCaMP5G)* (Böhm et al., 2016; Annex 2). Imaging laterally to identify ventral versus

dorsal CSF-cNs, a few dorsal CSF-cNs displayed rare calcium transients. Surprisingly, ventral CSF-cNs, not labeled in the *Tg(s1020t:gal4)* enhancer trap line displayed massive, uncorrelated, and long-lasting calcium transients in almost all neurons at 24-25 hpf (**Figure 2C-2D**).

In other experiments at larval stages, CSF-cNs did not appear to be active, so we asked whether this activity was restricted to early development and could reflect spontaneous network activity. To address this question, we imaged CSF-cNs in the *Tg(pk211:GCaMP5G)* daily from 1-5 dpf, stages during which embryonic behavior transitions to more mature larval locomotor networks, and CSF-cNs develop the morphology of a pear-shaped cell body with a brush of microvilli that extends into the central canal (**Figure 3A-3B**). Although spontaneous activity overall increased between embryonic (from 2 dpf) and larval stages, a period during which the transition to mature swimming occurs, the highest level of activity was restricted to the ventral CSF-cN population at 1 dpf (**Figure 3C**).

All CSF-cNs express *pk211* from 18 hpf (Djenoune et al. 2014), when spontaneous activity in the spinal cord starts, therefore we asked whether this channel contributes to this embryonic activity. I took advantage of a *pk211*^{-/-} mutant generated in the lab (Böhm et al., 2016) to test whether spontaneous activity was affected in CSF-cNs lacking Pkd211 (**Figure 4**). Activity was almost completely abolished in ventral cells at 1 dpf when dorsal CSF-cN activity was already low (**Figure 4A-4C**). Activity in both ventral and dorsal CSF-cNs increased in wild type larvae by 4 and 5 dpf, when larvae can execute mature swim bouts (**Figure 4C**). This activity was significantly reduced in the *pk211*^{-/-} mutant in ventral and dorsal CSF-cNs at 4 and 5 dpf (**Figure 4A-4B**). In both ventral and dorsal CSF-cNs, correlated activity between cells occurred in approximately 15% of fish from embryonic to larval stages (**Figure 5A, Table**). A small level of activity remained in the *pk211*^{-/-} mutant, which mostly occurred in the context these correlated events between CSF-cNs (**Figure 5B, Table**).

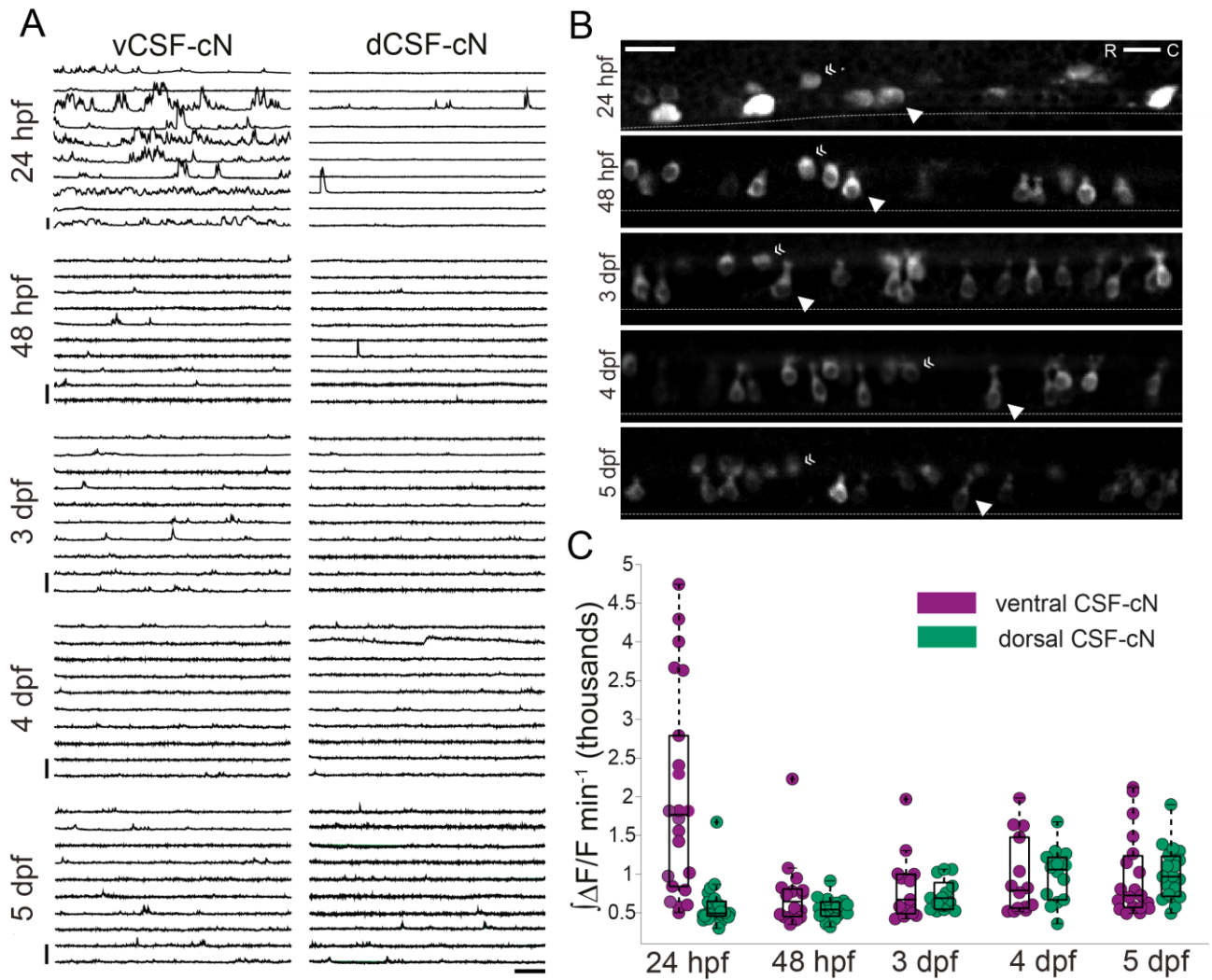


Figure 3. Spontaneous activity of CSF-cNs from embryonic to larval stages.

(A) Mean $\int \Delta F/F$ ten traces taken from ROIs from wild type embryos or larvae from 1 to 5 dpf. Scale is 100% $\int \Delta F/F$ (vertical) and 30 s (horizontal). (B) Representative examples of imaging planes of *Tg(pkd211:GCaMP5G)* for calcium imaging from 1 to 5 dpf. Each image is a lateral view maximum z-projection of the spinal cord taken from a subset of frames from one recorded embryo or larvae. Solid arrows indicate a characteristic ventral CSF-cN, double arrowheads indicate dorsal CSF-cN. Dotted lines demarcate the ventral limit of the spinal cord. Scale is 20 μm . (C) Quantification of $\int \Delta F/F$ from 1 to 5 dpf. Each point represents the average value for all ROIs from one embryo or larvae per minute, n fish = 22 (24 hpf), 16 (48 hpf), 13 (3 dpf), 14 (4 dpf), 19 (5 dpf). The central line on each boxplot indicates the median, the bottom and top edges indicate the 25th and 75th percentiles, respectively. The whiskers extend to the most extreme points not considered outliers, and the outliers are demarcated by a '+' symbol.

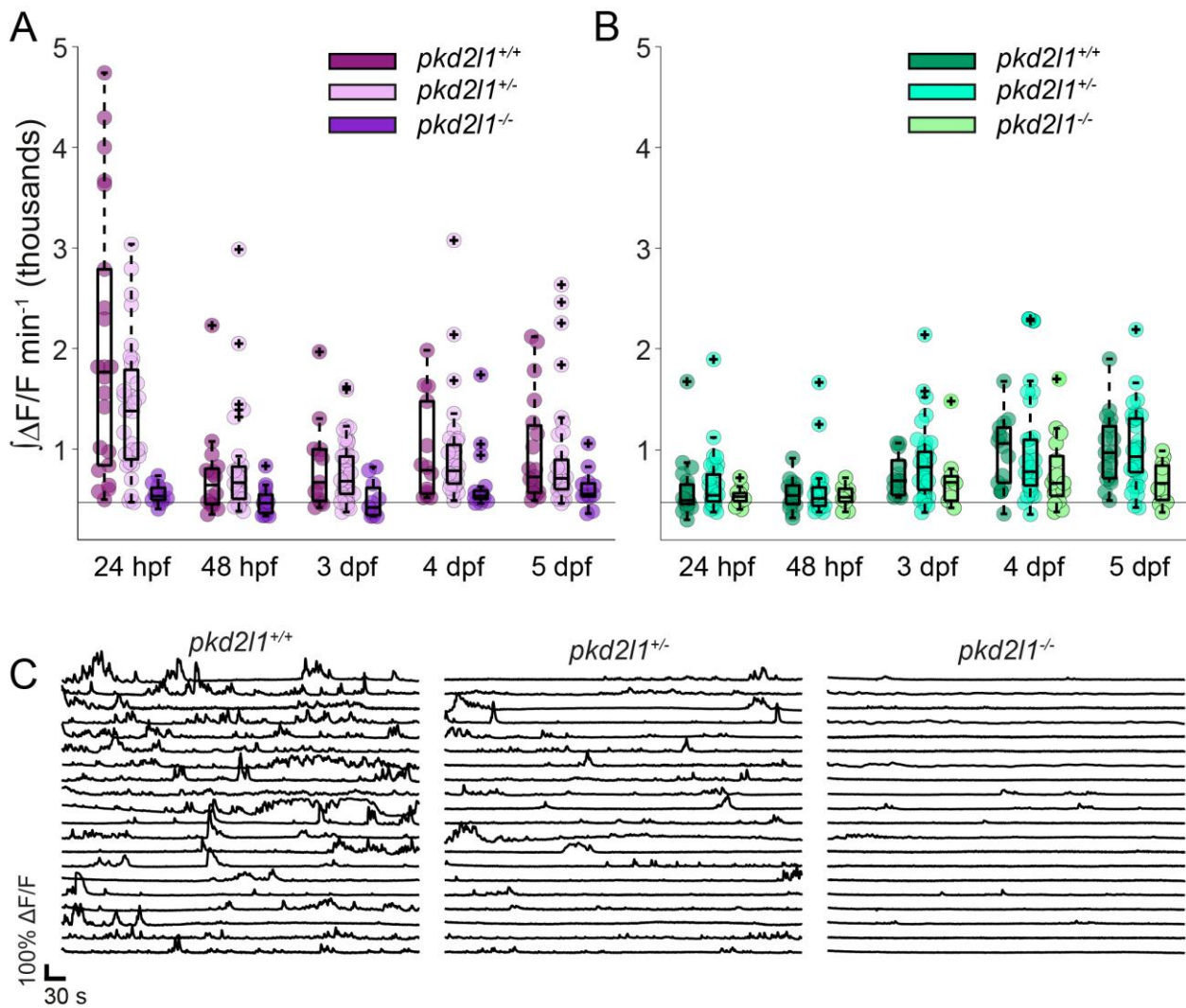


Figure 4. Spontaneous activity is lost in a *pkd211* mutant.

(A) Quantification of calcium activity from 1 to 5 dpf in ventral CSF-cNs of *pkd211*^{+/+}, *pkd211*^{+/-}, or *pkd211*^{-/-}; *Tg(pk211:GCaMP5G)* embryos or larvae. Each point represents the average activity of all ROIs from one embryo or larvae. All values are normalized to one minute. (B) Same as (A) for dorsal CSF-cNs. (C) Mean twenty $\Delta F/F$ traces taken from ROIs from wild type or mutant embryos or larvae for each developmental stage. For (A) and (B) Each point represents the average value for all ROIs from one embryo or larvae per minute, n fish (from left to right) = 22, 32, 12, 16, 28, 15, 13, 43, 11, 14, 34, 17, 19, 37, 12. The gray line horizontal line reflects the average background signal taken from one ROI within the dorsal spinal cord from twenty unique traces. The central line on each boxplot indicates the median, the bottom and top edges indicate the 25th and 75th percentiles, respectively. The whiskers extend to the most extreme points no considered outliers, and the outliers are demarcated by a '+' symbol. Effects of ventral versus dorsal, interaction between genotype, developmental stage, and interfish variability were evaluated with linear mixed effects analyses. Dorsal cells have significantly less activity than ventral cells in wild type fish at 24, 48 hpf, and 3 dpf ($p < 0.001$) but not 4 or 5 dpf. *pkd211*^{-/-} mutants have significantly reduced activity in ventral and dorsal cells (considered independently) at 24 and 48 hpf compared to wild type fish ($p < 0.05$). Overall activity (considering ventral and dorsal cells together) is decreased between wild type and *pkd211*^{-/-} mutants at all stages ($p < 0.05$).

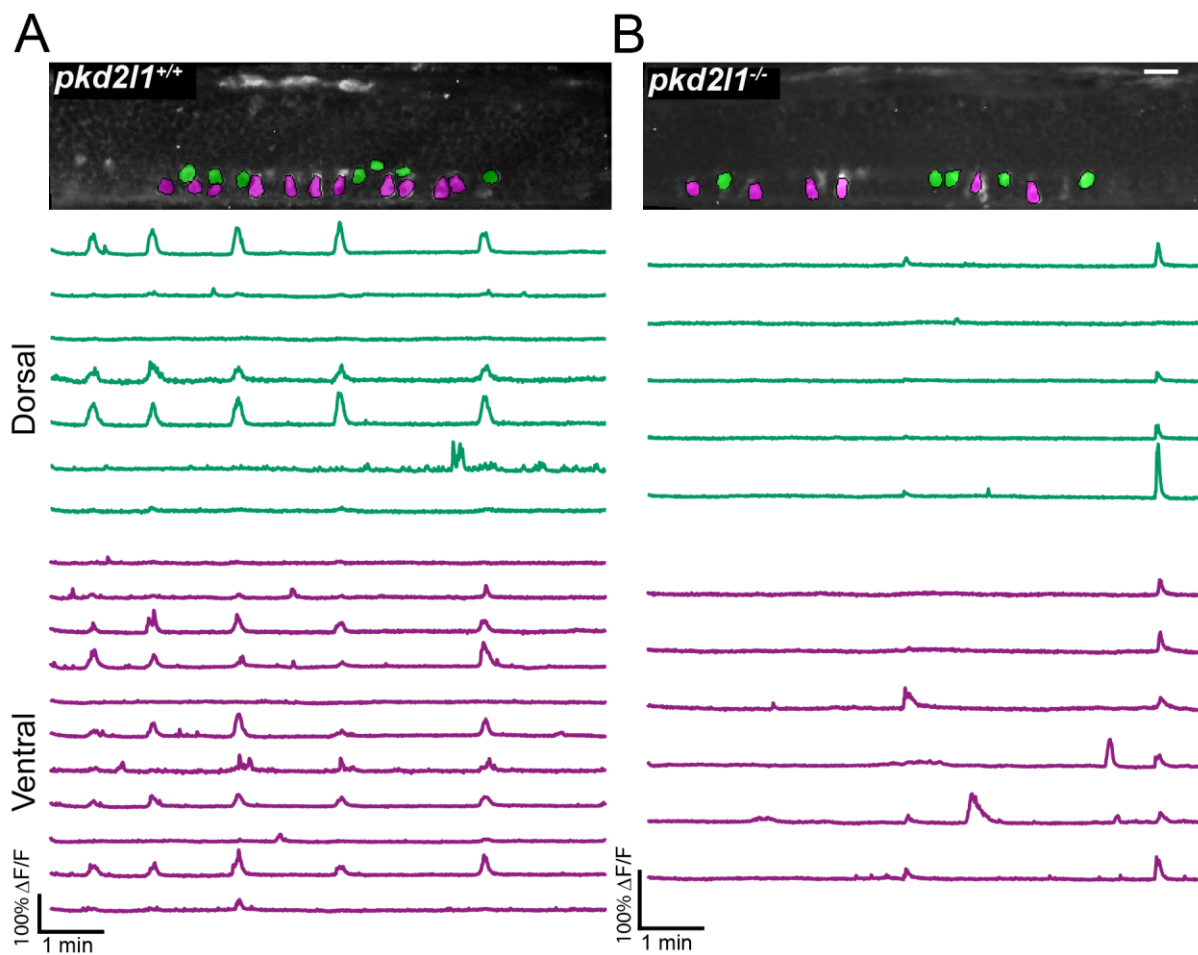


Figure 5. Correlated activity across CSF-cNs occasionally occurs.

Example calcium traces from 48 hpf wild type (A) and *pkd211*^{-/-} mutant (B) embryos. Top: Lateral view of ROI selection for CSF-cNs labeled in *Tg(pkd211:GCaMP5G)*. Dorsal CSF-cNs are indicated in green. Ventral CSF-cNs are indicated in magenta. Rostral is to the left. Scale is 20 μ M. Bottom: spontaneous calcium activity for selected ROIs.

Table. Correlated activity in CSF-cNs occurs across developmental stages.

Developmental stage	Number of fish showing correlated events between at least 3 cells (n = 40 for each stage)	<i>pkd211</i> ^{+/+}	<i>pkd211</i> ^{+/-}	<i>pkd211</i> ^{-/-}
24 hpf	8	3	4	1
48 hpf	5	3	1	1
3 dpf	6	1	4	1
4 dpf	7	2	3	2
5 dpf	6	2	3	1

II. Evaluation of developmental effects due to loss of activity

Calcium transients in GABAergic CSF-cNs predominated at embryonic stages during which the spinal cord has a high level of spontaneous network activity (**Figure 3A**) and was strongly reduced at embryonic and larval stages (**Figure 4A-4C**). Therefore, this activity could potentially contribute to development of a functional locomotor network. CSF-cNs project axons ipsilaterally and rostrally and express GABA from as early as 18 hpf (Djenoune et al., 2014, Bernhardt et al., 1992). GABA is known to play important roles in activity-dependent development, and GABA release also contributes to setting the excitability of oscillating networks to set frequency of oscillation, entraining a clock for developmental timing (Barbin et al., 1993; Represa and Ben-Ari, 2005; Kastanenka and Landmesser, 2013). We therefore postulated that early GABAergic release by CSF-cNs may contribute to proper development of the spinal cord or setting oscillation frequency for the developing motor network. GABA can be excitatory or shunting at early stages because chloride exporter KCC2 is only expressed starting at 2 dpf (Ben-Ari, 2002; Reynolds et al., 2008), and GABA release could condition the excitatory of the spinal cord, affecting the frequency of oscillations. In zebrafish, GABA does not drive spontaneous oscillations of motor neurons and other CPG neurons at embryonic stages (Saint Amant and Drapeau, 2000). However, GABA release could have an impact on neurotransmitter phenotype, number of CSF-cNs, development of synaptic connections, expression of neuropeptides, or neuron morphology.

To investigate whether the frequency of motor network oscillations was altered by CSF-cN activity, we assessed coiling frequency when synaptic release was silenced (**Chapter 2**) or in the *pkd2l1*^{-/-} mutant. Coiling was unaffected in both conditions. Wild type embryos performed coiling behavior at 0.58 Hz on average (n = 7 embryos), and similarly *pkd2l1*^{-/-} mutants coiled at 0.57 Hz (n = 6 embryos, p > 0.05, unpaired t-test).

Activity was lost in the *pkd2l1*^{-/-} mutant (**Figure 4**), and this loss of activity may affect development of the spinal cord. We performed morphology and axonal trajectory analysis,

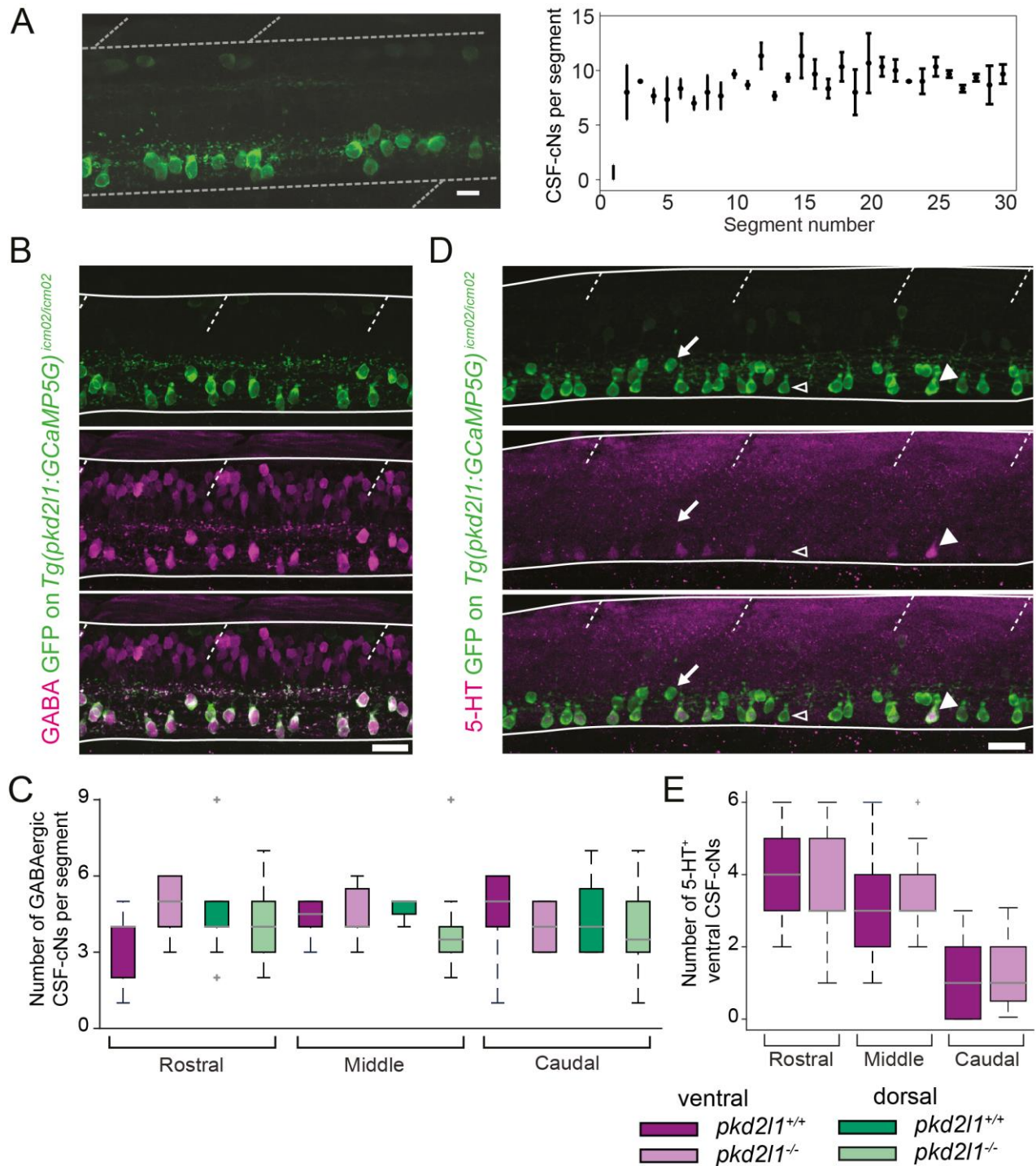


Figure 6. Pkd211 is not required for neurotransmitter specification or differentiation of CSF-cNs.

(A) Quantification of CSF-cNs in wild type larvae at 3 dpf. Cells were counted in *Tg(pkcd211:GCaMP5G)*, which labels all CSF-cNs (Annex 2). Scale is 10 μ m. (B) Immunohistochemistry for GABA and GFP in *pkd211*^{-/-} at 3 dpf. GFP staining shows CSF-cNs labeled in *Tg(pkcd211:GCaMP5G)* (top), GABA⁺ neurons (middle), and the merged image (bottom). Scale is 20 μ m. (C) Quantification of GABA⁺ CSF-cNs in rostral (segments 3-6), mid-cord (segments 10-13), or caudal (segments 23-26) regions of the spinal cord in the *pkd211*^{-/-} mutant. n = 40 segments counted from 5 *pkd211*^{-/-} larvae and n = 9 segments from 2 control larvae. (D) Immunohistochemistry for 5-HT and GFP in the *pkd211*^{-/-} mutant at 48 hpf. GFP staining shows CSF-cNs labeled in *Tg(pkcd211:GCaMP5G)* (top), 5-HT⁺ neurons (middle), and the merged image (bottom). Scale is 20 μ m. (E) Quantification of 5-HT⁺ CSF-cNs in the *pkd211*^{-/-} mutant. n = 30 segments from 4 control or mutant embryos. p > 0.05 for comparisons between wild type and mutant, Student's t-test.

analysis of neurotransmitter phenotype, quantification of CSF-cNs, and evaluation of synaptic connections with whole cell patch clamp recordings. CSF-cNs retained their standard morphology and axonal projections (Annex 2). Reducing the amount of GABA releases could generate an imbalance in excitatory versus inhibitory populations, affecting the GABAergic phenotype or number of CSF-cNs or other neurons. At 3 dpf the larval spinal cord has 267 ± 8 CSF-cNs in wild type larvae (**Figure 6A**). CSF-cNs retained their GABA expression (**Figure 6B-6C**) at 3 dpf showing comparable numbers with wild type larvae.

Serotonin transient expression is a feature of developing neural networks and is thought to contribute to proper development of neuronal circuits (Gaspar et al., 2003). CSF-cNs show transient serotonin expression (Montgomery et al., 2015; Annex 2). Yet, loss of spontaneous activity did not affect CSF-cN serotonin expression (**Figure 6D-6E**). In addition to morphology and development of correct neurotransmitter phenotype, spontaneous network activity contributes to formation of functional synaptic connections (Gonzalez-Islas and Wenner, 2006). CSF-cNs form monosynaptic connections with CaP primary motor neurons, a single spike inducing large amplitude short latency inward currents in a connected CaP (Chapter 2; Hubbard et al., *in revision*), involved in producing fast swimming movements as well as MCoDs (Fidelin et al., 2015), excitatory interneurons active during slow swimming (McLean et al., 2008).

The connection between CSF-cNs and CaP primary motor neurons is restricted to ventral CSF-cNs. The ventral population is highly active at early stages, and this connection is both easily identified by the characteristic basket shape formed by the CSF-cN axon and is 100% reliable in wild type larvae ($n = 37$, **Chapter 2**; Hubbard et al., *in revision*). Therefore I decided to test whether loss of Pkd211 and loss of spontaneous activity disrupted this connection. In order to address this question, homozygous *pkd211*^{-/-} mutants were injected at the single-cell stage with constructs for *pkd211:gal4* and *UAS:ChR2-mCherry* DNA constructs to sparsely label CSF-cNs with ChR2-mcherry. Larvae were screened at 3 dpf for the basket shape indicative of CaP innervation, and ChR2-mediated activation of CSF-cNs was coupled with a whole cell patch clamp

recording of the CaP *in vivo* to evaluate the reliability of this connection (**Figure 7A-7B**). In both control and *pkd211*^{-/-} larvae, a single spike induced short latency inward currents of similar amplitude in the recorded CaP (**Figure 7D**). The CSF-cN-CaP connection displays short term plasticity, habituating in response to high frequency repeated stimuli (Hubbard et al., *in revision*), which is conserved in the *pkd211*^{-/-} mutant (**Figure 7E-7F**).

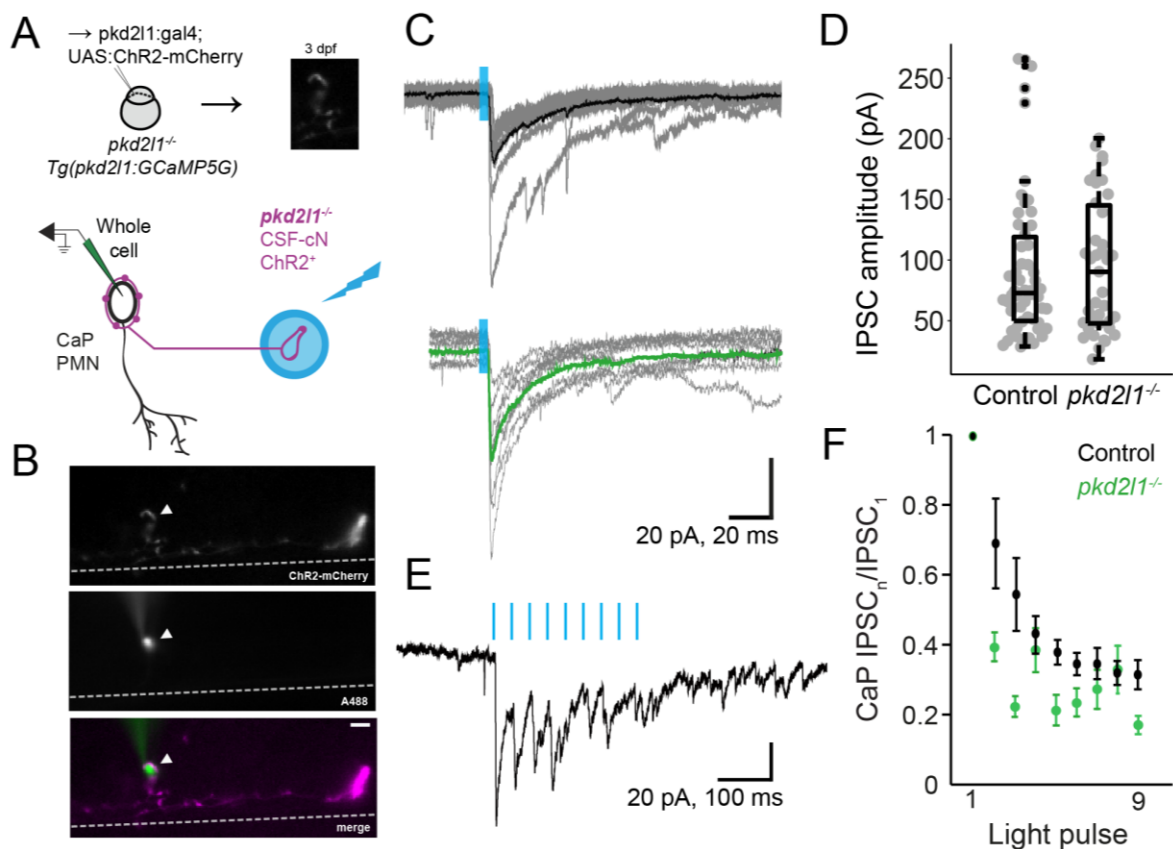


Figure 7. The monosynaptic connection from CSF-cNs on to CaP primary motor neurons is preserved in the *pkd211*^{-/-} mutant.

(A) Experimental Protocol. Fertilized *pkd211*^{-/-} homozygous mutant eggs were injected at the one cell stage with both *pkd211:gal4* and *UAS:ChR2-mCherry* DNA constructs. At 3 dpf, larvae were screened for CSF-cNs expressing ChR2-mCherry with the characteristic basket shape found around CSF-cN-innervated CaPs. Simultaneous optogenetic activation of CSF-cN was performed while performing whole-cell patch clamp recordings from the innervated CaP motor neuron. (B) Image of a CSF-cN expressing ChR2-mCherry with characteristic basket formed by CSF-cN axon onto CaP (top), Alexa-filled CaP (middle), merge (bottom). (C) Light-mediated activation of the CSF-cN induces a monosynaptic IPSC in the recorded CaP motor neuron in both control *pkd211*^{+/+} (top) and *pkd211*^{-/-} mutant (bottom). (D) Quantification of peak IPSC amplitude in control and *pkd211*^{-/-}. (E) The CSF-cN synapse onto CaP shows similar depression in *pkd211*^{-/-} and controls (5 ms pulses of blue light triggered at 30 Hz for 200 ms). Controls from C and D are reproduced from Chapter 2 results. Control in F represents larvae recorded from 3 to 7 dpf. Control data in F provided by Jeff Hubbard. $p > 0.05$, Student's t-test for (D).

Altogether, these results demonstrate that the *pkd211*^{-/-} mutant has preserved morphology, axonal trajectory, neurotransmitter phenotype, number of CSF-cNs, and synaptic connections. In addition to using the *pkd211*^{-/-} mutant to silence embryonic activity, we expressed botulinum neurotoxin in CSF-cNs to silence synaptic release (**Chapter 2**). Silencing synaptic release in a majority of CSF-cNs with genetically encoded botulinum neurotoxin did not affect coiling frequency or neurotransmitter phenotype of CSF-cNs and their putative synaptic partners (**Chapter 2, Figure 1, Supplemental Figure 2**). These results together suggest that the early spontaneous network activity of CSF-cNs during embryonic stages does not play a critical role in their development or development of functional spinal cord networks.

III. Spontaneous activity of CSF-cNs relies on Pkd211 channel activity.

Pkd211 conditions high activity at embryonic stages exclusively in ventral CSF-cNs (**Figure 3**). This activity related to Pkd211 appeared not critical for development, although some function may be compensated during development by the activity of other subpopulations of neurons. As the physiology of the PKD2L1 channel is complex (Clapham, 2003) and remains poorly understood, we investigated the role of this channel in driving spontaneous activity and sensory responses in CSF-cNs.

Although calcium imaging classically reflects spiking in response to varied stimuli, the diverse function of calcium within cells could hamper this analysis. Pkd211 forms heteromeric tetramers with a PKD1 partner in taste receptor cells in the mouse (Ishimaru et al., 2006), in primary cilia (Delling et al., 2013), and in CSF-cNs in the mouse (Petracca et al., 2016), which allows targeting of the channel to the plasma membrane (Murakami et al., 2005). However, this reports also demonstrated that Pkd211 can also form homomeric tetramers at the endoplasmic reticulum (Murakami et al., 2005), from which release of calcium could trigger calcium waves and calcium release that modulates excitability.

In order to determine the mechanisms underlying CSF-cN spontaneous activity, I used tetrodotoxin (TTX), a voltage-gated sodium channel blocker to silence synaptic activity systemically in the embryonic zebrafish and recorded calcium transients in either motor neurons of CSF-cNs using calcium imaging. TTX injected into the yolk effectively silenced motor neuron oscillations present at 24 hpf in *Tg(s1020t:gal4; UAS:GCaMP5G)* embryos (**Figure 8A-8C**), demonstrating effectiveness at embryonic stages. In *Tg(pkd211:GCaMP5G)* embryos, expressing GCaMP5G in CSF-cNs, the level of calcium activity in ventral CSF-cNs was significantly reduced but not abolished. (**Figure 8D-8G**). Control injections of artificial CSF into the yolk may also cause a decrease in the overall level of activity (**Figure 8F-8G**), possibly confounding interpretation of the absolute changes in calcium activity. These results indicate that TTX is effective as it silences motor neuron activity relying on TTX-sensitive sodium channels for generating spikes. In contrast, activity of CSF-cNs persists, indicating that the activity relies mainly on the Pkd211 channel and that sodium channels at most contribute to amplifying it.

If the spontaneous activity is intrinsic to CSF-cNs, the activity could reflect either action potentials or calcium-induced calcium release leading to high changes in calcium levels within CSF-cNs. Coupling calcium imaging in *Tg(pkd211:GCaMP5G)* with extracellular recordings in loose-patch configuration allowed simultaneous recording of electrical activity and calcium activity without influencing spontaneous patterns. Ventral CSF-cNs fired regular action potentials at 24-26 hpf (**Figure 9A**), while dorsal cells never spontaneously fired (**Figure 9B**). When simultaneously performing calcium imaging and loose-patch recordings, calcium transients typically corresponded to bursts of action potentials (**Figure 9C**). Single action potentials were usually not detected by GCaMP5G in *Tg(pkd211:GCaMP5G)* (**Figure 9C**).

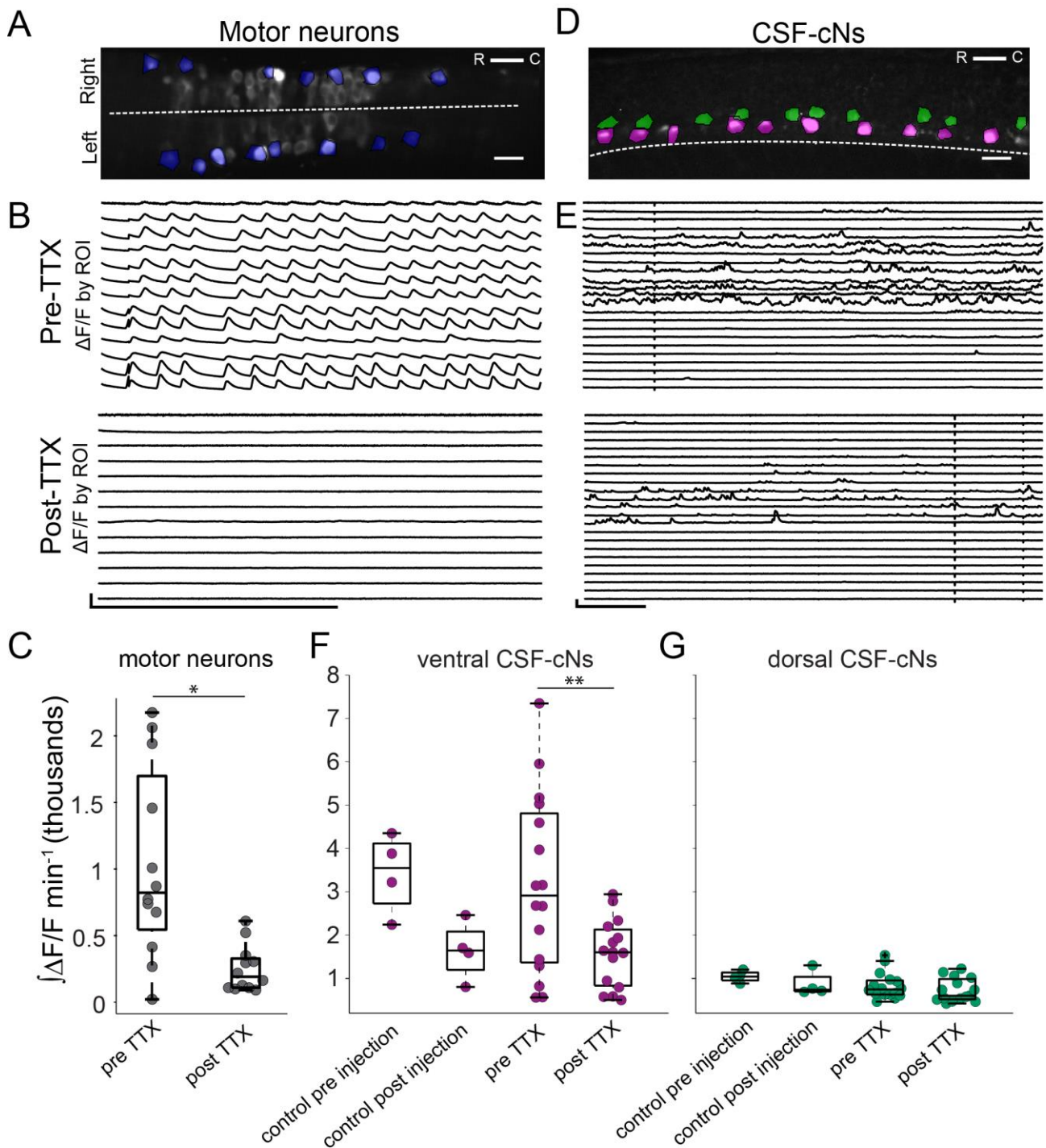


Figure 8. TTX application does not abolish calcium transients in CSF-cNs at 25 hpf.

(A) Example imaging region. Dorsal view of a *Tg(s1020t:gal4; UAS:GCaMP5G)* embryo. Image is a maximum z-projection of the acquired time series. The dotted line demarcates spinal hemicords. Scale is 20 μm . (B) Calcium transients in embryonic motor neurons before injection of TTX (top) and after (bottom). Rhythmic oscillations are abolished when TTX is applied. (C) Quantification of calcium signal from motor neurons before and after application of TTX. (D) Example imaging region. Lateral view of *Tg(pkd211:GCaMP5G)* embryo. Image is a maximum z-projection of the acquired time series. The dotted line demarcates the ventral boundary of the spinal cord. Scale is 20 μm . (E) Calcium transients in embryonic CSF-cNs before injection of TTX (top) and after (bottom). (F) Quantification of ventral CSF-cN activity in embryos injected with either artificial CSF or TTX. (G) Quantification dorsal CSF-cN activity in embryos injected with either artificial CSF or TTX. For (B) and (E) scale is 100% $\Delta F/F$ (vertical), 1 minute (horizontal). For (F) and (G), $n = 4$ embryos for controls injected with aCSF, $n = 15$ embryos injected with TTX. Paired t-test for comparisons within groups. * $p < 0.05$, ** $p < 0.01$.

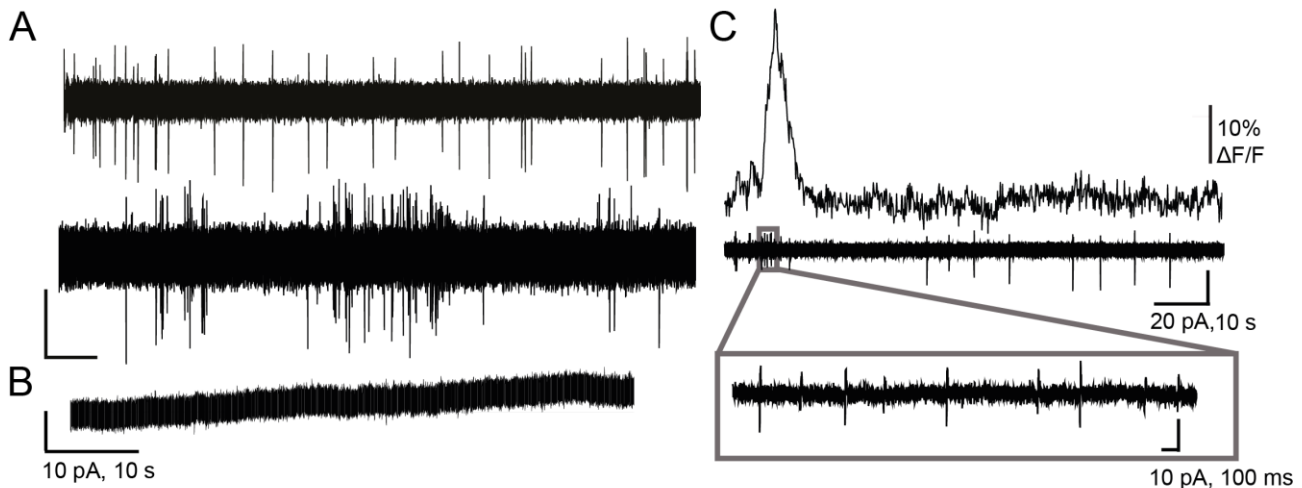


Figure 9. Ventral CSF-cNs fire spontaneous action potentials at 24 hpf.

(A) Loose patch extracellular recordings at 24 hpf in two ventral CSF-cNs from two embryos. (B) Loose patch extracellular recordings at 24 hpf in a dorsal CSF-cN ($n = 3$, firing rates over two minutes 0.7 Hz, 0.2 Hz, 3 Hz). Dorsal CSF-cNs never fired spontaneously ($n = 4$). (C) Simultaneous cell-attached recording and calcium imaging from a ventral CSF-cN in a *Tg(pkd211:GCaMP5G)* embryo at 24 hpf. Single spikes are usually not detected with GCaMP5G.

IV. Origins of activity in CSF-cNs

Together the results from TTX experiments (**Figure 8**) and loose-patch recordings (**Figure 9**) establish that ventral CSF-cNs spontaneously regularly fire action potentials at 1 dpf, generating large, long-lasting calcium transients. Additionally, this activity depends on Pkd211 because the activity is lost in a mutant lacking this ion channel. These results raised questions about the origin and role of Pkd211-driven activity in CSF-cNs. How could Pkd211, present in both ventral and dorsal CSF-cNs, drive activity in only one of these two populations? Several hypotheses arose:

1. Intrinsic properties of CSF-cNs differ, and only ventral CSF-cNs are capable of generating action potentials at 1 dpf. Pkd211 channel opening depolarizes the CSF-cNs and generates action potentials in ventral CSF-cNs.
2. Differences in translation or sub-cellular localization of Pkd211 in ventral and dorsal CSF-cNs: Pkd211 is present at the cell membrane in ventral CSF-cNs and its opening depolarizes the

membrane to generate an action potential in ventral CSF-cNs but does not have the requisite Pkd1-like partner necessary to be trafficked to the membrane in dorsal CSF-cNs.

3. The activity is not spontaneous. Extrinsic factors cause Pkd211 to open constitutively in ventral but not dorsal CSF-cNs.

CSF-cNs do not appear to fire action potentials in response to depolarizing currents from 22-24 hpf (Moreno and Ribera, 2014), however no previous studies have addressed electrical properties of CSF-cNs later in development when CSF-cNs are active. To test whether differences between intrinsic properties of dorsal and ventral CSF-cNs could lead to differences in spontaneous firing at 1 dpf, I performed fluorescence-guided whole cell patch clamp recordings at 24-29 hpf (**Figure 8**). From 24-29 hpf, most ventral and dorsal cells produced a single action potential in response to a small sustained depolarizing current of either 10 or 20 picoampere (pA) and a rebound action potential after a prolonged period of hyperpolarization (**Figure 10A-10D**). Membrane resistance and capacitance were not significantly different between ventral and dorsal cells, although the membrane time constant was significantly higher in ventral CSF-cNs (**Figure 10E-10G**), which could contribute to an integration of inputs over longer durations, leading to more frequent burst firing.

Both ventral and dorsal CSF-cNs in the zebrafish spinal cord express Pkd211 (Djenoune et al., 2014), but PKD2L1 requires a PKD partner to operate functionally at the cell surface (Ishimaru et al., 2006). CSF-cNs might have differential activity due to different subcellular localization of Pkd211 in ventral and dorsal CSF-cNs. Voltage-clamp recordings revealed that both ventral and dorsal cells have extensive single channel opening at 1 dpf (**Figure 11**). Channel activity reversed between 6-20 mV, in accordance with a cationic conductance. (**Figure 11A-11C**). CSF-cNs in zebrafish respond to mechanical stimuli and respond to decrease in osmolarity in the mouse (Orts-Del'Immagine et al., 2012). Analyzing frequency of channel open was thus hindered by a massive

increase in channel activity in the first 60 seconds of breaking into the cell, possibly due to a change in osmolarity induced by the step of breaking-in. Dorsal CSF-cNs showed high levels of single channel activity during the first five minutes of recording that declined to almost zero within 5-10 minutes of the beginning of recording, while ventral cells were less markedly affected by breaking into the cell and sustained channel activity at 1 Hz at 5-10 minutes of recording (**Figure 11D**). This relative difference in activity over time was preserved in shorter duration events that represented partial channel opening (**Figure 11E**). Altogether these results show that both ventral and dorsal populations have single channel openings, suggesting that Pkd211 is functionally expressed in both populations at the cell membrane but may have differences in channel opening probability leading to differences in spontaneous firing rates.

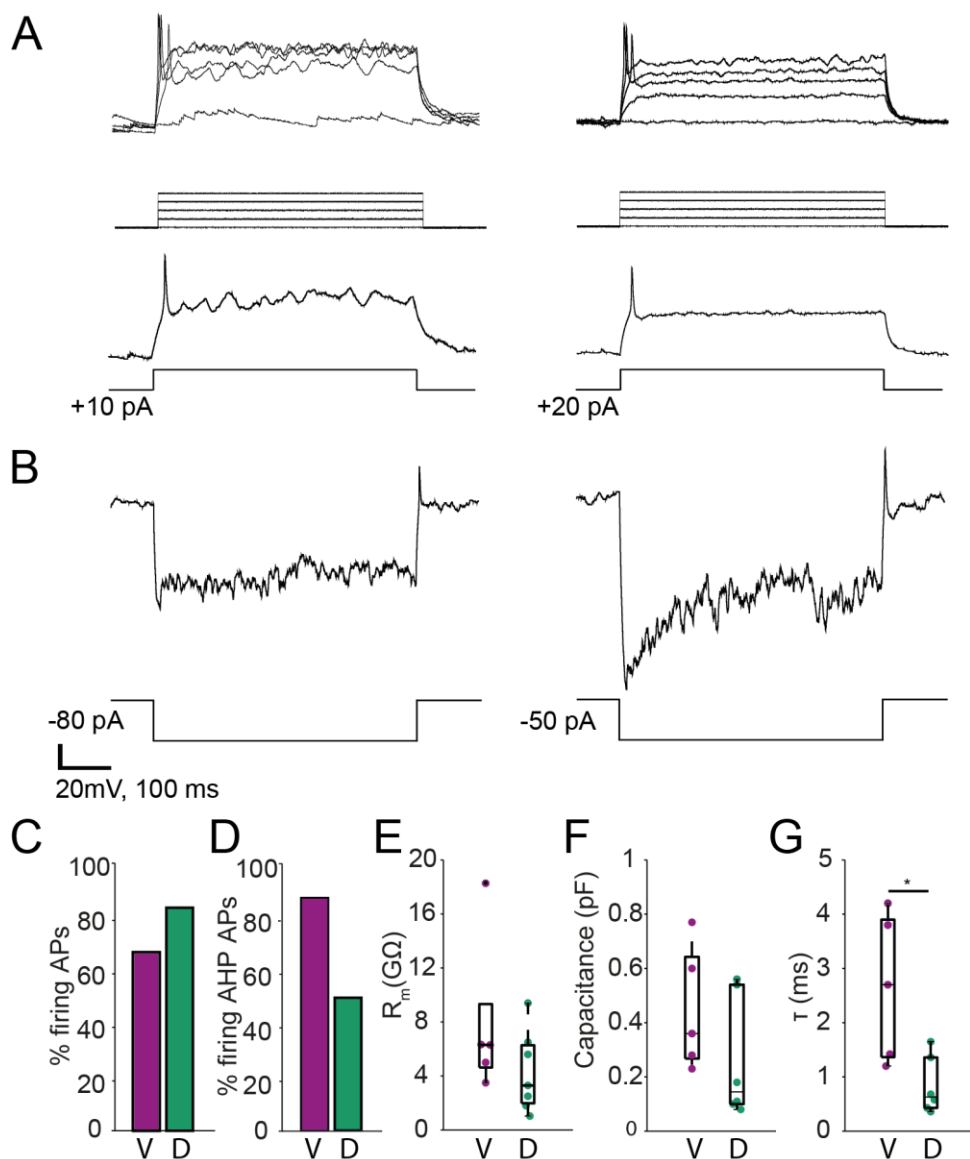


Figure 10. Intrinsic properties of ventral and dorsal CSF-cNs at 1 dpf. (A) Current clamp recordings from a ventral (left) and dorsal (right) CSF-cN at 24 hpf. Both populations fire single action potentials in response to a small depolarizing current step. (B) Both populations fire after-hyperpolarization (AHP) action potentials following a large hyperpolarizing step. (C). Percentage of CSF-cNs capable of generating APs in response to depolarizing current steps from 24-29 hpf. (D). Percentage of CSF-cNs that generate APs after hyperpolarization from 24-29 hpf. (E) Quantification of membrane resistance (F) capacitance and (G) the membrane time constant in ventral and dorsal CSF-cNs (n = 5 ventral CSF-cNs, n = 7 dorsal CSF-cNs). *p < 0.05, Student's t-test.

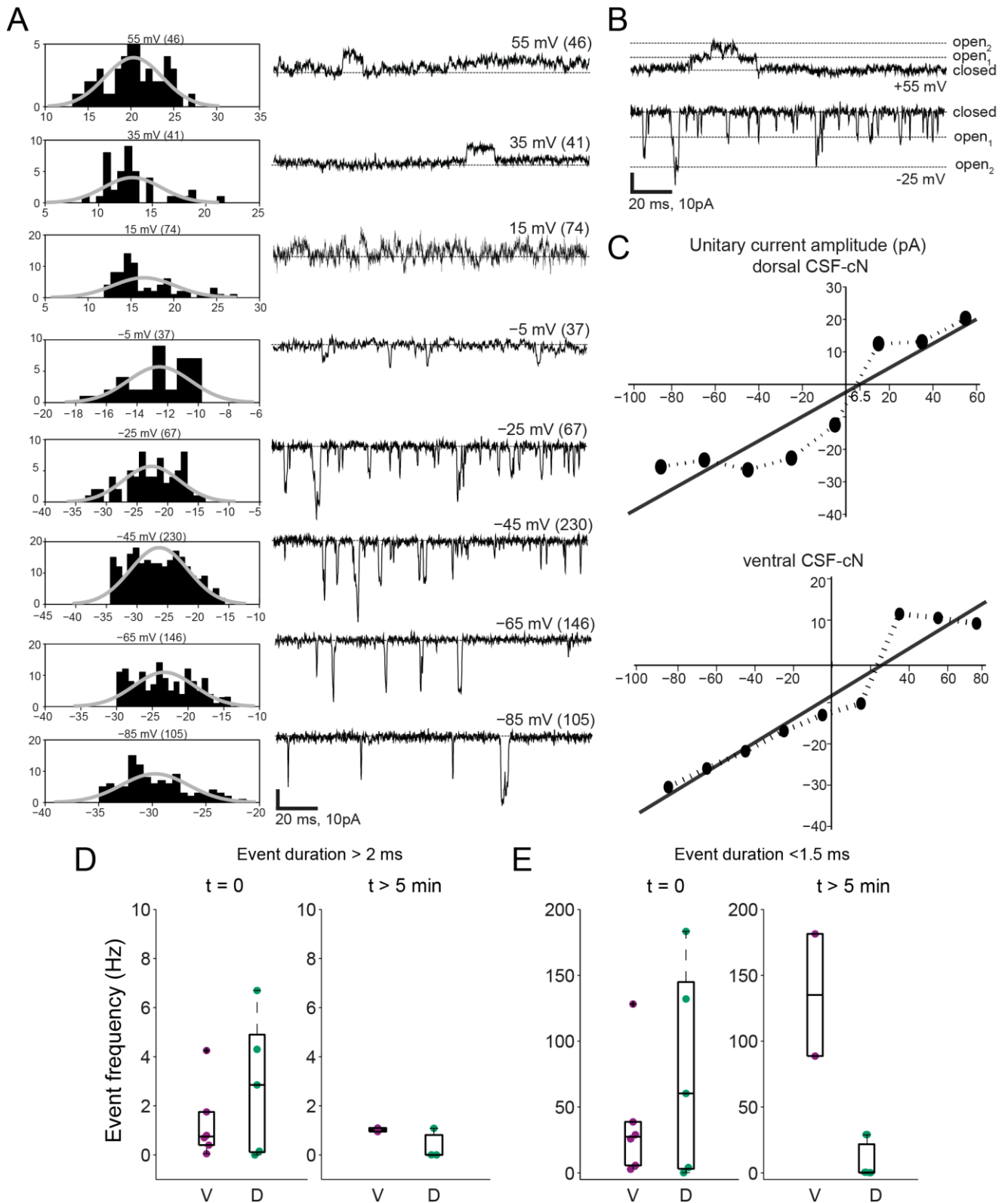


Figure 11. CSF-cNs have extensive single channel opening at 1 dpf in whole cell configuration.

(A) Voltage-clamp recording in a dorsal CSF-cN registers single channel events due to the high resistance of the cell. Histogram of events within manually set bandpass for single channel events (left). Sample traces (right). (B). Traces of recorded currents at holding potentials of +55 mV (top) or -25 mV (bottom). (C). Representative example of current voltage (I-V) curve for single channel openings. The reversal potential and channel conductance were based on a linear fit (solid black line). (D) Event frequency for long events in ventral and dorsal cells and (E) short duration events. n = 6 ventral CSF-cNs, n = 5 dorsal CSF-cNs. n = 2 ventral CSF-cNs, n = 3 dorsal CSF-cNs for t > 5 minutes.

In voltage-clamp recordings performed to detect spontaneous currents, no synaptic events were present, but current amplitude was highly variable. To determine if all of the spontaneous inward currents were related to Pkd211 activity, I performed whole cell patch clamp recordings in the *pkd211*^{-/-} mutant (**Figure 12**). CSF-cNs lacking Pkd211 retained the ability to fire action potentials in response to depolarizing current injection (**Figure 12A**) or as a rebound to a hyperpolarizing current step (**Figure 12B**). However, almost all spontaneous currents were abolished (**Figure 12C**). Membrane resistance, capacitance, and the time constant were within the ranges of wild type CSF-cNs. Single channel events lasting longer than 2 ms, reflecting complete opening of the channel, rarely occurred or appeared in bursts (**Figure 12C-12D**), which could reflect the remaining, often correlated, activity remaining in these neurons (**Figure 5, Table**). We can conclude that Pkd211 does not seem to affect neuronal properties, and almost all spontaneous inward current relies on Pkd211.

To ask whether differences between the two cell types could be due to intrinsic properties and high membrane resistance of CSF-cNs relative to later stages, I recorded from CSF-cNs at larval stages. At 1 dpf, a single channel opening generates enough inward current (approximately 20-25 pA) to depolarize a CSF-cN and generate an action potential (**Figure 11**). This is preserved at 4 dpf (**Figure 13A**). Some CSF-cNs also retain a rebound action potential following hyperpolarization (**Figure 13A-13B**). Membrane resistance is comparable, although capacitance and membrane time constant may be slightly higher than at embryonic stages (**Figure 13C**). In gap-free recordings performed in voltage clamp configuration, CSF-cNs at 4 dpf also show high frequency channel opening that persists over time (**Figure 13D-13E**). These results suggest that extrinsic factors likely determine the probability of channel opening and relay sensory information read out by CSF-cNs.

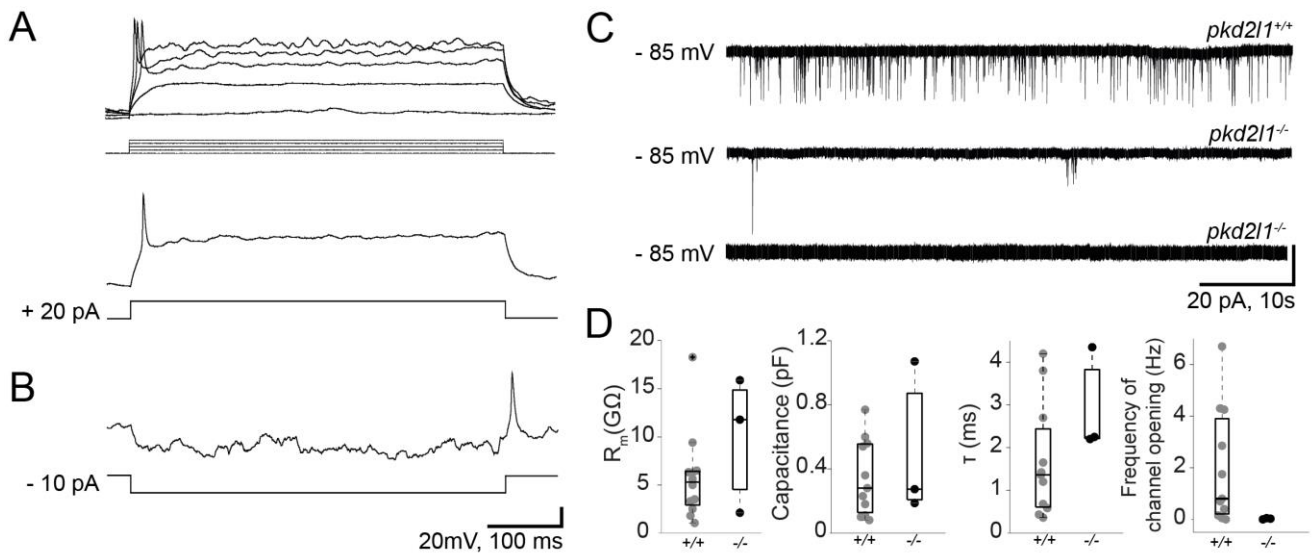


Figure 12. Intrinsic properties of CSF-cNs in *pkd211*^{-/-} at 1 dpf.

(A) Current clamp recordings from a CSF-cN in a *pkd211*^{-/-} embryo at 27 hpf. Example of a CSF-cN that fired a single action potential in response to a 20 pA depolarizing current step. (B) Example of a CSF-cN that fired a rebound action potential following hyperpolarization. (C) Example gap free voltage clamp traces from *pkd211*^{+/+} (top), and *pkd211*^{-/-} (middle and bottom) embryos. (D) Quantification of intrinsic properties and frequency of channel opening in *pkd211*^{+/+} and *pkd211*^{-/-}, n = 3 cells from 3 embryos.

If “spontaneous” activity is actually related to sensory function, how early do CSF-cNs carry sensory function and in what role does Pkd211 play? CSF-cNs sense pH, osmolarity, and relay mechanosensory information to spinal circuits. In the zebrafish, CSF-cNs respond to both passive and active bending of the tail at larval stages (5-6 dpf, Böhm et al., 2016), which depends on Pkd211. However, how Pkd211 participates in this response has not been investigated. Present on the cell surface as evidenced by whole cell recordings (**Figures 11-13**), Pkd211 could act as a direct mechanosensitive channel. In the lamprey, pharmacological block of ASIC channels blocks response to CSF flow, suggesting that PKD and ASIC channels may work together and possibly with other channels to carry a mechanosensory response (Jalalvand et al., 2016a). If CSF-cNs are responding to flow, one possibility is that other cells detect bending, and these signals are transmitted to CSF-cNs.

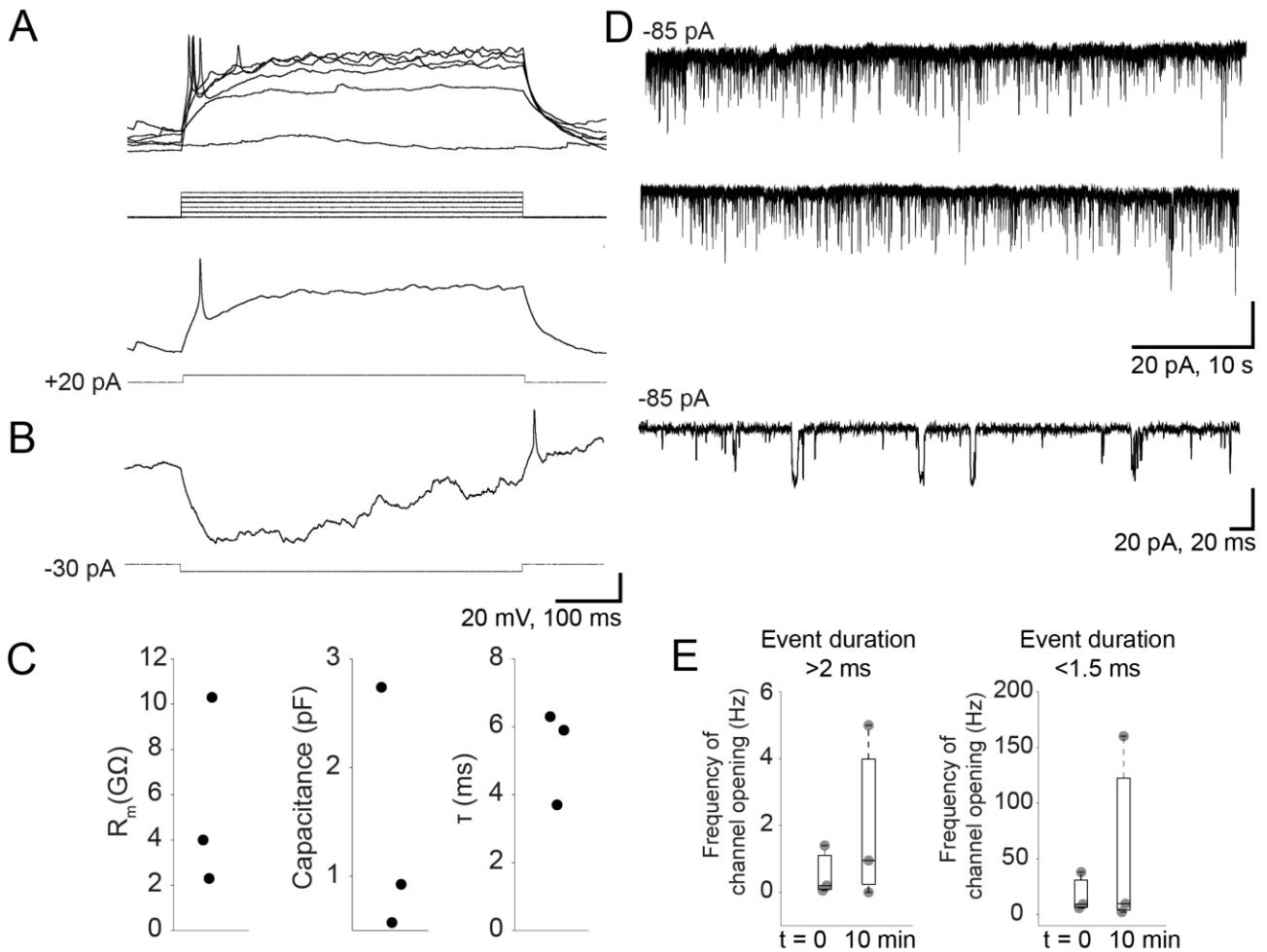


Figure 13. Intrinsic properties and channel activity in CSF-cNs at larval stages.

(A) Example current clamp recordings from a CSF-cN at 4 dpf. A depolarizing current step of 20 pA generates a single action potential in a CSF-cN. (B) Example of a CSF-cN that fired a rebound action potential following hyperpolarization. (C) Quantification of membrane resistance, capacitance, and membrane time constant. Each point represents one neuron. (D). Example gap free voltage clamp traces (E). Event frequency for long events and short duration channel opening events. $n = 3$ cells from 3 larvae.

If CSF-cNs respond to mechanosensory input at embryonic stages, early embryonic activity could relate to sensory function of CSF-cNs. To test whether CSF-cNs are activated during muscle contraction at embryonic stages, I performed calcium imaging in unparalyzed in *pkd21l*^{+/+} or *pkd21l*^{-/-} embryos expressing GCaMP5G and tagRFP under the *pkd21l* promoter, using the tagRFP expression as a reference for cellular location (**Figure 14A**) and quantified changes in GCaMP fluorescence following muscle contraction (**Figure 14A-14B**). CSF-cNs are activated when muscle contraction is initiated, suggesting their response to mechanical stimuli begins at 1 dpf. It also appeared that the *pkd21l*^{-/-} mutant may also retain some response to bending at this stage (**Figure**

14C). Further investigation will be necessary to determine whether the response was reduced but preserved in *pkd211*^{-/-} and if other ion channels could be involved in mechanosensory transduction in these neurons.

Thanks to genetic and pharmacological tools, it is now possible to test the relative contribution of Pkd211 and other ion channels to sensory function in CSF-cNs. I developed a preparation (**Figure 15A**) to test whether CSF-cNs respond directly to flow in the central canal. Neurons that do not contact the central canal do not respond to a brief water puff into the central canal (**Figure 15B**). At 1 dpf, a subset of CSF-cNs respond to a puff of artificial CSF applied within the central (**Figure 15C**) but not when applied in the spinal cord outside of the central canal (**Figure 15D**). CSF-cNs therefore detect flow in the central canal, and this open preparation can now be utilized to implement testing of the sensory response of CSF-cNs and the relative contribution of different ion channels to their sensory response *in vivo*.

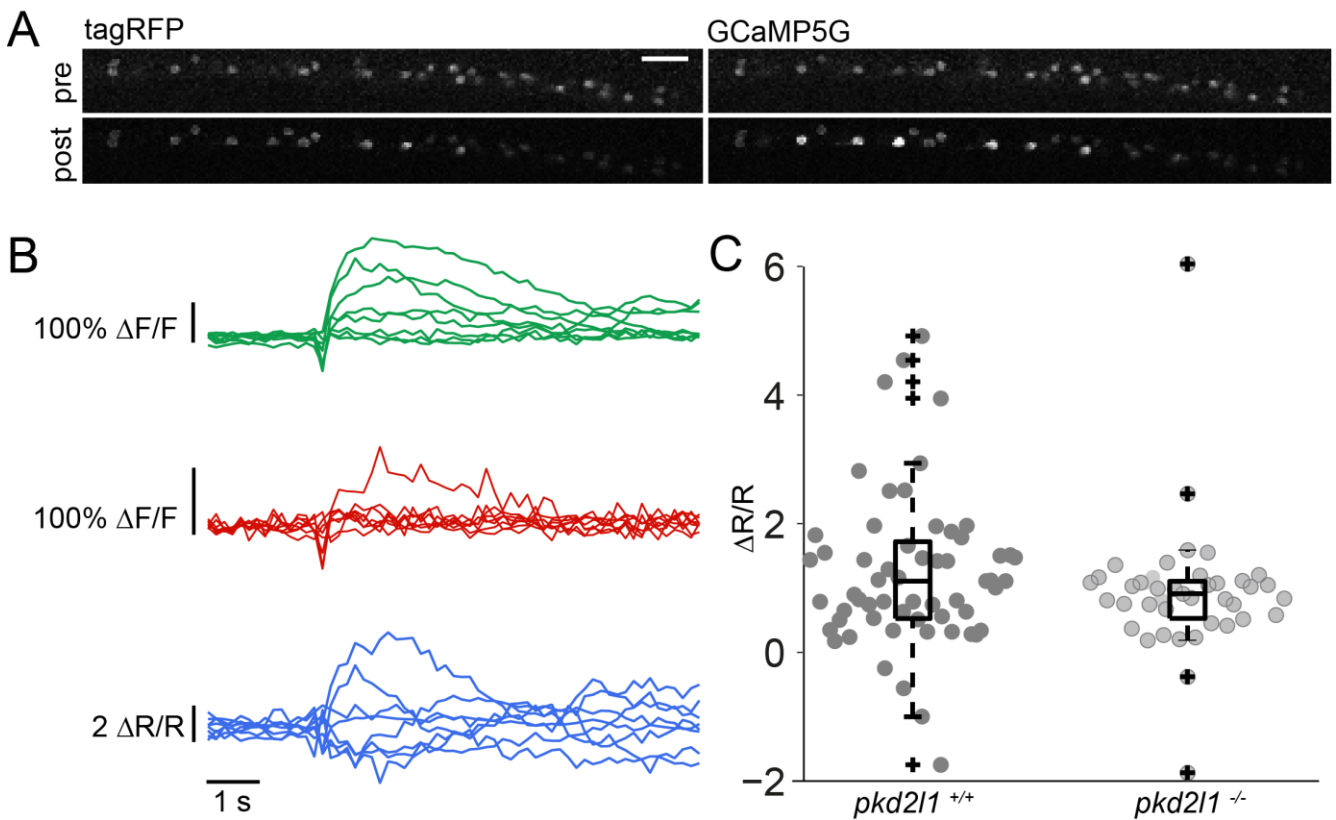


Figure 14. CSF-cNs are active during muscle contraction by 27-30 hpf.

(A) Two-photon imaging was performed in unparalyzed dual transgenic *Tg(pkd211:GCaMP5G; pkd211:tagRFP)* embryos. Top: signal in both channels prior to muscle contractions. Bottom: signal in both channels following muscle contraction. Scale bar 20 μM . (B) Example of $\Delta F/F$ for GCaMP5G signal (top), tagRFP signal (middle), and normalized $\Delta F/F$, bottom following a muscle contraction. (C) Quantification of $\Delta R/R$ for wild type and mutants. Experiments performed in $n = 23$ embryos 27-30 hpf, $pkd211^{+/-}$ showed responses similar to wild type and are excluded here. $n = 61$ cells from 6 embryos for $pkd211^{+/+}$, $n = 39$ cells from 5 embryos for $pkd211^{-/-}$.

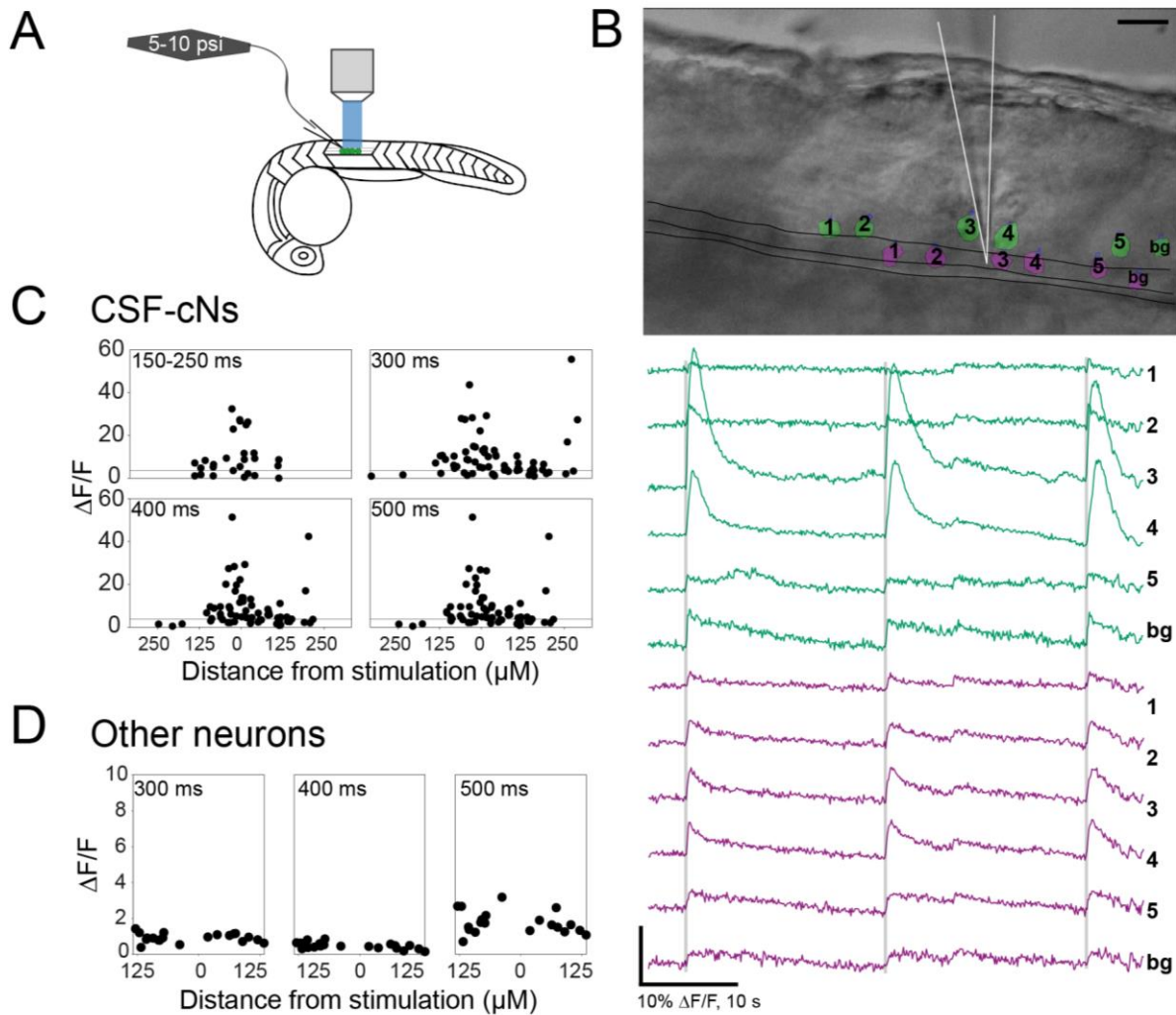


Figure 15. CSF-cNs respond to flow in the central canal at 27-30 hpf.

(A) Experimental setup for testing in vivo responses of CSF-cNs to flow in *Tg(pkd211:GCaMP5G)* embryos. Embryos are dissected as performed for electrophysiological recordings, leaving the spinal cord intact. A patch pipette filled with aCSF is connected to a picospritzer to deliver a timed stimulus of 5-10 psi in the central canal while calcium imaging is performed. (B) Top: superimposed transmitted light image and fluorescent image of *Tg(pkd211:GCaMP5G)*. The stimulus pipette is outlined in white. ROIs of dorsal CSF-cNs are green; ventral CSF-cNs are magenta. Bottom: $\Delta F/F$ or corresponding ROIs. Gray bars indicate time of stimulus delivery. Background ROIs, selected from nearby regions with no CSF-cN labeled are indicated by "bg". A small signal can be detected due diffracted photons related to the lack of optical sectioning on the widefield microscope. Scale is 20 μM . (C) Quantification of $\Delta F/F$ for CSF-cNs in *Tg(pkd211:GCaMP5G)* in response to stimuli of different durations. Distance from the stimuli pipette refers to more rostrally-located CSF-cNs (left of 0) or more caudally-located CSF-cNs (right of 0). The gray line indicates average $\Delta F/F$ for background regions. $n = 3$ stimulations each for 67 ROIs from 4 embryos. (D) Preliminary quantification of $\Delta F/F$ for CSF-cNs in *Tg(HuC:GCaMP5G)*, labeling most neurons, in response to stimuli of different durations ($n = 1$ embryo).

Overview

CSF-cNs consist of a heterogeneous population of sensory neurons located within the spinal cord. Ventral CSF-cNs arise from *nkx2.2*⁺ p3 progenitors and are distinct from dorsal CSF-cNs that derive from pMN and *olig2*⁺ progenitors (Park et al., 2004; Yang et al., 2010; Djenoune et al., 2014). Despite their unique origin, no work has described functional differences between the two classes. Evidence suggests that ventral CSF-cNs preferentially target motor circuits in the spinal cord (Fidelin et al., 2015, Hubbard et al., *in revision*), and peptides are generally expressed in subpopulations of dorsal or ventral CSF-cNs (Annex 2).

Spontaneous activity, characterized with calcium imaging, occurs in CSF-cNs at early embryonic and larval stages, though very high levels of activity predominate at 1 dpf in ventral CSF-cNs. This activity is dependent on the opening of transient receptor channel Pkd2l1. We showed that the loss of activity does not preclude development of synaptic connections, neurotransmitter phenotype, axonal guidance, or CSF-cN morphology. CSF-cNs fired action potentials that were associated with calcium transients, although pharmacological block of TTX-sensitive voltage-gated sodium channels did not abolish entirely their activity. This could be due to the recruitment of TTX-insensitive sodium channels or calcium voltage-dependent channels following the channel opening. Even though only ventral cells are highly active, dorsal and ventral CSF-cNs both have extensive single channel opening but not spontaneous synaptic inputs at embryonic and larval stages. Small differences in intrinsic properties, such as the membrane time constant, may underlie differences between groups. CSF-cNs gain sensory properties, responding to active bending of the tail and fluid flow in the central canal by 28 hpf. Early embryonic activity may thus reflect a development process not evaluated here, compensated by other mechanism, or an early sensory response within the spinal cord.

I. Embryonic activity in CSF-cNs and development

Activity was restricted primarily to 1 dpf, a time of intense neuronal birth, axon guidance, and wiring of early motor circuits (Drapeau et al., 2002; Lewis and Eisen; 2003). In many species, GABA contributes to developmental timing and synchrony for wiring during development (Milner and Landmesser, 1999; Ben-Ari, 2002; Wang et al., 2003). Because CSF-cNs are GABAergic, the idea that the activity at 1 dpf in ventral CSF-cNs might be involved in proper development of the spinal cord seemed probable. The *pkd211*^{-/-} mutant provided a means to silence embryonic activity and probe the function of early activity specifically.

Numbers and neurotransmitter phenotype of CSF-cNs were unaffected in the *pkd211*^{-/-} mutant by early larval stages. Evaluation of the *pkd211*^{-/-} mutant at early larval stages allowed for investigation at a stage in which mature circuits for locomotion at 4 dpf are mostly established. GABA signaling sets timing for development of the spinal cord in other species (Milner and Landmesser, 1999). Early activity or GABA release related to developmental timing could have led to developmental delay at embryonic stages when the high activity in CSF-cNs pervades, followed by compensation to have the correct number of neurons by larval stages.

Approximately 100 CSF-cNs are present in the spinal cord at 1 dpf (Djenoune et al., 2014), which increases to almost three times that number by early larval stages. Early-differentiated CSF-cNs active at embryonic may function as one subpopulation among the ventral CSF-cNs to target the fast motor circuitry, which develops before slow motor circuitry. By using photoconvertible proteins and morphology analysis, it may be possible to determine whether early-born ventral CSF-cNs comprise a subtype. At larval stages, the *pkd211*^{-/-} mutant displays decreased tail beat frequency during fast swimming (Bohm et al., 2016). As I demonstrated that the monosynaptic connection between CSF-cNs and CaP

primary motor neurons is preserved in the *pkd211*^{-/-} mutant, the difference underlying the larval behavioral phenotype is most likely due to the fact that sensory response to bending is decreased when the channel is mutated.

CSF-cNs and development

Although embryonic activity in CSF-cNs did not contribute detectibly to spinal cord development as shown by neurotransmitter identity, CSF-cNs may contribute to other developmental processes such as axonal migration that we did not quantify here. Furthermore, CSF-cNs express somatostatin in dorsal CSF-cNs from 24-55 hpf. Somatostatin increases the frequency of calcium transients and the initial rate of cell migration (Yacubova and Komuro, 2002). Expression of somatostatin in dorsal CSF-cNs during this period could contribute to neuronal migration. In addition, CSF-cNs also express serotonin (5-HT) specifically from 48-72 hpf, a period when many interneurons and secondary motor neurons are developing (Lewis and Eisen, 2003). Transient serotonin expression is a feature of developing neural circuits. Many neurons that do not express 5-HT at mature stages express serotonin transporter (SERT) and vesicular monoamine transporter (VMAT) during development (Lebrand et al., 1996; Hansson et al., 1998). Although no clear role has been established, suggested roles include (1) participating in a transition from electrical to chemical coupling, (2) creating a morphogenetic gradient between neurons that actively produce 5-HT and those that actively pump it, (3) serving as a "borrowed neurotransmitter," allowing neurons to produce pulse of 5-HT release in phase with incoming neural activity, or (4) serving to clear 5-HT away from the extracellular space when the serotonergic fiber network is not fully mature (Gaspar et al., 2003). In zebrafish, the period during which CSF-cNs are serotonergic corresponds to a wave of neurogenesis of secondary motor neurons (Lewis and Eisen, 2003). All of these are plausible roles of 5-HT in CSF-cNs. Understanding whether CSF-cNs play a role in

development of spinal cord networks will require cell-type specific block of somatostatin or block of 5-HT uptake or release.

TRP channels in development

During development, primary cilia sense extracellular signals (Berbari et al., 2009). Hedgehog is a secreted protein that regulates a diversity of developmental processes (Nusslein-Volhard and Wieschaus, 1980). Calcium signaling via TRPP channels (PKDs) in ciliary compartments drives transcriptional activation via Gli transcription factors (Haycraft et al., 2005; Kiprilov et al., 2008). The Wingless (Wnt) pathway also mediates effects via changes in intracellular calcium. Calcium influx via a Pkd211-Pkd1 like complex could contribute to transcriptional activation within zebrafish CSF-cNs.

Turning responses to netrin-1, BDNF, and MAG are mediated by TRPC1 channels in *Xenopus* spinal neurons and TRPC channels in rat cerebellar granule neurons (Li et al., 2005; Shim et al., 2005; Wang and Poo, 2005) TRPC5-receptor operated ion channels appear to constitute the calcium entry pathway generating spontaneous growth cone transients in cultured hippocampal neurons (Greka et al., 2003). Again, Pkd211 could serve a function compensated during development by other factors.

Possible contribution of gap junctions to CSF-cN activity

We used a *pkd211*^{-/-} mutant to study embryonic activity of CSF-cNs, in which uncorrelated calcium transients in CSF-cNs were abolished. Although activity was mostly uncorrelated between CSF-cNs, in some cases (at least one event in approximately fifteen percent of traces in *pkd211*^{+/+}, *pkd211*^{+/-}, *pkd211*^{-/-}, n = 200 embryos and larvae) synchronized activity occurred in CSF-cNs. These events occurred either in most or all CSF-cNs in the imaging plane, and occurred at both embryonic and larval stages. Electrical activity via gap

junctions contributes to synchronized activity in the developing nervous system (Ben-Ari 2002), and contributes to synaptogenesis (Personius et al., 2007), neuronal differentiation (Hartfield et al., 2011), migration (Cina et al., 2007), and neural circuit maturation (Maher et al., 2009; Hanganu et al., 2009) via calcium influx, metabolites, and second messengers that coordinate metabolism and transcription in developing neurons (Kandler and Katz, 1998). Although the uncorrelated activity silenced here did not have a detectable effect on development, these correlated events that resemble closely correlated spontaneous activity in other species may function in development.

Gap junction coupling mediating interactions between sensory neurons can be found in other systems, including *C. elegans*, in which electrical synapses mediate inhibitory and excitatory interactions between neurons (Chatzigeorgiou et al., 2011; Rabinowitch et al., 2013). Experiments using fictive recordings as a readout of locomotion demonstrated that when CSF-cNs are activated optogenetically during slow swimming in rostral regions of the spinal cord, locomotor output is silenced in caudal regions as well (Fidelin et al., 2015). This could result from CSF-cNs projecting onto descending interneurons or possibly from gap junction coupling between CSF-cNs to effect sensory function during distinct swimming modes.

Whether connexins are expressed and form gap junctions between CSF-cNs and whether this underlies some of the synchronous activity, asynchronous activity via subthreshold depolarizations, or function in locomotor circuits remains to be determined. We previously demonstrated that Granger causality could be used to demonstrate rostral to caudal propagation signals in the gap junction coupled synchronized motor networks during embryonic development (De Vico Fallani et al., 2015, Annex 3). It would be interesting to use causality analysis to investigate whether correlated activity results from signal propagation from specific CSF-cN hub neurons or in a rostral to caudal fashion similar to gap junction

coupled motor networks (Muto et al., 2011; De Vico Fallani et al., 2015, Annex 3).

Pharmacological manipulation to block gap junctions or gabazine could elucidate the mechanism of correlated events and function in either development or locomotion, though the relative rare occurrence of these events hinders study of their role.

Conclusions: embryonic activity and development

Understanding whether spontaneous activity during embryonic development plays a functional role may require more acute manipulations of spontaneous activity. Activity-dependent processes are often redundant and compensated in case of loss (Blankenship and Feller, 2010). Pkd211-driven spontaneous activity may play a redundant role during development or be compensated by early larval stages, when we evaluated effects of the mutation on development. Current methods for silencing either do not silence completely or are difficult to implement *in vivo* (Curado et al., 2008; Arrenberg et al., 2009). I previously used botulinum neurotoxin (Chapter 2) to investigate whether silencing synaptic output would affect development. However, neurotransmitter phenotype and number of neurons were the same as controls, the fish had normal rhythmic embryonic activity, and lived to adulthood without apparent health defects, all together suggesting synaptic release during development does not play a critical role. Release of GABA in a paracrine manner that acts independently of synaptic release promotes migration of embryonic neurons in the hippocampus of mice (Demarque et al., 2002; Manent et al., 2005), which could be a function of GABA release in CSF-cNs, otherwise undetectable by blocking synaptic release with botulinum neurotoxin. Targeted ablation may be a better option to eliminate CSF-cNs as circuit elements. Additionally, methods to block serotonin or somatostatin release from these neurons may reveal important functions for their expression in CSF-cNs for developmental processes.

II. Challenges and limitations of interpreting calcium imaging data

Immunohistochemistry showed that expression of PKD2L1 in CSF-cNs in mouse and macaque is enhanced in the terminal bud of the apical extension into the lumen of the central canal (Djenoune et al., 2014), suggesting expression is not confined to the endoplasmic reticulum. However, due to technical challenges of immunohistochemistry in the zebrafish, to date, subcellular localization of Pkd2l1 remains unknown. The PKD2L1 channel forms homomeric tetramers that are restricted to ER as well as heteromeric tetramers with a PKD1 partner that leads to expression on the cell surface (Murakami et al., 2005). At the level of the endoplasmic reticulum, Pkd2l1-Pkd2l1 complexes in zebrafish could participate in calcium release from internal stores and not participate in calcium influx at the level of the cell membrane.

Calcium release from internal stores contributes to action potentials and synaptic potentiation (Sandler and Barbara, 1999). Calcium entry during an action potential stimulates calcium release from the internal stores in dorsal root ganglia (DRG) (Shmigol et al., 1995; Usachev and Thayer, 1997) and could serve as coincidence detectors for synaptic potentiation. Calcium release via IP₃-receptor dependent calcium release contributes to stabilization of GABA_AR (Bannai et al., 2015). Function of PKD2L1-PKD2L1 complexes at the level of the endoplasmic reticulum has not been investigated, however, it could entrain one of these functions.

When beginning this study, Pkd2l1 expression in zebrafish was established in CSF-cNs via *in situ* hybridization (Djenoune et al., 2014) and expression of potential Pkd1 partners was unknown. Additionally, subcellular localization of PKD2L1 to the apical extension in other species was not established. Therefore, it then seemed reasonable that Pkd2l1 could form homomeric tetramers intracellularly and not be involved at all in intercellular signaling, and this activity was reflected in the calcium imaging instead of action potentials. Frequently,

neuroscientists rely on spike rate inference to predict firing rates from calcium imaging when a stimulus is delivered without ground truth electrophysiological recordings. Many neuroscientists and mathematicians are using various techniques to perform this computation including Bayesian inference (Vogelstein et al., 2009; Pnevmatikakis et al., 2016); deconvolution (Yaksi and Friedrich, 2006; Park et al., 2013), or template matching (Grewe et al., 2010; Onativia et al., 2013). However, in all cases these algorithms assume that the calcium activity corresponds to neuronal spiking.

In my experiments, the possibility that Pkd211 was sequestered inside the cell prevented assumption that these neurons were firing action potentials. Cell attached recordings demonstrated that CSF-cNs do fire action potentials regularly even during early development at 24 hpf. All activity visible on the calcium traces corresponded to action potentials. Experiments to block CICR from intracellular stores with thapsigargin, a sarco/endoplasmic reticulum Ca^{2+} ATPase (SERCA) inhibitor also did not impact CSF-cN activity, though pharmacological agents penetrate weakly in the embryo without dissection and without a positive control to ensure that the drug was entering cells, these data could not be fully interpreted (*data not shown*). Evidence now suggests that Pkd211 is localized to the cell membrane via a Pkd1 partner and is concentrated in the apical extension within the central canal of the spinal cord (Djenoune et al., 2014; *unpublished results*). Together these results suggest that Pkd211 is present and functional as a cationic selective channel at the cell membrane.

Experiments using TTX to block classical Na^+ action potentials did not abolish spontaneous activity in CSF-cNs as it did for rhythmic oscillations in motor networks. CSF-cN embryonic activity thus does not rely on synaptic transmission, more likely being intrinsic. The remaining activity when TTX is applied could be a result of (1) direct conductance of the Pkd211-Pkd1 complex, (2) calcium release from intracellular stores, or (3) calcium spikes. A

complete picture of the calcium activity taking place within the CSF-cNs and reflected in the calcium imaging remains to be determined.

III. Properties of CSF-cNs

In order to understand how subpopulations of CSF-cNs contribute to spinal cord development and locomotion, either via sensing CSF flow, contents, or other interactions, two questions still need to be addressed. Why are ventral cells highly active at 1 dpf, and what are the functional differences between dorsal and ventral CSF-cNs? *In vivo* electrophysiology demonstrated that Pkd211 ventral and dorsal CSF-cNs may have a different opening probability in the two cell types. However, whole cell patch clamp techniques affect channel opening probability without any additional stimulus. Calcium imaging alone allowed readout of cellular activity without stimulating the CSF-cNs, other than with light. Using whole cell recordings to better understand the origin of the activity and differences between subpopulations of CSF-cNs confounded interpretation by influencing basal activity of the CSF-cNs. CSF-cNs all showed changing levels of Pkd211 channel activity over the course of a recording.

At 4 dpf, when spontaneous activity is generally lower in CSF-cNs, whole cell recordings show similar channel opening frequency as at 1 dpf, suggesting that recording directly from cells alters the physiological channel activity. Whether ventral and dorsal CSF-cNs have different intrinsic excitability remains to be fully determined. The membrane input resistance varied from 3.5 to 18 G Ω in ventral CSF-cNs and 1-10 G Ω in dorsal CSF-cNs, membrane capacitance ranged from 0.25 to 0.75 in ventral CSF-cNs versus 0.8 to 0.55 in dorsal CSF-cNs, and the membrane time constant ranged from 1.2 to 4.2 ms in ventral CSF-cNs versus 0.3 to 1.7 in dorsal CSF-cNs. More recordings are needed to determine whether these

differences are sufficient to alter early activity or if the two classes of CSF-cNs (ventral or dorsal) can be divided into additional subpopulations.

Increased Pkd211 activity at the beginning of a whole cell recording could be related to sensory responses to osmolarity changes, although the small osmolarity differences between the intracellular or extracellular solution (5-10 mOsmol/kg) were lower than published changes necessary to elicit a response from PKD2L1 *in vitro* (500 mOsmol/kg in CSF-cNs, Orts-Del'Immagine et al., 2012; 40-50 mOsmol/kg *in vitro*, Shimizu et al., 2009), although the channel could be sensitive to much smaller changes *in vivo*. Ciliary PKD proteins regulate intracellular calcium signaling triggering downstream cascades (Koulen et al., 2005; Abou Alaiwi et al., 2009), and by washing out the intracellular milieu with an imposed intracellular solution, the properties of the cell could be affected. By varying calcium concentration within in the intracellular solution or performing perforated patch recordings, more physiological conditions for CSF-cNs and Pkd211 may be achieved.

PKD2L1 in mechanosensory function

Some TRP channels contribute to mechanosensation, but their function remains unclear (Christensen and Corey, 2007). In, *Drosophila* distinct TRP or other ion channels may function separately in sensory cells to mediate a mechanosensory response or amplify the signal (Göpfert et al., 2006; Lehnert et al., 2013), and in *C. elegans* TRPV channels and TRPA-1 are involved in mechanosensation, either as primary transducers or through a modulatory role (Kindt et al., 2007; Kang et al., 2010).

The PKD2L1 channel shows responses to changes in osmolarity, however its role in mechanosensation as for other PKDs is not clear. Previous work suggested PKD1 and PKD2 form mechanosensory channels in primary cilia in the kidney (Nauli et al., 2003; Nauli and Zhou, 2004). However, single cilia recordings show currents in response to mechanical

stimuli at higher pressures than known mechanosensitive channels (DeCaen et al., 2013). Other evidence points to PKD2 as a regulator of other nonselective cationic channels (currently unidentified) instead of a primary mechanosensory role (Sharif-Naeini et al., 2009). Hair cell transduction persists in double and triple PKD knockout mice (TRPM2, PKD2, PKD2L1, PKD2L2 and PKD1L3; Wu et al., 2016). PKD2L1 is strongly conserved in CSF-cNs across species (Djenoune et al., 2014; Orts-Del-Imagine et al., 2014) and likely PKD2L1 in CSF-cNs has a conserved role in vertebrates, though this role may not be direct transduction of mechanical stimuli.

In zebrafish, *Pkd2l1* mediates at least a part of responses to mechanosensory stimuli in CSF-cNs (Bohm et al., 2016). Whether PKD2L1 carries out the function of a mechanotransducer or whether CSF-cNs themselves are mechanosensors remains to be determined. At embryonic stages when CSF-cNs begin to respond to sensory stimuli, a small response may be preserved in the *pkd2l1*^{-/-} mutant. PKD2L1 may function in sensory transduction or amplifying a signal. Recent work demonstrated that PKD2L1-PKD1L3 complexes operate as gain control by generating calcium spikes in response to diverse sensory stimuli (Hu et al., 2015). Studying cultured CSF-cNs in isolation (Böhm et al., 2016) will provide evidence of whether they directly sense mechanical stimulus, and pharmacological stimulation *in vivo* can be used to elucidate relative contributions of different channels for sensory responses.

The function of PKD2L1 in CSF-cNS

In addition to responses to mechanical stimuli, CSF-cNs respond to changes in pH via PKD2L1 and acid sensing ion channels (ASICs) in mouse and lamprey (Orts-Del'Imagine et al., 2016; Jalalvand et al., 2016a; Jalalvand et al., 2016b). Pharmacological blockade of ASIC channels combined with a mutant for PKD2l1 indicated that ASIC channels carry

responses to acidic stimuli, whereas PKD2L1 carries responses to alkaline stimuli. Activation of either channel increases firing in CSF-cNs, which are inhibitory across species (Orts-Del'Immagine et al., 2016; Jalalvand et al., 2016a; Jalalvand et al., 2016b). In the lamprey, ASIC channels are also activated when CSF-cNs are mechanically stimulated through fluid flow in the central canal (Jalalvand et al., 2016a), though lack of genetic targeting or pharmacology for PKD2L1 prevented investigation of its function in mechanical responses. By developing a preparation in which CSF-cNs can be readily accessed by pharmacology, I can now investigate the relative contributions of these channels to mechanosensory function *in vivo* in wild type or *pkd2l1*^{-/-} mutants.

A role for CSF flow in embryonic activity?

CSF-cNs have sensory capabilities from 1 dpf, sensing bending of the tail and flow in the central canal starting from 26-28 hpf. Between intrinsic properties being similar and sensory properties developing early, high activity in ventral CSF-cNs at 1 dpf could result from extrinsic factors triggering Pkd2l1 channel opening.

Cilia beating of ependymal cells generates CSF flow, which provides directional information for the guidance of developing neurons (Sawamoto et al., 2006) and contributes to development of normal curvature of the spine (Grimes et al., 2016). In the central canal of the zebrafish spinal cord, radial glia have a motile cilium from 24 hpf and beat at approximately 12 Hz at 2.5 dpf (Kramer-Zucker et al., 2005). Additionally, CSF-cNs respond to fluid flow in the central canal starting around 25-28 hpf. Beating of cilia from radial glia at different rates ventrally or dorsally may trigger differential flow within the central canal that would increase CSF-cN activity in only ventral CSF-cNs via activation of Pkd2l1. Whether CSF flow affects CSF-cN activity at 1 dpf could be tested with motile cilia mutants, in which the CSF no longer flows in the central canal of the spinal cord, in combination with calcium

imaging using the transgenic line *Tg(pkd211:GCaMP5G)*. If flow at 1 dpf selectively altered CSF-cN activity, this activity could guide newborn neurons as previously found (Sawamoto et al., 2006), readout of calcium signals to selectively trigger intracellular cascades (Borodinsky et al., 2004; Swapna and Borodinsky, 2012), or these processes could be carried by neuroblasts (Sawamoto et al., 2006), and CSF-cN activity driven by Pkd211 at 1 dpf is simply a feature of the sensory capacities of these cells.

Relationship of activity to function in ventral and dorsal CSF-cNs

In both mammals and zebrafish, CSF-cNs form subpopulations that originate from two progenitor populations (Park et al., 2004; Yang et al., 2010; Petracca et al., 2016) and subgroups have unique morphological, molecular, and electrical properties (Petracca et al., 2016; Annex 2). Differential activity between ventral and dorsal CSF-cNs at early stages could have consequences or reflect functional differences between these two subpopulations that derive from unique origins. At larval stages, ventral CSF-cNs form monosynaptic connections with excitatory neurons involved in both slow and fast locomotion as well as primary motor neurons active during fast swimming, both revealed by optogenetic activation of CSF-cNs. Morphological analysis suggests as well that ventral CSF-cNs form more dorsally-projecting axons that innervate fast locomotor circuitry whereas axons of dorsal CSF-cNs remain ventral in the spinal cord (Annex 2).

What is the connectivity and function of dorsal CSF-cNs versus ventral CSF-cNs? Synaptic partners of dorsal CSF-cNs remain unknown, although this population preferentially responds over ventral CSF-cNs to active or passive lateral bending of the tail at larval stages using calcium imaging with GCaMP5 (Böhm et al., 2016). Together, preferential targeting of motor circuitry by ventral CSF-cNs and larger responses to lateral bending of dorsal CSF-cNs suggest the two populations play distinct roles. For instance, ventral CSF-cNs could respond

to bending via a single action potential rather than burst spiking of dorsal CSF-cNs that can be detected with GCaMP5 or they could detect bending along the vertical axis instead of the lateral directions. Addressing the connectivity of dorsal CSF-cNs, and mostly, the physiological activation of these cells *in vivo* will further expound on heterogeneity of the population that could be reflected by embryonic activity.

IV. Conclusions

CSF-cNs comprise a heterogeneous population of intraspinal neurons that display high levels of activity during development and expression of diverse signaling molecules that could impart unique functions to development or locomotion. Understanding the contribution of PKD2L1 and other ion channels to activity of CSF-cNs during development, in response to sensory stimuli, or even by secreting molecules into the CSF will create a larger picture of the possible roles of CSF-cNs in regulating activity in the spinal cord and the nervous system.

References

- Abou Alaiwi, W. A., S. T. Lo, and S. M. Nauli. "Primary Cilia: Highly Sophisticated Biological Sensors." *Sensors* 9, no. 9 (2009): 7003-20.
- Ahrens, M. B., M. B. Orger, D. N. Robson, J. M. Li, and P. J. Keller. "Whole-Brain Functional Imaging at Cellular Resolution Using Light-Sheet Microscopy." *Nat Methods* 10, no. 5 (2013): 413-20.
- Akerboom, J., T. W. Chen, T. J. Wardill, L. Tian, J. S. Marvin, S. Mutlu, N. C. Calderon, *et al.* "Optimization of a Gcamp Calcium Indicator for Neural Activity Imaging." *J Neurosci* 32, no. 40 (2012): 13819-40.
- Al-Mosawie, A., J. M. Wilson, and R. M. Brownstone. "Heterogeneity of V2-Derived Interneurons in the Adult Mouse Spinal Cord." *Eur J Neurosci* 26, no. 11 (2007): 3003-15.
- Ampatzis, K., J. Song, J. Ausborn, and A. El Manira. "Separate Microcircuit Modules of Distinct V2a Interneurons and Motoneurons Control the Speed of Locomotion." *Neuron* 83, no. 4 (2014): 934-43.
- Aoki, K. R., and B. Guyer. "Botulinum Toxin Type a and Other Botulinum Toxin Serotypes: A Comparative Review of Biochemical and Pharmacological Actions." *Eur J Neurol* 8 (2001): 21-9.
- Aoyagi, Y., R. B. Stein, A. Branner, K. G. Pearson, and R. A. Normann. "Capabilities of a Penetrating Microelectrode Array for Recording Single Units in Dorsal Root Ganglia of the Cat." *J Neurosci Methods* 128, no. 1 (2003): 9-20.
- Appelbaum, L., G. X. Wang, G. S. Maro, R. Mori, A. Tovin, W. Marin, T. Yokogawa, *et al.* "Sleep-Wake Regulation and Hypocretin-Melatonin Interaction in Zebrafish." *Proc Natl Acad Sci U S A* 106, no. 51 (2009): 21942-7.
- Arenkiel, B. R., M. E. Klein, I. G. Davison, L. C. Katz, and M. D. Ehlers. "Genetic Control of Neuronal Activity in Mice Conditionally Expressing Trpv1." *Nat Methods* 5, no. 4 (2008): 299-302.
- Armbruster, B., X. Li, M. H. Pausch, S. Herlitze, and B. Roth. "Evolving the Lock to Fit the Key to Create a Family of G Protein-Coupled Receptors Potently Activated by an Inert Ligand." *Proceedings of the National Academy of Sciences* 104, no. 12 (2007): 5163-68.
- Armstrong, C., E. Krook-Magnuson, M. Oijala, and I. Soltesz. "Closed-Loop Optogenetic Intervention in Mice." *Nat Protoc* 8, no. 8 (2013): 1475-93.
- Armstrong, D. M. "The Supraspinal Control of Mammalian Locomotion." *J Physiol* 405 (1988): 1-37.
- Arrenberg, A. B., F. Del Bene, and H. Baier. "Optical Control of Zebrafish Behavior with Halorhodopsin." *Proc Natl Acad Sci USA* 106, no. 42 (2009): 17968-73.
- Asakawa, K., and K. Kawakami. "Targeted Gene Expression by the Gal4-Uas System in Zebrafish." *Development, growth & differentiation* 50, no. 6 (2008): 391-99.
- Asakawa, K., M. L. Suster, K. Mizusawa, S. Nagayoshi, T. Kotani, A. Urasaki, Y. Kishimoto, M. Hibi, and K. Kawakami. "Genetic Dissection of Neural Circuits by Tol2 Transposon-Mediated Gal4 Gene and Enhancer Trapping in Zebrafish." *Proc Natl Acad Sci U S A* 105, no. 4 (2008): 1255-60.
- Bannai, H., F. Niwa, M. W. Sherwood, A. N. Shrivastava, M. Arizono, A. Miyamoto, K. Sugiura, *et al.* "Bidirectional Control of Synaptic Gabaar Clustering by Glutamate and Calcium." *Cell Rep* 13, no. 12 (2015): 2768-80.
- Barber, R. P., J. E. Vaughn, and E. Roberts. "The Cytoarchitecture of Gabaergic Neurons in Rat Spinal Cord." *Brain Res* 238, no. 2 (1982): 305-28.
- Barbin, G., H. Pollard, J. L. Gaiarsa, and Y. Ben-Ari. "Involvement of Gabaa Receptors in the Outgrowth of Cultured Hippocampal Neurons." *Neurosci Lett* 152, no. 1-2 (1993): 150-4.
- Ben-Ari, Y. "Excitatory Actions of Gaba During Development: The Nature of the Nurture." *Nat Rev Neurosci* 3, no. 9 (2002): 728-39.
- Berbari, N. F., A. K. O'Connor, C. J. Haycraft, and B. K. Yoder. "The Primary Cilium as a Complex Signaling Center." *Curr Biol* 19, no. 13 (2009): R526-35.
- Bernhardt, R. R., A. B. Chitnis, L. Lindamer, and J. Y. Kuwada. "Identification of Spinal Neurons in the Embryonic and Larval Zebrafish." *J Comp Neurol* 302, no. 3 (1990): 603-16.

References

- Bernhardt, R. R., C. K. Patel, S. W. Wilson, and J. Y. Kuwada. "Axonal Trajectories and Distribution of Gabaergic Spinal Neurons in Wildtype and Mutant Zebrafish Lacking Floor Plate Cells." *J Comp Neurol* 326, no. 2 (1992): 263-72.
- Bernstein, J. G., and E. S. Boyden. "Optogenetic Tools for Analyzing the Neural Circuits of Behavior." *Trends in cognitive sciences* 15, no. 12 (2011): 592-600.
- Bianco, I. H., A. R. Kampff, and F. Engert. "Prey Capture Behavior Evoked by Simple Visual Stimuli in Larval Zebrafish." *Front Syst Neurosci* 5 (2011): 101.
- Bito, L., H. Davson, E. Levin, M. Murray, and N. Snider. "The Concentrations of Free Amino Acids and Other Electrolytes in Cerebrospinal Fluid, in Vivo Dialysate of Brain, and Blood Plasma of the Dog." *Journal of neurochemistry* 13, no. 11 (1966): 1057-67.
- Blankenship, A. G., and M. B. Feller. "Mechanisms Underlying Spontaneous Patterned Activity in Developing Neural Circuits." *Nat Rev Neurosci* 11, no. 1 (2010): 18-29.
- Blaser, R. E., L. Chadwick, and G. C. McGinnis. "Behavioral Measures of Anxiety in Zebrafish (*Danio Rerio*)." *Behav Brain Res* 208, no. 1 (2010): 56-62.
- Bohm, U. L., A. Prendergast, L. Djenoune, S. Nunes Figueiredo, J. Gomez, C. Stokes, S. Kaiser, *et al.* "Csf-Contacting Neurons Regulate Locomotion by Relaying Mechanical Stimuli to Spinal Circuits." *Nat Commun* 7 (2016): 10866.
- Borla, M. A., B. Palecek, S. Budick, and D. M. O'Malley. "Prey Capture by Larval Zebrafish: Evidence for Fine Axial Motor Control." *Brain Behav Evol* 60, no. 4 (2002): 207-29.
- Borodinsky, L. N., C. M. Root, J. A. Cronin, S. B. Sann, X. Gu, and N. C. Spitzer. "Activity-Dependent Homeostatic Specification of Transmitter Expression in Embryonic Neurons." *Nature* 429, no. 6991 (2004): 523-30.
- Bouvier, J., V. Caggiano, R. Leiras, V. Caldeira, C. Bellardita, K. Balueva, A. Fuchs, and O. Kiehn. "Descending Command Neurons in the Brainstem That Halt Locomotion." *Cell* 163, no. 5 (2015): 1191-203.
- Boyden, E. S., F. Zhang, E. Bamberg, G. Nagel, and K. Deisseroth. "Millisecond-Timescale, Genetically Targeted Optical Control of Neural Activity." *Nat Neurosci* 8, no. 9 (2005): 1263-8.
- Bradbury, M. W., and W. Lathem. "A Flow of Cerebrospinal Fluid Along the Central Canal of the Spinal Cord of the Rabbit and Communications between This Canal and the Sacral Subarachnoid Space." *J Physiol* 181, no. 4 (1965): 785-800.
- Bramble, D. M., and D. R. Carrier. "Running and Breathing in Mammals." *Science* 219, no. 4582 (1983): 251-6.
- Branson, K., A. A. Robie, J. Bender, P. Perona, and M. H. Dickinson. "High-Throughput Ethomics in Large Groups of *Drosophila*." *Nat Methods* 6, no. 6 (2009): 451-7.
- Brown, A. E., E. I. Yemini, L. J. Grundy, T. Jucikas, and W. R. Schafer. "A Dictionary of Behavioral Motifs Reveals Clusters of Genes Affecting *Caenorhabditis Elegans* Locomotion." *Proc Natl Acad Sci U S A* 110, no. 2 (2013): 791-6.
- Brunger, A. T., R. Jin, and M. A. Breidenbach. "Highly Specific Interactions between Botulinum Neurotoxins and Synaptic Vesicle Proteins." *Cell Mol Life Sci* 65, no. 15 (2008): 2296-306.
- Buchanan, J. T., L. Brodin, T. Hokfelt, P. A. Van Dongen, and S. Grillner. "Survey of Neuropeptide-Like Immunoreactivity in the Lamprey Spinal Cord." *Brain Res* 408, no. 1-2 (1987): 299-302.
- Buchanan, J. T., and S. Grillner. "Newly Identified 'Glutamate Interneurons' and Their Role in Locomotion in the Lamprey Spinal Cord." *Science* 236, no. 4799 (1987): 312-4.
- Budick, S. A., and D. M. O'Malley. "Locomotor Repertoire of the Larval Zebrafish: Swimming, Turning and Prey Capture." *J Exp Biol* 203, no. Pt 17 (2000): 2565-79.
- . "Locomotor Repertoire of the Larval Zebrafish: Swimming, Turning and Prey Capture." [In eng]. *J Exp Biol* 203, no. Pt 17 (Sep 2000): 2565-79.
- Bulina, M. E., K. A. Lukyanov, O. V. Britanova, D. Onichtchouk, S. Lukyanov, and D. M. Chudakov. "Chromophore-Assisted Light Inactivation (Cali) Using the Phototoxic Fluorescent Protein Killerred." *Nat Protoc* 1, no. 2 (2006): 947-53.

References

- Buonomano, D. V., and W. Maass. "State-Dependent Computations: Spatiotemporal Processing in Cortical Networks." *Nat Rev Neurosci* 10, no. 2 (2009): 113-25.
- Burgess, H. A., and M. Granato. "Modulation of Locomotor Activity in Larval Zebrafish During Light Adaptation." *J Exp Biol* 210, no. Pt 14 (2007): 2526-39.
- . "Sensorimotor Gating in Larval Zebrafish." *J Neurosci* 27, no. 18 (2007): 4984-94.
- Bushman, J. D., W. Ye, and E. R. Liman. "A Proton Current Associated with Sour Taste: Distribution and Functional Properties." *FASEB J* 29, no. 7 (2015): 3014-26.
- Buske, C., and R. Gerlai. "Shoaling Develops with Age in Zebrafish (*Danio Rerio*)." *Prog Neuropsychopharmacol Biol Psychiatry* 35, no. 6 (2011): 1409-15.
- Cachat, J., A. Stewart, E. Utterback, P. Hart, S. Gaikwad, K. Wong, E. Kyzar, N. Wu, and A. V. Kalueff. "Three-Dimensional Neurophenotyping of Adult Zebrafish Behavior." *PLoS One* 6, no. 3 (2011): e17597.
- Caterina, M. J., M. A. Schumacher, M. Tominaga, T. A. Rosen, J. D. Levine, and D. Julius. "The Capsaicin Receptor: A Heat-Activated Ion Channel in the Pain Pathway." *Nature* 389, no. 6653 (1997): 816-24.
- Chalfie, M., J. E. Sulston, J. G. White, E. Southgate, J. N. Thomson, and S. Brenner. "The Neural Circuit for Touch Sensitivity in *Caenorhabditis Elegans*." *J Neurosci* 5, no. 4 (1985): 956-64.
- Chatzigeorgiou, M., and W. R. Schafer. "Lateral Facilitation between Primary Mechanosensory Neurons Controls Nose Touch Perception in *C. Elegans*." *Neuron* 70, no. 2 (2011): 299-309.
- Chen, S., C. N. Chiu, K. L. McArthur, J. R. Fetcho, and D. A. Prober. "Trp Channel Mediated Neuronal Activation and Ablation in Freely Behaving Zebrafish." *Nat Methods* 13, no. 2 (2016): 147-50.
- Chen, X. Z., P. M. Vassilev, N. Basora, J. B. Peng, H. Nomura, Y. Segal, E. M. Brown, *et al.* "Polycystin-L Is a Calcium-Regulated Cation Channel Permeable to Calcium Ions." *Nature* 401, no. 6751 (1999): 383-6.
- Chou, M. Y., R. Amo, M. Kinoshita, B. W. Cherng, H. Shimazaki, M. Agetsuma, T. Shiraki, *et al.* "Social Conflict Resolution Regulated by Two Dorsal Habenular Subregions in Zebrafish." *Science* 352, no. 6281 (2016): 87-90.
- Chow, B. Y., X. Han, A. S. Dobry, X. Qian, A. S. Chuong, M. Li, M. A. Henninger, *et al.* "High-Performance Genetically Targetable Optical Neural Silencing by Light-Driven Proton Pumps." *Nature* 463, no. 7277 (2010): 98-102.
- Christensen, A. P., and D. P. Corey. "Trp Channels in Mechanosensation: Direct or Indirect Activation?" *Nat Rev Neurosci* 8, no. 7 (2007): 510-21.
- Cina, C., J. F. Bechberger, M. A. Ozog, and C. C. Naus. "Expression of Connexins in Embryonic Mouse Neocortical Development." *J Comp Neurol* 504, no. 3 (2007): 298-313.
- Clapham, D. E. "Trp Channels as Cellular Sensors." *Nature* 426, no. 6966 (2003): 517-24.
- Coste, B., B. Xiao, J. S. Santos, R. Syeda, J. Grandl, K. S. Spencer, S. E. Kim, *et al.* "Piezo Proteins Are Pore-Forming Subunits of Mechanically Activated Channels." *Nature* 483, no. 7388 (2012): 176-81.
- Crisp, S. J., J. F. Evers, and M. Bate. "Endogenous Patterns of Activity Are Required for the Maturation of a Motor Network." *J Neurosci* 31, no. 29 (2011): 10445-50.
- Crone, S. A., K. A. Quinlan, L. Zagoraiou, S. Droho, C. E. Restrepo, L. Lundfald, T. Endo, *et al.* "Genetic Ablation of V2a Ipsilateral Interneurons Disrupts Left-Right Locomotor Coordination in Mammalian Spinal Cord." *Neuron* 60, no. 1 (2008): 70-83.
- Curado, S., R. M. Anderson, B. Jungblut, J. Mumm, E. Schroeter, and D. Y. Stainier. "Conditional Targeted Cell Ablation in Zebrafish: A New Tool for Regeneration Studies." *Dev Dyn* 236, no. 4 (2007): 1025-35.
- Curado, S., D. Y. Stainier, and R. M. Anderson. "Nitroreductase-Mediated Cell/Tissue Ablation in Zebrafish: A Spatially and Temporally Controlled Ablation Method with Applications in Developmental and Regeneration Studies." *Nat Protoc* 3, no. 6 (2008): 948-54.
- Dale, N. "Reciprocal Inhibitory Interneurons in the *Xenopus* Embryo Spinal Cord." *J Physiol* 363 (1985): 61-70.

References

- Dale, N., A. Roberts, O. P. Ottersen, and J. Storm-Mathisen. "The Development of a Population of Spinal Cord Neurons and Their Axonal Projections Revealed by Gaba Immunocytochemistry in Frog Embryos." *Proc R Soc Lond B Biol Sci* 232, no. 1267 (1987): 205-15.
- . "The Morphology and Distribution of 'Kolmer-Agdurh Cells', a Class of Cerebrospinal-Fluid-Contacting Neurons Revealed in the Frog Embryo Spinal Cord by Gaba Immunocytochemistry." *Proc R Soc Lond B Biol Sci* 232, no. 1267 (1987): 193-203.
- Dankert, H., L. Wang, E. D. Hoopfer, D. J. Anderson, and P. Perona. "Automated Monitoring and Analysis of Social Behavior in *Drosophila*." *Nat Methods* 6, no. 4 (2009): 297-303.
- Danos, N., and G. V. Lauder. "The Ontogeny of Fin Function During Routine Turns in Zebrafish *Danio Rerio*." *J Exp Biol* 210, no. Pt 19 (2007): 3374-86.
- de Chaumont, F., R. D. Coura, P. Serreau, A. Cressant, J. Chabout, S. Granon, and J. C. Olivo-Marin. "Computerized Video Analysis of Social Interactions in Mice." *Nat Methods* 9, no. 4 (2012): 410-7.
- DeCaen, P. G., M. Delling, T. N. Vien, and D. E. Clapham. "Direct Recording and Molecular Identification of the Calcium Channel of Primary Cilia." *Nature* 504, no. 7479 (2013): 315-8.
- Deisseroth, K. "Optogenetics: 10 Years of Microbial Opsins in Neuroscience." *Nat Neurosci* 18, no. 9 (2015): 1213-25.
- Delcomyn, F. "Neural Basis of Rhythmic Behavior in Animals." *Science* 210, no. 4469 (1980): 492-8.
- Delling, M., P. G. DeCaen, J. F. Doerner, S. Febvay, and D. E. Clapham. "Primary Cilia Are Specialized Calcium Signalling Organelles." *Nature* 504, no. 7479 (2013): 311-4.
- Delling, M., A. A. Indzhukulian, X. Liu, Y. Li, T. Xie, D. P. Corey, and D. E. Clapham. "Primary Cilia Are Not Calcium-Responsive Mechanosensors." *Nature* 531, no. 7596 (2016): 656-60.
- Demarque, M., A. Represa, H. Becq, I. Khalilov, Y. Ben-Ari, and L. Aniksztejn. "Paracrine Intercellular Communication by a Ca²⁺- and Snare-Independent Release of Gaba and Glutamate Prior to Synapse Formation." *Neuron* 36, no. 6 (2002): 1051-61.
- Desarmenien, M. G., and N. C. Spitzer. "Role of Calcium and Protein Kinase C in Development of the Delayed Rectifier Potassium Current in *Xenopus* Spinal Neurons." *Neuron* 7, no. 5 (1991): 797-805.
- Djenoune, L. "Molecular and Morphological Analysis of Spinal Cerebrospinal Fluid-Contacting Neurons." Doctoral Thesis, 2015.
- Djenoune, L., H. Khabou, F. Joubert, F. B. Quan, S. Nunes Figueiredo, L. Bodineau, F. Del Bene, *et al.* "Investigation of Spinal Cerebrospinal Fluid-Contacting Neurons Expressing Pkd211: Evidence for a Conserved System from Fish to Primates." *Front Neuroanat* 8 (2014): 26.
- Dougherty, K. J., and O. Kiehn. "Functional Organization of V2a-Related Locomotor Circuits in the Rodent Spinal Cord." *Ann N Y Acad Sci* 1198 (2010): 85-93.
- Dougherty, K. J., L. Zagoraoui, D. Satoh, I. Rozani, S. Doobar, S. Arber, T. M. Jessell, and O. Kiehn. "Locomotor Rhythm Generation Linked to the Output of Spinal Shox2 Excitatory Interneurons." *Neuron* 80, no. 4 (2013): 920-33.
- Douglass, A. D., S. Kraves, K. Deisseroth, A. F. Schier, and F. Engert. "Escape Behavior Elicited by Single, Channelrhodopsin-2-Evoked Spikes in Zebrafish Somatosensory Neurons." *Curr Biol* 18, no. 15 (2008): 1133-7.
- Downes, G. B., and M. Granato. "Supraspinal Input Is Dispensable to Generate Glycine-Mediated Locomotive Behaviors in the Zebrafish Embryo." *J Neurobiol* 66, no. 5 (2006): 437-51.
- Drapeau, P., L. Saint-Amant, R. R. Buss, M. Chong, J. R. McDermid, and E. Brustein. "Development of the Locomotor Network in Zebrafish." *Prog Neurobiol* 68, no. 2 (2002): 85-111.
- Drew, T., S. Prentice, and B. Schepens. "Cortical and Brainstem Control of Locomotion." *Prog Brain Res* 143 (2004): 251-61.
- Driever, W., L. Solnica-Krezel, A. F. Schier, S. C. Neuhauss, J. Malicki, D. L. Stemple, D. Y. Stainier, *et al.* "A Genetic Screen for Mutations Affecting Embryogenesis in Zebrafish." *Development* 123 (1996): 37-46.

References

- Duysens, J., and K. G. Pearson. "Inhibition of Flexor Burst Generation by Loading Ankle Extensor Muscles in Walking Cats." *Brain Res* 187, no. 2 (1980): 321-32.
- E., Agduhr. "Über Ein Zentrales Sinnesorgan (?) Bei Den Vertebraten." *Z. Anat. Entwickl. Gesch* 66 (1922): 223-360.
- Eaton, R. C., and R. D. Farley. "Spawning Cycle and Egg Production of Zebrafish, *Brachydanio Rerio*, in the Laboratory." *Copeia* (1974): 195-204.
- Eklof-Ljunggren, E., S. Haupt, J. Ausborn, I. Dehnisch, P. Uhlen, S. Higashijima, and A. El Manira. "Origin of Excitation Underlying Locomotion in the Spinal Circuit of Zebrafish." *Proc Natl Acad Sci U S A* 109, no. 14 (2012): 5511-6.
- Elbaz, I., L. Yelin-Bekerman, J. Nicenboim, G. Vatine, and L. Appelbaum. "Genetic Ablation of Hypocretin Neurons Alters Behavioral State Transitions in Zebrafish." *J Neurosci* 32, no. 37 (2012): 12961-72.
- Fallani Fde, V., M. Corazzol, J. R. Sternberg, C. Wyart, and M. Chavez. "Hierarchy of Neural Organization in the Embryonic Spinal Cord: Granger-Causality Graph Analysis of in Vivo Calcium Imaging Data." *IEEE Trans Neural Syst Rehabil Eng* 23, no. 3 (2015): 333-41.
- Fidelin, K., L. Djenoune, C. Stokes, A. Prendergast, J. Gomez, A. Baradel, F. Del Bene, and C. Wyart. "State-Dependent Modulation of Locomotion by Gabaergic Spinal Sensory Neurons." *Current Biology* 25, no. 23 (2015): 3035-47.
- Fields, H. "State-Dependent Opioid Control of Pain." *Nat Rev Neurosci* 5, no. 7 (2004): 565-75.
- Fischer, JA, E Giniger, T Maniatis, and M Ptashne. "Gal4 Activates Transcription in *Drosophila*." *Nature* 332, no. 6167 (1988): 853.
- Fleisch, V. C., and S. C. Neuhaus. "Visual Behavior in Zebrafish." *Zebrafish* 3, no. 2 (2006): 191-201.
- Flint, A. C., R. S. Dammerman, and A. R. Kriegstein. "Endogenous Activation of Metabotropic Glutamate Receptors in Neocortical Development Causes Neuronal Calcium Oscillations." *Proc Natl Acad Sci U S A* 96, no. 21 (1999): 12144-9.
- Fontaine, E., D. Lentink, S. Kranenbarg, U. K. Muller, J. L. van Leeuwen, A. H. Barr, and J. W. Burdick. "Automated Visual Tracking for Studying the Ontogeny of Zebrafish Swimming." *J Exp Biol* 211, no. Pt 8 (2008): 1305-16.
- Foreman, M. B., and R. C. Eaton. "The Direction Change Concept for Reticulospinal Control of Goldfish Escape." *J Neurosci* 13, no. 10 (1993): 4101-13.
- Friedmann, D., A. Hoagland, S. Berlin, and E. Y. Isacoff. "A Spinal Opsin Controls Early Neural Activity and Drives a Behavioral Light Response." *Curr Biol* 25, no. 1 (2015): 69-74.
- Gahtan, E., P. Tanger, and H. Baier. "Visual Prey Capture in Larval Zebrafish Is Controlled by Identified Reticulospinal Neurons Downstream of the Tectum." *J Neurosci* 25, no. 40 (2005): 9294-303.
- Galli, L., and L. Maffei. "Spontaneous Impulse Activity of Rat Retinal Ganglion Cells in Prenatal Life." *Science* 242, no. 4875 (1988): 90-91.
- Garaschuk, O., E. Hanse, and A. Konnerth. "Developmental Profile and Synaptic Origin of Early Network Oscillations in the Ca1 Region of Rat Neonatal Hippocampus." *J Physiol* 507 (1998): 219-36.
- Gaspar, P., O. Cases, and L. Maroteaux. "The Developmental Role of Serotonin: News from Mouse Molecular Genetics." *Nat Rev Neurosci* 4, no. 12 (2003): 1002-12.
- Gautrais, J., F. Ginelli, R. Fournier, S. Blanco, M. Soria, H. Chate, and G. Theraulaz. "Deciphering Interactions in Moving Animal Groups." *PLoS Comput Biol* 8, no. 9 (2012): e1002678.
- Getting, P. A. "Mechanisms of Pattern Generation Underlying Swimming in *Tritonia*. Iii. Intrinsic and Synaptic Mechanisms for Delayed Excitation." *J Neurophysiol* 49, no. 4 (1983): 1036-50.
- Gonzalez-Islas, C., and P. Wenner. "Spontaneous Network Activity in the Embryonic Spinal Cord Regulates Ampaergic and Gabaergic Synaptic Strength." *Neuron* 49, no. 4 (2006): 563-75.
- Gopfert, M. C., J. T. Albert, B. Nadrowski, and A. Kamikouchi. "Specification of Auditory Sensitivity by *Drosophila* Trp Channels." *Nat Neurosci* 9, no. 8 (2006): 999-1000.

References

- Gorostiza, P., and E. Y. Isacoff. "Optical Switches for Remote and Noninvasive Control of Cell Signaling." *Science* 322, no. 5900 (2008): 395-9.
- Gosgnach, S., G. M. Lanuza, S. J. Butt, H. Saueressig, Y. Zhang, T. Velasquez, D. Riethmacher, *et al.* "V1 Spinal Neurons Regulate the Speed of Vertebrate Locomotor Outputs." *Nature* 440, no. 7081 (2006): 215-9.
- Goulding, M. "Circuits Controlling Vertebrate Locomotion: Moving in a New Direction." *Nat Rev Neurosci* 10, no. 7 (2009): 507-18.
- Granato, M., F. J. van Eeden, U. Schach, T. Trowe, M. Brand, M. Furutani-Seiki, P. Haffter, *et al.* "Genes Controlling and Mediating Locomotion Behavior of the Zebrafish Embryo and Larva." *Development* 123 (1996): 399-413.
- Greka, A., B. Navarro, E. Oancea, A. Duggan, and D. E. Clapham. "Trpc5 Is a Regulator of Hippocampal Neurite Length and Growth Cone Morphology." *Nat Neurosci* 6, no. 8 (2003): 837-45.
- Grewe, B. F., D. Langer, H. Kasper, B. M. Kampa, and F. Helmchen. "High-Speed in Vivo Calcium Imaging Reveals Neuronal Network Activity with near-Millisecond Precision." *Nat Methods* 7, no. 5 (2010): 399-405.
- Grillner, S. "The Motor Infrastructure: From Ion Channels to Neuronal Networks." *Nat Rev Neurosci* 4, no. 7 (2003): 573-86.
- Grillner, S., T. Deliagina, O. Ekeberg, A. el Manira, R. H. Hill, A. Lansner, G. N. Orlovsky, and P. Wallen. "Neural Networks That Co-Ordinate Locomotion and Body Orientation in Lamprey." *Trends Neurosci* 18, no. 6 (1995): 270-9.
- Grillner, S., and A. El Manira. "The Intrinsic Operation of the Networks That Make Us Locomote." *Curr Opin Neurobiol* 31 (2015): 244-9.
- Grillner, S., and T. M. Jessell. "Measured Motion: Searching for Simplicity in Spinal Locomotor Networks." *Curr Opin Neurobiol* 19, no. 6 (2009): 572-86.
- Grillner, S., A. Kozlov, P. Dario, C. Stefanini, A. Menciassi, A. Lansner, and J. Hellgren Kotaleski. "Modeling a Vertebrate Motor System: Pattern Generation, Steering and Control of Body Orientation." *Prog Brain Res* 165 (2007): 221-34.
- Grillner, S., and M. L. Shik. "On the Descending Control of the Lumbosacral Spinal Cord from the "Mesencephalic Locomotor Region"." *Acta Physiol Scand* 87, no. 3 (1973): 320-33.
- Grillner, S., and P. Wallen. "Central Pattern Generators for Locomotion, with Special Reference to Vertebrates." *Annu Rev Neurosci* 8 (1985): 233-61.
- Grillner, S., P. Wallen, L. Brodin, and A. Lansner. "Neuronal Network Generating Locomotor Behavior in Lamprey: Circuitry, Transmitters, Membrane Properties, and Simulation." *Annu Rev Neurosci* 14 (1991): 169-99.
- Grillner, S., and P. Zangger. "On the Central Generation of Locomotion in the Low Spinal Cat." *Exp Brain Res* 34, no. 2 (1979): 241-61.
- Grimes, D. T., C. W. Boswell, N. F. Morante, R. M. Henkelman, R. D. Burdine, and B. Ciruna. "Zebrafish Models of Idiopathic Scoliosis Link Cerebrospinal Fluid Flow Defects to Spine Curvature." *Science* 352, no. 6291 (2016): 1341-4.
- Grunwald, D. J., and J. S. Eisen. "Headwaters of the Zebrafish -- Emergence of a New Model Vertebrate." *Nat Rev Genet* 3, no. 9 (2002): 717-24.
- Gu, X., and N. C. Spitzer. "Distinct Aspects of Neuronal Differentiation Encoded by Frequency of Spontaneous Ca²⁺ Transients." *Nature* 375, no. 6534 (1995): 784-7.
- Haffter, P., and C. Nusslein-Volhard. "Large Scale Genetics in a Small Vertebrate, the Zebrafish." *Int J Dev Biol* 40, no. 1 (1996): 221-7.
- Hale, M. E. "Locomotor Mechanics During Early Life History: Effects of Size and Ontogeny on Fast-Start Performance of Salmonid Fishes." *J Exp Biol* 202 (1999): 1465-79.
- Hale, M. E., D. A. Ritter, and J. R. Fetcho. "A Confocal Study of Spinal Interneurons in Living Larval Zebrafish." *J Comp Neurol* 437, no. 1 (2001): 1-16.
- Hamburger, V., and M. Balaban. "Observations and Experiments on Spontaneous Rhythmical Behavior in the Chick Embryo." *Dev Biol* 6 (1963): 533-45.

References

- Hanganu, I. L., A. Okabe, V. Lessmann, and H. J. Luhmann. "Cellular Mechanisms of Subplate-Driven and Cholinergic Input-Dependent Network Activity in the Neonatal Rat Somatosensory Cortex." *Cereb Cortex* 19, no. 1 (2009): 89-105.
- Hanson, M. G., and L. T. Landmesser. "Increasing the Frequency of Spontaneous Rhythmic Activity Disrupts Pool-Specific Axon Fasciculation and Pathfinding of Embryonic Spinal Motoneurons." *J Neurosci* 26, no. 49 (2006): 12769-80.
- Hansson, S. R., E. Mezey, and B. J. Hoffman. "Serotonin Transporter Messenger Rna in the Developing Rat Brain: Early Expression in Serotonergic Neurons and Transient Expression in Non-Serotonergic Neurons." *Neuroscience* 83, no. 4 (1998): 1185-201.
- Harris-Warrick, R. M., and E. Marder. "Modulation of Neural Networks for Behavior." *Annu Rev Neurosci* 14 (1991): 39-57.
- Hartfield, E. M., F. Rinaldi, C. P. Glover, L. F. Wong, M. A. Caldwell, and J. B. Uney. "Connexin 36 Expression Regulates Neuronal Differentiation from Neural Progenitor Cells." *PLoS One* 6, no. 3 (2011): e14746.
- Haverkamp, L. J. "Anatomical and Physiological Development of the Xenopus Embryonic Motor System in the Absence of Neural Activity." *J Neurosci* 6, no. 5 (1986): 1338-48.
- Haycraft, C. J., B. Banizs, Y. Aydin-Son, Q. Zhang, E. J. Michaud, and B. K. Yoder. "Gli2 and Gli3 Localize to Cilia and Require the Intraflagellar Transport Protein Polaris for Processing and Function." *PLoS Genet* 1, no. 4 (2005): e53.
- Hernandez, O., E. Papagiakoumou, D. Tanese, K. Fidelin, C. Wyart, and V. Emiliani. "Three-Dimensional Spatiotemporal Focusing of Holographic Patterns." *Nat Commun* 7 (2016): 11928.
- Higuchi, T., T. Shimizu, T. Fujii, B. Nilius, and H. Sakai. "Gating Modulation by Heat of the Polycystin Transient Receptor Potential Channel Pkd211 (Trpp3)." *Pflugers Arch* 466, no. 10 (2014): 1933-40.
- Hirata, H., L. Saint-Amant, G. B. Downes, W. W. Cui, W. Zhou, M. Granato, and J. Y. Kuwada. "Zebrafish Bandoneon Mutants Display Behavioral Defects Due to a Mutation in the Glycine Receptor Beta-Subunit." *Proc Natl Acad Sci U S A* 102, no. 23 (2005): 8345-50.
- Hooker, D. "Early Human Fetal Behavior, with a Preliminary Note on Double Simultaneous Fetal Stimulation." *Res Publ Assoc Res Nerv Ment Dis* 33 (1954): 98-113.
- Horio, N., R. Yoshida, K. Yasumatsu, Y. Yanagawa, Y. Ishimaru, H. Matsunami, and Y. Ninomiya. "Sour Taste Responses in Mice Lacking Pkd Channels." *PLoS One* 6, no. 5 (2011): e20007.
- Hoyt, D. F., and C. R. Taylor. "Gait and the Energetics of Locomotion in Horses." *Nature* (1981).
- Hu, M., Y. Liu, J. Wu, and X. Liu. "Influx-Operated Ca(2+) Entry Via Pkd2-L1 and Pkd1-L3 Channels Facilitates Sensory Responses to Polymodal Transient Stimuli." *Cell Rep* 13, no. 4 (2015): 798-811.
- Huang, K. H., M. B. Ahrens, T. W. Dunn, and F. Engert. "Spinal Projection Neurons Control Turning Behaviors in Zebrafish." *Curr Biol* 23, no. 16 (2013): 1566-73.
- Hubbard, J.M., U.L. Böhm, A. Prendergast, P.-E. Tseng, M. Newman, C. Stokes, and C. Wyart. "Intraspinal Sensory Neurons Provide Powerful Inhibition to Motor Circuits Ensuring Postural Control During Locomotion." (In revision).
- Hugnot, J. P., and R. Franzen. "The Spinal Cord Ependymal Region: A Stem Cell Niche in the Caudal Central Nervous System." *Front Biosci (Landmark Ed)* 16 (2011): 1044-59.
- Inada, H., F. Kawabata, Y. Ishimaru, T. Fushiki, H. Matsunami, and M. Tominaga. "Off-Response Property of an Acid-Activated Cation Channel Complex Pkd113-Pkd211." *EMBO Rep* 9, no. 7 (2008): 690-7.
- Ishimaru, Y., H. Inada, M. Kubota, H. Zhuang, M. Tominaga, and H. Matsunami. "Transient Receptor Potential Family Members Pkd113 and Pkd211 Form a Candidate Sour Taste Receptor." *Proc Natl Acad Sci U S A* 103, no. 33 (2006): 12569-74.
- Jacobs, G. A., J. P. Miller, and Z. Aldworth. "Computational Mechanisms of Mechanosensory Processing in the Cricket." *J Exp Biol* 211, no. 11 (2008): 1819-28.
- Jalalvand, E., B. Robertson, H. Tostivint, P. Wallen, and S. Grillner. "The Spinal Cord Has an Intrinsic System for the Control of Ph." *Curr Biol* 26, no. 10 (2016): 1346-51.

References

- Jalalvand, E., B. Robertson, P. Wallen, and S. Grillner. "Ciliated Neurons Lining the Central Canal Sense Both Fluid Movement and Ph through *Asic3*." *Nat Commun* 7 (2016): 10002.
- Jalalvand, E., B. Robertson, P. Wallen, R. H. Hill, and S. Grillner. "Laterally Projecting Cerebrospinal Fluid-Contacting Cells in the Lamprey Spinal Cord Are of Two Distinct Types." *J Comp Neurol* 522, no. 8 (2014): Spc1.
- Jessell, T. M. "Neuronal Specification in the Spinal Cord: Inductive Signals and Transcriptional Codes." *Nat Rev Genet* 1, no. 1 (2000): 20-9.
- Jhuang, H., E. Garrote, J. Mutch, X. Yu, V. Khilnani, T. Poggio, A. D. Steele, and T. Serre. "Automated Home-Cage Behavioural Phenotyping of Mice." *Nat Commun* 1 (2010): 68.
- Jordan, L. M., J. Liu, P. B. Hedlund, T. Akay, and K. G. Pearson. "Descending Command Systems for the Initiation of Locomotion in Mammals." *Brain research reviews* 57, no. 1 (2008): 183-91.
- Jordt, S. E., D. M. Bautista, H. H. Chuang, D. D. McKemy, P. M. Zygmunt, E. D. Hogestatt, I. D. Meng, and D. Julius. "Mustard Oils and Cannabinoids Excite Sensory Nerve Fibres through the Trp Channel *Anktm1*." *Nature* 427, no. 6971 (2004): 260-5.
- Jouary, Adrien, and German Sumbre. "Automatic Classification of Behavior in Zebrafish Larvae." *bioRxiv* (2016): 052324.
- Kabra, M., A. A. Robie, M. Rivera-Alba, S. Branson, and K. Branson. "Jaaba: Interactive Machine Learning for Automatic Annotation of Animal Behavior." *Nat Methods* 10, no. 1 (2013): 64-7.
- Kandler, K., and L. C. Katz. "Coordination of Neuronal Activity in Developing Visual Cortex by Gap Junction-Mediated Biochemical Communication." *J Neurosci* 18, no. 4 (1998): 1419-27.
- Kang, L., J. Gao, W. R. Schafer, Z. Xie, and X. Z. Xu. "C. Elegans Trp Family Protein Trp-4 Is a Pore-Forming Subunit of a Native Mechanotransduction Channel." *Neuron* 67, no. 3 (2010): 381-91.
- Kao, I., D. B. Drachman, and D. L. Price. "Botulinum Toxin: Mechanism of Presynaptic Blockade." *Science* 193, no. 4259 (1976): 1256-8.
- Karunaratne, A., M. Hargrave, A. Poh, and T. Yamada. "Gata Proteins Identify a Novel Ventral Interneuron Subclass in the Developing Chick Spinal Cord." *Dev Biol* 249, no. 1 (2002): 30-43.
- Kastanenka, K. V., and L. T. Landmesser. "Optogenetic-Mediated Increases in in Vivo Spontaneous Activity Disrupt Pool-Specific but Not Dorsal-Ventral Motoneuron Pathfinding." *Proc Natl Acad Sci U S A* 110, no. 43 (2013): 17528-33.
- Katz, L. C., and C. J. Shatz. "Synaptic Activity and the Construction of Cortical Circuits." *Science* 274, no. 5290 (1996): 1133-8.
- Katz, P. S., P. A. Getting, and W. N. Frost. "Dynamic Neuromodulation of Synaptic Strength Intrinsic to a Central Pattern Generator Circuit." *Nature* 367, no. 6465 (1994): 729-31.
- Katz, Y., K. Tunstrom, C. C. Ioannou, C. Huepe, and I. D. Couzin. "Inferring the Structure and Dynamics of Interactions in Schooling Fish." *Proc Natl Acad Sci U S A* 108, no. 46 (2011): 18720-5.
- Kay, J. N., K. C. Finger-Baier, T. Roeser, W. Staub, and H. Baier. "Retinal Ganglion Cell Genesis Requires *Lakritz*, a Zebrafish *Atonal* Homolog." *Neuron* 30 (Jun 2001): 725-36.
- Khor, B. S., M. F. Jamil, M. I. Adenan, and A. C. Shu-Chien. "Mitragnine Attenuates Withdrawal Syndrome in Morphine-Withdrawn Zebrafish." *PLoS One* 6, no. 12 (2011): e28340.
- Kiehn, O. "Decoding the Organization of Spinal Circuits That Control Locomotion." *Nat Rev Neurosci* 17, no. 4 (2016): 224-38.
- Kimmel, C. B., W. W. Ballard, S. R. Kimmel, B. Ullmann, and T. F. Schilling. "Stages of Embryonic Development of the Zebrafish." *Dev Dyn* 203, no. 3 (1995): 253-310.
- Kimura, Y., Y. Okamura, and S. Higashijima. "Alx, a Zebrafish Homolog of *Chx10*, Marks Ipsilateral Descending Excitatory Interneurons That Participate in the Regulation of Spinal Locomotor Circuits." *J Neurosci* 26, no. 21 (2006): 5684-97.

References

- Kimura, Y., C. Satou, S. Fujioka, W. Shoji, K. Umeda, T. Ishizuka, H. Yawo, and S. Higashijima. "Hindbrain V2a Neurons in the Excitation of Spinal Locomotor Circuits During Zebrafish Swimming." *Curr Biol* 23, no. 10 (2013): 843-9.
- Kimura, Y., C. Satou, and S. Higashijima. "V2a and V2b Neurons Are Generated by the Final Divisions of Pair-Producing Progenitors in the Zebrafish Spinal Cord." *Development* 135, no. 18 (2008): 3001-5.
- Kindt, K. S., V. Viswanath, L. Macpherson, K. Quast, H. Hu, A. Patapoutian, and W. R. Schafer. "Caenorhabditis Elegans Trpa-1 Functions in Mechanosensation." *Nat Neurosci* 10, no. 5 (2007): 568-77.
- Kiprilov, E. N., A. Awan, R. Desprat, M. Velho, C. A. Clement, A. G. Byskov, C. Y. Andersen, *et al.* "Human Embryonic Stem Cells in Culture Possess Primary Cilia with Hedgehog Signaling Machinery." *J Cell Biol* 180, no. 5 (2008): 897-904.
- Kirkby, L. A., G. S. Sack, A. Firl, and M. B. Feller. "A Role for Correlated Spontaneous Activity in the Assembly of Neural Circuits." *Neuron* 80, no. 5 (2013): 1129-44.
- Kjaerulff, O., and O. Kiehn. "Distribution of Networks Generating and Coordinating Locomotor Activity in the Neonatal Rat Spinal Cord in Vitro: A Lesion Study." *J Neurosci* 16, no. 18 (1996): 5777-94.
- Knaut, H., P. Blader, U. Strahle, and A. F. Schier. "Assembly of Trigeminal Sensory Ganglia by Chemokine Signaling." *Neuron* 47, no. 5 (2005): 653-66.
- Knogler, L. D., J. Ryan, L. Saint-Amant, and P. Drapeau. "A Hybrid Electrical/Chemical Circuit in the Spinal Cord Generates a Transient Embryonic Motor Behavior." *J Neurosci* 34, no. 29 (2014): 9644-55.
- Kohashi, T., N. Nakata, and Y. Oda. "Effective Sensory Modality Activating an Escape Triggering Neuron Switches During Early Development in Zebrafish." *J Neurosci* 32, no. 17 (2012): 5810-20.
- Kohashi, T., and Y. Oda. "Initiation of Mauthner- or Non-Mauthner-Mediated Fast Escape Evoked by Different Modes of Sensory Input." *J Neurosci* 28, no. 42 (2008): 10641-53.
- Kokel, D., J. Bryan, C. Laggner, R. White, C. Y. Cheung, R. Mateus, D. Healey, *et al.* "Rapid Behavior-Based Identification of Neuroactive Small Molecules in the Zebrafish." *Nat Chem Biol* 6, no. 3 (2010): 231-37.
- Kolmer, W. "Das 'Sagittallorgan' Der Wirbeltiere." *Z. Anat. EntwGesch* 60 (1921 1921): 652-717.
- . "Über Das Sagittalorgan, Ein Zentrales Sinnesorgan Der Wirbeltiere, Insbesondere Beim Affen." *Z. Zellforsch* 13 (1931): 236-48.
- Korn, H., and D. S. Faber. "The Mauthner Cell Half a Century Later: A Neurobiological Model for Decision-Making?". *Neuron* 47, no. 1 (2005): 13-28.
- Koulen, P., R. S. Duncan, J. Liu, N. E. Cohen, J. A. Yannazzo, N. McClung, C. L. Lockhart, M. Branden, and M. Buechner. "Polycystin-2 Accelerates Ca²⁺ Release from Intracellular Stores in Caenorhabditis Elegans." *Cell Calcium* 37, no. 6 (2005): 593-601.
- Kramer, R. H., D. L. Fortin, and D. Trauner. "New Photochemical Tools for Controlling Neuronal Activity." *Curr Opin Neurobiol* 19, no. 5 (2009): 544-52.
- Kramer-Zucker, A. G., F. Olale, C. J. Haycraft, B. K. Yoder, A. F. Schier, and I. A. Drummond. "Cilia-Driven Fluid Flow in the Zebrafish Pronephros, Brain and Kupffer's Vesicle Is Required for Normal Organogenesis." *Development* 132, no. 8 (2005): 1907-21.
- Kucenas, S., N. Takada, H. C. Park, E. Woodruff, K. Broadie, and B. Appel. "Cns-Derived Glia Ensheath Peripheral Nerves and Mediate Motor Root Development." *Nat Neurosci* 11, no. 2 (2008): 143-51.
- Kurita, R., H. Sagara, Y. Aoki, B. A. Link, K. Arai, and S. Watanabe. "Suppression of Lens Growth by Aa-Crystallin Promoter-Driven Expression of Diphtheria Toxin Results in Disruption of Retinal Cell Organization in Zebrafish." *Dev Biol* 255, no. 1 (2003): 113-27.
- Kuwada, J. Y., R. R. Bernhardt, and N. Nguyen. "Development of Spinal Neurons and Tracts in the Zebrafish Embryo." *J Comp Neurol* 302, no. 3 (1990): 617-28.
- Kwan, K. M., E. Fujimoto, C. Grabher, B. D. Mangum, M. E. Hardy, D. S. Campbell, J. M. Parant, *et al.* "The Tol2kit: A Multisite Gateway-Based Construction Kit for Tol2 Transposon Transgenesis Constructs." *Dev Dyn* 236, no. 11 (2007): 3088-99.

References

- Lambert, A. M., J. L. Bonkowsky, and M. A. Masino. "The Conserved Dopaminergic Diencephalospinal Tract Mediates Vertebrate Locomotor Development in Zebrafish Larvae." *J Neurosci* 32, no. 39 (2012): 13488-500.
- Lanuza, G. M., S. Gosgnach, A. Pierani, T. M. Jessell, and M. Goulding. "Genetic Identification of Spinal Interneurons That Coordinate Left-Right Locomotor Activity Necessary for Walking Movements." *Neuron* 42, no. 3 (2004): 375-86.
- Lauterbach, M. A., E. Ronzitti, J. R. Sternberg, C. Wyart, and V. Emiliani. "Fast Calcium Imaging with Optical Sectioning Via Hilo Microscopy." *PLoS One* 10, no. 12 (2015): e0143681.
- Lebrand, C., O. Cases, C. Adelbrecht, A. Doye, C. Alvarez, S. El Mestikawy, I. Seif, and P. Gaspar. "Transient Uptake and Storage of Serotonin in Developing Thalamic Neurons." *Neuron* 17, no. 5 (1996): 823-35.
- Lee, A., A. S. Mathuru, C. Teh, C. Kibat, V. Korzh, T. B. Penney, and S. Jesuthasan. "The Habenula Prevents Helpless Behavior in Larval Zebrafish." *Curr Biol* 20, no. 24 (2010): 2211-6.
- Lee, K. J., and T. M. Jessell. "The Specification of Dorsal Cell Fates in the Vertebrate Central Nervous System." *Annu Rev Neurosci* 22 (1999): 261-94.
- Lehnert, B. P., A. E. Baker, Q. Gaudry, A. S. Chiang, and R. I. Wilson. "Distinct Roles of Trp Channels in Auditory Transduction and Amplification in Drosophila." *Neuron* 77, no. 1 (2013): 115-28.
- Leifer, A. M., C. Fang-Yen, M. Gershow, M. J. Alkema, and A. D. Samuel. "Optogenetic Manipulation of Neural Activity in Freely Moving Caenorhabditis Elegans." *Nat Methods* 8, no. 2 (2011): 147-52.
- Leinekugel, X., I. Medina, I. Khalilov, Y. Ben-Ari, and R. Khazipov. "Ca²⁺ Oscillations Mediated by the Synergistic Excitatory Actions of Gaba(a) and Nmda Receptors in the Neonatal Hippocampus." *Neuron* 18, no. 2 (1997): 243-55.
- Lewis, K. E., and J. S. Eisen. "From Cells to Circuits: Development of the Zebrafish Spinal Cord." *Prog Neurobiol* 69, no. 6 (2003): 419-49.
- Li, W. C., S. Higashijima, D. M. Parry, A. Roberts, and S. R. Soffe. "Primitive Roles for Inhibitory Interneurons in Developing Frog Spinal Cord." *J Neurosci* 24, no. 25 (2004): 5840-8.
- Li, Y., Y. C. Jia, K. Cui, N. Li, Z. Y. Zheng, Y. Z. Wang, and X. B. Yuan. "Essential Role of Trpc Channels in the Guidance of Nerve Growth Cones by Brain-Derived Neurotrophic Factor." *Nature* 434, no. 7035 (2005): 894-8.
- Lima, S. Q., and G. Miesenbock. "Remote Control of Behavior through Genetically Targeted Photostimulation of Neurons." *Cell* 121, no. 1 (2005): 141-52.
- Liman, E. R., D. P. Corey, and C. Dulac. "Trp2: A Candidate Transduction Channel for Mammalian Pheromone Sensory Signaling." *Proc Natl Acad Sci U S A* 96, no. 10 (1999): 5791-6.
- Lin, S. Y., and D. P. Corey. "Trp Channels in Mechanosensation." *Curr Opin Neurobiol* 15, no. 3 (2005): 350-7.
- Liu, K. S., and J. R. Fetcho. "Laser Ablations Reveal Functional Relationships of Segmental Hindbrain Neurons in Zebrafish." *Neuron* 23, no. 2 (1999): 325-35.
- Liu, Y., Q. Li, M. Tan, Y. Y. Zhang, E. Karpinski, J. Zhou, and X. Z. Chen. "Modulation of the Human Polycystin-L Channel by Voltage and Divalent Cations." *FEBS Lett* 525, no. 1-3 (2002): 71-6.
- Liu, Y. C., I. Bailey, and M. E. Hale. "Alternative Startle Motor Patterns and Behaviors in the Larval Zebrafish (Danio Rerio)." *J Comp Physiol A Neuroethol Sens Neural Behav Physiol* 198, no. 1 (2012): 11-24.
- Ljunggren, E. E., S. Haupt, J. Ausborn, K. Ampatzis, and A. El Manira. "Optogenetic Activation of Excitatory Premotor Interneurons Is Sufficient to Generate Coordinated Locomotor Activity in Larval Zebrafish." *J Neurosci* 34, no. 1 (2014): 134-9.
- Loeb, G. E., M. J. Bak, and J. Duysens. "Long-Term Unit Recording from Somatosensory Neurons in the Spinal Ganglia of the Freely Walking Cat." *Science* 197, no. 4309 (1977): 1192-94.
- LoTurco, J. J., D. F. Owens, M. J. Heath, M. B. Davis, and A. R. Kriegstein. "Gaba and Glutamate Depolarize Cortical Progenitor Cells and Inhibit DNA Synthesis." *Neuron* 15, no. 6 (1995): 1287-98.

References

- Lundfald, L., C. E. Restrepo, S. J. Butt, C. Y. Peng, S. Droho, T. Endo, H. U. Zeilhofer, K. Sharma, and O. Kiehn. "Phenotype of V2-Derived Interneurons and Their Relationship to the Axon Guidance Molecule Epha4 in the Developing Mouse Spinal Cord." *Eur J Neurosci* 26, no. 11 (2007): 2989-3002.
- Ma, Q. "Labeled Lines Meet and Talk: Population Coding of Somatic Sensations." *J Clin Invest* 120, no. 11 (2010): 3773-8.
- Maher, B. J., M. J. McGinley, and G. L. Westbrook. "Experience-Dependent Maturation of the Glomerular Microcircuit." *Proc Natl Acad Sci U S A* 106, no. 39 (2009): 16865-70.
- Mahn, M., M. Prigge, S. Ron, R. Levy, and O. Yizhar. "Biophysical Constraints of Optogenetic Inhibition at Presynaptic Terminals." *Nat Neurosci* 19, no. 4 (2016): 554-6.
- Manent, J. B., M. Demarque, I. Jorquera, C. Pellegrino, Y. Ben-Ari, L. Aniksztejn, and A. Represa. "A Noncanonical Release of Gaba and Glutamate Modulates Neuronal Migration." *J Neurosci* 25, no. 19 (2005): 4755-65.
- Marder, E., and R. L. Calabrese. "Principles of Rhythmic Motor Pattern Generation." *Physiol Rev* 76, no. 3 (1996): 687-717.
- Marder, E., T. O'Leary, and S. Shruti. "Neuromodulation of Circuits with Variable Parameters: Single Neurons and Small Circuits Reveal Principles of State-Dependent and Robust Neuromodulation." *Annu Rev Neurosci* 37 (2014): 329-46.
- Marder, E., and K. J. Rehm. "Development of Central Pattern Generating Circuits." *Curr Opin Neurobiol* 15, no. 1 (2005): 86-93.
- Marder, E., and V. Thirumalai. "Cellular, Synaptic and Network Effects of Neuromodulation." *Neural Netw* 15, no. 4-6 (Jun-Jul 2002): 479-93.
- Marques, J. C. "Density Valley Clustering Reveals New Swim Types of the Zebrafish Larvae." (2016).
- Masino, M. A., and J. R. Fetcho. "Fictive Swimming Motor Patterns in Wild Type and Mutant Larval Zebrafish." *J Neurophysiol* 93, no. 6 (2005): 3177-88.
- Mathias, J. R., Z. Zhang, M. T. Saxena, and J. S. Mumm. "Enhanced Cell-Specific Ablation in Zebrafish Using a Triple Mutant of Escherichia Coli Nitroreductase." *Zebrafish* 11, no. 2 (2014): 85-97.
- Mattis, J., K. M. Tye, E. A. Ferenczi, C. Ramakrishnan, D. J. O'Shea, R. Prakash, L. A. Gunaydin, *et al.* "Principles for Applying Optogenetic Tools Derived from Direct Comparative Analysis of Microbial Opsins." *Nat Methods* 9, no. 2 (2012): 159-72.
- McElligott, M. B., and M. O'Malley D. "Prey Tracking by Larval Zebrafish: Axial Kinematics and Visual Control." *Brain Behav Evol* 66, no. 3 (2005): 177-96.
- McLean, D. L., J. Fan, S. Higashijima, M. E. Hale, and J. R. Fetcho. "A Topographic Map of Recruitment in Spinal Cord." *Nature* 446, no. 7131 (2007): 71-5.
- McLean, D. L., M. A. Masino, I. Y. Koh, W. B. Lindquist, and J. R. Fetcho. "Continuous Shifts in the Active Set of Spinal Interneurons During Changes in Locomotor Speed." *Nat Neurosci* 11, no. 12 (2008): 1419-29.
- Meister, M., R. O. Wong, D. A. Baylor, and C. J. Shatz. "Synchronous Bursts of Action Potentials in Ganglion Cells of the Developing Mammalian Retina." *Science* 252, no. 5008 (1991): 939-43.
- Menelaou, E., C. VanDunk, and D. L. McLean. "Differences in the Morphology of Spinal V2a Neurons Reflect Their Recruitment Order During Swimming in Larval Zebrafish." *J Comp Neurol* 522, no. 6 (2014): 1232-48.
- Metcalfe, W. K., C. B. Kimmel, and E. Schabtach. "Anatomy of the Posterior Lateral Line System in Young Larvae of the Zebrafish." *J Comp Neurol* 233, no. 3 (1985): 377-89.
- Miller, N., and R. Gerlai. "From Schooling to Shoaling: Patterns of Collective Motion in Zebrafish (Danio Rerio)." *PLoS One* 7, no. 11 (2012): e48865.
- Milner, L. D., and L. T. Landmesser. "Cholinergic and Gabaergic Inputs Drive Patterned Spontaneous Motoneuron Activity before Target Contact." *J Neurosci* 19, no. 8 (1999): 3007-22.
- Mirat, O., J. R. Sternberg, K. E. Severi, and C. Wyart. "Zebrazoom: An Automated Program for High-Throughput Behavioral Analysis and Categorization." *Front Neural Circuits* 7 (2013): 107.

References

- Montgomery, J. E., T. D. Wiggin, L. M. Rivera-Perez, C. Lillesaar, and M. A. Masino. "Intraspinal Serotonergic Neurons Consist of Two, Temporally Distinct Populations in Developing Zebrafish." *Dev Neurobiol* 76, no. 6 (2016): 673-87.
- Moody, W. J., and M. M. Bosma. "Ion Channel Development, Spontaneous Activity, and Activity-Dependent Development in Nerve and Muscle Cells." *Physiol Rev* 85, no. 3 (2005): 883-941.
- Moore, M. S., J. DeZazzo, A. Y. Luk, T. Tully, C. M. Singh, and U. Heberlein. "Ethanol Intoxication in Drosophila: Genetic and Pharmacological Evidence for Regulation by the Camp Signaling Pathway." *Cell* 93, no. 6 (1998): 997-1007.
- Moreno, R. L., and A. B. Ribera. "Spinal Neurons Require Islet1 for Subtype-Specific Differentiation of Electrical Excitability." *Neural Dev* 9 (2014): 19.
- Murakami, M., T. Ohba, F. Xu, S. Shida, E. Satoh, K. Ono, I. Miyoshi, *et al.* "Genomic Organization and Functional Analysis of Murine Pkd211." *J Biol Chem* 280, no. 7 (2005): 5626-35.
- Muto, A., M. Ohkura, T. Kotani, S. Higashijima, J. Nakai, and K. Kawakami. "Genetic Visualization with an Improved Gcamp Calcium Indicator Reveals Spatiotemporal Activation of the Spinal Motor Neurons in Zebrafish." *Proc Natl Acad Sci U S A* 108, no. 13 (2011): 5425-30.
- Myers, C. P., J. W. Lewcock, M. G. Hanson, S. Gosgnach, J. B. Aimone, F. H. Gage, K. F. Lee, L. T. Landmesser, and S. L. Pfaff. "Cholinergic Input Is Required During Embryonic Development to Mediate Proper Assembly of Spinal Locomotor Circuits." *Neuron* 46, no. 1 (2005): 37-49.
- Nagel, G., D. Ollig, M. Fuhrmann, S. Kateriya, A. M. Musti, E. Bamberg, and P. Hegemann. "Channelrhodopsin-1: A Light-Gated Proton Channel in Green Algae." *Science* 296, no. 5577 (2002): 2395-8.
- Nagel, G., T. Szellas, W. Huhn, S. Kateriya, N. Adeishvili, P. Berthold, D. Ollig, P. Hegemann, and E. Bamberg. "Channelrhodopsin-2, a Directly Light-Gated Cation-Selective Membrane Channel." *Proc Natl Acad Sci U S A* 100, no. 24 (2003): 13940-5.
- Nauli, S. M., F. J. Alenghat, Y. Luo, E. Williams, P. Vassilev, X. Li, A. E. Elia, *et al.* "Polycystins 1 and 2 Mediate Mechanosensation in the Primary Cilium of Kidney Cells." *Nat Genet* 33, no. 2 (2003): 129-37.
- Nauli, S. M., and J. Zhou. "Polycystins and Mechanosensation in Renal and Nodal Cilia." *Bioessays* 26, no. 8 (2004): 844-56.
- Nelson, T. M., N. D. Lopezjimenez, L. Tessarollo, M. Inoue, A. A. Bachmanov, and S. L. Sullivan. "Taste Function in Mice with a Targeted Mutation of the Pkd113 Gene." *Chem Senses* 35, no. 7 (2010): 565-77.
- Neuhauss, S. C., O. Biehlmaier, M. W. Seeliger, T. Das, K. Kohler, W. A. Harris, and H. Baier. "Genetic Disorders of Vision Revealed by a Behavioral Screen of 400 Essential Loci in Zebrafish." *J Neurosci* 19, no. 19 (1999): 8603-15.
- Ni, T. T., J. Lu, M. Zhu, L. A. Maddison, K. L. Boyd, L. Huskey, B. Ju, *et al.* "Conditional Control of Gene Function by an Invertible Gene Trap in Zebrafish." *Proc Natl Acad Sci U S A* 109, no. 38 (2012): 15389-94.
- Nishimaru, H., and M. Kakizaki. "The Role of Inhibitory Neurotransmission in Locomotor Circuits of the Developing Mammalian Spinal Cord." *Acta Physiol (Oxf)* 197, no. 2 (2009): 83-97.
- Nusslein-Volhard, C., and E. Wieschaus. "Mutations Affecting Segment Number and Polarity in Drosophila." *Nature* 287, no. 5785 (1980): 795-801.
- Odenthal, J., K. Rossnagel, P. Haffter, R. N. Kelsh, E. Vogelsang, M. Brand, F. J. van Eeden, *et al.* "Mutations Affecting Xanthophore Pigmentation in the Zebrafish, Danio Rerio." *Development* 123 (1996): 391-8.
- O'Malley, D. M., N. S. Sankrithi, M. A. Borla, S. Parker, S. Banden, E. Gahtan, and H. W. Detrich, 3rd. "Optical Physiology and Locomotor Behaviors of Wild-Type and Nacre Zebrafish." *Methods Cell Biol* 76 (2004): 261-84.
- Onativia, J., S. R. Schultz, and P. L. Dragotti. "A Finite Rate of Innovation Algorithm for Fast and Accurate Spike Detection from Two-Photon Calcium Imaging." *J Neural Eng* 10, no. 4 (2013): 046017.
- Orger, M. B., A. R. Kampff, K. E. Severi, J. H. Bollmann, and F. Engert. "Control of Visually Guided Behavior by Distinct Populations of Spinal Projection Neurons." *Nat Neurosci* 11, no. 3 (2008): 327-33.

References

- Ornitz, David M, Randall W Moreadith, and Philip Leder. "Binary System for Regulating Transgene Expression in Mice: Targeting Int-2 Gene Expression with Yeast Gal4/Uas Control Elements." *Proceedings of the National Academy of Sciences* 88, no. 3 (1991): 698-702.
- Orts-Del'Imagine, A., A. Kastner, V. Tillement, C. Tardivel, J. Trouslard, and N. Wanaverbecq. "Morphology, Distribution and Phenotype of Polycystin Kidney Disease 2-Like 1-Positive Cerebrospinal Fluid Contacting Neurons in the Brainstem of Adult Mice." *PLoS One* 9, no. 2 (2014): e87748.
- Orts-Del'Imagine, A., R. Seddik, F. Tell, C. Airault, G. Er-Raoui, M. Najimi, J. Trouslard, and N. Wanaverbecq. "A Single Polycystic Kidney Disease 2-Like 1 Channel Opening Acts as a Spike Generator in Cerebrospinal Fluid-Contacting Neurons of Adult Mouse Brainstem." *Neuropharmacology* 101 (2016): 549-65.
- Orts-Del'Imagine, A., N. Wanaverbecq, C. Tardivel, V. Tillement, M. Dallaporta, and J. Trouslard. "Properties of Subependymal Cerebrospinal Fluid Contacting Neurons in the Dorsal Vagal Complex of the Mouse Brainstem." *J Physiol* 590, no. 16 (2012): 3719-41.
- Otchy, T. M., S. B. Wolff, J. Y. Rhee, C. Pehlevan, R. Kawai, A. Kempf, S. M. Gobes, and B. P. Olveczky. "Acute Off-Target Effects of Neural Circuit Manipulations." *Nature* 528, no. 7582 (2015): 358-63.
- Owsianik, G., K. Talavera, T. Voets, and B. Nilius. "Permeation and Selectivity of Trp Channels." *Annu Rev Physiol* 68 (2006): 685-717.
- Park, H. C., J. Shin, and B. Appel. "Spatial and Temporal Regulation of Ventral Spinal Cord Precursor Specification by Hedgehog Signaling." *Development* 131, no. 23 (2004): 5959-69.
- Park, I. J., Y. V. Bobkov, B. W. Ache, and J. C. Principe. "Quantifying Bursting Neuron Activity from Calcium Signals Using Blind Deconvolution." *J Neurosci Methods* 218, no. 2 (2013): 196-205.
- Peier, A. M., A. Moqrich, A. C. Hergarden, A. J. Reeve, D. A. Andersson, G. M. Story, T. J. Earley, *et al.* "A Trp Channel That Senses Cold Stimuli and Menthol." *Cell* 108, no. 5 (2002): 705-15.
- Pellizzari, R., O. Rossetto, G. Schiavo, and C. Montecucco. "Tetanus and Botulinum Neurotoxins: Mechanism of Action and Therapeutic Uses." *Philos Trans R Soc Lond B Biol Sci* 354, no. 1381 (1999): 259-68.
- Perez, C. A., L. Huang, M. Rong, J. A. Kozak, A. K. Preuss, H. Zhang, M. Max, and R. F. Margolskee. "A Transient Receptor Potential Channel Expressed in Taste Receptor Cells." *Nat Neurosci* 5, no. 11 (2002): 1169-76.
- Personius, K. E., Q. Chang, G. Z. Mentis, M. J. O'Donovan, and R. J. Balice-Gordon. "Reduced Gap Junctional Coupling Leads to Uncorrelated Motor Neuron Firing and Precocious Neuromuscular Synapse Elimination." *Proc Natl Acad Sci U S A* 104, no. 28 (2007): 11808-13.
- Petracca, Y. L., M. M. Sartoretti, D. J. Di Bella, A. Marin-Burgin, A. L. Carcagno, A. F. Schinder, and G. M. Lanuza. "The Late and Dual Origin of Cerebrospinal Fluid-Contacting Neurons in the Mouse Spinal Cord." *Development* 143, no. 5 (2016): 880-91.
- Petzold, A. M., D. Balciunas, S. Sivasubbu, K. J. Clark, V. M. Bedell, S. E. Westcot, S. R. Myers, *et al.* "Nicotine Response Genetics in the Zebrafish." *Proc Natl Acad Sci U S A* 106, no. 44 (2009): 18662-7.
- Pfaff, S. L. "Development of a Spinal Sensorimotor Node That Modulates Limb Position in Response to Painful Stimuli." Paper presented at the 21st Biennial Meeting of the International Society for Developmental Neuroscience, France, 2016.
- Pnevmatikakis, E. A., D. Soudry, Y. Gao, T. A. Machado, J. Merel, D. Pfau, T. Reardon, *et al.* "Simultaneous Denoising, Deconvolution, and Demixing of Calcium Imaging Data." *Neuron* 89, no. 2 (2016): 285-99.
- Praetorius, H. A., and K. R. Spring. "A Physiological View of the Primary Cilium." *Annu Rev Physiol* 67 (2005): 515-29.
- Quan, F. B., C. Dubessy, S. Galant, N. B. Kenigfest, L. Djenoune, J. Leprince, C. Wyart, I. Lihmann, and H. Tostivint. "Comparative Distribution and in Vitro Activities of the Urotensin Ii-Related Peptides Urp1 and Urp2 in Zebrafish: Evidence for Their Colocalization in Spinal Cerebrospinal Fluid-Contacting Neurons." *PLoS One* 10, no. 3 (2015): e0119290.
- Rabinowitch, I., M. Chatzigeorgiou, and W. R. Schafer. "A Gap Junction Circuit Enhances Processing of Coincident Mechanosensory Inputs." *Curr Biol* 23, no. 11 (2013): 963-7.

References

- Raimondo, J. V., L. Kay, T. J. Ellender, and C. J. Akerman. "Optogenetic Silencing Strategies Differ in Their Effects on Inhibitory Synaptic Transmission." *Nat Neurosci* 15, no. 8 (2012): 1102-4.
- Reali, C., A. Fernandez, M. Radmilovich, O. Trujillo-Cenoz, and R. E. Russo. "Gabaergic Signalling in a Neurogenic Niche of the Turtle Spinal Cord." *J Physiol* 589, no. Pt 23 (2011): 5633-47.
- Represa, A., and Y. Ben-Ari. "Trophic Actions of Gaba on Neuronal Development." *Trends Neurosci* 28, no. 6 (2005): 278-83.
- Reynolds, A., E. Brustein, M. Liao, A. Mercado, E. Babilonia, D. B. Mount, and P. Drapeau. "Neurogenic Role of the Depolarizing Chloride Gradient Revealed by Global Overexpression of Kcc2 from the Onset of Development." *J Neurosci* 28, no. 7 (2008): 1588-97.
- Rihel, J., D. A. Prober, A. Arvanites, K. Lam, S. Zimmerman, S. Jang, S. J. Haggarty, *et al.* "Zebrafish Behavioral Profiling Links Drugs to Biological Targets and Rest/Wake Regulation." *Science* 327, no. 5963 (2010): 348-51.
- Rihel, J., and A. F. Schier. "Behavioral Screening for Neuroactive Drugs in Zebrafish." *Dev Neurobiol* 72, no. 3 (2012): 373-85.
- Ritter, D. A., D. H. Bhatt, and J. R. Fetcho. "In Vivo Imaging of Zebrafish Reveals Differences in the Spinal Networks for Escape and Swimming Movements." *J Neurosci* 21, no. 22 (2001): 8956-65.
- Roberts, A., W. C. Li, and S. R. Soffe. "How Neurons Generate Behavior in a Hatchling Amphibian Tadpole: An Outline." *Front Behav Neurosci* 4 (2010): 16.
- Roberts, B. L., and G. E. Meredith. "Immunohistochemical Study of a Dopaminergic System in the Spinal Cord of the Ray, *Raja Radiata*." *Brain Res* 437, no. 1 (1987): 171-5.
- Roberts, B. L., G. E. Meredith, and S. Maslam. "Immunocytochemical Analysis of the Dopamine System in the Brain and Spinal Cord of the European Eel, *Anguilla Anguilla*." *Anat Embryol (Berl)* 180, no. 4 (1989): 401-12.
- Rockhill, W., J. L. Kirkman, and M. M. Bosma. "Spontaneous Activity in the Developing Mouse Midbrain Driven by an External Pacemaker." *Dev Neurobiol* 69, no. 11 (2009): 689-704.
- Roeser, T., and H. Baier. "Visuomotor Behaviors in Larval Zebrafish after Gfp-Guided Laser Ablation of the Optic Tectum." *J Neurosci* 23, no. 9 (2003): 3726-34.
- Rogan, S. C., and B. L. Roth. "Remote Control of Neuronal Signaling." *Pharmacol Rev* 63, no. 2 (2011): 291-315.
- Rossignol, S., R. Dubuc, and J. P. Gossard. "Dynamic Sensorimotor Interactions in Locomotion." *Physiol Rev* 86, no. 1 (2006): 89-154.
- Saint-Amant, L., and P. Drapeau. "Motoneuron Activity Patterns Related to the Earliest Behavior of the Zebrafish Embryo." *J Neurosci* 20, no. 11 (2000): 3964-72.
- . "Synchronization of an Embryonic Network of Identified Spinal Interneurons Solely by Electrical Coupling." *Neuron* 31, no. 6 (2001): 1035-46.
- . "Time Course of the Development of Motor Behaviors in the Zebrafish Embryo." *J Neurobiol* 37, no. 4 (1998): 622-32.
- Sakurai, A., and P. S. Katz. "Spike Timing-Dependent Serotonergic Neuromodulation of Synaptic Strength Intrinsic to a Central Pattern Generator Circuit." *J Neurosci* 23, no. 34 (2003): 10745-55.
- Sandler, V. M., and J. G. Barbara. "Calcium-Induced Calcium Release Contributes to Action Potential-Evoked Calcium Transients in Hippocampal Ca1 Pyramidal Neurons." *J Neurosci* 19, no. 11 (1999): 4325-36.
- Satoh, D., C. Pudenz, and S. Arber. "Context-Dependent Gait Choice Elicited by Epha4 Mutation in Lbx1 Spinal Interneurons." *Neuron* 89, no. 5 (2016): 1046-58.
- Satou, C., Y. Kimura, H. Hirata, M. L. Suster, K. Kawakami, and S. Higashijima. "Transgenic Tools to Characterize Neuronal Properties of Discrete Populations of Zebrafish Neurons." *Development* 140, no. 18 (2013): 3927-31.
- Sawamoto, K., H. Wichterle, O. Gonzalez-Perez, J. A. Cholfin, M. Yamada, N. Spassky, N. S. Murcia, *et al.* "New Neurons Follow the Flow of Cerebrospinal Fluid in the Adult Brain." *Science* 311, no. 5761 (2006): 629-32.

References

- Schafer, M., D. Kinzel, and C. Winkler. "Discontinuous Organization and Specification of the Lateral Floor Plate in Zebrafish." *Dev Biol* 301, no. 1 (2007): 117-29.
- Scheer, Nico, and José A Campos-Ortega. "Use of the Gal4-Uas Technique for Targeted Gene Expression in the Zebrafish." *Mechanisms of development* 80, no. 2 (1999): 153-58.
- Schiavo, G., F. Benfenati, B. Poulain, O. Rossetto, P. Polverino de Laureto, B. R. DasGupta, and C. Montecucco. "Tetanus and Botulinum-B Neurotoxins Block Neurotransmitter Release by Proteolytic Cleavage of Synaptobrevin." *Nature* 359, no. 6398 (1992): 832-5.
- Scholz, H., J. Ramond, C. M. Singh, and U. Heberlein. "Functional Ethanol Tolerance in Drosophila." *Neuron* 28, no. 1 (2000): 261-71.
- Schoonheim, P. J., A. B. Arrenberg, F. Del Bene, and H. Baier. "Optogenetic Localization and Genetic Perturbation of Saccade-Generating Neurons in Zebrafish." *J Neurosci* 30, no. 20 (2010): 7111-20.
- Scott, E. K., L. Mason, A. B. Arrenberg, L. Ziv, N. J. Gosse, T. Xiao, N. C. Chi, *et al.* "Targeting Neural Circuitry in Zebrafish Using Gal4 Enhancer Trapping." *Nat Methods* 4, no. 4 (2007): 323-6.
- Seitz, R., J. Lohler, and G. Schwendemann. "Ependyma and Meninges of the Spinal Cord of the Mouse. A Light- and Electron-Microscopic Study." *Cell Tissue Res* 220, no. 1 (1981): 61-72.
- Severi, K. E., R. Portugues, J. C. Marques, D. M. O'Malley, M. B. Orger, and F. Engert. "Neural Control and Modulation of Swimming Speed in the Larval Zebrafish." *Neuron* 83, no. 3 (2014): 692-707.
- Sharif-Naeni, R., J. H. Folgering, D. Bichet, F. Duprat, I. Lauritzen, M. Arhatte, M. Jodar, *et al.* "Polycystin-1 and -2 Dosage Regulates Pressure Sensing." *Cell* 139, no. 3 (2009): 587-96.
- Sherrington, C. S. "Observations on the Scratch-Reflex in the Spinal Dog." *J Physiol* 34, no. 1-2 (1906): 1-50.
- Shim, S., E. L. Goh, S. Ge, K. Sailor, J. P. Yuan, H. L. Roderick, M. D. Bootman, *et al.* "Xtrpc1-Dependent Chemotropic Guidance of Neuronal Growth Cones." *Nat Neurosci* 8, no. 6 (2005): 730-5.
- Shimizu, T., T. Higuchi, T. Fujii, B. Nilius, and H. Sakai. "Bimodal Effect of Alkalinization on the Polycystin Transient Receptor Potential Channel, Pkd211." *Pflugers Arch* 461, no. 5 (2011): 507-13.
- Shimizu, T., A. Janssens, T. Voets, and B. Nilius. "Regulation of the Murine Trpp3 Channel by Voltage, Ph, and Changes in Cell Volume." *Pflugers Arch* 457, no. 4 (2009): 795-807.
- Shirasaki, R., and S. L. Pfaff. "Transcriptional Codes and the Control of Neuronal Identity." *Annu Rev Neurosci* 25 (2002): 251-81.
- Shmigol, A., A. Verkhratsky, and G. Isenberg. "Calcium-Induced Calcium Release in Rat Sensory Neurons." *J Physiol* 489 (Pt 3) (1995): 627-36.
- Simpson, L. L. "Identification of the Major Steps in Botulinum Toxin Action." *Annu Rev Pharmacol Toxicol* 44 (2004): 167-93.
- Singer, J. H., R. R. Mirotznik, and M. B. Feller. "Potentiation of L-Type Calcium Channels Reveals Nonsynaptic Mechanisms That Correlate Spontaneous Activity in the Developing Mammalian Retina." *J Neurosci* 21, no. 21 (2001): 8514-22.
- Smith, J. C., and J. L. Feldman. "In Vitro Brainstem-Spinal Cord Preparations for Study of Motor Systems for Mammalian Respiration and Locomotion." *J Neurosci Methods* 21, no. 2-4 (1987): 321-33.
- Spitzer, N. C. "Electrical Activity in Early Neuronal Development." *Nature* 444, no. 7120 (2006): 707-12.
- Stecher, B., U. Weller, E. Habermann, M. Gratzl, and G. Ahnert-Hilger. "The Light Chain but Not the Heavy Chain of Botulinum a Toxin Inhibits Exocytosis from Permeabilized Adrenal Chromaffin Cells." *FEBS Lett* 255, no. 2 (1989): 391-4.
- Steeves, J. D., and L. M. Jordan. "Localization of a Descending Pathway in the Spinal Cord Which Is Necessary for Controlled Treadmill Locomotion." *Neurosci Lett* 20, no. 3 (1980): 283-8.
- Stephens, G. J., B. Johnson-Kerner, W. Bialek, and W. S. Ryu. "Dimensionality and Dynamics in the Behavior of C. Elegans." *PLoS Comput Biol* 4, no. 4 (2008): e1000028.
- Sternson, S. M., and B. L. Roth. "Chemogenetic Tools to Interrogate Brain Functions." *Annu Rev Neurosci* 37 (2014): 387-407.

References

- Stirman, J. N., M. M. Crane, S. J. Husson, S. Wabnig, C. Schultheis, A. Gottschalk, and H. Lu. "Real-Time Multimodal Optical Control of Neurons and Muscles in Freely Behaving *Caenorhabditis Elegans*." *Nat Methods* 8, no. 2 (2011): 153-8.
- Stoeckel, M. E., S. Uhl-Bronner, S. Hugel, P. Veinante, M. J. Klein, J. Mutterer, M. J. Freund-Mercier, and R. Schlichter. "Cerebrospinal Fluid-Contacting Neurons in the Rat Spinal Cord, a Gamma-Aminobutyric Acidergic System Expressing the P2x2 Subunit of Purinergic Receptors, Psa-Ncam, and Gap-43 Immunoreactivities: Light and Electron Microscopic Study." *J Comp Neurol* 457, no. 2 (2003): 159-74.
- Streisinger, G., C. Walker, N. Dower, D. Knauber, and F. Singer. "Production of Clones of Homozygous Diploid Zebra Fish (*Brachydanio Rerio*)." *Nature* 291, no. 5813 (1981): 293-6.
- Strotmann, R., C. Harteneck, K. Nunnenmacher, G. Schultz, and T. D. Plant. "Otrpc4, a Nonselective Cation Channel That Confers Sensitivity to Extracellular Osmolarity." *Nat Cell Biol* 2, no. 10 (2000): 695-702.
- Sukharev, S. I., P. Blount, B. Martinac, F. R. Blattner, and C. Kung. "A Large-Conductance Mechanosensitive Channel in *E. Coli* Encoded by MscL Alone." *Nature* 368, no. 6468 (1994): 265-8.
- Suster, M. L., and M. Bate. "Embryonic Assembly of a Central Pattern Generator without Sensory Input." *Nature* 416, no. 6877 (2002): 174-8.
- Sutton, R. B., D. Fasshauer, R. Jahn, and A. T. Brunger. "Crystal Structure of a Snare Complex Involved in Synaptic Exocytosis at 2.4 Å Resolution." *Nature* 395, no. 6700 (1998): 347-53.
- Suzuki, Satoshi. "Topological Structural Analysis of Digitized Binary Images by Border Following." *Computer Vision, Graphics, and Image Processing* 30, no. 1 (1985): 32-46.
- Swapna, I., and L. N. Borodinsky. "Interplay between Electrical Activity and Bone Morphogenetic Protein Signaling Regulates Spinal Neuron Differentiation." *Proc Natl Acad Sci U S A* 109, no. 40 (2012): 16336-41.
- Swierczek, N. A., A. C. Giles, C. H. Rankin, and R. A. Kerr. "High-Throughput Behavioral Analysis in *C. Elegans*." *Nat Methods* 8, no. 7 (2011): 592-8.
- Talpalari, A. E., J. Bouvier, L. Borgius, G. Fortin, A. Pierani, and O. Kiehn. "Dual-Mode Operation of Neuronal Networks Involved in Left-Right Alternation." *Nature* 500, no. 7460 (2013): 85-8.
- Teh, C., D. M. Chudakov, K. L. Poon, I. Z. Mamedov, J. Y. Sek, K. Shidlovsky, S. Lukyanov, and V. Korzh. "Optogenetic in Vivo Cell Manipulation in Killerred-Expressing Zebrafish Transgenics." *BMC Dev Biol* 10 (2010): 110.
- Thorsen, D. H., J. J. Cassidy, and M. E. Hale. "Swimming of Larval Zebrafish: Fin-Axis Coordination and Implications for Function and Neural Control." *J Exp Biol* 207, no. Pt 24 (2004): 4175-83.
- Tong, H., and J. R. McDermid. "Pacemaker and Plateau Potentials Shape Output of a Developing Locomotor Network." *Curr Biol* 22, no. 24 (2012): 2285-93.
- Tovote, P., M. S. Esposito, P. Botta, F. Chaudun, J. P. Fadok, M. Markovic, S. B. Wolff, et al. "Midbrain Circuits for Defensive Behaviour." *Nature* 534, no. 7606 (2016): 206-12.
- Tritsch, N. X., E. Yi, J. E. Gale, E. Glowatzki, and D. E. Bergles. "The Origin of Spontaneous Activity in the Developing Auditory System." *Nature* 450, no. 7166 (2007): 50-5.
- Usachev, Y. M., and S. A. Thayer. "All-or-None Ca²⁺ Release from Intracellular Stores Triggered by Ca²⁺ Influx through Voltage-Gated Ca²⁺ Channels in Rat Sensory Neurons." *J Neurosci* 17, no. 19 (1997): 7404-14.
- Vanhoutte, P., and H. Bading. "Opposing Roles of Synaptic and Extrasynaptic Nmda Receptors in Neuronal Calcium Signalling and Bdnf Gene Regulation." *Curr Opin Neurobiol* 13, no. 3 (2003): 366-71.
- Vaziri, A., and V. Emiliani. "Reshaping the Optical Dimension in Optogenetics." *Curr Opin Neurobiol* 22, no. 1 (2012): 128-37.
- Vermoesen, K., A. S. Serruys, E. Loyens, T. Afrikanova, A. Massie, A. Schallier, Y. Michotte, et al. "Assessment of the Convulsant Liability of Antidepressants Using Zebrafish and Mouse Seizure Models." *Epilepsy Behav* 22, no. 3 (2011): 450-60.
- Vigh, B., and I. Vigh-Teichmann. "Actual Problems of the Cerebrospinal Fluid-Contacting Neurons." *Microsc Res Tech* 41, no. 1 (1998): 57-83.

References

- . "Comparative Ultrastructure of the Cerebrospinal Fluid-Contacting Neurons." *Int Rev Cytol* 35 (1973): 189-251.
- . "Structure of the Medullo-Spinal Liquor-Contacting Neuronal System." *Acta Biol Acad Sci Hung* 22, no. 2 (1971): 227-43.
- Vigh-Teichmann, I., and B. Vigh. "Structure and Function of the Liquor Contacting Neurosecretory System." In *Aspects of Neuroendocrinology*. 329-37: Springer, 1970.
- Voets, T., G. Droogmans, U. Wissenbach, A. Janssens, V. Flockerzi, and B. Nilius. "The Principle of Temperature-Dependent Gating in Cold- and Heat-Sensitive Trp Channels." *Nature* 430, no. 7001 (2004): 748-54.
- Voets, T., K. Talavera, G. Owsianik, and B. Nilius. "Sensing with Trp Channels." *Nat Chem Biol* 1, no. 2 (2005): 85-92.
- Vogelstein, J. T., B. O. Watson, A. M. Packer, R. Yuste, B. Jedynek, and L. Paninski. "Spike Inference from Calcium Imaging Using Sequential Monte Carlo Methods." *Biophys J* 97, no. 2 (2009): 636-55.
- Wallen, P., and T. L. Williams. "Fictive Locomotion in the Lamprey Spinal Cord in Vitro Compared with Swimming in the Intact and Spinal Animal." *J Physiol* 347 (1984): 225-39.
- Wan, H., S. Korzh, Z. Li, S. P. Mudumana, V. Korzh, Y. J. Jiang, S. Lin, and Z. Gong. "Analyses of Pancreas Development by Generation of Gfp Transgenic Zebrafish Using an Exocrine Pancreas-Specific Elastase Gene Promoter." *Exp Cell Res* 312, no. 9 (2006): 1526-39.
- Wang, D. D., D. D. Krueger, and A. Bordey. "Gaba Depolarizes Neuronal Progenitors of the Postnatal Subventricular Zone Via Gabaa Receptor Activation." *J Physiol* 550 (2003): 785-800.
- Wang, G. X., and M. M. Poo. "Requirement of Trpc Channels in Netrin-1-Induced Chemotropic Turning of Nerve Growth Cones." *Nature* 434, no. 7035 (2005): 898-904.
- Wark, B., B. N. Lundstrom, and A. Fairhall. "Sensory Adaptation." *Curr Opin Neurobiol* 17, no. 4 (2007): 423-9.
- Warp, E., G. Agarwal, C. Wyart, D. Friedmann, C. S. Oldfield, A. Conner, F. Del Bene, *et al.* "Emergence of Patterned Activity in the Developing Zebrafish Spinal Cord." *Curr Biol* 22, no. 2 (2012): 93-102.
- Wilson, Rachel I. "Constraints on Sensory Processing." In *Cognitive Neuroscience: The Biology of the Mind*, edited by Michael S. Gazzaniga, Richard B. Ivry and George R. Mangun. 261-70: MIT Press, 2014.
- Wu, M. C., L. A. Chu, P. Y. Hsiao, Y. Y. Lin, C. C. Chi, T. H. Liu, C. C. Fu, and A. S. Chiang. "Optogenetic Control of Selective Neural Activity in Multiple Freely Moving Drosophila Adults." *Proc Natl Acad Sci U S A* 111, no. 14 (2014): 5367-72.
- Wu, X., A. A. Indzhukulian, P. D. Nicksch, R. M. Webber, M. Garcia-Gonzalez, T. Watnick, J. Zhou, M. A. Vollrath, and D. P. Corey. "Hair-Cell Mechanotransduction Persists in Trp Channel Knockout Mice." *PLoS One* 11, no. 5 (2016): e0155577.
- Wyart, C., F. Del Bene, E. Warp, E. K. Scott, D. Trauner, H. Baier, and E. Y. Isacoff. "Optogenetic Dissection of a Behavioural Module in the Vertebrate Spinal Cord." *Nature* 461, no. 7262 (2009): 407-10.
- Yacubova, E., and H. Komuro. "Stage-Specific Control of Neuronal Migration by Somatostatin." *Nature* 415, no. 6867 (2002): 77-81.
- Yaksi, E., and R. W. Friedrich. "Reconstruction of Firing Rate Changes across Neuronal Populations by Temporally Deconvolved Ca²⁺ Imaging." *Nat Methods* 3, no. 5 (2006): 377-83.
- Yang, L., S. Rastegar, and U. Strahle. "Regulatory Interactions Specifying Kolmer-Agduhr Interneurons." *Development* 137, no. 16 (2010): 2713-22.
- Yizhar, O., L. E. Fenno, T. J. Davidson, M. Mogri, and K. Deisseroth. "Optogenetics in Neural Systems." *Neuron* 71, no. 1 (2011): 9-34.
- Yorozu, S., A. Wong, B. J. Fischer, H. Dankert, M. J. Kernan, A. Kamikouchi, K. Ito, and D. J. Anderson. "Distinct Sensory Representations of Wind and near-Field Sound in the Drosophila Brain." *Nature* 458, no. 7235 (2009): 201-5.
- Yoshida, S., H. Shiratori, I. Y. Kuo, A. Kawasumi, K. Shinohara, S. Nonaka, Y. Asai, *et al.* "Cilia at the Node of Mouse Embryos Sense Fluid Flow for Left-Right Determination Via Pkd2." *Science* 338, no. 6104 (2012): 226-31.

References

- Yu, Y., M. H. Ulbrich, M. H. Li, S. Dobbins, W. K. Zhang, L. Tong, E. Y. Isacoff, and J. Yang. "Molecular Mechanism of the Assembly of an Acid-Sensing Receptor Ion Channel Complex." *Nat Commun* 3 (2012): 1252.
- Zakhary, S. M., D. Ayubcha, F. Ansari, K. Kamran, M. Karim, J. R. Leheste, J. M. Horowitz, and G. Torres. "A Behavioral and Molecular Analysis of Ketamine in Zebrafish." *Synapse* 65, no. 2 (2011): 160-7.
- Zelenchuk, T. A., and J. L. Bruses. "In Vivo Labeling of Zebrafish Motor Neurons Using an Mnx1 Enhancer and Gal4/Uas." *Genesis* 49, no. 7 (2011): 546-54.
- Zhang, F., L. P. Wang, M. Brauner, J. F. Liewald, K. Kay, N. Watzke, P. G. Wood, *et al.* "Multimodal Fast Optical Interrogation of Neural Circuitry." *Nature* 446, no. 7136 (2007): 633-9.
- Zhang, J., G. M. Lanuza, O. Britz, Z. Wang, V. C. Siembab, Y. Zhang, T. Velasquez, *et al.* "V1 and V2b Interneurons Secure the Alternating Flexor-Extensor Motor Activity Mice Require for Limbed Locomotion." *Neuron* 82, no. 1 (2014): 138-50.
- Zhang, Y., S. Narayan, E. Geiman, G. M. Lanuza, T. Velasquez, B. Shanks, T. Akay, *et al.* "V3 Spinal Neurons Establish a Robust and Balanced Locomotor Rhythm During Walking." *Neuron* 60, no. 1 (2008): 84-96.
- Zhdanova, I. V., R. J. Wurtman, M. M. Regan, J. A. Taylor, J. P. Shi, and O. U. Leclair. "Melatonin Treatment for Age-Related Insomnia." *J Clin Endocrinol Metab* 86, no. 10 (2001): 4727-30.
- Zheng, W., S. Hussein, J. Yang, J. Huang, F. Zhang, S. Hernandez-Anzaldo, C. Fernandez-Patron, *et al.* "A Novel Pkd21l C-Terminal Domain Critical for Trimerization and Channel Function." *Sci Rep* 5 (2015): 9460.
- Zheng, Y., P. J. Brockie, J. E. Mellem, D. M. Madsen, and A. V. Maricq. "Neuronal Control of Locomotion in *C. Elegans* Is Modified by a Dominant Mutation in the Glr-1 Ionotropic Glutamate Receptor." *Neuron* 24, no. 2 (1999): 347-61.
- Zhong, G., K. Sharma, and R. M. Harris-Warrick. "Frequency-Dependent Recruitment of V2a Interneurons During Fictive Locomotion in the Mouse Spinal Cord." *Nat Commun* 2 (2011): 274.
- Ziv, L., A. Muto, P. J. Schoonheim, S. H. Meijnsing, D. Strasser, H. A. Ingraham, M. J. Schaaf, K. R. Yamamoto, and H. Baier. "An Affective Disorder in Zebrafish with Mutation of the Glucocorticoid Receptor." *Mol Psychiatry* 18, no. 6 (2013): 681-91.

Chapter 1

Olivier Mirat and Claire Wyart conceived the original project of developing automated tracking and classification of larval zebrafish behavior, and I worked with them to design the behavioral setup. I designed experiments with Claire Wyart, and I independently performed all of these experiments. I manually classified behaviors to evaluate the automatic algorithm and wrote the publication with Claire Wyart and Kristen Severi.

Chapter 2

I designed this project with Kristen Severi and Claire Wyart. I performed and analyzed embryonic behavior and calcium imaging, whole cell patch clamp confirmation of loss of synaptic input from CSF-cNs to PMNs, fictive recordings combined with calcium imaging, and quantification of changes in neurotransmitter expression when GABAergic CSF-cNS expressed BoTxBLC-GFP (Figures 1D-J, Figure 2, Figure 4G-J, and Supplemental Figures). I wrote the paper with Kristen Severi, with input from Claire Wyart and Kevin Fidelin. Max Suster generated the optimized UAS:BoTxBLC-GFP. Kristen Severi and Yara Alcheikh performed and analyzed larval behavioral experiments. Kevin Fidelin acquired and analyzed the initial dataset of fictive recordings.

Chapter 3

I performed multi-day calcium imaging with Lydia Djenoune and Andrew Prendergast. Johanna Gomez performed serotonin immunohistochemistry shown. Lydia Djenoune and Johanna Gomez contributed to quantification of GABA and serotonin expression in the *pkd211*^{-/-} mutant. I designed, performed, and analyzed all other experiments.

Contributions in annexes

Annex 2 – I performed and analyzed GABA immunohistochemistry in *pkd211*^{+/+} and *pkd211*^{-/-} and analyzed serotonin immunohistochemistry in *pkd211*^{+/+} and *pkd211*^{-/-}.

Annex 3 – I designed, performed, and analyzed $\Delta F/F$ for all experiments in this article and contributed to writing relevant sections of the manuscript. FDVF, MC, and MC performed and supervised Granger causality analysis.

Annex 4 – I designed (with CW) and performed (with ML and ER) all calcium imaging experiments in this article.

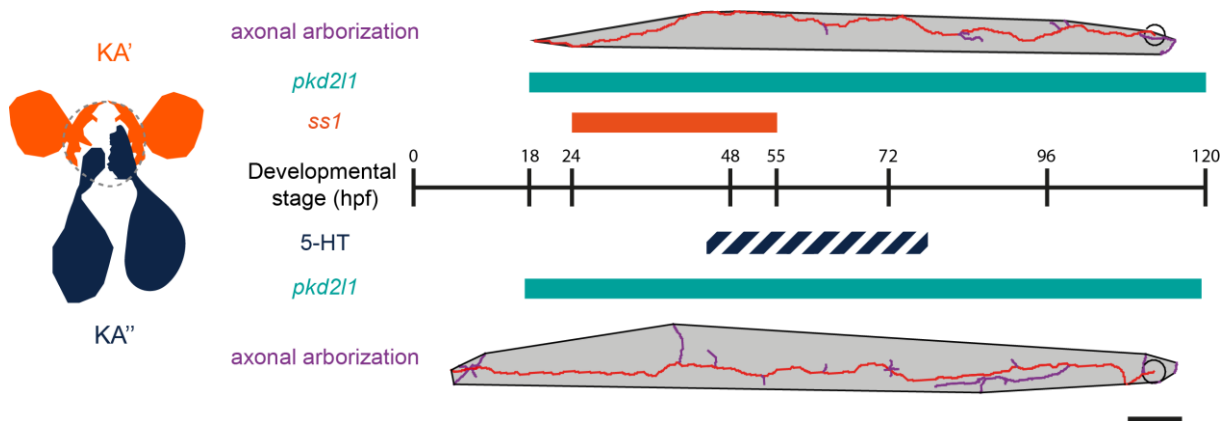
Annex 2

Spinal cerebrospinal fluid-contacting neurons segregate by morphology and molecular markers

Article in preparation

Lydia Djenoune, Laura Desban, Johanna Gomez, Andrew Prendergast, Jenna R. Sternberg, Thomas O. Auer, Filippo Del Bene, Pierre-Luc Bardet, Claire Wyart

Graphical Abstract



Abstract

Multiple evidence indicate that molecular and mechanical cues from the cerebrospinal fluid (CSF) can affect the development and function of the central nervous system (CNS). However, the mechanisms by which these cues are detected and relayed to the CNS remain elusive. Cerebrospinal fluid contacting neurons (CSF-cNs) being situated at the interface between the CSF and the CNS are in an ideal location to convey such information to local networks. In the spinal cord, these GABAergic neurons expressing the channel PKD2L1 extend an apical extension bearing microvilli into the CSF and an axon projecting rostrally. Evidence in zebrafish and mouse indicate that spinal CSF-cNs originate from at least two distinct progenitor domains. Here we ask whether these two groups of CSF-cNs differ by their morphology and molecular features. We show in zebrafish larva that morphology of the apical extension as well as the axon projection distinguish spinal CSF-cNs. In addition, each type is characterized by the expression of specific neuromodulator and peptides. Altogether our study demonstrates that spinal CSF-cNs identified by their developmental origins also corresponds to at least two cell types characterized by specific morphologies of the apical extension, axonal projections and neuromodulators. This work opens new research paths to understand how these cell types carry specific functions in spinal cord formation, locomotion and posture.

Introduction

The cerebrospinal fluid (CSF) is a complex solution circulating around the entire central nervous system (CNS). It has classically been assumed that CSF insured the homeostasis of the CNS (Davson et al., 1962; Di Terlizzi and Platt, 2006; Iliff et al., 2012). Multiple studies indicate that the CSF also conveys signals that can modulate the development and output functions of the nervous CNS, such as feeding, sleep, and locomotion (Pappenheimer et al., 1967; Martin et al., 1973; Lerner et al., 1994; Nishino et al., 2001; Gato et al., 2005; Sawamoto et al., 2006; Xie et al., 2013). This phenomenon implies that chemical or mechanical cues from the CSF can act on neurons in the brain and spinal cord. Cerebrospinal fluid-contacting neurons (CSF-cNs) are located precisely at the interface between the CSF in the central canal and the neuronal circuits (Vigh and Vigh-Teichmann, 1971; Vigh and Vigh-Teichmann, 1998).

In the vertebrate spinal cord, CSF-cNs reside around the central canal (Kolmer, 1921; Agduhr, 1922; Kolmer, 1931; Dale et al., 1987; Huang et al., 2006; Wyart et al., 2009; Djenoune et al., 2014; Jalalvand et al., 2014; Fidelin et al., 2015; Jalalvand et al., 2016). These cells project an apical dendritic extension that contacts the CSF (Vigh et al., 1974; 1977; Jaeger et al., 1983; Schueren and DeSantis, 1985; LaMotte, 1987; Vigh and Vigh-Teichmann, 1998; Stoeckel et al., 2003; Marichal et al., 2009) and an axon projecting locally axon (Ochi and Hosoya, 1974; Vigh et al., 1977; Dale et al., 1987a; b; Christenson et al., 1991b; Megias et al., 2003; Vigh et al., 2004; Jalalvand et al., 2014a) to modulate the activity of other neurons (Christenson et al., 1991a; Wyart et al., 2009; Fidelin et al., 2015).

One essential first step to understand spinal CSF-cN functions lies in identifying specific markers for these cells. In this regard, the polycystic kidney disease 2 like 1 (PKD2L1) channel also called TRPP3 (Delmas, 2004b; 2005) belonging to the Transient Potential Receptor (TRP) family appears as a robust candidate to label CSF-cNs (Huang et al., 2006; Orts-Del'immagine et al., 2012, 2015; Djenoune et al., 2014). PKD2L1, originally identified as the sour taste receptor in the taste buds, has been found in mouse spinal CSF-cNs (Huang et al., 2006, Orts-Del'immagine et al., 2014; Djenoune et al., 2014; Petracca et al., 2016) as well as macaques (Djenoune et al., 2014). The opening of the PKD2L1 channel is modulated by variations in pH (Ishimaru et al., 2006; Inada et al., 2008; Shimizu et al., 2011; Orts-Del'immagine et al., 2012) and osmolarity (Shimizu et al., 2009; Orts-Del'immagine et al., 2012; Jalalvand et al., 2016). Although the physiological amplitude of pH and osmolarity variations in the CSF are not well known, these observations suggest that CSF-cNs could be interoceptors modulated by chemical cues in the CSF.

There is evidence that spinal CSF-cNs do not constitute a homogeneous population of neurons. They originate from distinct progenitor domains and are specified differentially by several cascades of transcription factors (Park et al., 2004; Yang et al., 2010; Huang et al., 2012; Petracca et al., 2016). In zebrafish, CSF-cNs are subdivided into the ventral population (also named KA'') originating from the progenitor domain p3 and the dorsal one (also named KA') originating from pMN (Park et al., 2004; Yang et al., 2010; Huang et al., 2012). In mouse, spinal CSF-cNs were recently shown to originate mainly from the p3 and p2 progenitor domains (Petracca et al., 2016).

The zebrafish has emerged as an ideal model organism to study the development (Park et al., 2004; Yang et al., 2010; Huang et al., 2012; Djenoune et al., 2014), morphology and functions of CSF-cNs *in vivo* due to its transparency at early stages (Wyart et al., 2009; Fidelin et al., 2015; Bohm et al., 2016). Yet, few functional markers of CSF-cNs have been identified in this species. Here, we investigated whether the two types of spinal CSF-cNs defined by their developmental origins had distinct morphology and molecular markers. We show that ventral and dorsal CSF-cNs exhibit distinct shapes of apical extension as well as different axonal projections. Interestingly we demonstrate that these two cell types are also characterized by the transient expression of distinct modulators and peptides. While ventral CSF-cNs transiently express serotonin, dorsal CSF-cNs transiently express the *sst1.1* somatostatin

paralogue. We report that the Pkd2l1 channel is not required for CSF-cN differentiation of their axonal projection, as well as for the expression of serotonin nor somatostatin. Altogether, our results show that spinal GABAergic Pkd2l1⁺ CSF-cNs constitute at least two cell types that differ in apical and axonal morphology as well as in the expression of molecular markers.

Materials and Methods

Animal care

Zebrafish (*Danio rerio*) adults and larvae were maintained and raised on a 14/10 hour light cycle. Water was regulated at 28.5°C, conductivity at 500µS and pH at 7.4 (Westerfield, 2000). Embryos were dechorionated and staged as described (Kimmel et al., 1995). All embryos and larvae were anesthetized in 0.02% tricaine methane sulfonate (MS 222) (Sandoz, Levallois-Perret, France) and killed in 0.2% MS 222 prior to fixation. Animal handling and procedures were validated by the Institut du Cerveau et de la Moelle épinière (ICM), Paris and the French National Ethics Committee (Comité National de Réflexion Ethique sur l'Expérimentation Animale-Ce5/2011/056) in agreement with European Union legislation.

Description of transgenic lines and mutants

Transgenic lines and mutants generated for and used in this study along with the spinal cell populations targeted are referenced in Table 1.

Table 1: Transgenic lines used in our study.

Transgenic/mutant	Labelling in the spinal cord	Original publication
<i>Tg(pkd2l1:GCaMP5G)icm07</i>	CSF-cNs	Böhm et al., 2016
<i>Tg(pkd2l1:GCaMP5G)icm07;pkd2l1^{icm02}</i>	CSF-cNs	Böhm et al., 2016
<i>Tg(mnx1:GFP)</i>	Motor neurons	Flanagan-Steet et al., 2005
<i>Tg(pkd2l1:Gal4)icm10</i>	CSF-cNs	Fidelin et al., 2015
<i>Tg(UAS:TagRFP-CAAX;cmlc2:eGFP)icm22</i>	Heart (for <i>cmlc2</i>)	This study

Genotype protocol for the *pkd2l1^{icm02}* mutants was described in Böhm et al., 2016.

Generation of transgenic lines

In order to generate the *Tg(UAS:TagRFP-CAAX;cmlc2:eGFP)icm22* line, the TagRFP-CAAX sequence was amplified using a TagRFP-forward (5'-CCCGGGATCCACATGGTGTCTAAGGGCGAAG-3') and reverse primer (5'-GATCGCGGCCGCTCAGGAGAGCACACACTTGCAGCTCATGCAGCCGGGGCCACTCTCATCAGGAGGGTTCAGCTTATTAAGTTTGTGCCC-3') and inserted into the pME-MCS vector (Kwan et al., 2007) via BamHI/NotI restriction digestion. The resulting pME-TagRFP-CAAX vector was recombined via a Gateway reaction (MultiSite Gateway Three-Fragment Vector Construction Kit) with p5E-4nrUAS (Auer et al., 2015), p3E-pA and pDest-Tol2; *cmlc2:eGFP* (Kwan et al., 2007) resulting in p4nrUAS:TagRFP-CAAX-pA-Tol2;*cmlc2:eGFP*. Microinjection of this plasmid was performed with Tol2 mRNA (25ng/µl) following standard protocols. Transgenic founder fish *Tg(UAS:TagRFP-CAAX;cmlc2:eGFP)icm22* were screened based on GFP expression in the heart and transactivation of the TagRFP transgene when crossed with various Gal4 transgenic lines.

Plasmid design

To generate the *Tg(UAS:LifeAct-TagRFP;cryaaC)* DNA construct, we first extracted the coding sequence of the tagged protein LifeAct-TagRFP from the plasmid *mTagRFP-T-LifeAct-7* (Addgene #54586, kind gift from Michael Davidson) by PCR using a forward (GGGGACAAGTTTGTACAAAAAAGCAGGCTAGATCTCTGCCACCATGGGCGTGGC CGACTTGATC) and a reverse (GGGGACCACTTTGTACAAGAAAGCTGGGTACTAGTTTACTTGTACAGCTCGTCCA TGCC) primer. LifeAct-TagRFP was then inserted into the plasmid pDONR221 by a BP reaction to produce the pME_LifeAct-TagRFP plasmid. A three-way gateway reaction was then performed using pME_LifeAct-TagRFP, pDest_cry:aaC, p5'E_10XUAS and p3'E_polyA plasmids to produce the *Tg(UAS:LifeAct-TagRFP;cryaaC)* construct.

Analysis of the apical dendritic extension of CSF-cNs

To investigate the shape of CSF-cNs apical dendritic extension, we used two different strategies to access to their morphology at a high resolution. First, we took advantage of a membrane-tagged red fluorescent protein (RFP) by crossing *Tg(UAS:TagRFP-CAAX;cmlc2:eGFP)icm22* fish to *Tg(pkd211:Gal4)icm10*. In a second approach, we injected both *Tg(pkd211:Gal4)* (Fidelin et al., 2015) and *Tg(UAS:LifeAct-TagRFP;cryaaC)* DNA constructs into *Tg(pkd211:GCaMP5)icm07* eggs at the one cell stage in order to specifically label F-actin (Riedl et al., 2008) in CSF-cNs. 3 dpf larvae were then selected for specific expression in CSF-cNs and fixed using 4% PFA during 4 hours at 4°C. Immunostainings were performed based on the procedures described below. 50 µm-thick transverse sections were done on larvae mounted in 4% low melting point agarose using a vibratome (HM 650V Microtome, Thermo Scientific). For each cell, Z-stacks (step size 0.25 µm) were acquired to image the entire apical extension. To assess whether a CSF-cN was ventral or dorsal, we first calculated its position (P) relative to the ventral limit of the central canal (VCC) by the ratio between its dorso-ventral position in the spinal cord (D-V_soma) and the dorso-ventral position of the VCC (D-V_VCC) (**Figure 3B**, see below for the detail of the calculation of the D-V position). $P > 1$ indicates that the cell is dorsal with a soma located above the VCC while $P < 1$ indicates that the cell is ventral. To characterize the shape of the apical extension, we modeled its spread (S) by calculating the ratio between the width of the spread along the central canal (W) and the height of the extension within the central canal (H). W and H were extracted by drawing a polygon around the apical extension using the polygon tool in Fiji and then estimated by the parallel and perpendicular axis, respectively, of the best fitting ellipse (**Figure 3B**).

Single cell labeling

To assess whether *pkd211* mutation led to a disruption of CSF-cN axonal refinement, we injected at 25 ng/µl the *Tg(pkd211:TagRFP)* construct generated with a three-fragment Gateway recombineering reaction (Fidelin et al., 2015) into single-cell stage embryos from *pkd211^{icm02/+}* incrosses. 3 dpf larvae selected for single CSF-cN expression were fixed with 4% PFA for 3 hours and immunostained following procedures described below. Genotyping of the larvae was performed after immunostaining.

Analysis of the axonal arborization of isolated CSF-cNs

For each cell, multiple Z-stacks (step size 1 μm) were acquired to capture the entire arborization of the axon. Multiple stacks from a single cell were combined using the Pairwise stitching and Grid/Collection stitching plugins in Fiji (Preibisch et al., 2009) or the XuvTools stitching software (Emmenlauer et al., 2009). The combined files were then exported in Fiji (Schindelin et al., 2012) and the cell morphology was reconstructed into a three-dimensional image using the Simple Neurite Tracer (SNT) plugin in Fiji (Longair et al., 2011) (**Figure 4B**). The area was measured in MATLAB as the smallest polygon that included all axonal endings (grey area, **Figure 4C**). The total axon length and the number of branches were obtained from SNT (red and purple segments in **Figure 4C**). The traces obtained from SNT were then imported in MATLAB and morphological parameters were extracted using a custom made script available upon request. The dorso-ventral soma positions were measured from the center of the cell body and normalized to the limits of the spinal cord where the ventral edge corresponds to 0 and the dorsal edge to 1 (**Figure 4B**, D-V_soma). The attribution of dorsal versus ventral CSF-cN (Park et al., 2004) was based on the soma location relative to the central canal. The total axon length was the sum of the length of the main axon and all branches. The minimum dorso-ventral axon position referred to the most ventral position reached by the axon. The maximum dorso-ventral axon position referred to the most dorsal position reached by the axon. The dorso-ventral axonal range was the difference between the two. For illustration purposes, the cell reconstruction images were processed in Photoshop CS5 in order to assign them a color according to their genotype and to display them according to their dorso-ventral index.

Fluorescent in situ (FISH)

The *pkd211* ISH probe was generated as previously described (Djenoune et al., 2014). The *sst1.1* plasmid originates from the Argenton lab, Padova, Italy, (Argenton et al., 1999; Devos et al., 2002). *pkd211* and *sst1.1* plasmids were respectively linearized with NotI and SalI. Digoxigenin (DIG)- and fluorescein (Fluo)-labeled probes were synthesized using SP6 RNA polymerase with the RNA Labeling Kit (Roche Applied Science, Basel, Switzerland) to generate both *pkd211* and *sst1.1* antisense probes. All probes were purified using the mini Quick Spin RNA Column (Roche, Basel, Switzerland). Whole-mount ISH were performed as previously described (Parmentier et al., 2011; Alunni et al., 2013, Djenoune et al., 2014) on embryos or larvae fixed in 4% PFA in PBS overnight at 4°C.

Immunohistochemistry (IHC)

For 5-HT IHC, embryos and larvae were fixed in 4% PFA, 1% dimethyl sulfoxide (DMSO), washed, incubated in 50mM of glycine in 0.1% PBS-Triton X-100 (PBSTx), washed in PBSTx, blocked for 2h in 1% DMSO, 1% NGS, 1% BSA, and 0.7% Triton X-100 and incubated with primary antibody (rabbit anti-5-HT, 1:2000 from Dr Steinbusch, Maastricht University, Netherlands) in blocking buffer overnight at 4°C. After several washes in PBSTx, fish were incubated in corresponding Alexa conjugated secondary antibodies IgG (1:500, Invitrogen, Carlsbad, CA, USA) in blocking buffer overnight at 4°C. Fish were then washed in PBSTx several times before mounting. For TagRFP immunostaining, after 3h of 4% PFA

fixation, larvae were washed in successive baths of PBS-Tween 0.1% (PBST). After 1h blocking in a solution of 10% normal goat serum (NGS), 1% DMSO, 0.5% Triton X-100 in PBS 1X, we incubated embryos with the primary rabbit anti-TagRFP antibody (1:500, Invitrogen R10367, Carlsbad, CA, USA) overnight at 4°C in a solution of 1% NGS, 1% DMSO, 0.5% Triton X-100 in PBS 1X. After several washes in PBST, larvae were incubated with corresponding Alexa conjugated secondary antibodies IgG (1:500, Invitrogen, Carlsbad, CA, USA) overnight at 4°C and washed several times with PBST. For GABA immunostaining, larvae were fixed for 3h at 4°C in 4% PFA, 0.1% glutaraldehyde, washed in successive baths of PBST, dehydrated stepwise in increasing concentration of methanol (MeOH), stored in MeOH for at least two hours at -20°C then rehydrated stepwise. Larvae were digested with 0.5U/mL dispase (1X, Invitrogen 17105-041, Carlsbad, CA, USA) for 90 min. Larvae were blocked for at least two hours in 2% BSA, 5% NGS, 1% DMSO, PBST and incubated with the primary rabbit anti-GABA (1:2,000, Sigma-Aldrich A2052, St. Louis, MO, USA) overnight at 4°C in a solution of 2% BSA, 2% NGS, 1% DMSO, PBST. After several washes in 1% DMSO, 1% NGS, PBST, larvae were incubated in corresponding Alexa conjugated secondary antibodies IgG (1:500, Invitrogen, Carlsbad, CA, USA) overnight at 4°C. Note that for GABA and 5-HT IHC at 3dpf, 30% sucrose was added in fixation solutions, fish were treated prior to staining with 0.2mg/ml collagenase in PBS for 5min and skin was removed with forceps to increase permeabilization.

FISH coupled to IHC

Procedures were described in Djenoune et al., 2014. Briefly, *pkd21l* and *sst1.1* FISH were performed prior to IHC against green fluorescent protein (GFP): embryos and larvae were washed and immunostained with the chicken anti-GFP antibody (1:500 dilution, Abcam ab13970, Cambridge, UK) overnight at 4°C, and then incubated with the corresponding Alexa-conjugated secondary antibodies IgG (1:500, Invitrogen A11039, Carlsbad, CA, USA) combined with DAPI (2.5 µg/ml, Invitrogen D3571, Carlsbad, CA, USA).

Cell counting

To allow a systematic comparison and quantification between different markers investigated, we systematically imaged 3 regions along the rostrocaudal axis of the fish: segments 3-6 (referred as rostral), 10-13 (referred as middle) and 23-26 (referred as caudal). For consistency in all figures, we displayed the region corresponding to segments 10-13.

Imaging

Images were acquired using an Olympus FV1000 confocal microscope equipped with a 20 and 40x water immersion objective using the 405, 473nm and 543nm laser lines. To determine the overlap of GFP in the *Tg(pkd21l:GCaMP5G)^{icm07}* transgenic embryos and larvae with *pkd21l*, *sst1.1* FISH or GABA and 5-HT IHC, fish were mounted laterally in 1,5% agarose covered of Vectashield Mounting Medium (Vectorlabs, CA, USA). To analyze apical extensions, slices were transferred into Vectashield mounting medium as well (Vectorlab, CA, USA) and images were acquired using the 488, 543 and 633 nm laser lines on a confocal microscope (Olympus FV-1000) equipped with a 60x oil immersion objective. Images were

processed using Fiji (Schindelin et al., 2012) and Adobe Illustrator (Adobe Systems, Mountain View, CA, USA) softwares.

Statistics

For the morphological comparison of ventral versus dorsal WT CSF-cNs and WT versus homozygous *pkd2l1^{icm02/icm02}* mutant CSF-cNs, Student's t-tests were performed. Two-way ANOVAs were performed to test the interaction between the genotypes and the regions where cells were counted. The level of significance was $p < 0.05$ for all datasets.

Results

pkd2l1 promoter drives expression selectively in spinal CSF-cNs

Taking advantage of *pkd2l1* expression in CSF-cNs (Djenoune et al., 2014), we used the *Tg(pkd2l1:GCaMP5G)icm07* transgenic line to selectively target CSF-cNs (Böhm et al., 2016). To validate the line, we performed FISH for *pkd2l1* mRNA coupled to a GFP IHC to amplify the endogenous GCaMP5G signal at different stages of development from 24hpf to 5dpf (**Figure 1A-E**). We found that *Tg(pkd2l1:GCaMP5G)icm07* line (green signal, **Figure 1A-E**) selectively labeled *pkd2l1*⁺ cells (red signal, **Figure 1A-E**) at all stages investigated, that is to say ventral CSF-cNs (**Figure 1E**, arrowhead) and dorsal ones (**Figure 1E**, arrow). Moreover, we found that all GFP⁺ cells around the central canal (green, **Figure 1F**) were GABAergic (red, **Figure 1F**) confirming further that they were CSF-cNs. Altogether, these results indicate that the *Tg(pkd2l1:GCaMP5G)icm07* line is a reliable tool to target all CSF-cNs in the zebrafish spinal cord.

CSF-cNs display different shapes of apical extensions

Given that ventral and dorsal CSF-cNs do not share the same developmental origin, we tested whether they also displayed specific morphological properties. We investigated the shape of CSF-cN apical extension at 3 dpf using either *Tg(pld2l1:Gal4;UAS:TagRFP;CAAX;cryaaC)icm22* embryos or *Tg(pkd2l1:GCaMP5)icm07* embryos injected with two DNA constructs: *Tg(pkd2l1:Gal4)* and *Tg(UAS:LifeAct-TagRFP,cryaaC)*. With both labeling techniques, we observed different shapes of apical extensions for ventral and dorsal CSF-cNs (**Figure 2A**). We found that dorsal CSF-cNs consistently formed an apical extension spread along the border of the central canal (**Figure 2A1**, arrow) while ventral CSF-cNs exhibited a compact and dense apical extension (80.8%, n = 21 out of 26 ventral cells, **Figures 2A1**, arrowhead). The shape of this last population appears more diverse, with a small proportion of ventral CSF-cNs displaying a spread apical extension (19.2%, n = 5 out of 26 ventral cells, **Figure 2A2**, empty arrow). To characterize the shape of the apical extension for each cell, we performed a systematic analysis of its spread (**Figure 2B**). The distribution of the cells according to both the spread and the position showed a good correlation between cell body position and spread of the apical extension (**Figure 2C1**); the more dorsal a CSF-cN is, the more spread its brush is. The comparison of the spread of the apical extension of these two populations (**Figure 2C2**) indicated that dorsal CSF-cNs possess a significantly more extended apical extension than ventral ones (p = 3.23.10⁻⁵, 13 dorsal CSF-cNs, 26 ventral CSF-cNs). Notably, among the ventral population, we observed some outliers with high spreads (**Figure 2C2**), confirming the existence of a small proportion of ventral CSF-cNs displaying a highly spread apical extension similar to dorsal ones. These results provide the first evidence of morphological heterogeneity among zebrafish spinal CSF-cNs between ventral and dorsal CSF-cNs and suggest a morphological heterogeneity within ventral CSF-cNs themselves.

Ventral and dorsal spinal CSF-cNs possess specific axonal projections

In order to assess whether CSF-cNs could also be classified regarding their axonal projections, we injected the *Tg(pkd211-TagRFP)* DNA construct to label single cells (**Figure 3A**) and reconstruct their axon (**Figure 3B,C**). All CSF-cN axonal projections were ventral, ipsilateral and ascending (consistent with Fidelin et al., 2015), yet they were heterogeneous along the rostrocaudal axis of the spinal cord (**Figure 3B, Supplemental Figure 1**). We performed a systematic comparison between the ventral and dorsal populations for the parameters we extrapolated from each cell (**Figure 3C**). We detected significant differences between the two populations for all of the morphological parameters investigated (**Figure 3D**). Indeed, ventral CSF-cNs have a wider axonal arborization ($p=0.0025$), a longer axon ($p=0.0014$), reach more ventral domains of the spinal cord ($p=8.67 \cdot 10^{-4}$), cover a larger dorso-ventral (D-V) range ($p=1.13 \cdot 10^{-4}$) with more axonal branches ($p=0.0138$). These results strongly indicate that ventral and dorsal CSF-cNs have axonal differences suggesting that they may not target the same cell types within the ventral spinal cord. Nonetheless, we could not detect from our analysis whether ventral CSF-cNs segregated in different clusters based on axonal projections.

Investigation of the molecular heterogeneity of spinal CSF-cNs leads to specific profiles in ventral and dorsal CSF-cNS

In order to confirm that ventral and dorsal CSF-cNs are two distinct functional populations, we tested whether they expressed differentially two selected markers that have been previously reported as expressed in a restricted number of CSF-cNs. Somatostatin was found in restricted CSF-cNs (in lamprey: Buchanan et al., 1987; Christenson et al., 1991a; Jalalvand et al., 2014; in Mexican burrowing caecilian: Lopez et al., 2007). In zebrafish, somatostatin immunoreactivity has previously been reported (Wyart et al., 2009). Nonetheless, there are 6 different paralogues of the peptide in this species: *sst1.1* (also referred as SS1), *sst1.2* (also referred as SS3), *sst2* (also SS4), *sst3* (also SS2 and named cortistatin in mammals), *sst5* (also SS5) and *sst6* (also SS6) (Tostivint et al., 2004; 2008; 2013). We tested which form was expressed in zebrafish CSF-cNs and did not detect their expression in these cells except for *sst1.1*. Indeed, by combining FISH for *sst1.1* with GFP IHC from 24 to 120 hpf *Tg(pkd211:GCaMP5G)icm07* embryos and larvae, we observed at 24 and 48 hpf restricted expression of *sst1.1* in dorsal CSF-cNs (**Figure 4A,B**, arrows) mainly in the rostral part of the spinal cord, from segment 1 to 13 approximately. Since *sst1.1* had been reported as expressed transiently in motor neurons from 19 hpf until 55 hpf (Devos et al., 2002), we combined FISH for *sst1.1* and GFP IHC on 24 hpf *Tg(mnx1:GFP)* embryos in which GFP expression labels motor neurons (Flanagan-Steet et al., 2005). *sst1.1* expression was distinct from GFP expression in this line (**Figure 4C**) excluding the motor neuronal expression of *sst1.1*. The expression of *sst1.1* not being detected in the spinal cord after 55 hpf (Devos et al., 2002; *data not shown*), our results show that *sst1.1* is transiently expressed in dorsal CSF-cNs at early stages of development and is excluded from motor neurons.

Likewise, the serotonin has been reported in a restricted number of CSF-cNs of multiple fish species (Sims, 1977; Ochi et al., 1979; Parent and Northcutt, 1982; Chiba and Oka, 1999). We

thus tested whether zebrafish CSF-cNs were serotonergic by performing double IHC for 5-HT and GFP on *Tg(pkd211:GCaMP5G)icm07* embryos and larvae from 24 hpf to 72 hpf. At 24 hpf, no 5-HT immunostaining was detected in the zebrafish spinal cord (*data not shown*). At 48 hpf, we detected 5-HT in ventral CSF-cNs (**Figure 4D**, arrowheads) mainly in the rostral part of the spinal cord (from segment 1 to about 24). Notably, this expression was restricted only in a subset of ventral CSF-cNs (**Figure 4D**). The proportion of these 5-HT⁺ cells along the rostrocaudal axis of the spinal cord decreases from the rostral part to the caudal one; segments 3 to 6: $88.6 \pm 16.0\%$ of 5-HT⁺ ventral CSF-cNs (96 cells counted); segments 10 to 13: $73.2 \pm 27.3\%$ 5-HT⁺ ventral CSF-cNs (100 cells counted); segments 23 to 26: $31.2 \pm 33.3\%$ 5-HT⁺ ventral CSF-cNs (94 cells counted). Nonetheless, at 72 hpf, 5-HT staining was clearly distinct from the GFP labelling (**Figure 4E**) in the rostral cord but was still detected in restricted ventral CSF-cNs of the caudal part (*data not shown*). In conclusion, we identified a novel marker expressed in zebrafish spinal CSF-cNs, the *sst1.1* in dorsal CSF-cNs and showed that a subpopulation of the ventral CSF-cNs population is transiently serotonergic.

***pkd211* null mutation does not impact on the differentiation of spinal CSF-cNs**

PKD2L1 channel is expressed in spinal CSF-cNs across multiple vertebrate species (Djenoune et al., 2014). This conservation strongly suggests a critical role of the channel within the cells. In order to assess Pkd211 contribution to zebrafish spinal CSF-cNs, we generated a mutant using TALENs in the *Tg(pkd211:GCaMP5G)icm07* background (Böhm et al., 2016). We tested whether the mutation impacted on the molecular differentiation of the cells and observed that in *pkd21^{icm02/icm02}* mutants, CSF-cNs still expressed GABA (**Figure 5A**) and that a large proportion of ventral CSF-cNs were still serotonergic (**Figure 5B**). We counted the number of ventral and dorsal CSF-cNs in the three regions along the rostrocaudal axis of the spinal cord and did not count any significant difference in the number of CSF-cNs in the mutants compared to the WT (**Figure 5C**). We did not detect a difference in the proportion of 5-HT⁺ ventral CSF-cNs neither (**Figure 5D**). We next tested whether the loss of Pkd211 could lead to the alteration of CSF-cNs axonal development. We did not find any significant difference for any of the reported axonal parameters between the two genotypes both for ventral and dorsal CSF-cNs, while the same differences observed between ventral and dorsal CSF-cNs in WT were still present in the mutant (**Figure 5E**). Altogether, our results indicate that *pkd211* function is not required for proper CSF-cNs differentiation.

Discussion

Using zebrafish spinal cord as a model, we identified a heterogeneity of spinal CSF-cNs at different levels. First, they harbor different and specific morphological features. Second, ventral and dorsal CSF-cNs populations selectively express 5-HT and *sst1.1* respectively. Third, Pkd211 is not necessary for the differentiation of any of the CSF-cNs classes. Altogether, our results demonstrate that zebrafish spinal CSF-cNs are more heterogeneous than reported so far and suggest that the CSF-cNs system might sustain multiple functions within the vertebrate spinal cord.

Distinct morphology of ventral and dorsal CSF-cNs for distinct functions?

Due to their peculiar apical extension contacting the CSF and their morphology reminiscent of sensory cells, it has been hypothesized that CSF-cNs may have sensory properties to detect cues or movements of the CSF (Kolmer 1921; Agduhr 1922; Vigh and Vigh-Teichmann, 1971; 1973; Vigh et al., 1977; Huang et al., 2006; Orts-Del'immagine et al., 2012) or that they may release compounds into the CSF (Leonhardt, 1967; Vigh and Vigh-Teichmann, 1971; 1973; Vigh et al., 1977). Nonetheless, whether all spinal CSF-cNs share the same sensory properties is not clear. Previous studies reported that spinal CSF-cNs can harbor different morphologies. In rat, spinal GABAergic CSF-cNs were first classified into three subtypes according to the shape of their soma (Barber et al., 1982). Four morphological types of CSF-cNs were then described based on the shape of their soma, their axonal projection, and on the expression of the peptide Met-Enk-Arg-Gly-Leu (Shimosegawa et al., 1986). These indications together with our data reveal a high level of heterogeneity among spinal CSF-cNs which remained poorly understood.

Regarding the shape of their apical extension, we showed that dorsal CSF-cNs exhibit a spread contact with the CSF, whereas ventral ones are more compact. Notably, among the ventral population of CSF-cNs, we found another level of heterogeneity with at least two types of apical extensions. We cannot exclude that the few ventrally positioned cells are originating from the dorsal domain and have slightly shifted down during development. However, this may reflect a subdivision of the ventral population into more different cell types, as suggested by the 5-HT staining (see below). As for the functional meaning of the dorso-ventral difference, we can assume that a particular shape is associated with specific integration and/or the release of given cues in the CSF. The recent study in which we demonstrated that CSF-cNs respond to passive and active bending of the spinal cord (Böhm et al., 2016) reinforces this hypothesis. Indeed, we showed that dorsal CSF-cNs respond to tail bending selectively on the contracting side while contralateral dorsal and ventral cells remained mostly silent (Böhm et al., 2016). These results suggest that the different populations of CSF-cNs could bear specific sensory properties sustained by distinct ultrastructural features. The mechanisms underlying the formation of a spread apical extension as opposed to a more compact one are still not understood. Whether a given molecular profile (e.g. the expression of 5-HT at 48 hpf by a subpopulation of ventral CSF-cNs) can be associated to the development of a particular type of apical extension remains to be determined. Although distinct molecular pathways could be responsible for the differences observed between ventral and dorsal CSF-cN apical extensions, we cannot exclude that they might be due to specific physical constraints.

By a single cell labelling approach, we found that ventral CSF-cNs had on average a longer and broader axonal arborization covering a higher dorso-ventral spinal cord range and possessing more axonal branches than dorsal CSF-cNs. Our results thus demonstrate that ventral and dorsal CSF-cNs populations have distinct morphological features and support the idea that these cells are two different populations. These axonal differences between the two

populations suggest that they might have specific targets within the spinal cord. In a previous study, we observed that CSF-cNs preferentially form presynaptic boutons in the ventral spinal cord (between 0.2-0.4) (Fidelin et al., 2015). We demonstrated that CSF-cNs form active GABAergic synapses onto glutamatergic descending V0-v interneurons and that they modulate slow locomotor events (Fidelin et al., 2015). We also showed that CSF-cNs contact and modulate the activity of CaPs primary motor neurons, indicating their participation in fast swimming (Hubbard et al., in revision). Together with our results demonstrating that ventral CSF-cNs innervate a more dorsal D-V range of the spinal cord than dorsal ones, it could thus be hypothesized that ventral CSF-cNs preferentially innervate CaPs while dorsal CSF-cNs mainly contact V0-v. Demonstrating whether one type of CSF-cNs specifically project onto slow locomotor circuits and the other type onto fast ones would require further investigations.

Molecular classification of zebrafish spinal CSF-cNs

Multiple markers have been found in subpopulations of CSF-cNs across species: somatostatin (in lamprey: Buchanan et al., 1987; Christenson et al., 1991a; Jalalvand et al., 2014; in coho salmon: Yulis and Lederis, 1986; Yulis and Lederis, 1988a; b; in Mexican burrowing caecilian: Lopez et al., 2007; in zebrafish: Wyart et al., 2009), dopamine (in lamprey: Schotland et al., 1995, 1996; Barreiro-Iglesias et al., 2008; Rodicio et al., 2008; in xenopus: Binor and Heathcote, 2001; in ray: Roberts and Meredith, 1987; in eels: Roberts et al., 1989, 1995; in pigeon: Acerbo et al., 2003) or serotonin (in salamander: Sims, 1977; in lamprey and Hagfish: Ochi et al., 1979; in garfish: Parent and Northcutt, 1982; in spotted gar: Chiba and Oka, 1999; in chick: Sako et al., 1986). Notably, the expression of most of these markers was reported only in a restricted number of CSF-cNs. In order to further characterize the expression patterns of each population in zebrafish, we tested whether these markers also showed restricted expression patterns among CSF-cNs in this model. Interestingly, we found that ventral CSF-cNs were at 48 hpf transiently serotonergic as previously described in other species (salamander: Sims, 1977; lamprey and hagfish: Ochi et al., 1979; garfish: Parent and Northcutt, 1982; chick: Sako et al., 1986; spotted gar: Chiba and Oka, 1999) in accordance with findings from Montgomery et al., 2015. Nonetheless, we demonstrated here that, even at 48 hpf, not all ventral CSF-cNs were clearly 5-HT⁺ as many cells were dimly or not labelled. There may be different subtypes of ventral CSF-cNs based on 5-HT expression. Moreover, Montgomery et al., 2015 also suggest that the rate-limiting enzyme involved in 5-HT synthesis *tryptophan hydroxylase 1 a* (*tph1a*) (Bellipanni et al., 2002; Teraoka et al., 2004) may be expressed in the ventral spinal cord at 24 and 48 hpf. This suggests that ventral CSF-cNs transient expression of 5-HT could be a transient source of serotonin at early stages. One possible reason for the disappearance of 5-HT expression in ventral CSF-cNs could be the appearance of 5-HT expressing descending neurons from the brainstem raphe nuclei during the same time window, from 48 hpf onwards (Bellipanni et al., 2002), that would suppress the monoaminergic expression of ventral CSF-cNs as suggested in rodents (Branchereau et al., 2002; Allain et al., 2010; Wienecke et al., 2014). The physiological relevance of the transient 5-HT expression among this ventral population of CSF-cNs remains to be elucidated.

Testing the somatostatin phenotype of zebrafish CSF-cNs, we found that among the six SST paralogues, *sst1.1* was expressed in CSF-cNs. Notably, we demonstrated that the expression of the peptide is specific and restricted to the dorsal population of CSF-cNs, identifying for the first time a specific marker of dorsal CSF-cNs, contrary to its reported expression in motor neurons (Devos et al., 2002). Motor neurons originate from the same pMN domain (Myers et al., 1986; Park et al., 2004) as dorsal CSF-cNs (Park et al., 2004; Yang et al., 2010; Djenoune et al., 2014). The proximity of both populations can explain how *sst1.1* could have been mistaken for motor neurons. The physiological relevance of *sst1.1* expression by dorsal CSF-cNs is not yet established. In mammals and lamprey, it has been shown that somatostatin can modulate the frequency of locomotion in reducing the global level of fictive locomotor activity (Barriere et al., 2005; Miles and Sillar, 2011; Jalalvand et al., 2016). The release of SST by CSF-cNs thus may modulate the frequency of locomotor events. Moreover, among the UII family of neuropeptides, *urp1* and *urp2* are specifically expressed in ventral CSF-cNs (Quan et al., 2015). Coupled with the specific expression of *sst1.1* in dorsal CSF-cNs, we show in zebrafish what Yulis and Lederis (1988b) reported in the coho salmon: a UII-like immunoreactive ventral population of CSF-cNs and a distinct somatostatinergic one. Taken together, the results of the molecular characterization of zebrafish CSF-cNs we performed indicate that ventral and dorsal CSF-cNs are molecularly distinct populations and suggest that these classes may be conserved across species and have specific functional properties sustained by the pool of markers they possess or given their physiological context.

Altogether, in addition to reinforcing the classification in two classes of the CSF-cNs system in the zebrafish spinal cord, our study demonstrates that this system is more heterogeneous than reported so far. The multiple morphologies and functional markers CSF-cNs bear could underlie the multiple roles they perform at the CSF/CNS interface and within motor circuits. How these molecular and morphological features are connected to their physiological contributions within the vertebrate spinal cord remains to be elucidated.

Contributions

Lydia D performed the *in situ* for *pkd211* and *sst1.1*, injected the *Tg(pkd211:TagRFP)*, reconstructed and analyzed the axonal projections with the help of JG and AP. Laura D performed the morphological analysis on CSF-cN apical extension. JG performed the 5-HT and JRS the GABA IHCs. Lydia D, JG and JRS counted cells. TOA generated the *Tg(UAS:TagRFP-CAAX;cmc2:eGFP)icm22* line in FDB's lab. Lydia D, PLB, FDB and CW supervised research. Lydia D analyzed data. Lydia D wrote and CW edited the manuscript with feedback from all authors.

Acknowledgments

We thank Natalia Maties and Bogdan Buzurin from Animalliance for expert fish care. We thank Prof. Hervé Tostivint for precious feedback regarding the somatostatin experiments. We thank Déborah Delpuch for help with genotyping and Sophie Nunes Figueiredo for technical assistance. We thank Peter Steenbergen, Dr Soojin Ryu, Freiburg University, Germany and Dr Heiko Loehr, University of Cologne, Germany for providing the *sst1.1* plasmid. We thank

Vincent Guillemot from the ICM Biostatistics/Bioinformatics core facility for advices on statistics and the imaging facility PICPS from ICM supported by 'Investissements d'avenir' ANR-10-IAIHU-06. This work received support from the ERC starting grant 'Optoloco' # 311673 and the HFSP research grant # RGP0063/2014.

Figures

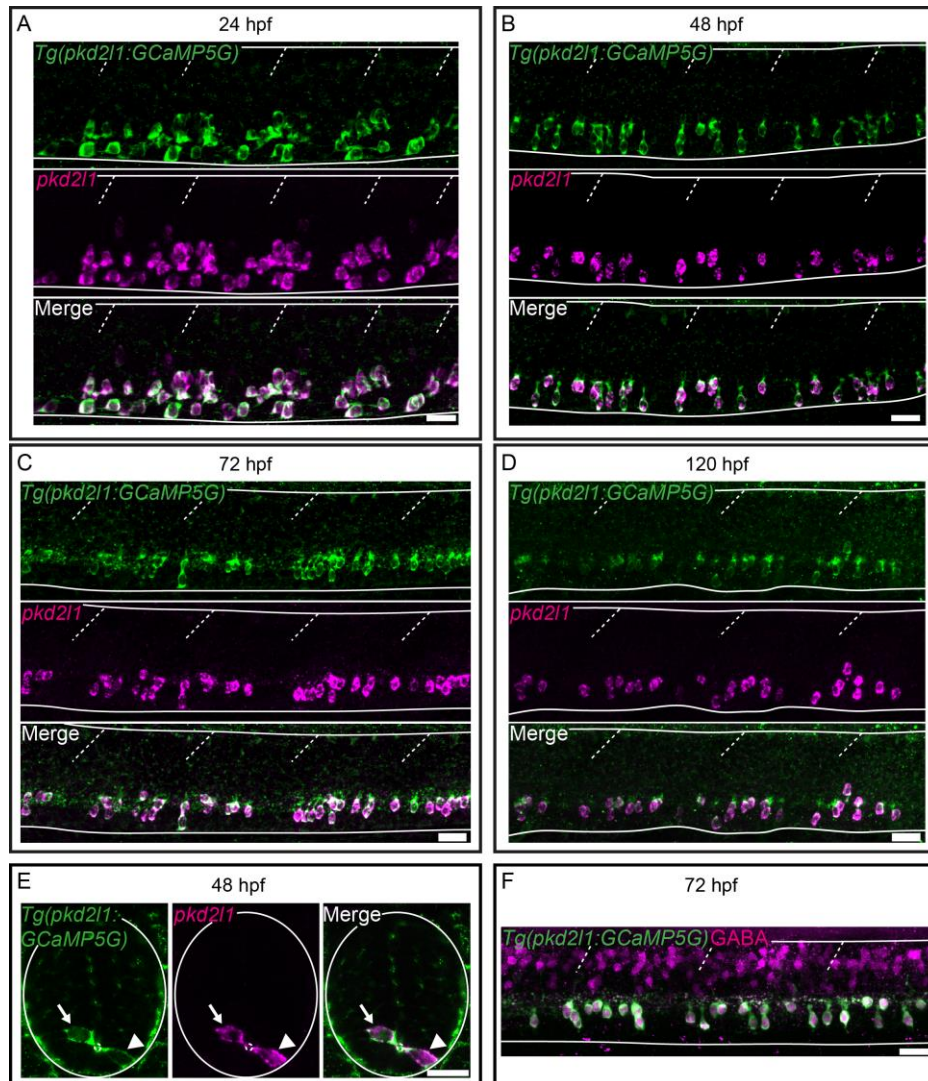


Figure 1: The *Tg(pkcd2l1:GCaMP5G)icm07* transgenic line recapitulates endogenous *pkcd2l1* mRNA expression.

FISH for *pkcd2l1* (magenta) coupled to GFP IHC (green) on *Tg(pkcd2l1:GCaMP5G)* embryos and larvae at 24 hpf (A), 48 hpf (B, E), 72 hpf (C) and 120 hpf (D). (A-D) Lateral views of the spinal cord from segments 10 to 13 show that all GFP⁺ cells (green) in the *Tg(pkcd2l1:GCaMP5G)* line are *pkcd2l1*⁺ (magenta). (E) Transverse sections of the spinal cord of 48 hpf embryos show the dorso-ventral distribution of a ventral CSF-cN (arrowhead) ventral to the central canal (small dotted circle) and a dorsal CSF-cNs (arrow) above it. (F) All CSF-cNs in the *Tg(pkcd2l1:GCaMP5G)* line (green) express GABA (magenta). Horizontal lines represent the limits of the spinal cord and slash dashed lines represent somites boundaries. Scale bars= 20μm.

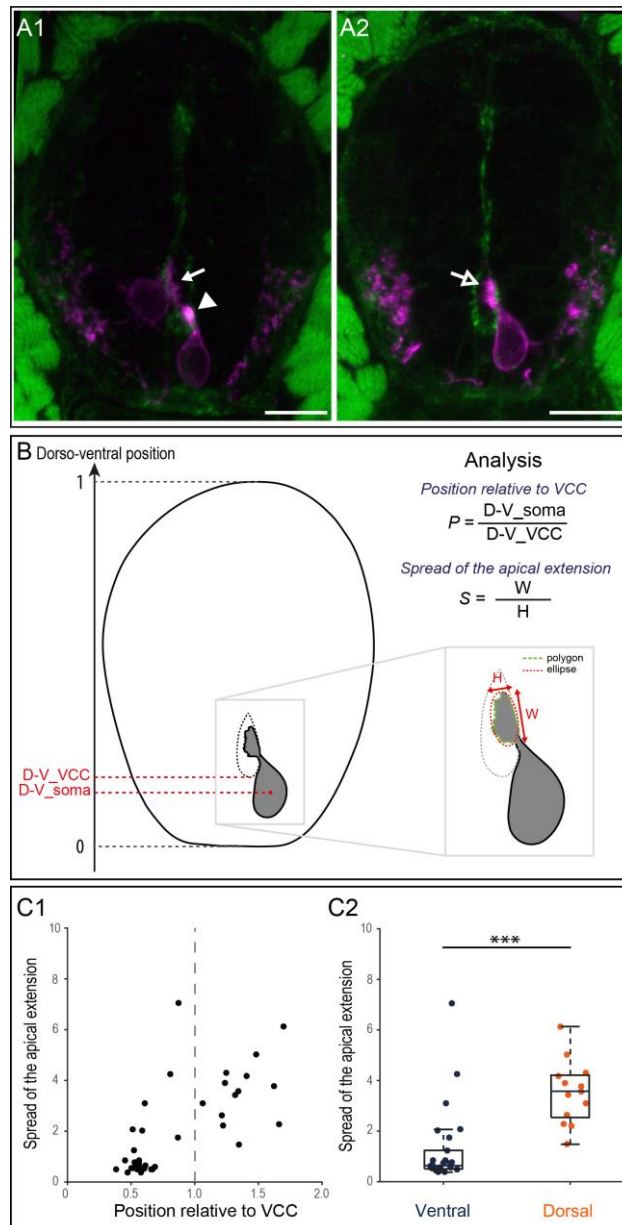


Figure 2: The analysis of CSF-cNs apical extension reveals heterogeneous shapes

Transverse sections showing ventral and dorsal TagRFP-CAAX⁺ (magenta) CSF-cNs at 3 dpf displaying the different types of apical extension characterized in our study. **(A1)** Dorsal CSF-cNs possess an apical extension spreading along the central canal border (arrow) while most ventral CSF-cNs (80.8%) form compact ones (arrowhead). **(A2)** A small subpopulation of ventral CSF-cNs (19.2%) exhibit the typical spread of dorsal apical extensions (arrow with empty head). Phalloïdine staining (green). Scale bar, 10µm. **(B)** Schematics of the analysis of the apical extension performed on each cell. For illustration purpose, we based our schematics on the cell displayed in A2. **(C)** Analysis for 39 CSF-cNs. **(C1)** Graph showing the distribution of the CSF-cNs considering the spread of their apical extension ($S =$ ratio between the width of the spread along the central canal (W) and the height of the extension within the central canal (H)) and their position (P) relative to VCC. The vertical grey line represents the physiological cutoff between ventral ($P < 1.0$) and dorsal ($P > 1.0$) position taking the VCC as a reference. **(C2)** Statistical analysis comparing the spread of the apical extension between 26 ventral and 13 dorsal CSF-cNs distinguished systematically based on the cutoff at $P = 1$ as shown in C1. Two-sample t-tests to compare two populations were performed for significance is indicated by the triple stars ($p < 0.05$).

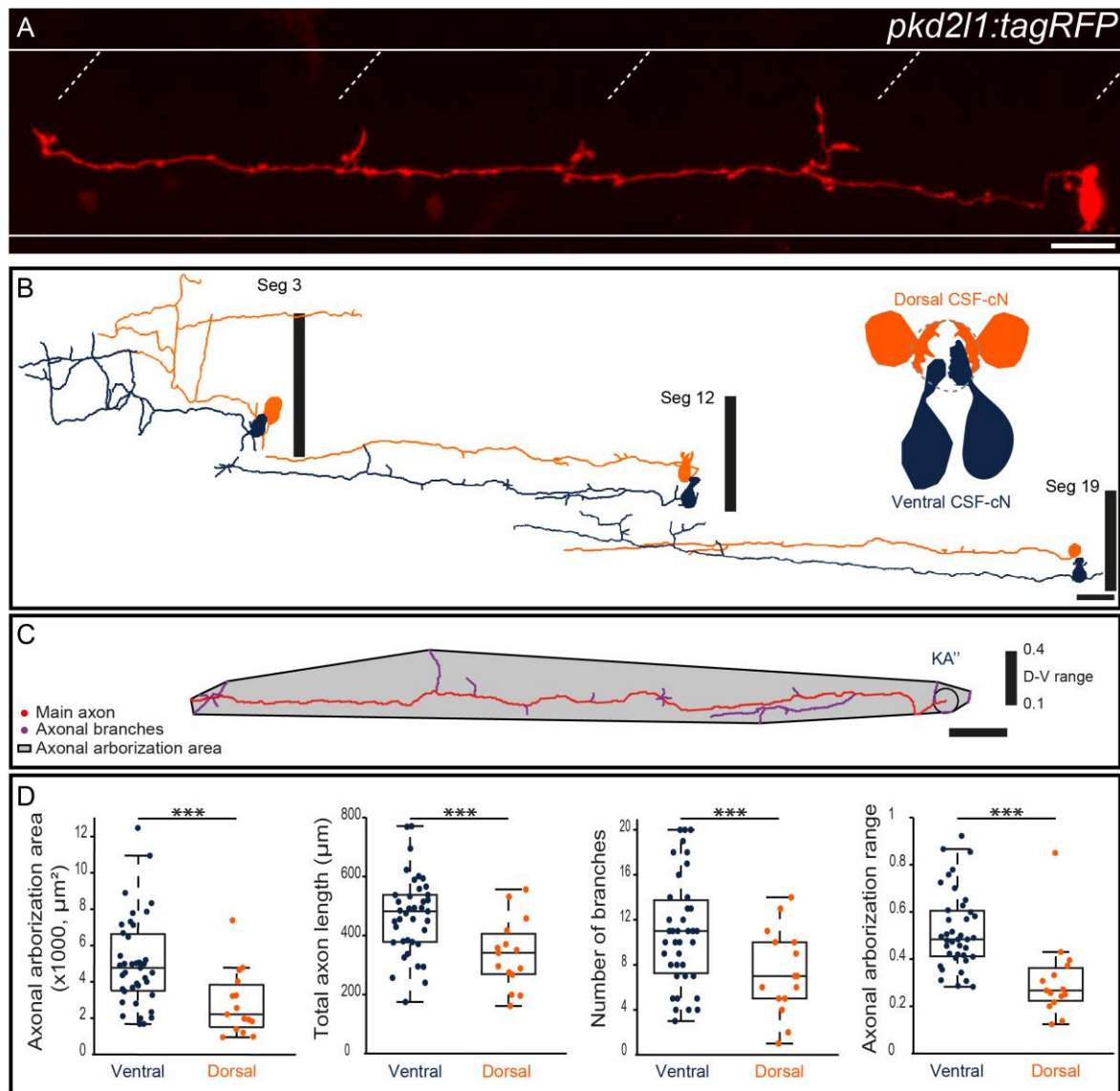


Figure 3: Ventral and dorsal CSF-cNs exhibit specific morphological properties

(A) Projection obtained from z-stacks of a single CSF-cN in a wild-type larva previously injected with *Tg(pkd211-TagRFP)*. (B) The reconstruction of 3 ventral CSF-cNs (dark blue) and 3 dorsal CSF-cNs (orange) from segment 3, 12 and 19 show that along the rostrocaudal axis, ventral CSF-cNs are morphologically different from dorsal ones. (B) Illustration of the reconstruction of one ventral CSF-cN displays the area covered by the axon and the axonal arborization nomenclature. (C) Statistical analysis of 39 ventral CSF-cNs and 15 dorsal ones comparing the two populations for the axonal arborization area, the total axon length, the number of branches and the axonal arborization dorso-ventral range. Each dot represents one cell. Two-sample t-tests to compare the two populations were performed for the given parameter and significance is indicated by the triple stars ($p < 0.05$). Scale bars = 20 μm .

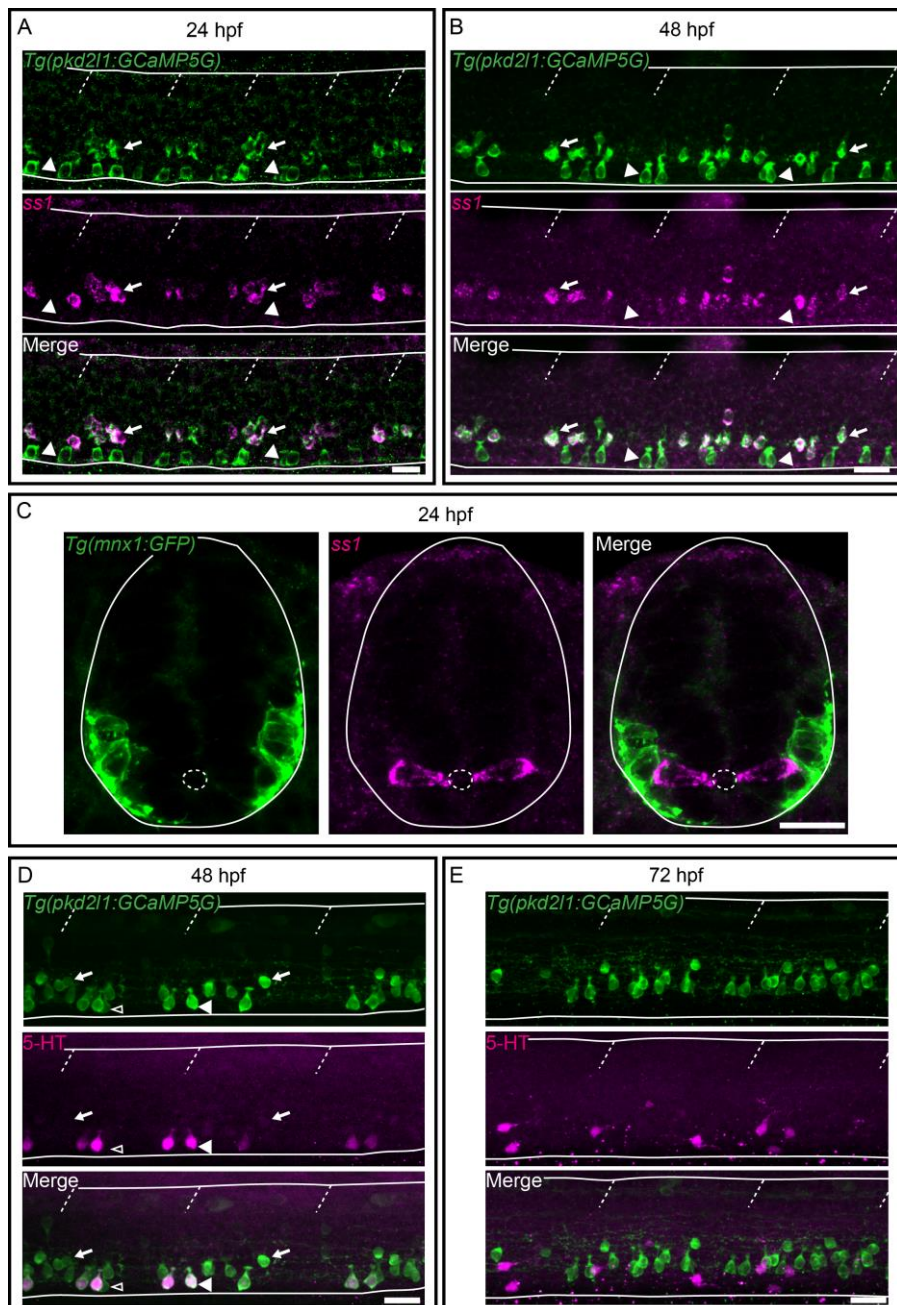


Figure 4: Dorsal CSF-cNs specifically express the somatostatin paralogue *ss1.1* when ventral CSF-cNs are partially and transiently serotonergic at early stages of development in the zebrafish spinal cord.

(A-C) FISH for *ss1.1* (magenta) coupled to GFP IHC (green) on *Tg(pkcd211:GCaMP5G)* (A, B) and *Tg(mnx1:GFP)* (C) embryos and larvae at 24 hpf and 48 hpf. (A-B) Lateral views of the spinal cord show that *ss1.1* expression is restricted to dorsal CSF-cNs (arrows). (C) Transverse sections of the spinal cord demonstrate that *ss1.1* (magenta) is not expressed in motor neurons (green) as previously reported (Devos et al. 2002). (D-E) 5-HT IHC (magenta) coupled to GFP IHC (green) on *Tg(pkcd211:GCaMP5G)* larvae at 48 hpf (D) and 72 hpf (E). (D) At 48 hpf, a large proportion of ventral CSF-cNs express 5-HT (arrowhead) but not all (empty arrowhead). Note that dorsal CSF-cNs (arrows) are not labelled by 5-HT. (E) At 72 hpf, ventral CSF-cNs are not serotonergic anymore in the rostral part of the spinal cord. Horizontal dashed lines represent the limits of the spinal cord and slash dashed lines represent somites boundaries. Small dotted ellipses represent respectively the limit of the central canal. Scale bars= 20 μ m.

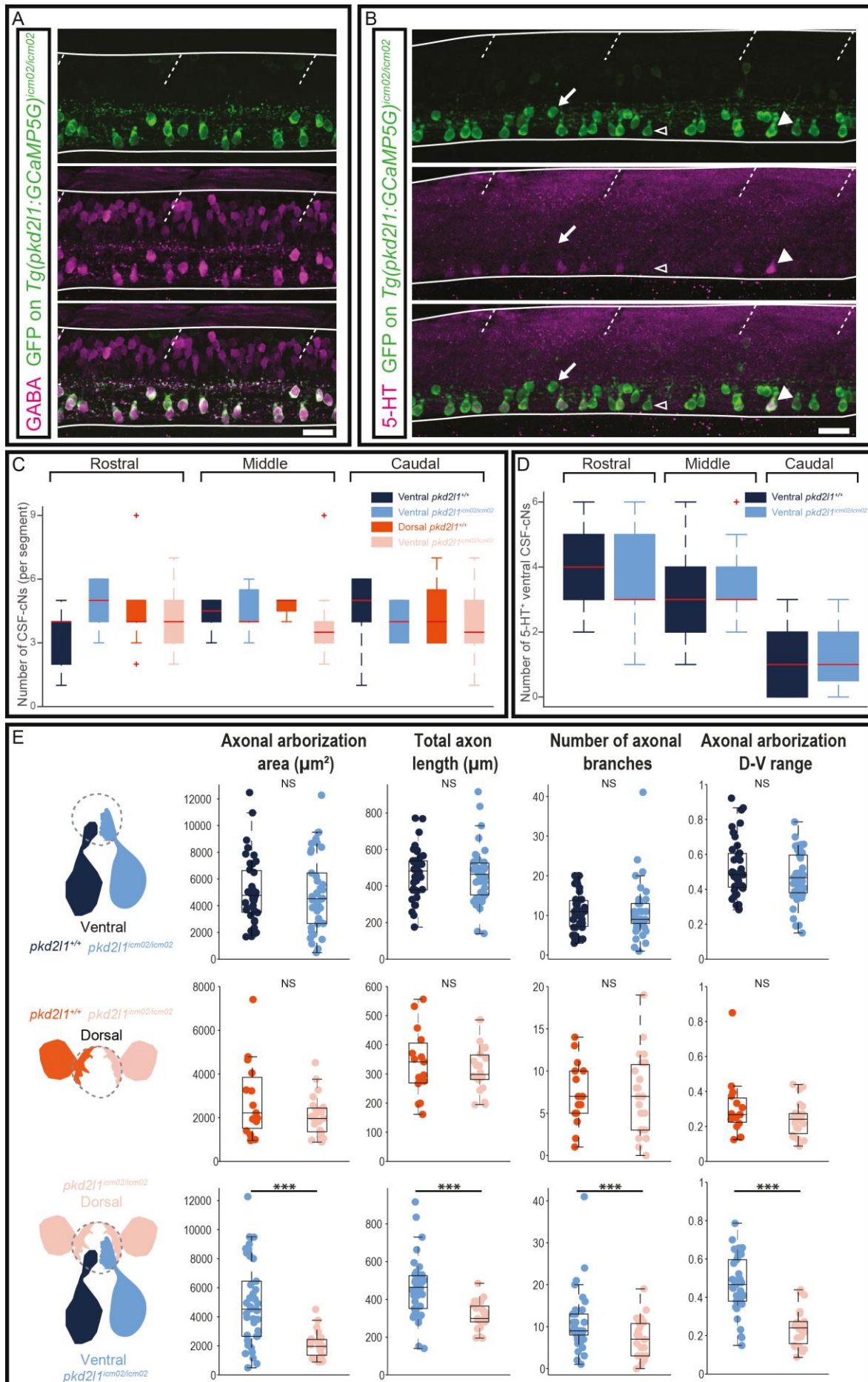


Figure 5: Pkd2l1 is not required for the proper differentiation of spinal CSF-cNs
GABA (**A**, magenta), 5-HT (**B**, magenta) and GFP (**A-B**, green) IHCs on *pkd2l1^{icm02/icm02}* mutants carrying *Tg(pkd2l1:GCaMP5G)^{icm07}* (thus named *Tg(pkd2l1:GCaMP5G)^{icm02/icm02}*). (**A**) All CSF-cNs in the mutants express GABA at 72 hpf. (**B**) At 48 hpf, a large proportion of ventral CSF-cNs in the mutants express the 5-HT. Horizontal dashed lines represent the limits of the spinal cord and slash dashed lines represent somites boundaries. Scale bars= 20µm. (**C-E**) *pkd2l1^{+/+}* and *pkd2l1^{icm02/icm02}* ventral CSF-cNs are represented in two shades of orange from dark to light respectively. *pkd2l1^{+/+}* and *pkd2l1^{icm02/icm02}* dorsal CSF-cNs are similarly represented in two shades of blue. (**C**) Counting of the number of ventral and dorsal CSF-cNs in WT and *pkd2l1^{icm02/icm02}* larvae at 3 dpf in three regions of the spinal cord; rostral from segments 3 to 6; middle from segments 10 to 13 and caudal from segments 23 to 26. (**D**) Counting of the number of 5-HT⁺ ventral CSF-cNs in 48hpf WT and *pkd2l1^{icm02/icm02}* embryos. Two-way ANOVAs were performed to test the interaction between the genotypes and the regions where cells were counted. (**E**) Statistical analysis of 39 WT and 38 *pkd2l1^{icm02/icm02}* ventral CSF-cNs, 15 WT and 23 *pkd2l1^{icm02/icm02}* dorsal CSF-cNs, and 38 *pkd2l1^{icm02/icm02}* ventral and 23 *pkd2l1^{icm02/icm02}* dorsal CSF-cNs comparing the two populations for the axonal arborization area, the total axon length, the number of branches and the axonal arborization dorso-ventral range. Each dot represents one cell. Two-sample t-tests to compare two populations were performed for the given parameter and significance is indicated by the triple stars ($p < 0.05$).

Annex 3

Hierarchy of Neural Organization in the Embryonic Spinal Cord: Granger-Causality Graph Analysis of In Vivo Calcium Imaging Data

Fabrizio De Vico Fallani, Martina Corazzol, Jenna R. Sternberg, Claire Wyart, and Mario Chavez

Published in:
IEEE Transactions on Neural Systems and Rehabilitation Engineering
VOL. 23, NO. 3, MAY 2015 333

Hierarchy of Neural Organization in the Embryonic Spinal Cord: Granger-Causality Graph Analysis of *In Vivo* Calcium Imaging Data

Fabrizio De Vico Fallani, *Member, IEEE*, Martina Corazzol, Jenna R. Sternberg, Claire Wyart, and Mario Chavez

Abstract—The recent development of genetically encoded calcium indicators enables monitoring *in vivo* the activity of neuronal populations. Most analysis of these calcium transients relies on linear regression analysis based on the sensory stimulus applied or the behavior observed. To estimate the basic properties of the functional neural circuitry, we propose a network approach to calcium imaging recorded at single cell resolution. Differently from previous analysis based on cross-correlation, we used Granger-causality estimates to infer information propagation between the activities of different neurons. The resulting functional network was then modeled as a directed graph and characterized in terms of connectivity and node centralities. We applied our approach to calcium transients recorded at low frequency (4 Hz) in ventral neurons of the zebrafish spinal cord at the embryonic stage when spontaneous coiling of the tail occurs. Our analysis on population calcium imaging data revealed a strong ipsilateral connectivity and a characteristic hierarchical organization of the network hubs that supported established propagation of activity from rostral to caudal spinal cord. Our method could be used for detecting functional defects in neuronal circuitry during development and pathological conditions.

Index Terms—Functional connectivity, GCaMP3 fluorescence, graph modeling, neuronal networks, zebrafish.

Manuscript received January 23, 2014; revised June 11, 2014; accepted July 16, 2014. Date of publication August 06, 2014; date of current version May 06, 2015. The work of M. Chavez was supported in part by the EU-LASAGNE Project under Contract 318132 (FET STREP). This work was supported in part by the program “Investissements d’avenir” ANR-10-IAIHU-06, by the Paris School of Neuroscience (ENP), by the Fondation Bettencourt Schueller (FBS), by Mr. P. Belle, the City of Paris Emergence program, by the Atip/Avenir junior program from INSERM and CNRS, by the Fyssen foundation, by an International Reintegration Grant from Marie Curie Actions Framework Program 6, and by the European Research Council (ERC) starter grant “OptoLoco”.

This paper has supplementary downloadable material available at <http://ieeexplore.ieee.org>, provided by the authors.

F. De Vico Fallani is with INRIA Paris-Rocquencourt, Aramis Project-Team, Paris, France, the Institut du Cerveau et de la Moelle épinière (ICM), Paris, France, the INSERM, U1127, Paris, France, the CNRS, UMR7225, Paris, France, and also with the Sorbonne Université, UPMC Université Paris 06, UMR S1127, Paris, France (e-mail: fabrizio.devicofallani@gmail.com).

M. Corazzol was with the CNRS, UMR7225, Paris, France, and the Institut du Cerveau et de la Moelle épinière (ICM), Paris, France. She is now with the Centre de Neurosciences Cognitive, CNRS UMR5229, Bron, France.

J. R. Sternberg and C. Wyart are with the INSERM U1127, Paris, France, and with the CNRS, UMR7225, Paris, France, and with the Sorbonne Université, UPMC Université Paris 06, UMR S1127, Paris, France, as well as with the Institut du Cerveau et de la Moelle épinière (ICM), Paris, France (e-mail: claire.wyart@inserm.fr).

M. Chavez is with the CNRS, UMR7225, Paris, France.

Color versions of one or more of the figures in this paper are available online at <http://ieeexplore.ieee.org>.

Digital Object Identifier 10.1109/TNSRE.2014.2341632

I. INTRODUCTION

NEURAL circuits in the spinal cord play essential roles in vertebrate locomotion [1]. During early development, spontaneous coordinated activity rises from newborn neurons across the entire spinal cord. Embryonic and larval zebrafish provide a unique model to investigate the mechanisms involved in generating rhythmic patterns of neuronal activity due to their transparency, relatively small size and amenability to genetic manipulation [2]. Notably, the combination of genetics and optical imaging has been recently developed to investigate non-invasively the neuronal circuit function at single-cell resolution [3], [4]. In contrast to conventional electrophysiology, which records the activity of few neuronal cells through electrode insertion, calcium fluorescence imaging techniques allow us to optically record from multiple neurons the Ca²⁺ influx associated with their activity and in systems as diverse as neuronal cultures, hippocampal brain slices, nematodes and zebrafish [5]–[13].

It has been reported that zebrafish embryos show spontaneous activity as early as 17 hours post-fertilization (hpf) [14]. This spontaneous activity consists of the contraction of the left and right trunk muscles alternatively without any external stimulus. This coiling behavior precedes touch-evoked escape response and swimming, which emerge in later developmental stages. Conventional electrophysiology analyses showed evidence in the paralyzed embryo for periodic and synchronized activity of motoneurons within one side of the spinal cord and alternation between the two hemicords [15]. Similar results were also replicated by using genetically encoded calcium indicators [16]; the latter approach, based on high frequency imaging (20 Hz), has also shown rostral-caudal propagation of activity [16]. From a methodological perspective synchronized coordination between neurons has been generally evaluated by cross-correlation analyses, which are basic indexes of undirected functional connectivity [17]–[19]. Synchronization does not inform on the propagation of such activity, which could instead describe how the information flows across neuronal populations [20]. Current methods for investigating activity propagation in calcium fluorescence imaging data largely rely on the computation of either inter-spike delays between different signals [16], [17] or onset times of neuronal activation [10], [13], that can be seen as an heuristic instance of the more general cross-lagged correlation [21]. The arbitrary selection of several parameters (e.g., amplitude thresholds, refractory periods) to be fixed *a priori*, as well as the sensitivity to spurious noisy peaks, make this heuristic

method suboptimal in terms of general applicability. Interestingly, a recent *in vitro* study suggests that theoretically grounded methods, like the transfer entropy, can be effectively used to reconstruct activity propagation from calcium signals of neuronal cultures [12]. Despite its theoretical advantages, transfer entropy requires very long data to obtain reliable estimates of activity propagation [22]. This technical requirement represents a limiting factor when dealing with *in vivo*, generally shorter, data.

In the present study, we use a more robust principled method to infer activity propagation by exploiting the entire dynamics of *in vivo* recorded calcium signals. Specifically, we refer here to the Granger-causality (*GC*), a statistical concept, based on prediction error that is commonly used to quantify the information flow between neurophysiological signals [23]. Estimating Granger-causality between all the available calcium signals gives a functional connectivity pattern that describes in a compact way the directed interactions between all the neuronal cells. This functional connectivity pattern is shaped to some extent by the underlying synaptic connectivity [24] and provides complementary information about the putative dynamic flow within the neuronal network. Functional connectivity patterns can be probed as graphs or networks, i.e., mathematical objects composed of nodes corresponding to neurons and weighted directed links (*GC* values). Finally, we exploit graph theoretical approaches to: i) characterize at a system level the putative functional circuitry in the spinal cord of the zebrafish embryo and ii) identify the neuronal “hubs” of information flow that subserve the spontaneous activity.

II. METHODS

A. Experimental Data and Preprocessing

All experiments were performed on Danio rerio embryos between 23 and 24 hours post-fertilization. AB and TL strains of wild-type (WT) larvae were obtained from our laboratory stock of adults. Embryos and larvae were raised in an incubator at 28.5°C until 60%–75% epiboly, then maintained at 26°C until shortly before recordings were performed. All procedures were approved by the Institutional Ethics Committee at the Institut du Cerveau et de la Moelle épinière (ICM). Five 28–30 somite-stage *Tg{sl1020t:Gal4; UAS:GCaMP3}* [25] transgenic embryos were used for this study. Before recordings were performed, embryos were dechorionated and screened for fluorescence. Embryos screened for GCaMP3 fluorescence were staged at 23 hpf and embedded in 1.5% agarose with the dorsal side of the spinal cord oriented up. Embryos were anesthetized in MS-222 before being paralyzed with 0.5 mM α -bungarotoxin (Sigma-Aldrich, USA) diluted in phenol red solution via injection of caudal muscle (segments 15–18). Data were acquired with a 3i spinning disk confocal microscope. Calcium imaging was performed during spontaneous activity for 250 seconds at 4 Hz with a 488 nm laser. A 20x objective allowed simultaneous imaging of five segments of the spinal cord from somites 3 to 7. After the experiment was performed, embryos were staged again to confirm that imaging reflected activity of 30-somite stage embryos (corresponding to 24 hpf). Images were acquired with Slidebook software and analyzed offline with ImageJ and MATLAB (The Mathworks, USA).

Neurons expressing in these lines and implicated in the spontaneous activity are mainly motoneurons. They were identified based on the amplitude of the change of GCaMP3 fluorescence that is related to intracellular calcium concentration. ROIs for motoneurons on each side were manually selected based on the standard deviation image calculated over the entire recording. For each ROI, the fluorescence value was computed as $\Delta F/F = (F(t) - F_0)/(F_0 - F_{bg})$, where $F(t)$ was the fluorescence signal averaged across the pixels within the ROI, the baseline fluorescence F_0 was calculated as the mean of the first ten frames acquired and F_{bg} was calculated in a region outside of the embryo (Fig. 1).

B. Neuronal Functional Connectivity

To elucidate how different motoneurons were collectively recruited, we referred to the concept of functional connectivity [26]. Here, the organization of neural circuits is estimated on the basis of the model-free Granger-causality [27], which tests whether the prediction of the present value in one time series can be significantly improved by including information from another time series. If so, the second time series is said to have a Granger causal effect on the first, and the degree of significance of the improvement may be taken as the strength of *GC*. The *GC* measure is typically implemented by autoregressive (AR) modeling. In AR modeling, a stationary signal $x_j(t)$ can be expressed by a linear regression of its past values according to the formula

$$x_j(t) = \sum_{k=1}^q a_j(k) x_j(t-k) + e_j(t) \quad (1)$$

where $a_j(k)$ are the regression coefficients of the univariate AR model, q is the model order, and $e_j(t)$ is the respective prediction error. By introducing the information from a second stationary signal $x_i(t)$ the formula can be rewritten as

$$x_j(t) = \sum_{k=1}^q a_j(k) x_j(t-k) + \sum_{k=1}^q a_i(k) x_i(t-k) + e_{ij}(t) \quad (2)$$

where $a_j(k)$ and $a_i(k)$ are the new regression coefficients of the bivariate AR model, and $e_{ij}(t)$ is the new prediction error obtained by including also the past of $x_i(t)$ in the linear regression of $x_j(t)$.

The *GC* between $x_i(t)$ and $x_j(t)$ is then measured by the log ratio of the prediction error variances for the bivariate and univariate model:

$$GC_{i \rightarrow j} = \ln \left(\frac{\text{var}[e_{ij}(t)]}{\text{var}[e_j(t)]} \right). \quad (3)$$

GC is a positive number; the higher $GC_{i \rightarrow j}$, the stronger the influence of x_i on x_j is. Such influence is often considered to reflect the existence of an information flow outgoing from the system i to the system j [28]. Finally, *GC* is generally asymmetric ($GC_{i \rightarrow j} \neq GC_{j \rightarrow i}$), which is an important feature to infer causal or driving relationships.

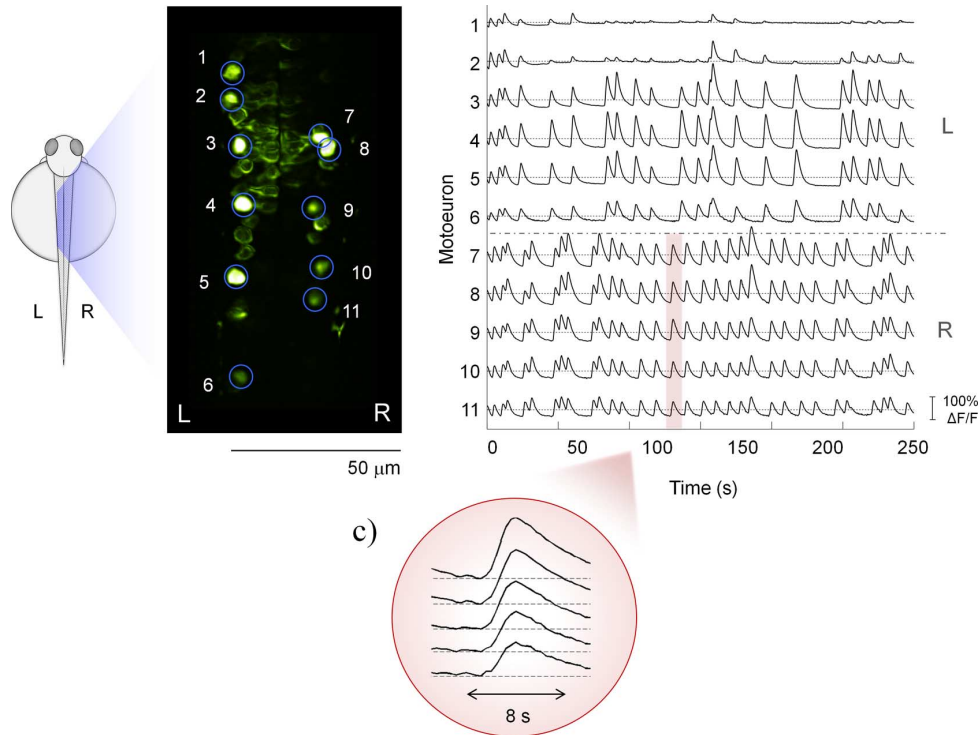


Fig. 1. Optical imaging of calcium transients recorded in a 30-somite stage representative embryo in the stable transgenic zebrafish line *Tg(s1020:Gal4; UAS:GCaMP3)*. Panel a) Dorsal side showing the field of view. Scale bar = 50 μm . Rostral is up, “L” for left and “R” for right side of the spinal cord. Each motoneuron selected for analysis is circled (from 1 to 6 on the left side, and 7 to 11 on the right side). Panel b) $\Delta F/F$ fluorescence signals (related to calcium activity) for each motoneuron selected in a). Motoneurons 1 and 2 have a smaller $\Delta F/F$ signal-to-noise ratio, which may be due to their position slightly shifted compared to the focal plan. Panel c) Inset shows a zoomed view of a representative calcium transient for the motoneurons in the right hemicord.

1) *Application to Calcium Fluorescence Imaging Data:* In our study the neuronal GCaMP3 fluorescence signals exhibited steady oscillations (see Fig. 1 for a representative embryo). Specifically, the 98.5% of the pooled data satisfied the stationary test [29] and we computed $GC_{i \rightarrow j}$ values, with $i, j = 1 \dots N$ where N is the number of the identified motoneurons in each zebrafish embryo. The regression coefficients of the AR models were computed according to the ordinary least-squares minimization of the Yule-walker equations. The model order q was selected for each zebrafish embryo according to the Akaike criterion [30]. This criterion tries to find the optimal q that minimizes the following cost function: $IC(q) = \ln(\det(\Sigma_2)) + 8q/T$, where Σ_2 is the noise covariance matrix of the bivariate AR model and T is the number of samples of the time series. Basically, this cost function balances the variance accounted for by the AR model against the number of coefficients to be estimated. Obtained values across zebrafish embryos ranged between 8 and 20, corresponding to sliding regression windows of 2 and 5 s, a temporal period which is compatible with the dynamics of single calcium transients (see Fig. 1). For each zebrafish embryo a full connectivity pattern was constructed by estimating the GC influences between the activities of all the identified motoneurons in the spinal cord. The statistical significance of the obtained influences was established by means of a F -test under the null hypothesis $GC_{i \rightarrow j} = 0$ [23]. According to this procedure, only the GC values corresponding to percentiles inferior to a statistical threshold of $\alpha = 0.01$, Bonferroni corrected for multiple comparisons were retained.

C. Graph Modeling of Functional Connectivity

The obtained functional connectivity patterns were then analyzed by means of a graph theoretical approach, which is a powerful tool to characterize the organization of several connected systems including the brain [31]. According to this framework, functional connectivity patterns can be regarded as graphs (or networks) composed of nodes (motoneurons) and directed weighted links (pairwise GC values). The mathematical representation of such network is an asymmetric square weighted matrix W of size N , where N is the number of motoneurons. The generic weight $w(i, j)$ corresponds to the magnitude of the information flow estimated between the motoneuron i and the motoneuron j . Thus, $w(i, j) = GC_{i \rightarrow j}$ if the corresponding GC value is statistically significant and $w(i, j) = 0$ otherwise.

1) *Connectivity Matrix Factorization:* In general, functional networks describing neuronal systems are peculiar in that the nodes of the network represent neurons that are spatially embedded [32]. Human brain networks, for example, consist of two large subsets of neural assemblies coincident with the two hemispheres, this evidence playing an important role for the overall organization [33], [34]. Here, the obtained neuronal networks are embedded in a physical space coincident with the two sides of the spinal cord (i.e., hemicords) of the zebrafish embryo, where nodes are primary rhythmically active motoneurons [17]. Without loss of generality, we can assume that the first M nodes of the network belong to the left side (L) and the remaining N

– M to the right side (R). The connectivity matrix W can be then usefully split in two subcomponents describing the ipsilateral and contralateral connectivity of the two hemicords

$$W = W_{IL} + W_{IR} + W_C = W_I + W_C \quad (4)$$

where W_{IL} is a $N \times N$ matrix containing the first block $M \times M$ on the main diagonal of W and 0 elsewhere; W_{IR} is a $N \times N$ matrix containing the second block $(N - M) \times (N - M)$ on the main diagonal of W and 0 elsewhere; W_I is the sum of the blocks W_{IL} and W_{IR} corresponding to the ipsilateral connectivity of the hemicords; W_C is a $N \times N$ matrix containing the two remaining blocks $(N - M) \times M$ and $M \times (N - M)$ on the second diagonal of W that correspond to the contralateral connectivity of the hemicords, and 0 elsewhere.

2) *Connection Intensity*: We considered the ipsilateral and contralateral connectivity separately according to the factorization of W . The global intensity of connectivity was defined as the sum of all the weighted links within (ipsi) or between (contra) the two sides of the spinal cord and it was measured by the connection intensity C

$$C_{\text{ipsi}} = \sum_{i \neq j=1}^N W_I(i, j), \quad C_{\text{contra}} = \sum_{i \neq j=1}^N W_C(i, j). \quad (5)$$

By definition C_{ipsi} and C_{contra} are positive numbers; higher values of C reflect more intense connectivity. Connection intensity can be seen as the weighted version of the connection density for unweighted graphs [31].

3) *Node Strength*: At the local level we considered separately the connectivity of each node i with respect to its ipsi/contralateral hemicord. Furthermore, we distinguished between incoming and outgoing connectivity. The local information flow was then measured by the node strength (or weighted degree), which considers the sum of all the incoming/outgoing weighted links

$$D_{\text{ipsi}}^{\text{in}}(i) = \sum_{j=1}^N W_I(j, i), \quad D_{\text{ipsi}}^{\text{out}}(i) = \sum_{j=1}^N W_I(i, j) \quad (6)$$

$$D_{\text{contra}}^{\text{in}}(i) = \sum_{j=1}^N W_C(j, i), \quad D_{\text{contra}}^{\text{out}}(i) = \sum_{j=1}^N W_C(i, j). \quad (7)$$

By definition, node strengths are always positive and they are characterized by a very intuitive interpretation: nodes with high in-strength are highly influenced by others and represent potential receivers of information flow; nodes with high out-strength are central in the way they influence others and represent possible neural transmitter of information flow.

4) Δ *Centrality*: We also defined an index that integrates the node strengths and gives a unique value of node centrality (or importance). This index of delta centrality Δ was computed

as the difference between the out- and in-strength and it was defined either for the connectivity within (ipsi) and between (contra) hemicords

$$\Delta_{\text{ipsi}}(i) = D_{\text{ipsi}}^{\text{out}}(i) - D_{\text{ipsi}}^{\text{in}}(i) \quad (8)$$

$$\Delta_{\text{contra}}(i) = D_{\text{contra}}^{\text{out}}(i) - D_{\text{contra}}^{\text{in}}(i) \quad (9)$$

Δ centrality values quantify the tendency of the nodes to act more as transmitter ($\Delta > 0$) or receiver ($\Delta < 0$) of information flow.

5) *Normalization by Random Graphs*: Due to experimental constraints (e.g., manual selection of motoneurons based on the variability of the fluorescence signal, see Section II-A), the resulting GC networks can have different sizes across embryos in terms of number of nodes and weighted links. The measured network indexes (i.e., connection intensity, node strength, delta centrality) were then normalized in each embryo to compensate possible biases on the network topology due to the different size [35]. Specifically, for each embryo, the measured network indexes were normalized by those obtained from a distribution of 100 equivalent graphs generated by randomly shuffling the weighted links of the actual GC network. From this distribution the mean and standard deviation were computed and used to normalize (Z-score) the actual network indexes. Eventually, a positive Z-score indicates that a network index measured on the actual GC network is higher than what expected in random graphs, a negative Z-score indicates the opposite, and a Z-score close to zero indicates that the network index measured on the actual GC network is similar to that obtained in equivalent random configurations.

III. RESULTS

By performing calcium imaging within one plane of the ventral and rostral spinal cord, we observed that motoneurons of zebrafish 30-somite stage embryos generated large calcium transients reflecting synchronous bursting activity (see Fig. 1, for a representative embryo). Motoneurons were highly synchronized on each side, as illustrated in the cross-correlation connectivity matrix of Fig. 2(a). Reciprocal coordination is usually estimated by the standard cross-correlation coefficient (CC), which can only detect undirected relationships between neuronal activities, i.e., $w(j, i) = w(i, j)$. Here, we used Granger-causality estimates to infer the activity propagation between the calcium transients of the motoneurons. Such nonreciprocal relationships allow identifying a directed neuronal network as revealed by the asymmetric connectivity matrix W of the representative embryo [Fig. 2(b)]. In this matrix the elements above the main diagonal represent influences from rostral to caudal motoneurons, the elements below the main diagonal indicating the opposite direction. Since active neurons were selected based on the standard deviation of the fluorescence signal for the length of the recording, the number of considered motoneurons could differ across distinct embryos.

By using a graph theoretical approach, we found that the ipsilateral connectivity intensity C_{ipsi} was significantly higher

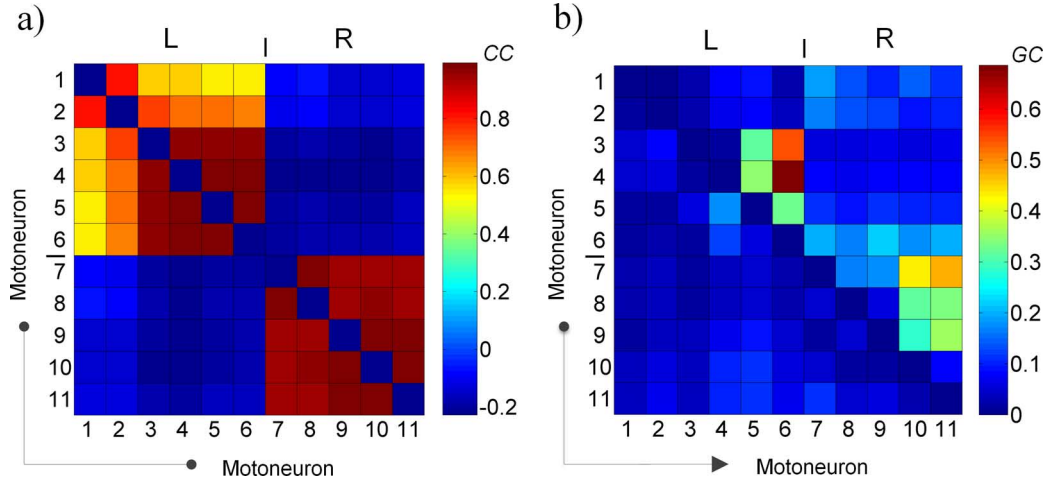


Fig. 2. Cross-correlation (CC) versus Granger-causality (GC) connectivity matrix W of the representative zebrafish embryo. Functional connectivity between motoneurons is coded by the elements of the W matrices. In these matrices, each element w_{ij} contains the magnitude of functional connectivity between the activity of the neuron i and j according to the respective color bar. Elements on the main diagonal, indicating self-connections, were excluded due to their trivial interpretation and coded by a blue color (i.e., absence of connectivity). The first block identified by the rows and columns from 1 to 6 represent the connectivity between the motoneurons in the left hemicord (L), while the second block of rows and columns from 7 to 11 represent the connectivity between the motoneurons in the right hemicord (R). Intensity of the pairwise connectivity is coded by the colorbar. Panel a) CC matrix shows a strong undirected (the matrix is symmetric) connectivity between ipsilateral motoneurons. Panel b) Asymmetric GC matrix shows a general tendency of the rostral motoneurons (lower identifier numbers) in each hemicord to influence caudal motoneurons (higher identifier numbers). Note that motoneurons 1 and 2 had a smaller $\Delta F/F$ signal-to-noise ratio [see Fig. 1(b)] and they are less involved in the connectivity matrices, i.e., low CC/GC values in the first two rows and columns of W .

TABLE I
NORMALIZED VALUES OF IPSILATERAL AND CONTRALATERAL CONNECTION INTENSITY FOR NEURONAL GRANGER-CAUSALITY NETWORKS. ASTERISKS DENOTE SIGNIFICANT DEVIATIONS ($\text{abs}(Z\text{-score}) > 1.96$, $p < 0.05$) FROM EQUIVALENT RANDOM GRAPHS. GROUP-AVERAGED VALUES ARE ALSO REPORTED AT THE END OF THE TABLE

Embryo #	GC networks	
	C_{ipsi} (Z-score)	C_{contra} (Z-score)
<i>E1</i>	4.412*	-9.124*
<i>E2</i>	1.982	-4.436*
<i>E3</i>	2.641*	-5.183*
<i>E4</i>	2.653*	-5.203*
<i>E5</i>	1.408	-2.200*
Group-average	2.619	-5.229

($p < 0.05$) compared with that obtained by randomly reshuffling the links (i.e., pairwise GC) among all the available motoneurons (here also referred as nodes). On the contrary, the contralateral connectivity intensity C_{contra} was significantly lower ($p < 0.05$) with respect to random graphs (Table I). In general, C_{ipsi} values tend to be higher than C_{contra} (Wilcoxon Z-value = -1.75 , $p = 0.079$), this indicating that spontaneous coiling in the zebrafish was functionally characterized by a strong exchange of information between the nodes in the same hemicord.

At a local level, we characterized each node in terms of its outgoing/incoming information flow. The resulting information flows were preferably distributed along the same side of the spinal cord as compared to random graphs, i.e., $D_{\text{ipsi}}^{\text{in}} > D_{\text{contra}}^{\text{in}}$, $D_{\text{ipsi}}^{\text{out}} > D_{\text{contra}}^{\text{out}}$ (see Supplementary Fig. 1). Given the scarce level of contralateral connectivity, both at the global and local scale, the ipsilateral graph metrics were expected to give more relevant information about the network organization. In particular, by fusing the information from the ipsilateral out-strength $D_{\text{ipsi}}^{\text{out}}$ and in-strength $D_{\text{ipsi}}^{\text{in}}$ we defined

a compact delta centrality index (Δ_{ipsi}) to identify the nodes acting as connectivity ‘‘hubs’’, i.e., nodes with relatively high information flow. The characteristic spatial organization of the Δ_{ipsi} values shows that rostral nodes tend to have a larger amount of outgoing information flow while caudal nodes have a higher tendency to receive information flow (see Fig. 3, for the representative embryo). By exploiting the actual longitudinal position of the motoneurons as measured by their Cartesian Y-coordinate from the field of view of the spinal cord, we tested whether the node Δ_{ipsi} centrality values and the normalized Y-coordinates of the corresponding motoneurons were statistically correlated. A first analysis considering the nodes in both the hemicords revealed a significant positive correlation for the pooled data (Spearman $R = 0.4157$, $p = 0.0006$; data not shown here). An even higher significant correlation ($R = 0.6001$, $p = 0.0003$) was obtained when we used the representative side of the spinal cord that gave the signals with better quality in each embryo [Fig. 4(a)]. Given that the calcium imaging data are obtained by optical sectioning on a

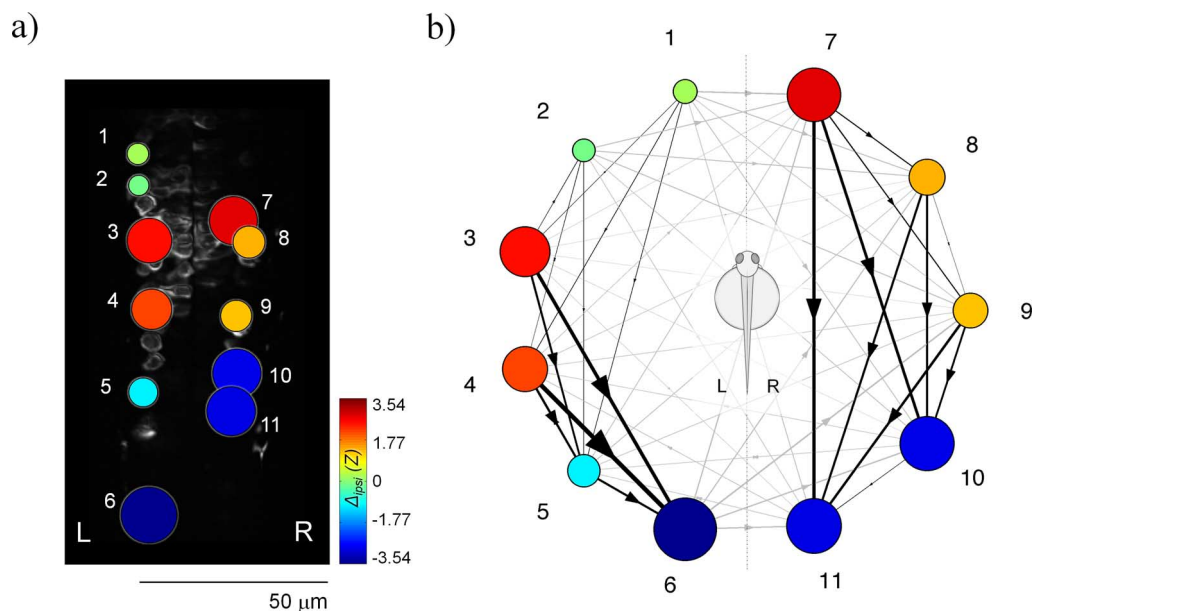


Fig. 3. Rostro-caudal distribution of the nodal delta centrality in the representative zebrafish embryo. Panel a) Normalized Δ_{ipsi} value is represented for each node (motoneuron) as a colored circle superimposed on the field of view. The larger the circle, the more central is the node in terms of its tendency to act as a transmitter (red color, positive value) or receiver (blue color, negative value) hub of information flow. Panel b) Same normalized Δ_{ipsi} centrality values are here represented within the neuronal GC network. Statistically significant GC influences are illustrated as directed arrows. The thicker the arrow the stronger the GC value is. Inter-hemicord directed links are illustrated in grey color for the sake of simplicity.

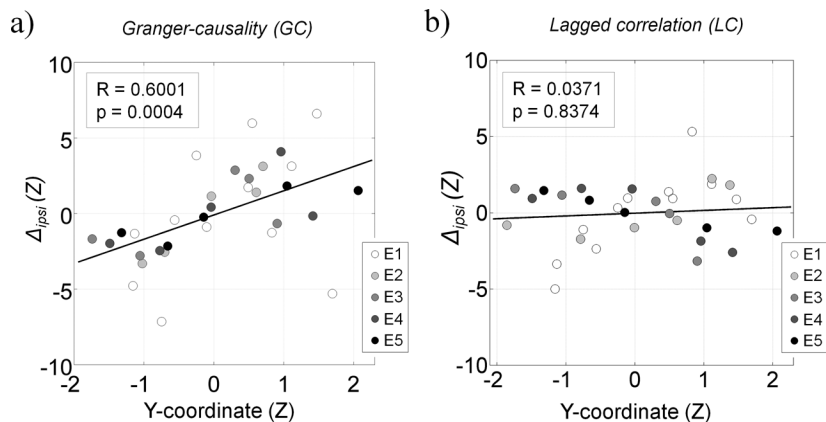


Fig. 4. Spearman correlation between nodal delta centrality and longitudinal position of the motoneurons for the pooled data. Each circle in the panels represents the normalized Y-coordinate (x-axis, whereby positive values correspond to more rostral positions and negative values indicate more caudal positions) and the Δ_{ipsi} value (y-axis) for a node of a zebrafish embryo's neuronal network. Colors of the circles code the identifier of the embryo according to the legend. Panel a) shows a significant positive correlation for the neuronal networks obtained by computing Granger-causality between the calcium imaging signals. Panel b) No significant correlation was reported for the network obtained by using lagged correlation.

single plane across the spinal cord, one side of the cord often shows signals with higher amplitude and signal-to-noise ratio than the other. This is a well-known issue due to the difficulty to obtain in the same focal plane $\Delta F/F$ signals with exactly the same quality from neurons on both the hemicords (see for example Fig. 1(b), motoneurons 1 and 2).

Such node spatial hierarchy also could be revealed, albeit marginally, by solely using node in-strength and out-strength values (see Supplementary Fig. 2). The observed node hierarchy reflecting the rostro-caudal propagation of activity can be attributed to the superiority of the GC method over standard techniques using for instance lagged correlation (LC) to infer directionality [21]. To demonstrate this, the Δ centralities were computed for the LC networks obtained in each zebrafish embryo (see Supplementary Fig. 3) and then correlated with the longi-

tudinal position of the motoneurons. No significant Spearman correlation was reported when considering either the sides of the spinal cord ($R = -0.089$, $p = 0.482$ data not shown here) or the representative side ($R = 0.037$, $p = 0.837$) [see Fig. 4(b)].

IV. DISCUSSION

Functional connectivity is considered fundamental to understand how neural assemblies exchange information and how the resulting network leads to physiological and pathological behavior [36]. Despite the high potential of connectivity-based approach in humans, neuroimaging techniques such as electroencephalography (EEG), magnetoencephalography (MEG) or functional magnetic resonance imaging (fMRI), only allow sampling of activity across a fraction of the entire neuronal network. This limitation restrains the power of subsequent analysis and results interpretation.

The transparency and small size of the zebrafish nervous system provide an opportunity to optically record calcium-transients reflecting neuronal activity from the entire neuronal network [9], [16], [17], [37], [38]. Recently, the combination of optical and genetic techniques has allowed us to record networks composed of thousands of neurons at single-cell resolution level [3], [4], [18], [19], [39], [40]. In the zebrafish embryonic spinal cord we show here that Granger-causality graph analysis of calcium imaging data, obtained from a single plane at the single cell resolution and low acquisition rate, can resolve the well-known rostro-caudal propagation in the spinal cord where cross-correlation analysis did fail. These findings are in line with previous studies showing that motoneurons are coupled via GAP junctions at this stage and that excitation most likely comes from descending fibers from the hindbrain [15], [41].

Applied to Z-scan measurements, our methodological approach could provide new insights on mechanisms underlying activity propagation and information flows between larger populations of neurons in dataset acquired on the whole brain [4], [18], [19], [39], [40], [42] and at faster acquisition rates [43]. However, when considering a large number of neurons ($N \gg 10$), particular attention should be paid to the statistical validation of the estimated *GC* networks. In our study, the statistical threshold that filters out the less-significant links (Section II-B1, Bonferroni criterion for multiple comparisons) inversely depends on the total number of possible of links $L = N * (N - 1)$, i.e., the higher L , the more stringent the threshold is. This choice could lead to very sparse *GC* networks when $N \gg 10$ and less stringent statistical procedures, based for example on false discovery rates [44], can be considered to retain a sufficiently higher number of weighted links describing the functional network.

Here, the resulting *GC* networks are factorized in order to disentangle the role of the connectivity within (ipsi) and between (contra) the two sides of the spinal cord. Our results suggest that the neuronal activity underlying the rhythmic dynamics at this early embryonic stage entails functional directed networks that foster the information propagation between ipsilateral neurons while discouraging contralateral connectivity flows. This outcome is in line with the previous findings obtained with undirected connectivity analyses, which reported high ipsilateral activity coordination and low contralateral correlation [10], [11]. The directed connectivity approach further revealed a characteristic spatial hierarchy of the network hubs, i.e., nodes with a relatively high incoming/outgoing information flow. Network hubs have a crucial structural role in connected systems as they convey the large part of the available information and mediate such information between other nodes [45]. The obtained results show that there are two classes of network hubs in the spinal cord of the zebrafish that underlie the early spontaneous activity: i) the *transmitter hubs*, i.e., nodes with a relatively high rate of outgoing information flow, and ii) the *receiver hubs*, i.e., those with a relatively high rate of incoming information flow. Interestingly, the transmitter hubs are located in the rostral zone of the spinal cord while the receiver hubs are rather located in the more caudal site (Figs. 3 and 4).

Although our approach is limited in that it cannot directly unveil the underlying basic mechanisms giving rise to the measured *GC* networks, the observed characteristic network hub organization supports previous evidence demonstrating rostro-caudal activity propagation in terms of inter-spike delay between neurons [1], [16]. In those studies, rostro-caudal activity propagation had been observed with electrophysiology techniques and higher acquisition rate. Here, we show that such hub organization cannot be determined when using temporal delays (i.e., cross-lagged correlation) between calcium imaging signals recorded at a low acquisition rate [Fig. 4(b)]. Hence, the proposed network approach describing the functional circuitry in terms of information propagation between multiple neural activities appears to be: i) more general, i.e., Granger-causality considers prediction error between signals whereas cross-lagged correlation takes into account simple delay and ii) more robust, i.e., rostro-caudal activity propagation can be characterized in terms of connectivity at lower acquisition rates.

In this study, the information propagation is estimated by means of bivariate AR models of Granger-causality (see Section II-B). Although other methods based on information theory [46] or multivariate autoregressive models (MVAR) could be used to assess directionality [47], practical evidence shows that they require generally longer data and strong assumptions on the absence of latent variables that could introduce spurious connectivity [48], [49]. Using MVAR models when these assumptions are marginally satisfied (like in our case) could lead to unreliable connectivity patterns. For the sake of completeness we have also computed the MVAR *GC* networks (data not shown here). A statistical procedure similar to the bivariate case (i.e., statistical threshold of $\alpha = 0.01$, Bonferroni corrected for multiple comparisons) is used to retain the significant *GC* influences. For these networks no significant hub hierarchy distribution is reported when correlating Δ_{ipsi} centrality values with the normalized Y-coordinates of the respective motoneurons either in both the sides of the spinal cord ($R = 0.107$, $p = 0.393$ data not shown here) or the representative side ($R = -0.019$, $p = 0.916$ data not shown here).

V. CONCLUSION

We used Granger-causality and graph theory to characterize the organization of neural functional connectivity patterns in the spinal cord of zebrafish embryos during spontaneous motor-like activity at the 30-somite stage. The obtained results allowed us to identify a characteristic network structure that supports ipsilateral neural connectivity and rostro-caudal activity propagation. This general framework can provide effective network-based biomarkers for functional circuitry alteration of the spinal cord during natural development as well as in induced or spontaneous pathological conditions.

REFERENCES

- [1] M. A. Masino and J. R. Fetcho, "Fictive swimming motor patterns in wild type and mutant larval zebrafish," *J. Neurophysiol.*, vol. 93, no. 6, pp. 3177–3188, Jun. 2005.

- [2] J. R. Fetcho and K. S. Liu, "Zebrafish as a model system for studying neuronal circuits and behavior," *Ann. N.Y. Acad. Sci.*, vol. 860, pp. 333–345, Nov. 1998.
- [3] C. Wyart and F. Del Bene, "Let there be light: Zebrafish neurobiology and the optogenetic revolution," *Rev. Neurosci.*, vol. 22, no. 1, Jan. 2011.
- [4] T. Panier, S. A. Romano, R. Olive, T. Pietri, G. Sumbre, R. Candelier, and G. Debrégeas, "Fast functional imaging of multiple brain regions in intact zebrafish larvae using selective plane illumination microscopy," *Front Neural Circuits*, vol. 7, p. 65, 2013.
- [5] J. R. Fetcho, K. J. Cox, and D. M. O'Malley, "Monitoring activity in neuronal populations with single-cell resolution in a behaving vertebrate," *Histochem. J.*, vol. 30, no. 3, pp. 153–167, Mar. 1998.
- [6] D. A. Ritter, D. H. Bhatt, and J. R. Fetcho, "In vivo imaging of zebrafish reveals differences in the spinal networks for escape and swimming movements," *J. Neurosci.*, vol. 21, no. 22, pp. 8956–8965, Nov. 2001.
- [7] M. B. Orger, A. R. Kampff, K. E. Severi, J. H. Bollmann, and F. Engert, "Control of visually guided behavior by distinct populations of spinal projection neurons," *Nat. Neurosci.*, vol. 11, no. 3, pp. 327–333, Mar. 2008.
- [8] F. Del Bene, C. Wyart, E. Robles, A. Tran, L. Looger, E. K. Scott, E. Y. Isacoff, and H. Baier, "Filtering of visual information in the tectum by an identified neural circuit," *Science*, vol. 330, no. 6004, pp. 669–673, Oct. 2010.
- [9] E. Brustein, N. Marandi, Y. Kovalchuk, P. Drapeau, and A. Konnerth, "In vivo monitoring of neuronal network activity in zebrafish by two-photon Ca²⁺ imaging," *Pflugers Arch.—Eur. J. Physiol.*, vol. 446, no. 6, pp. 766–773, Sep. 2003.
- [10] P. Bonifazi, M. Goldin, M. A. Picardo, I. Jorquera, A. Cattani, G. Bianconi, A. Represa, Y. Ben-Ari, and R. Cossart, "GABAergic hub neurons orchestrate synchrony in developing hippocampal networks," *Science*, vol. 326, no. 5958, pp. 1419–1424, Dec. 2009.
- [11] X. Liu, T. Quan, S. Zeng, and X. Lv, "Identification of the direction of the neural network activation with a cellular resolution by fast two-photon imaging," *J. Biomed. Opt.*, vol. 16, no. 8, pp. 080506–080506-3, 2011.
- [12] O. Stetter, D. Battaglia, J. Soriano, and T. Geisel, "Model-free reconstruction of excitatory neuronal connectivity from calcium imaging signals," *PLoS Comput. Biol.*, vol. 8, no. 8, p. e1002653, Aug. 2012.
- [13] J. G. Orlandi, J. Soriano, E. Alvarez-Lacalle, S. Teller, and J. Casademunt, "Noise focusing and the emergence of coherent activity in neuronal cultures," *Nature Phys.*, vol. 9, no. 9, pp. 582–590, Jul. 2013.
- [14] L. Saint-Amant and P. Drapeau, "Time course of the development of motor behaviors in the zebrafish embryo," *J. Neurobiol.*, vol. 37, no. 4, pp. 622–632, 1998.
- [15] L. Saint-Amant and P. Drapeau, "Synchronization of an embryonic network of identified spinal interneurons solely by electrical coupling," *Neuron*, vol. 31, no. 6, pp. 1035–1046, Sep. 2001.
- [16] A. Muto, M. Ohkura, T. Kotani, S. Higashijima, J. Nakai, and K. Kawakami, "Genetic visualization with an improved GCaMP calcium indicator reveals spatiotemporal activation of the spinal motor neurons in zebrafish," *PNAS*, vol. 108, no. 13, pp. 5425–5430, Mar. 2011.
- [17] E. Warp, G. Agarwal, C. Wyart, D. Friedmann, C. S. Oldfield, A. Conner, F. D. Bene, A. B. Arrenberg, H. Baier, and E. Y. Isacoff, "Emergence of patterned activity in the developing zebrafish spinal cord," *Current Biol.*, vol. 22, no. 2, pp. 93–102, Jan. 2012.
- [18] M. B. Ahrens, J. M. Li, M. B. Orger, D. N. Robson, A. F. Schier, F. Engert, and R. Portugues, "Brain-wide neuronal dynamics during motor adaptation in zebrafish," *Nature*, vol. 485, no. 7399, pp. 471–477, May 2012.
- [19] M. B. Ahrens, M. B. Orger, D. N. Robson, J. M. Li, and P. J. Keller, "Whole-brain functional imaging at cellular resolution using light-sheet microscopy," *Nat. Methods*, vol. 10, no. 5, pp. 413–420, May 2013.
- [20] M. Kamiński, M. Ding, W. A. Truccolo, and S. L. Bressler, "Evaluating causal relations in neural systems: Granger causality, directed transfer function and statistical assessment of significance," *Biol. Cybern.*, vol. 85, no. 2, pp. 145–157, Aug. 2001.
- [21] P. Soelberg, *Causal Inference From Cross-Lagged Correlation Coefficients Fact or Fancy?*. Cambridge, MA, USA: M.I.T. Press, 1967.
- [22] M. Chávez, J. Martinerie, and M. Le Van Quyen, "Statistical assessment of nonlinear causality: Application to epileptic EEG signals," *J. Neurosci. Methods*, vol. 124, no. 2, pp. 113–128, Apr. 2003.
- [23] S. L. Bressler and A. K. Seth, "Wiener–Granger Causality: A well established methodology," *NeuroImage*, vol. 58, no. 2, pp. 323–329, Sep. 2011.
- [24] D. Zhou, Y. Xiao, Y. Zhang, Z. Xu, and D. Cai, "Granger causality network reconstruction of conductance-based integrate-and-fire neuronal systems," *PLoS ONE*, vol. 9, no. 2, p. e87636, Feb. 2014.
- [25] C. Wyart, F. Del Bene, E. Warp, E. K. Scott, D. Trauner, H. Baier, and E. Y. Isacoff, "Optogenetic dissection of a behavioural module in the vertebrate spinal cord," *Nature*, vol. 461, no. 7262, pp. 407–410, Sep. 2009.
- [26] K. J. Friston, "Functional and effective connectivity in neuroimaging: A synthesis," *Human Brain Mapping*, vol. 2, no. 1–2, pp. 56–78, 1994.
- [27] C. W. J. Granger, "Investigating causal relations by econometric models and cross-spectral methods," *Econometrica*, vol. 37, no. 3, p. 424, Aug. 1969.
- [28] M. J. Kamiński and K. J. Blinowska, "A new method of the description of the information flow in the brain structures," *Biol. Cybern.*, vol. 65, no. 3, pp. 203–210, 1991.
- [29] D. Kwiatkowski, P. C. B. Phillips, P. Schmidt, and Y. Shin, "Testing the null hypothesis of stationarity against the alternative of a unit root: How sure are we that economic time series have a unit root?," *J. Econometrics*, vol. 54, no. 1–3, pp. 159–178, 1992.
- [30] H. Akaike, "A new look at the statistical model identification," *IEEE Trans. Automat. Contr.*, vol. 19, no. 6, pp. 716–723, Jun. 1974.
- [31] F. De Vico Fallani, J. Richiardi, M. Chavez, and S. Achard, "Graph analysis of functional brain networks: Practical issues in translational neuroscience," *Phil. Trans. Roy. Soc. B.*, vol. 369, no. 1653, p. 20130521.
- [32] P. E. Vértes, A. F. Alexander-Bloch, N. Gogtay, J. N. Giedd, J. L. Rapoport, and E. T. Bullmore, "Simple models of human brain functional networks," *Proc. Nat. Acad. Sci. USA*, vol. 109, no. 15, pp. 5868–5873, 2012.
- [33] K. W. Doron, D. S. Bassett, and M. S. Gazzaniga, "Dynamic network structure of interhemispheric coordination," *PNAS*, vol. 109, no. 46, pp. 18661–18668, Nov. 2012.
- [34] F. De Vico Fallani, F. Pichiorri, G. Morone, M. Molinari, F. Babiloni, F. Cincotti, and D. Mattia, "Multiscale topological properties of functional brain networks during motor imagery after stroke," *NeuroImage*, vol. 83, pp. 438–449, Dec. 2013.
- [35] B. C. M. van Wijk, C. J. Stam, and A. Daffertshofer, "Comparing brain networks of different size and connectivity density using graph theory," *PLoS ONE*, vol. 5, no. 10, p. e13701, Oct. 2010.
- [36] F. Varela, J.-P. Lachaux, E. Rodriguez, and J. Martinerie, "The brainweb: Phase synchronization and large-scale integration," *Nature Rev. Neurosci.*, vol. 2, no. 4, pp. 229–239, 2001.
- [37] S. Higashijima, M. A. Masino, G. Mandel, and J. R. Fetcho, "Imaging neuronal activity during zebrafish behavior with a genetically encoded calcium indicator," *J. Neurophysiol.*, vol. 90, no. 6, pp. 3986–3997, Dec. 2003.
- [38] P. V. Plazas, X. Nicol, and N. C. Spitzer, "Activity-dependent competition regulates motor neuron axon pathfinding via PlexinA3," *PNAS*, vol. 110, no. 4, pp. 1524–1529, Jan. 2013.
- [39] F. Kubo, B. Hablitzel, M. Dal Maschio, W. Driever, H. Baier, and A. B. Arrenberg, "Functional architecture of an optic flow-responsive area that drives horizontal eye movements in zebrafish," *Neuron*, vol. 81, no. 6, pp. 1344–1359, Mar. 2014.
- [40] R. Portugues, C. E. Feierstein, F. Engert, and M. B. Orger, "Whole-brain activity maps reveal stereotyped, distributed networks for visuo-motor behavior," *Neuron*, vol. 81, no. 6, pp. 1328–1343, Mar. 2014.
- [41] H. Tong and J. R. McDearmid, "Pacemaker and plateau potentials shape output of a developing locomotor network," *Current Biol.*, vol. 22, no. 24, pp. 2285–2293, Dec. 2012.
- [42] A. B. Arrenberg and W. Driever, "Integrating anatomy and function for zebrafish circuit analysis," *Front Neural Circuits*, vol. 7, Apr. 2013.
- [43] R. Prevedel, Y.-G. Yoon, M. Hoffmann, N. Pak, G. Wetzstein, S. Kato, T. Schrödel, R. Raskar, M. Zimmer, E. S. Boyden, and A. Vaziri, "Simultaneous whole-animal 3D imaging of neuronal activity using light-field microscopy," *Nat. Meth.*, vol. Advance online publication, May 2014.
- [44] Y. Benjamini and D. Yekutieli, "The control of the false discovery rate in multiple testing under dependency," *Ann. Statistics*, vol. 29, no. 4, pp. 1165–1188, 2001.
- [45] M. Newman, *Networks: An Introduction*. New York, NY, USA: Oxford Univ. Press, 2010.
- [46] M. Lungarella and O. Sporns, "Mapping information flow in sensorimotor networks," *PLoS Comput. Biol.*, vol. 2, no. 10, p. e144, Oct. 2006.
- [47] P. O. Amblard and O. J. J. Michel, "On Directed Information Theory and Granger Causality Graphs ArXiv, 2010, e-print 1002.1446.

[48] M. Eichler, Graphical Modelling of Dynamic Relationships in Multivariate Time Series Maastricht Univ., 2006, Open Access publications from Maastricht University, urn:nbn:nl:ui:27-13757.

[49] M. Kaminski and H. Liang, "Causal influence: Advances in neurosignal analysis," *Crit. Rev. Biomed. Eng.*, vol. 33, no. 4, pp. 347–430, 2005.

Fabrizio De Vico Fallani, photograph and biography not available at the time of publication.

Martina Corazzol, photograph and biography not available at the time of publication.

Jenna R. Sternberg, photograph and biography not available at the time of publication.

Claire Wyart, photograph and biography not available at the time of publication.

Mario Chavez, photograph and biography not available at the time of publication.

Annex 4

Fast Calcium Imaging with Optical Sectioning via HiLo Microscopy

Marcel A. Lauterbach, Emiliano Ronzitti, Jenna R. Sternberg, Claire
Wyart, and Valentina Emiliani

Published in:
PLOS One
VOL. 10, NO. 12, DECEMBER 2015

RESEARCH ARTICLE

Fast Calcium Imaging with Optical Sectioning via HiLo Microscopy

Marcel A. Lauterbach^{1☯✉}, Emiliano Ronzitti^{1☯}, Jenna R. Sternberg², Claire Wyart², Valentina Emiliani^{1*}

1 Wavefront-Engineering Microscopy Group, Neurophotonics Laboratory, CNRS UMR8250, University Paris Descartes, Sorbonne Paris Cité, Paris, France, **2** Institut du Cerveau et de la Moelle Epinière (ICM), INSERM U1127, CNRS UMR 7225, Sorbonne Paris Cité, University Pierre et Marie Curie Paris 06 UMR S 1127, Paris, France

☯ These authors contributed equally to this work.

✉ Current address: Max Planck Institute for Brain Research, Department of Neural Systems, Frankfurt am Main, Germany

* valentina.emiliani@parisdescartes.fr



OPEN ACCESS

Citation: Lauterbach MA, Ronzitti E, Sternberg JR, Wyart C, Emiliani V (2015) Fast Calcium Imaging with Optical Sectioning via HiLo Microscopy. PLoS ONE 10(12): e0143681. doi:10.1371/journal.pone.0143681

Editor: Filippo Del Bene, Institut Curie, FRANCE

Received: August 9, 2015

Accepted: November 9, 2015

Published: December 1, 2015

Copyright: © 2015 Lauterbach et al. This is an open access article distributed under the terms of the [Creative Commons Attribution License](https://creativecommons.org/licenses/by/4.0/), which permits unrestricted use, distribution, and reproduction in any medium, provided the original author and source are credited.

Data Availability Statement: All relevant data are within the paper and its Supporting Information files.

Funding: M.A.L. received funding from the People Programme (Marie Curie Actions) of the European Union's Seventh Framework Programme (FP7/2007–2013) under REA grant agreement no. PIEF-GA-2011-297917. E.R. acknowledges the "Fondation pour la Recherche Médicale". This work received financial support from the network Ecole des Neurosciences de Paris (ENP), the Atip/Avenir junior program from INSERM and CNRS, the International Reintegration Grant from Marie Curie Actions Framework Program 6 # 277200, and the European Research Council (ERC) starter grant "OptoLoco" # 311673. This work was supported by the Human

Abstract

Imaging intracellular calcium concentration via reporters that change their fluorescence properties upon binding of calcium, referred to as calcium imaging, has revolutionized our way to probe neuronal activity non-invasively. To reach neurons densely located deep in the tissue, optical sectioning at high rate of acquisition is necessary but difficult to achieve in a cost effective manner. Here we implement an accessible solution relying on HiLo microscopy to provide robust optical sectioning with a high frame rate *in vivo*. We show that large calcium signals can be recorded from dense neuronal populations at high acquisition rates. We quantify the optical sectioning capabilities and demonstrate the benefits of HiLo microscopy compared to wide-field microscopy for calcium imaging and 3D reconstruction. We apply HiLo microscopy to functional calcium imaging at 100 frames per second deep in biological tissues. This approach enables us to discriminate neuronal activity of motor neurons from different depths in the spinal cord of zebrafish embryos. We observe distinct time courses of calcium signals in somata and axons. We show that our method enables to remove large fluctuations of the background fluorescence. All together our setup can be implemented to provide efficient optical sectioning *in vivo* at low cost on a wide range of existing microscopes.

Introduction

Calcium imaging enables the study of activity in large populations of neurons with high sensitivity and high frame rates [1]. Camera-based imaging in wide-field (WF) mode can be fast, but imaging in thick specimen might require optical sectioning to suppress spurious out-of-focus signals [2]. Since the brain is an inherently three-dimensional structure, such sectioning is essential for resolving neuronal signals and deciphering its function. Two-photon excitation microscopy achieves optical sectioning at high penetration depth in highly scattering media;

Frontier Science Program (RGP0013/2010), the "Fondation pour la Recherche Médicale" through the program "FRM équipe" the "Agence Nationale de la Recherche" (and ANR-10-INSB-04-01, France-BioImaging Infrastructure network), the FRC and the Rotary Club through the program "Espoir en Tête" 2012 and the National Institutes of Health (NIH 1-U01-NS090501-01). The funders had no role in study design, data collection and analysis, decision to publish, or preparation of the manuscript.

Competing Interests: The authors have declared that no competing interests exist.

accordingly, it is the common approach for deep calcium imaging studies in the brain. On the contrary, for thin samples or weakly-scattering tissue-investigations, single-photon (1P) excitation can be sufficient and optical sectioning is usually provided by confocal laser scanning microscopy [3]. The major limitation of a 1P scanning system with respect to a WF mode is essentially the acquisition speed. Implementations with resonant scan mirrors or acousto-optical deflectors [4] can increase scan speed but they remain point scanning techniques. Apart from technical constraints, the available fluorescence signal limits ultimately the dwell time and hence the achievable speed.

Methods enabling WF imaging, where all pixels of the image are recorded in parallel, while preserving the optical sectioning capability of the point scanning methods would be optimal. Optical approaches have been conceived based either on a parallelization of the confocal principle using multiple pinholes (Spinning Disk Confocal Microscopy, SDCM) [4], on a rearrangement of the illumination to induce excitation only in the focal plane (Single/Selective Plane Illumination Microscopy, SPIM) [5, 6], or on a spatial modulation of the light to encode only in-focus information (Structured Illumination Microscopy, SIM) [7–9]. Although SDCM can image at video rate, inter-pinhole cross-talk impairs the out-of-focus light rejection in thick tissue with dense labeling [10]. SPIM demands side-on access and imposes constraints on handling of the sample, limiting its applications.

SIM offers a compromise between recording speed, sectioning capability, ease of integration into a standard WF microscope, and cost. Optical sectioning by SIM is essentially based on the elementary property of a WF microscope to blur fine details of the image when moving the sample away from the focal plane [11]. SIM structures the excitation light in order to create artificially fine high-contrasted details in the sample. This enables recognizing the in-focus portion of an object (the in-focus portion is the one where details are seen sharply), even in the absence of intrinsic details of the sample. A few raw images are computationally combined to separate the artificially superimposed structures in the image from intrinsic details and to calculate an optically sectioned image, i.e. to isolate the part of the object in focus. Relatively high imaging speed is maintained as the total frame rate is equivalent to the one in WF mode just reduced by a factor corresponding to the number of raw images required for the computation of the sectioned image.

HiLo microscopy [8] is a SIM technique, which needs only two images: one image with structured illumination and one with conventional uniform illumination ("HIGH" and "LOW" contrast images). Structured illumination either with a grating or with laser speckles introduces fine details that enable the computation of the optically sectioned image. Combination with the uniformly illuminated image allows recovering all structural information without the need to combine several non-uniform illumination patterns [12]. HiLo imaging can be fast, since only two raw images are needed to obtain the sectioned image. It has been used for imaging *c. elegans* and *danio rerio* (zebrafish) at 7 frames per second (fps) [13], chick embryos with up to 9.5 fps [14], *xenopus laevis* embryos with 25 fps [15] and externally induced calcium signals at cellular resolution in the brain of *drosophila melanogaster* with 30 fps [16].

Here, we present a fast optical configuration for HiLo microscopy that enables rapid switching between structured and uniform illumination to obtain optically sectioned images, thus allowing high-speed image recording (up to 100 fps) and demonstrate its capabilities by recording calcium transients in motor neurons in the embryonic *danio rerio* spinal cord.

Results

The optical set up for HiLo microscopy is built up around a commercial upright microscope (Fig 1). In order to realize high-frame-rate HiLo, fast switching between the speckled (SWF)

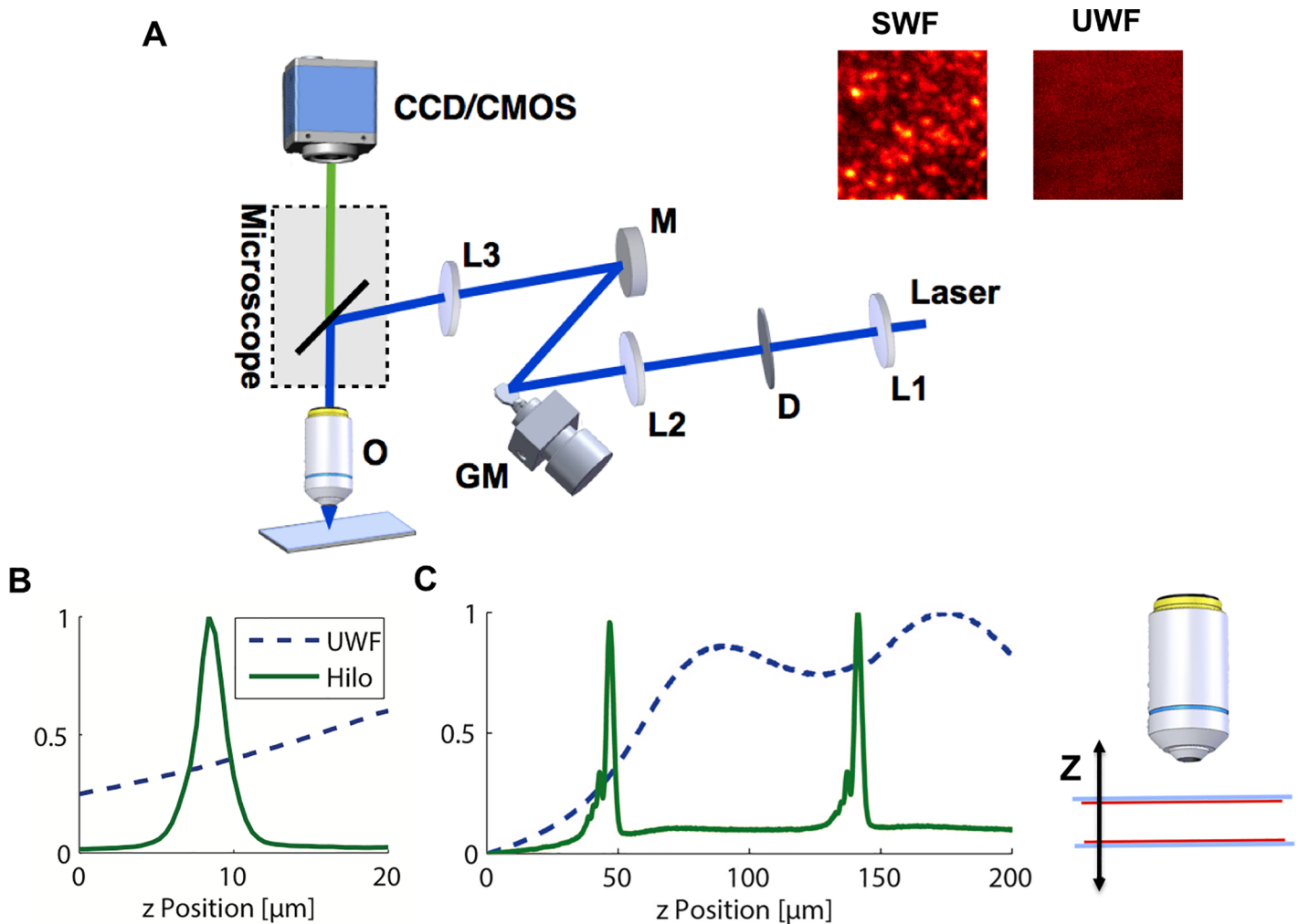


Fig 1. Implementation of HiLo Microscopy to enable optical sectioning at high frame rate in thick biological tissue. (A) Setup: A 473nm laser beam is expanded with lens L1 to a divergent beam to illuminate the diffuser D. The diffuser is imaged by lens L2 onto the galvanometric mirror GM. The galvanometric mirror is then imaged by lens L3 into a conjugated plane of the back focal plane of the objective O within the microscope body. Fluorescence images are acquired either with a CCD camera or a CMOS camera. (Inset) Fluorescent Rhodamine layer imaged with speckled (SWF) and uniform (UWF) widefield illumination at 200 frames per second (fps), confirming successful uniform/speckled illumination. (B–C) Illustration of the optical sectioning: (B) A single fluorescent layer appears as a sharp intensity peak (width 2.1 μm) in a z-stack in HiLo mode (solid green line), but with almost constant intensity in uniform wide-field (UWF) mode (blue dotted line). (C) Two Rhodamine layers can be separated in HiLo mode (solid green line), but in UWF mode only broad peaks (due to spherical aberration) whose positions do not correspond to the layers are visible. Inset: Experimental arrangement: red: Rhodamine layers; gray: supporting coverslips.

doi:10.1371/journal.pone.0143681.g001

and the uniform widefield illumination (UWF) is required. This is here achieved with a static diffuser imaged onto a galvanometric mirror, which is in turn projected into the back focal plane of the objective (Fig 1A). Each position of the galvanometric mirror generates a differently shifted speckle pattern (Fig 1A inset, SWF) at the sample plane. When the mirror is vibrated with a period that is much shorter than the exposure time of the imaging camera, the different speckle patterns are averaged giving a uniform illumination (Fig 1A inset, UWF). With this configuration we could acquire HiLo images up to 100 fps.

To quantify the optical sectioning achievable in our HiLo microscope, we recorded a z-stack of a thin fluorescent layer and determined the fluorescence intensity (averaged over the whole

image) as a function of Z position (Fig 1B). Whereas UWF microscopy showed an almost constant intensity with no sectioning (Fig 1B, dashed blue line), HiLo microscopy showed a sharp peak at the position of the fluorescent layer (Fig 1B, green line; full width at half maximum (FWHM) = 2.1 μm).

To achieve efficient optical sectioning *in vivo*, the ability to separate several objects along the optical axis is critical. We tested this with two fluorescent layers spaced by 94 μm (Fig 1C). UWF microscopy showed broad intensity peaks due to spherical aberrations that do not correspond to the position of the fluorescent layers (Fig 1C, dashed blue line). On the contrary, HiLo microscopy permits to clearly separate the two fluorescent layers showing sharp peaks at 47 μm and 141 μm Z position (Fig 1C, green line).

In order to demonstrate the capability of the microscope for optical sectioning in living samples, we imaged the nervous system of zebrafish embryos (between the 26- and the 30-somite-stage) from transgenic animals expressing genetically encoded calcium indicator GCaMP5 [17] in either motor neurons with *Tg(UAS:GCaMP5G^{icm08}; Et(e1b:Gal4-VP16) s1020t)* or pan-neuronally with *Tg(elavl3:GCaMP5G)* [18–20]. The HiLo microscope enabled the visualization of optical sections revealing the distribution of GCaMP5 (Fig 2A), not visible in epifluorescence illumination (Fig 2B). Finally, we performed a three-dimensional reconstruction of the neurons in the spinal cord of the embryo imaged from a lateral view (Fig 2C and 2D). Neurons from both sides of the embryonic spinal cord were clearly visualized due to the sectioning capability of the HiLo microscopy (Fig 2C, S1 Movie) while they remained blurred with UWF illumination (Fig 2D).

The high-frame-rate acquisition reachable with our implementation of HiLo microscopy was then used to record calcium transients in zebrafish embryos expressing GCaMP5 at the embryonic 26- to 30-somite stage, when motor neurons are alternatively activated on the left and on the right side of the embryo [21, 22].

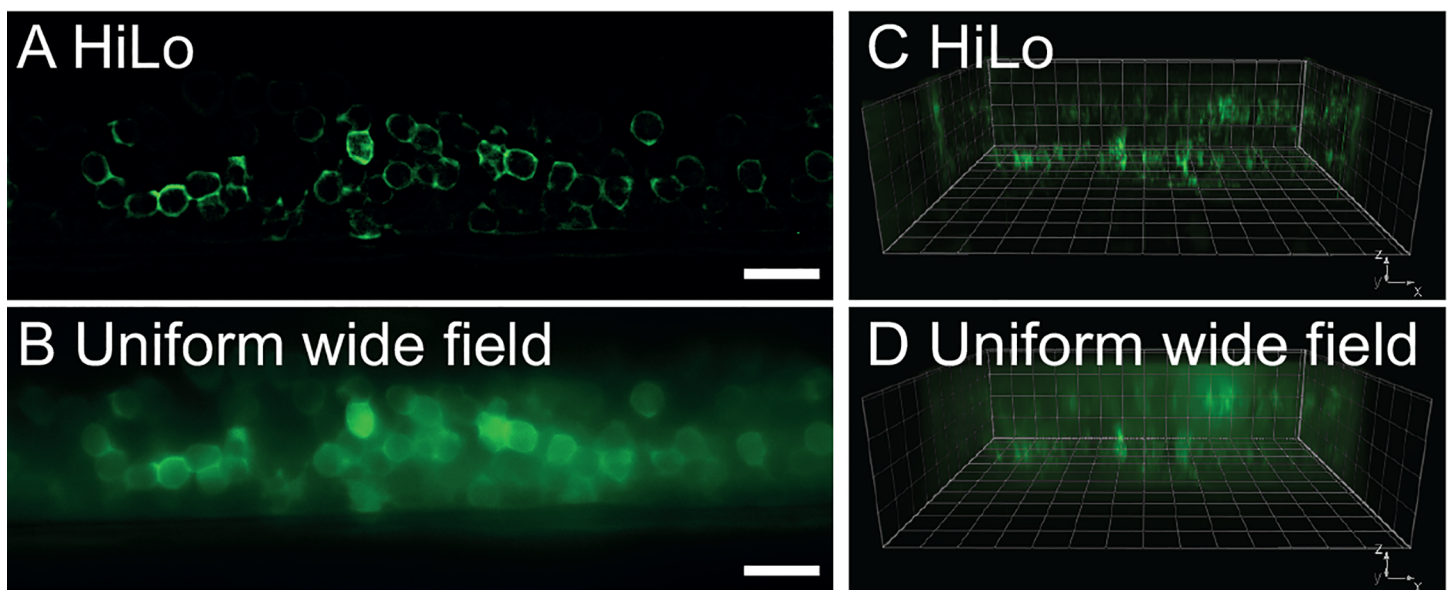


Fig 2. Optical section in embryonic spinal cord of zebrafish obtained with HiLo microscopy. (A) Lateral view of the spinal cord of transgenic zebrafish embryo expressing the fluorescent protein GCaMP5 pan-neuronally in *Tg(elavl3:GCaMP5G)* obtained with HiLo microscopy. (B) Same image obtained in UWF mode. The spatial distribution of GCaMP5G remains hidden under a haze of background fluorescence due to missing optical sectioning. Scale bars in both panels are 20 μm . (C) Corresponding z-stack in 3D visualization, imaged in HiLo mode. The pools of neurons on each side of the spinal cord are visible in two separate planes. (D) Same reconstruction in WF mode (grid step 10 $\mu\text{m}/\text{line}$). See also S1 Movie.

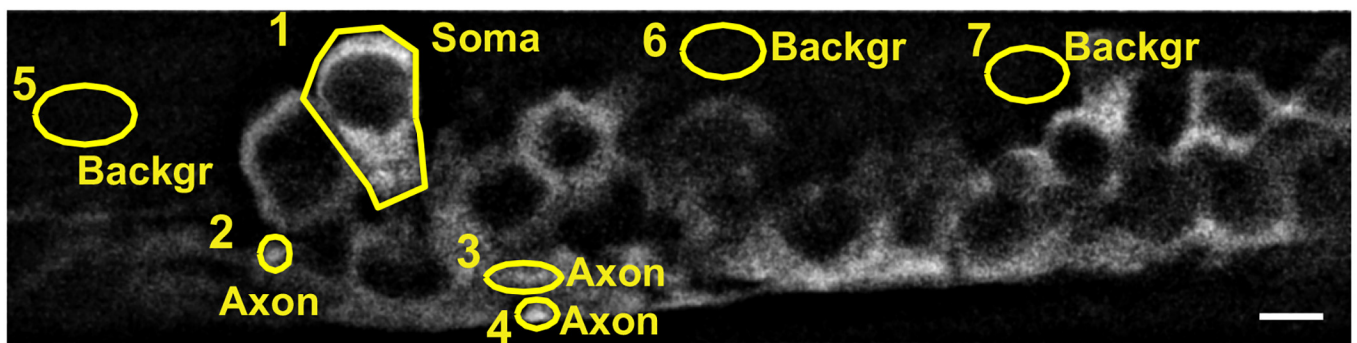
doi:10.1371/journal.pone.0143681.g002

In order to study the HiLo capability for calcium imaging, fluorescence variations ($\Delta F/F$) of the calcium indicator measured from selected regions of interest (ROIs; cell bodies, axons and background) in HiLo and UWF mode have been compared in *Tg(Et(e1b:Gal4-VP16)s1020t; UAS:GCaMP5G^{icm08})* (Fig 3A). Two main benefits can be noted in the HiLo mode:

First, substantially increased $\Delta F/F$ amplitudes are observable with HiLo (Fig 3, S2 Movie). Already on the cell bodies, which gave a strong signal, HiLo microscopy led to a gain of a factor of 2.5 in signal-to-baseline ratio ($\Delta F/F$) compared to UWF microscopy. (Fig 3B) This gain reached up to a factor 10 for less bright regions as axons (Fig 3C). Such an activity detection boost, due to a reduction of the out-of-focus stray light contribution, reveals the higher sensitivity of HiLo for identifying cellular activity with respect to a conventional WF observation.

Second, a set of lower-level peaks present in the UWF calcium signals (Fig 4A) was suppressed in the HiLo recording (Fig 4B). Peculiarly, contrary to the principal peaks, these secondary peaks were not localized to a specific ROI and were present also in the background signal (Fig 4A, Background ROIs 5–7). These secondary fluorescence variations are thus not

A Regions of interest (ROIs)



B Soma (ROI 1) C Axon (ROI 4)

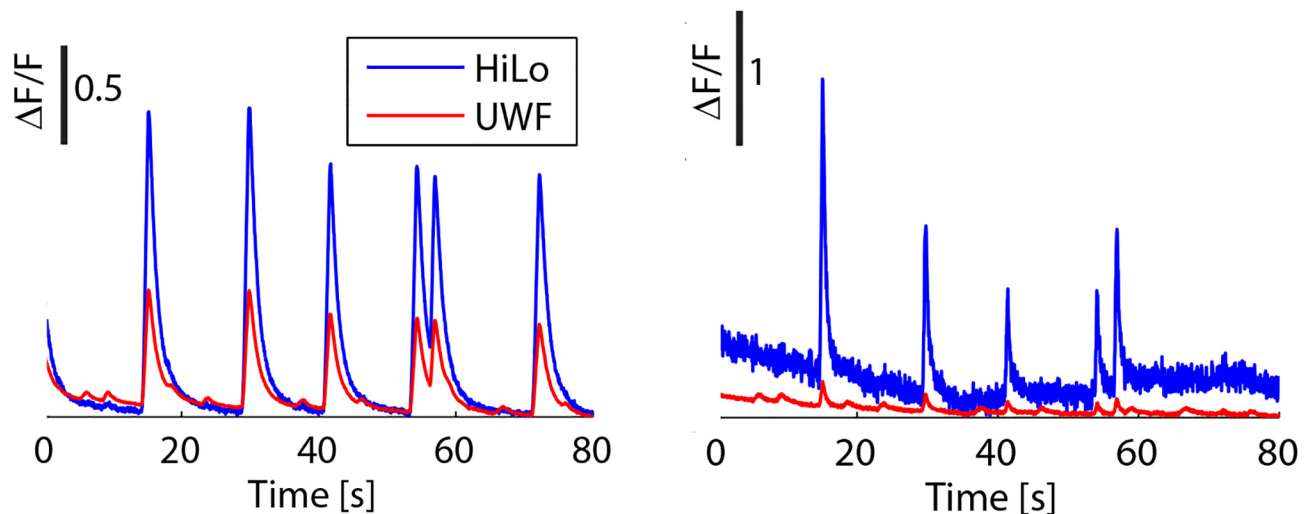


Fig 3. HiLo microscopy enhances calcium signals. (A) *In vivo* HiLo image of motor neurons of a zebrafish embryo expressing GCaMP5G in soma (ROI1), axons (ROIs 2–4), or background (ROIs 5–7). Scale bar 5 μ m. (B) $\Delta F/F$ time series in the soma (ROI 1) shows that HiLo mode leads to a larger signal than UWF mode. (C) For axons (ROI 4) the gain in HiLo mode is even larger. Acquisition rate was 25fps.

doi:10.1371/journal.pone.0143681.g003

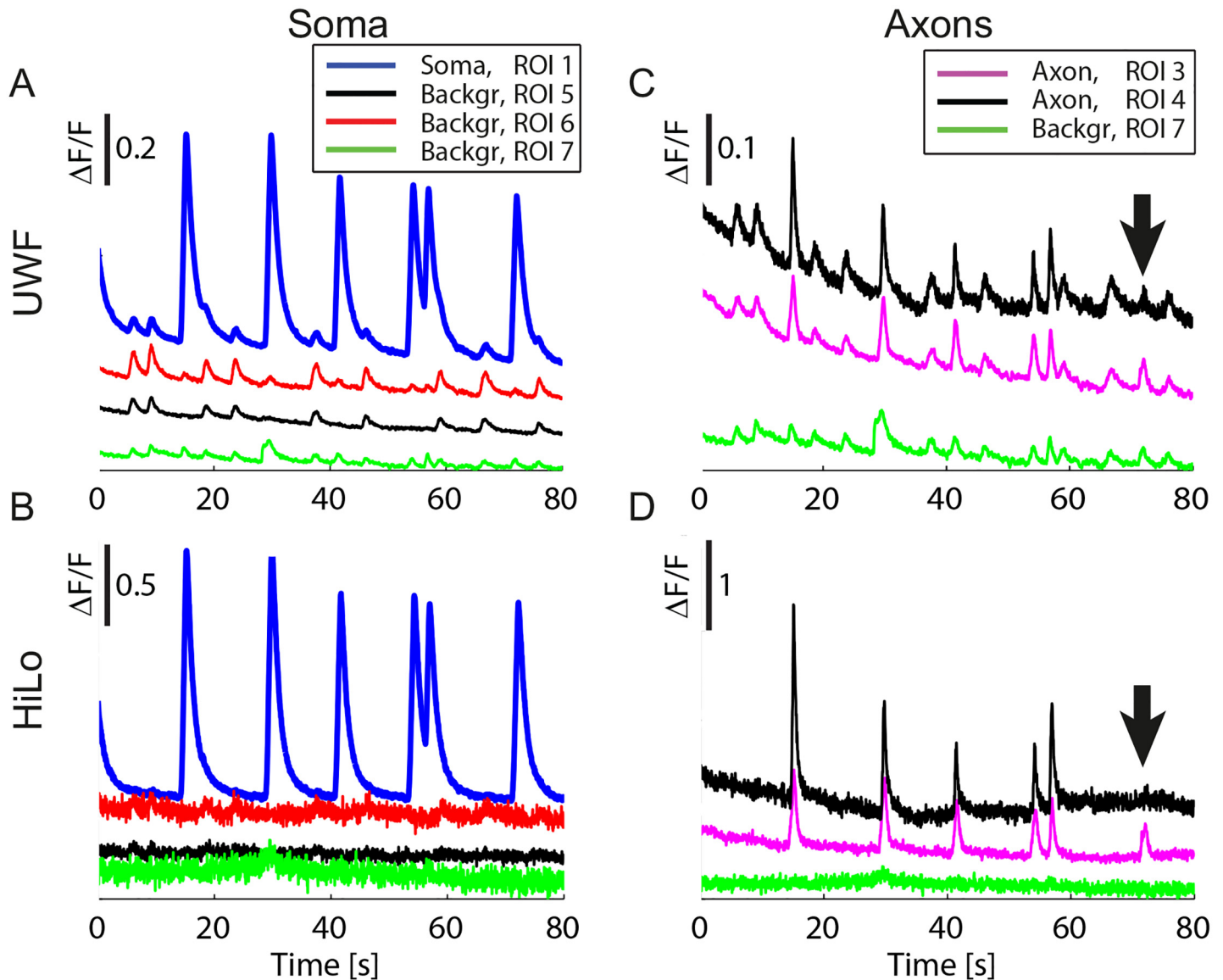


Fig 4. Suppression of non-specific signals. Nonspecific signals appeared in UWF mode (A, C) and were suppressed in HiLo mode (B, D) (ROIs numbered as in Fig 3A). The benefit is consistent in the somatic signal (A, B) and particularly important for the axonal signals (C, D) which are smaller and therefore more difficult to distinguish from the unspecific signals. Furthermore HiLo mode allows observing that calcium spikes occasionally did not occur in a single axon (black trace, arrow), despite occurrence in the neighboring axon (magenta trace) (D), while UWF mode hindered the observation of this phenomenon (C). Note that some bleaching is seen over the 80 s recording time. Traces were offset vertically for visualization. Raw data are shown in all panels. Acquisition rate was 25 fps.

doi:10.1371/journal.pone.0143681.g004

linked to an activity of the targeted cell, but originate from out-of-focus planes where anti-correlated neuronal activity was produced from the pool of contralateral motor neurons [21, 22]. Although for relatively strong signals, the real specific targeted activity can be distinguished from the out-of-focus contributions on the basis of the amplitude (Fig 4A), in many other circumstances the two contributions become hardly distinguishable, possibly leading to an erroneous interpretation of the cellular activity (Fig 4C and 4D). Being able to acquire only the fluorescence signal from the in-focus region of the sample, HiLo suppresses such unwanted peaks both in the cells and in the background (Fig 4B and 4D). Especially, we were able to

resolve with HiLo microscopy that neuronal activity is not always transmitted to all cells: ROI 4 on the axonal track does not show any calcium signal at 72 s (Fig 4D, black trace, arrow), despite a strong signal in the adjacent ROI (ROI 3, magenta trace in Fig 4D). This missing peak is in stark contrast with all other calcium peaks in this recording, which were faithfully spread to all ROIs (peaks at 15 s, 30 s, 42 s, 54 s, 57 s). Normal wide-field imaging shows a spurious signal at this time point (Fig 4C, black trace, arrow), which is indistinguishable from true neuronal signals. Only HiLo microscopy allowed here to detect the singular absence of signal transmission.

Thus, compared to conventional widefield microscopy, HiLo microscopy offers a higher sensitivity for fluorescence-variation detection and higher specificity in terms of spatial localization of the calcium signals. Since a fundamental requirement of calcium-signal recording is being able to follow fast cellular kinetics, such HiLo benefits can become of authentic advantage if HiLo imaging can be performed at very high frame rates.

We therefore verified HiLo-calcium-imaging performance up to 100 fps (200 fps raw-data rate) (Fig 5, S3 Movie), a frame-rate at which cellular sub-compartmental kinetics can be extensively investigated. This temporal resolution allows clearly observing that calcium transients rose first in axons and then in the soma (Fig 5A and 5B). Moreover, the intracellular calcium concentration rise was faster in the initial segment (Fig 5A and 5B, ROI 4, ROI 5, light blue and magenta) than in the rest of the soma (ROI 2, ROI 3, orange and dark blue). In the soma a close to linear rise of intracellular calcium was observed, followed by an exponential decay with a time constant of 1.7 s (Fig 5C, Inset: blue data/red-dotted fit). The sequence and kinetics of the calcium transients were stable over time, as seen when recording neuronal activity 2.5 min later (Fig 5C).

Discussion

We have demonstrated high rate *in vivo* HiLo microscopy on zebrafish embryos enabling fast calcium imaging up to 100 fps on a field of view of $\sim 100 \mu\text{m} \times 50 \mu\text{m}$ with optical sectioning.

We have shown an axial resolution of $\sim 2 \mu\text{m}$, permitting to resolve single axonal and dendritic processes. Correct targeting of the genetically encoded marker GCaMP5G could be visualized without the haze of out-of-focus fluorescence due to subcellular resolution.

The optical sectioning provided by HiLo microscopy increased the amplitudes of the recorded calcium signal and permitted the rejection of out-of-focus signals originating from motor neurons in the contralateral side. This suppression of spurious calcium signals by HiLo microscopy allowed a distinction between small signals that originate from the structure of interest and stray signals from other neurons. This capability is particularly relevant for a correct interpretation and localization of the neuronal signals. Indeed in UWF, the stray signals originating from neuronal activity from out-of-focus planes can be almost as strong as the signal arising from small regions of observation as axonal portions, making a distinction of true signals and spurious signals almost impossible (Fig 4).

HiLo recordings have been shown with up to 100 fps, demonstrating that fast cellular dynamics can be studied. This high imaging rate allows resolving differences in rise time of calcium transients for soma and axon. The calcium-concentration rise in the initial segments was faster than in the soma. By eliminating the out-of-focus light, we could detect failures to generate spikes in some axons.

It is worth mentioning that speckles are an inevitable interference phenomenon in laser illumination [23]. Fully developed speckles are therefore resistant against misalignment and optical aberrations [24]. Compared to alternative HiLo methods that project gratings into the sample plane, speckle projection is therefore more robust to optical aberrations induced by the microscope and sample.

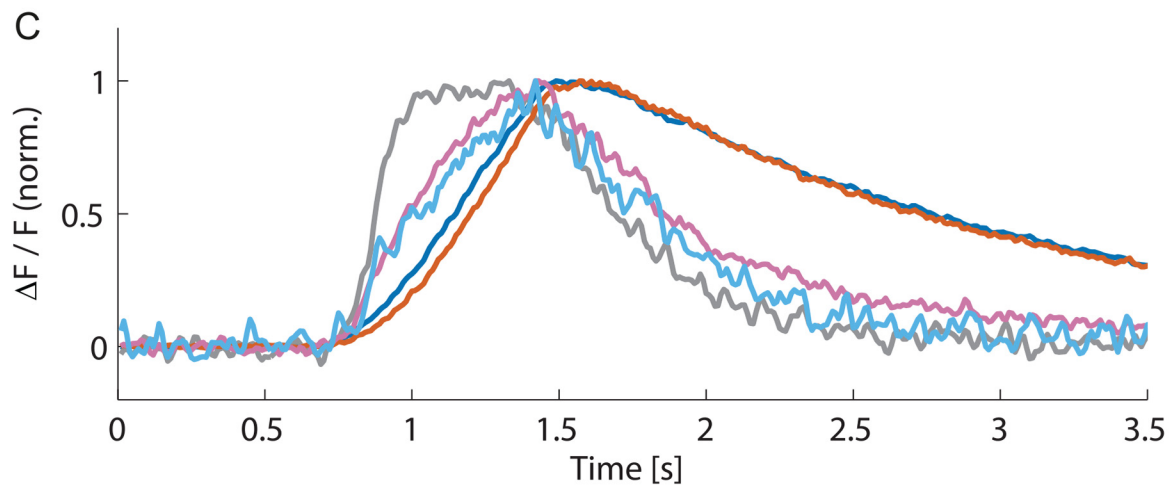
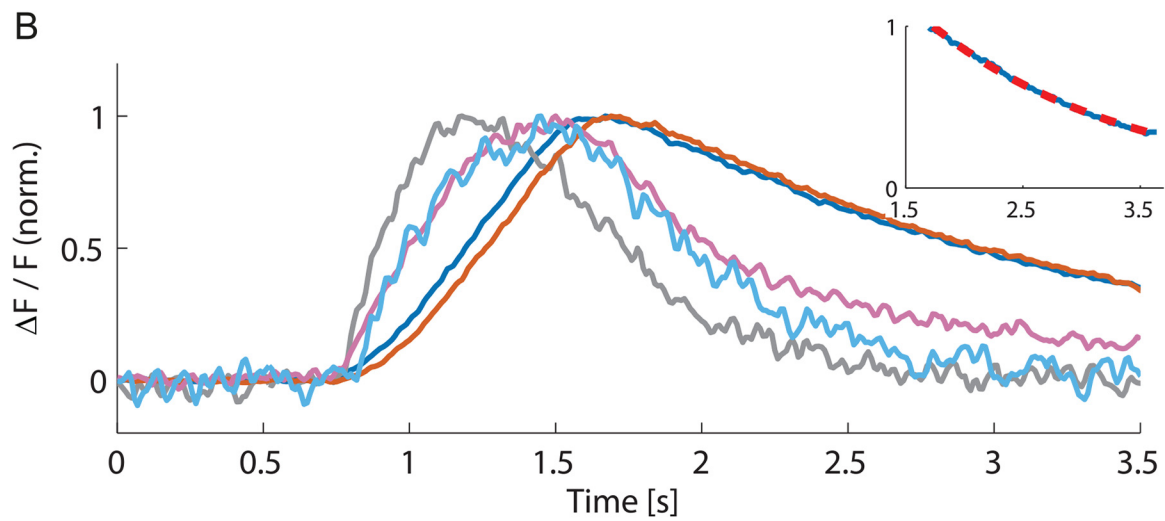
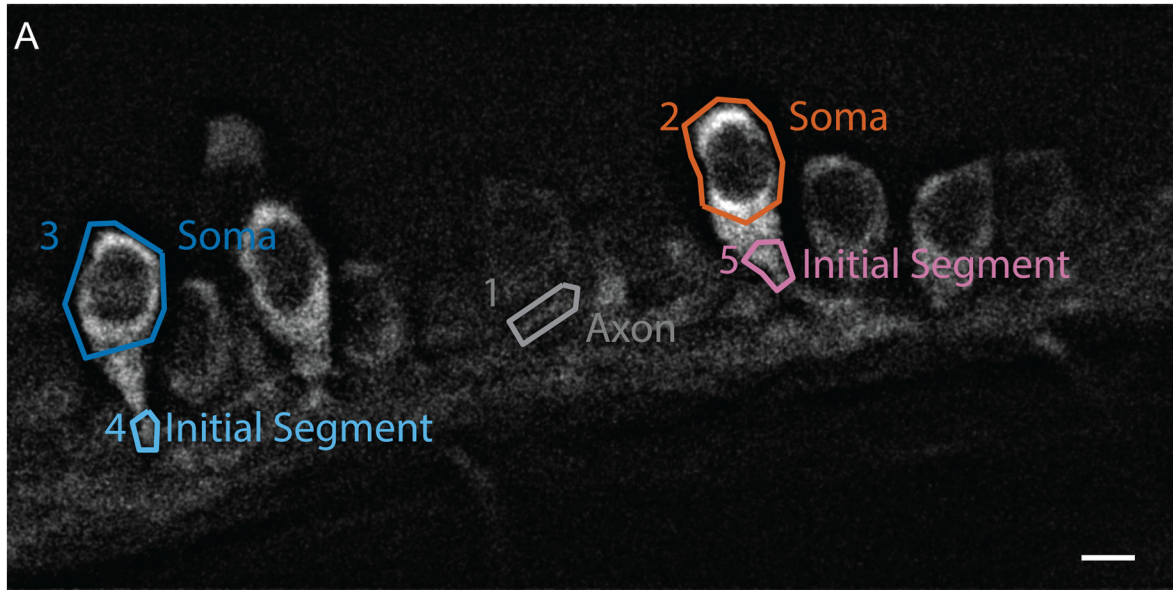


Fig 5. Fast calcium imaging at 100 fps with HiLo microscopy reveals different dynamics in soma and initial segment. (A) HiLo image of motor neurons expressing GCaMP5G with ROIs. Scale bar 5 μm . (B) Time course of calcium signals in soma, initial segment and axon, recorded at 100 fps. In the axon (ROI 1, gray) and the initial segments (ROI 4, light blue; ROI 5, magenta) a much faster rise is observed than in the somata (ROI 2, orange; ROI 3, dark blue). Somatic signals show a linear rise and a mono-exponential decay (Inset: blue somatic signal with red dotted fit, decay time 1.7 s, $R^2 = 0.998$). (C) The kinetics of calcium transients in different compartments were stable over time as shown with a recording performed 2.5 min later.

doi:10.1371/journal.pone.0143681.g005

We demonstrate that a fast-switching design can allow following calcium signals in zebrafish up to 100 fps, permitting accurate analysis of calcium kinetics. The system has an extremely simple design using a standard static diffuser in combination with a one-axis scan mirror that has to operate just in two states: stationary and moving. This is achieved by turning a sinusoidal command voltage on and off.

In this study, we demonstrated single-color HiLo imaging; however, extension to multiple colors would be straightforward and only require adding a second laser and the corresponding filter cube without further changes in the optical path. In addition HiLo microscopy can easily be combined with electrophysiology. Also combination with other optical widefield methods remains possible, e.g. to stimulate neurons optogenetically either via uniform [25] or targeted [26] illumination. Application to functional imaging other than calcium concentration, e.g. imaging of voltage-sensitive dyes should be feasible as well.

High-frame-rate optical sectioning for dynamic imaging can be alternatively obtained via Spinning Disk Confocal Microscopy (SDCM) or Single Plane Illumination Microscopy (SPIM). SDCM extends the confocal principle with a parallelized detection through multiple pinholes to speed up the scanning. Although a single-pinhole physical rejection of out-of-focus-light is often superior over computational SIMs in thick tissues [9], with multi-pinhole detection the inter-pinhole cross-talk hampers the optical sectioning, leading to background signals [21,22]. Thus, when optical sectioning and high-frame rate are required as for calcium imaging, HiLo is an advantageous alternative to SDCM. Moreover, confocal microscopy requires lasers of high beam quality as this determines the reachable resolution, while for HiLo microscopy the demand on laser-beam quality is lower, because the laser illuminates just a diffuser.

SPIM delivers sidewise illumination to illuminate just a single plane of the sample. Since the optical sectioning is fully provided through a selective plane illumination, the detection can be fully equivalent to a conventional microscope, thus basically speed-limited only by the camera performance and available signal [18, 27]. However, the need for two orthogonal optical paths restricts the access to the sample, representing a major limitation. Moreover, the sample scattering and aberrations can broaden and distort the plane of illumination, reducing the optical sectioning. On the contrary, clear access to the sample is maintained in HiLo since it is based on WF epifluorescence imaging.

Conclusions

In summary this study highlights a simple, easy-to-implement and cost-efficient method for fast calcium imaging in thick low-scattering samples. Optical sectioning is achieved due to alignment- and aberration-insensitive structured illumination with laser speckles. Images are acquired on a camera as in conventional WF microscopy, which is fast since no scanning is necessary. We showed here that this approach was powerful to perform *in vivo* calcium imaging with a genetically encoded calcium sensor at a speed of 100 fps on motor neurons of the zebrafish embryonic spinal cord.

Materials and Methods

Optical setup

A HiLo microscope using laser speckles for structured illumination ([Fig 1A](#)) was implemented on a commercial microscope body (Axio Examiner.Z1, Zeiss). A laser (MBL-F-473-500, Laser 2000, Wessling, Germany) with an emission wavelength of 473 nm and a power of 500 mW served as light source. The beam was expanded to a divergent beam with lens L1 ([Fig 1A](#)) to illuminate a static diffuser D (scattering angle 1°, 20DKIT-C1, Newport, Irvine, CA, USA). The diffuser was then imaged onto the galvanometric mirror GM (Cambridge Technology) with lens L2. Since the mirror had a size of only 4 mm, this image was demagnified. Note that a 4f geometry that preserves collimation of beams is not necessary. The galvanometric mirror was then imaged with lens L3 ($f = 30$ mm) through the rear port of the microscope onto an intermediate back focal plane in the microscope stand. The illumination was reflected to the objective O (Zeiss W Plan-Apochromat 63x/1.0) with a filter cube (Semrock, FITC-3540C-000) of the microscope. Fluorescence images were acquired either with a CCD camera (Coolsnap ES², Photometrics, Tucson, AZ, USA,) or a CMOS camera (Orca Flash, C11440, Hamamatsu, Massy, France). Illumination power was 2.8 mW.

The microscope and the CCD camera were controlled with the software Slidebook (Intelligent Imaging Innovations, Denver, CO, USA), the CMOS camera with the software HCImage (Hamamatsu).

To obtain structured illumination, the galvanometric mirror was kept stationary; for uniform illumination it was vibrated with a frequency much faster than the frame rate. To this end the galvanometric mirror was vibrated with a sine wave (700 Hz) from a function generator (203047, Jeulin, Evreux, France).

The vibration could be turned on and off via a TTL signal, which allowed control of the vibration via the microscope's software Slidebook. Alternatively this TTL signal was derived directly from the camera. The frame clock of the camera was divided by two with custom built electronics, giving a high TTL signal (galvo moving) for every other frame.

Fluorescent layers

Fluorescent layers for validation of optical sectioning ([Fig 1B and 1C](#)) were made of Rhodamine 6G in polymethyl-methacrylate (PMMA): 20 μ l of a Rhodamine 6G solution (1M Rhodamine in a 2% w/v PMMA-in-chloroform solution) were spin coated onto glass cover slips (#1, 25 mm, BK-7, diameter 18 mm, Marienfeld Superior, Menzel-Gläser GmbH, Braunschweig, Germany) at 8500 rpm.

The fluorescent double layer for testing the optical sectioning ([Fig 1B and 1C](#)) was fabricated by gluing two such spin coated cover slips together with double-sided adhesive tape. The Rhodamine layers were facing the tape. The space between the cover slips was filled with water.

Zebrafish care and strains

Danio rerio embryos of the AB and Tubingen Longfin (TL) genetic backgrounds were raised in egg water [28], at 28.5°C until 75% epiboly and then at 26°C to delay development for experimentation until the 24-somite stage. GCaMP5G-positive embryos originating from the cross of *Tg(Et(e1b:Gal4-VP16)s1020t; UAS:GCaMP5G^{icm08})* or *Tg(elavl3:GCaMP5G)* with wild type adults were dechorionated, mounted laterally in 1.5% agar at the 24-somite stage, and paralyzed with injections of 0.5 mM α -bungarotoxin (Sigma-Aldrich, USA) into caudal muscle of the tail. Experiments were performed at the 26–30 somite stages at room temperature. Embryo staging was performed according to stages described in Kimmel et al. [29]. All procedures were

approved by the Institutional Ethics Committee “Charles Darwin” at the Institut du Cerveau et de la Moelle épinière (ICM), Paris, France, and received subsequent approval from the EEC (2010/63/EU).

Data analysis

Images were acquired in 16 bit and exported in tiff format. All further data processing was performed with MATLAB (Mathworks, Natick, MA, USA).

HiLo. Raw images were recorded alternatingly with uniform illumination and speckled illumination. Optically sectioned images (“HiLo images”) were calculated from pairs of a speckled image (SWF) followed by a uniformly illuminated image (UWF) with the algorithm previously described [12]. A plugin for Image J (Rasband, W.S., ImageJ, U. S. National Institutes of Health, Bethesda, Maryland, USA, <http://imagej.nih.gov/ij/>, 1997–2014) is available from the group of Jerome Mertz (<http://biomicroscopy.bu.edu/>). We generated custom made Matlab scripts based on initial code kindly provided by Daryl Lim and Jerome Mertz. We favored the Matlab implementation for greater control of parameters and for the possibility of automating data processing. Since two raw images are used to obtain one HiLo image, the frame rate of the raw images is twice the frame rate of the HiLo images. All UWF images presented in the article are the images with uniform illumination that were also used for the calculation of the HiLo images.

Optical sectioning. To test the resolution of optical sectioning (Fig 1), image stacks of fluorescent Rhodamine 6G layers were recorded with a long distance 63X, NA 1.0 water-dipping objective. Fluorescence intensity was averaged over the whole field of view and plotted against axial position. Raw data without further smoothing are displayed.

Calcium imaging. For time series of calcium transients, the average fluorescence intensity was determined in the HiLo and the UWF images in ROIs as indicated. Fluorescence changes ΔF were normalized to the minimal fluorescence F in each time series. To show small peaks without overlay with other graphs, traces in Fig 4A and 4C were offset vertically by 0.1, traces in Fig 4B by 0.2, and traces in Fig 4D by 0.4. No temporal averaging was applied to the calcium signals.

Supporting Information

S1 Fig. Same data as in Fig 3C not normalized to $\Delta F/F$, but shown as raw signals.
(PDF)

S1 Movie. 3D-view of the spinal cord of double transgenic zebrafish embryo expressing the fluorescent protein GCaMP5 in motor neurons obtained with HiLo microscopy.
(WMV)

S2 Movie. Comparison of calcium transients imaged in HiLo and wide-field modes at 25 fps. (Upper Panel) *In vivo* HiLo image of motor neurons of a zebrafish embryo expressing GCaMP5G. Optical sectioning in HiLo mode visualizes the membraneous distribution of GCaMP5G and the calcium transients of spontaneous activity. (Lower Panel) Same recording in normal widefield mode with uniform illumination (UWF). Due to a lack of sectioning the localization of GCaMP5G and the calcium transients remain hidden in a haze.
(MP4)

S3 Movie. Stop-motion imaging of calcium transients at 100 fps. HiLo microscopy reaches up to 100 fps (upper panel) and provides the necessary optical sectioning, whereas the neurons are not clearly resolved in widefield mode (UWF) (lower panel).
(MP4)

Acknowledgments

We thank Karl Kilborn and Glen Redford from Intelligent Imaging Innovations for their help in controlling the instrument with Slidebook, Cathie Ventalon for useful discussions on the HiLo algorithm optimization and help in the construction of the initial HiLo configuration, Christophe Tourain for custom-built electronics, Marc Guillon for helpful discussions, Daryl Lim, and Jerome Mertz for providing the HiLo code. We are grateful to David Ogden for lending the galvanometric mirror. M.A.L. received funding from the People Programme (Marie Curie Actions) of the European Union's Seventh Framework Programme (FP7/2007–2013) under REA grant agreement no. PIEF-GA-2011-297917. E.R. acknowledges the "Fondation pour la Recherche Médicale". This work received financial support from the network Ecole des Neurosciences de Paris (ENP), the Atip/Avenir junior program from INSERM and CNRS, the International Reintegration Grant from Marie Curie Actions Framework Program 6 # 277200, and the European Research Council (ERC) starter grant "OptoLoco" # 311673. This work was supported by the Human Frontier Science Program (RGP0013/2010), the "Fondation pour la Recherche Médicale" through the program "FRM équipe", the "Agence Nationale de la Recherche" (and ANR-10-INSB-04-01, France-BioImaging Infrastructure network), the FRC and the Rotary Club through the program "Espoir en Tête" 2012 and the National Institutes of Health (NIH 1-U01-NS090501-01).

Author Contributions

Conceived and designed the experiments: MAL ER JS CW VE. Performed the experiments: MAL ER JS CW. Analyzed the data: MAL. Contributed reagents/materials/analysis tools: MAL ER. Wrote the paper: MAL ER CW VE.

References

1. Chen T-W, Wardill TJ, Sun Y, Pulver SR, Renninger SL, Baohan A, et al. Ultrasensitive fluorescent proteins for imaging neuronal activity. *Nature*. 2013; 499:295–300. doi: [10.1038/nature12354](https://doi.org/10.1038/nature12354) PMID: [23868258](https://pubmed.ncbi.nlm.nih.gov/23868258/)
2. Mertz J. Optical sectioning microscopy with planar or structured illumination. *Nat. Methods*. 2011; 8:811–9. doi: [10.1038/nmeth.1709](https://doi.org/10.1038/nmeth.1709) PMID: [21959136](https://pubmed.ncbi.nlm.nih.gov/21959136/)
3. Minsky M. Microscopy Apparatus. US Pat. 3013467. 1961.
4. Pawley J. Handbook of Biological Confocal Microscopy. 3rd Ed. New York: Springer Science+Business Media, LLC; 2006.
5. Huisken J, Swoger J, Del Bene F, Wittbrodt J, Stelzer EHK. Optical sectioning deep inside live embryos by selective plane illumination microscopy. *Science*. 2004; 305:1007–9. PMID: [15310904](https://pubmed.ncbi.nlm.nih.gov/15310904/)
6. Dodt H-U, Leischner U, Schierloh A, Jährling N, Mauch CP, Deininger K, et al. Ultramicroscopy: three-dimensional visualization of neuronal networks in the whole mouse brain. *Nat. Methods*. 2007; 4:331–6. PMID: [17384643](https://pubmed.ncbi.nlm.nih.gov/17384643/)
7. Neil M a, Juskaitis R, Wilson T. Method of obtaining optical sectioning by using structured light in a conventional microscope. *Opt. Lett.* 1997; 22:1905–7. PMID: [18188403](https://pubmed.ncbi.nlm.nih.gov/18188403/)
8. Lim D, Chu KK, Mertz J. Wide-field fluorescence sectioning with hybrid speckle and uniform-illumination microscopy. *Opt. Lett.* 2008; 33:1819–21. PMID: [18709098](https://pubmed.ncbi.nlm.nih.gov/18709098/)
9. Gustafsson MGL, Shao L, Carlton PM, Wang CJR, Golubovskaya IN, Cande WZ, et al. Three-dimensional resolution doubling in wide-field fluorescence microscopy by structured illumination. *Biophys. J.* 2008; 94:4957–70. doi: [10.1529/biophysj.107.120345](https://doi.org/10.1529/biophysj.107.120345) PMID: [18326650](https://pubmed.ncbi.nlm.nih.gov/18326650/)
10. Conchello J-A, Lichtman JW. Optical sectioning microscopy. *Nat. Methods*. 2005; 2:920–31. PMID: [16299477](https://pubmed.ncbi.nlm.nih.gov/16299477/)
11. Wilson T. Optical sectioning in fluorescence microscopy. *J. Microsc.* 2011; 242:111–6. doi: [10.1111/j.1365-2818.2010.03457.x](https://doi.org/10.1111/j.1365-2818.2010.03457.x) PMID: [21118248](https://pubmed.ncbi.nlm.nih.gov/21118248/)
12. Santos S, Chu KK, Lim D, Bozinovic N, Ford TN, Hourtoulle C, et al. Optically sectioned fluorescence endomicroscopy with hybrid-illumination imaging through a flexible fiber bundle. *J. Biomed. Opt.* 2011; 14:030502.

13. Lim D, Ford TN, Chu KK, Mertz J. Optically sectioned in vivo imaging with speckle illumination HiLo microscopy. *J. Biomed. Opt.* 2011; 16:016014. doi: [10.1117/1.3528656](https://doi.org/10.1117/1.3528656) PMID: [21280920](https://pubmed.ncbi.nlm.nih.gov/21280920/)
14. Ford TN, Lim D, Mertz J. Fast optically sectioned fluorescence HiLo endomicroscopy. *J. Biomed. Opt.* 2012; 17:021105. doi: [10.1117/1.JBO.17.2.021105](https://doi.org/10.1117/1.JBO.17.2.021105) PMID: [22463023](https://pubmed.ncbi.nlm.nih.gov/22463023/)
15. Muro E, Vermeulen P, Ioannou A, Skourides P, Dubertret B, Fragola A, et al. Single-shot optical sectioning using two-color probes in HiLo fluorescence microscopy. *Biophys. J. Biophysical Society*; 2011; 100:2810–9.
16. Masson A, Pedrazzani M, Benrezzak S, Tchenio P, Preat T, Nutarelli D. Micromirror structured illumination microscope for high-speed in vivo drosophila brain imaging. *Opt. Express*. 2014; 22:516–29.
17. Akerboom J, Chen T-W, Wardill TJ, Tian L, Marvin JS, Mutlu S, et al. Optimization of a GCaMP calcium indicator for neural activity imaging. *J. Neurosci.* 2012; 32:13819–40. doi: [10.1523/JNEUROSCI.2601-12.2012](https://doi.org/10.1523/JNEUROSCI.2601-12.2012) PMID: [23035093](https://pubmed.ncbi.nlm.nih.gov/23035093/)
18. Ahrens MB, Orger MB, Robson DN, Li JM, Keller PJ. Whole-brain functional imaging at cellular resolution using light-sheet microscopy. *Nat Methods*. 2013; 10:413–20. doi: [10.1038/nmeth.2434](https://doi.org/10.1038/nmeth.2434) PMID: [23524393](https://pubmed.ncbi.nlm.nih.gov/23524393/)
19. Fidelin K, Djenoune L, Stokes C, Prendergast A, Gomez J, Baradel A, Del Bene F, Wyart C. State-dependent modulation of locomotion by GABAergic spinal sensory neurons. *Current Biology (in press)*.
20. Scott EK, Mason L, Arrenberg AB, Ziv L, Gosse NJ, Xiao T, et al. Targeting neural circuitry in zebrafish using GAL4 enhancer trapping. *Nat. Methods*. 2007; 4:323–6. PMID: [17369834](https://pubmed.ncbi.nlm.nih.gov/17369834/)
21. Warp E, Agarwal G, Wyart C, Friedmann D, Oldfield CS, Conner A, et al. Emergence of patterned activity in the developing zebrafish spinal cord. *Curr. Biol.* 2012; 22:93–102. doi: [10.1016/j.cub.2011.12.002](https://doi.org/10.1016/j.cub.2011.12.002) PMID: [22197243](https://pubmed.ncbi.nlm.nih.gov/22197243/)
22. Muto A, Ohkura M, Kotani T, Higashijima S, Nakai J, Kawakami K. Genetic visualization with an improved GCaMP calcium indicator reveals spatiotemporal activation of the spinal motor neurons in zebrafish. *Proc. Natl. Acad. Sci. U. S. A.* 2011; 108:5425–30. doi: [10.1073/pnas.1000887108](https://doi.org/10.1073/pnas.1000887108) PMID: [21383146](https://pubmed.ncbi.nlm.nih.gov/21383146/)
23. Goodman JW. *Speckle phenomena in optics: theory and applications*. 1st ed. Roberts and Company Publishers; 2010.
24. Murphy PK, Allebach J., Gallagher NC. Effect of optical aberrations on laser speckle. *J. Opt. Soc. Am. A.* 1986; 3:215–22.
25. Boyden ES, Zhang F, Bamberg E, Nagel G, Deisseroth K. Millisecond-timescale, genetically targeted optical control of neural activity. *Nat. Neurosci.* 2005; 8:1263–8. PMID: [16116447](https://pubmed.ncbi.nlm.nih.gov/16116447/)
26. Papagiakoumou E, Anselmi F, Bègue A, de Sars V, Glückstad J, Isacoff EY, et al. Scanless two-photon excitation of channelrhodopsin-2. *Nat. Methods*. 2010; 7:848–54. doi: [10.1038/nmeth.1505](https://doi.org/10.1038/nmeth.1505) PMID: [20852649](https://pubmed.ncbi.nlm.nih.gov/20852649/)
27. Panier T, Romano S a, Olive R, Pietri T, Sumbre G, Candelier R, et al. Fast functional imaging of multiple brain regions in intact zebrafish larvae using selective plane illumination microscopy. *Front. Neural Circuits*. 2013; 7:65. doi: [10.3389/fncir.2013.00065](https://doi.org/10.3389/fncir.2013.00065) PMID: [23576959](https://pubmed.ncbi.nlm.nih.gov/23576959/)
28. Westerfield M. *The zebrafish book. A guide for the laboratory use of zebrafish (Danio rerio)*. 4th ed. Univ. of Oregon Press; 2000.
29. Kimmel CB, Ballard WW, Kimmel SR, Ullmann B, Schilling TF. Stages of embryonic development of the zebrafish. *Dev. Dyn.* 1995; 203:253–310. PMID: [8589427](https://pubmed.ncbi.nlm.nih.gov/8589427/)